Entanglement and quench dynamics in quantum spin chains

Pierre Wendenbaum

UNIVERSITÉ DE LORRAINE

Thèse

présentée en vue de l'obtention du titre de

Docteur de l'Université de Lorraine

en Physique

par

Pierre Wendenbaum

Intrication et dynamique de trempe dans les chaînes de spins quantiques

Entanglement and quench dynamics in quantum spin chains

Soutenance publique devant la commission d'examen le 8 décembre 2014

Composition du jury:

Président:	M. Bertrand Berche	Professeur, Université de Lorraine
Rapporteurs:	M. Stéphane Attal	Professeur, Université Claude Bernard, Lyon I
	M. Gunter Schütz	Professeur, Forschungszentrum, Jülich, Allemagne
Examinateurs:	M. Dragi Karevski	Professeur, Université de Lorraine (directeur de thèse)
	M. Thierry Platini	Senior Lecturer, Coventry University, Royaume-Uni
	M. Guillaume Roux	Maître de Conférences, Université Paris-Sud

Institut Jean Lamour - Département de Physique de la Matière et des Matériaux
Université de Lorraine - U.F.R Faculté des Sciences et Technologies - Vandœuvre-lès-Nancy
Secteur Physique Géosciences Chimie Mécanique
École doctorale EMMA

"-Bonjour, dit le Petit Prince.
- Bonjour dit le marchand."
C'était un marchand de pilules perfectionnées qui apaisent la soif. On en avale une par semaine et l'on n'éprouve plus le besoin de boire.
"-Pourquoi vends tu ça ? dit le Petit Prince.
- C'est une grosse économie de temps, dit le marchand. Les experts ont fait des calculs. On épargne cinquante-trois minutes par semaine.
- Et que fait on des cinquante-trois minutes ?
- On en fait ce qu'on veut...
- Moi, dit le Petit Prince, si j'avais cinquante-trois minutes à dépenser, je marcherais tout doucement vers une fontaine..."

Antoine de Saint Exupéry
Le Petit Prince

Remerciements / Acknowledgements

"Un seul mot, usé, mais qui brille comme
une vieille pièce de monnaie: merci !"

Pablo Neruda

Le moment est maintenant venu de s'asseoir et de regarder en arrière vers ces dernières années. En se retournant, on voit un long chemin. Ce long chemin de trois ans que constitue une thèse de doctorat, je ne l'ai, heureusement, pas arpenté seul. Peu importe la suite donnée à cette thèse, les rencontres effectuées ont été source d'un grand enrichissement, tant scientifique qu'humain. Un grand nombre de personnes, scientifiques ou non, a contribué de près ou de loin à la réussite de cette entreprise. Je doute pouvoir nommément lister toutes ces personnes, aussi, que celles qui ne trouvent pas leur nom ci-dessous soient gratifiées de ma reconnaissance.

Je tiens en tout premier lieu à remercier Stéphane Attal et Gunter Schütz d'avoir accepté de prendre un peu de leur temps pour être rapporteurs de ce manuscrit. Merci également à Bertrand Berche d'avoir présidé mon jury, et à Thierry Platini et Guillaume Roux d'avoir accepté d'en faire partie.

Cette thèse s'est déroulée au sein du département de Physique de la Matière et des Matériaux de l'Institut Jean Lamour. Je remercie donc son directeur Michel Vergnat pour son accueil.

Je tiens évidemment à exprimer ma profonde et sincère gratitude à Dragi Karevski, mon directeur de thèse. Merci pour la confiance que tu m'as témoignée, notamment à l'issue de mon stage de master en cherchant un moyen pour que je puisse continuer en thèse avec toi, alors que ce n'était pas ce qui était initialement prévu. Tes connaissances sur les systèmes quantiques hors équilibre, ton expérience de la recherche, ton soutien et la grande autonomie que tu m'as laissée m'ont été précieux et ont été l'un des moteurs de ce travail.
C'est avec un grand plaisir que je remercie chaleureusement tous les membres de l'équipe de physique statistique pour les bons moments que j'ai passés avec chacun d'entre eux, et pour l'environnement scientifique très stimulant qu'ils ont crée. Les pauses autour d'un café ont été des moments de détente appréciables, où j'ai pu en apprendre bien plus sur le fonctionnement en "off" d'institutions comme l'université ou le laboratoire. Ce sera sûrement avec une pointe de nostalgie que je continureai de suivre vos recherches et la vie du groupe. J'ai une pensée toute particulière pour

touts les thésards et thésardes passés et présents de la 106 que j'ai eu le bonheur de côtoyer durant ces trois ans et demi: Mario Collura, Xavier Durang, Sophie Mantelli, Nelson Bolivar, Nicolas Allegra, Dimitris Voliotis, Mariana Krasnytska, Emilio Flores, Sascha Wald et Hugo Tschirhart. Partager son bureau avec des gens venus de contrées lointaines pour certains apporte un certain enrichissement culturel, merci pour cela. Je vous souhaite à tous bonheur et épanouissement dans vos projets et vie futurs.
Je remercie particulièrement Bertand, alors chef du département de physique, pour avoir démêlé une situation bien mal embarquée concernant mon monitorat.
Je remercie également toutes les personnes membres d'autres équipes de l'ijl, ainsi que tous les autres thésards que j'ai pu cotoyer.

I spent a non negligible part of my Ph.D in the Theoretical Quantum Physics Group of the Saarland University. I would like to thank its leader Giovanna Morigi to have welcomed me in the group, and to have proposed me an interesting research subject. Even if the original plan has not been fulfilled, I really appreciated the human and scientific environment of the team. There are two peoples that I would like to thank specially. The first one is Endre Kajari. Thanks for having taken care of me when I arrived in these unknown country and group. Your enthusiasm for my work, your disponibility to answer all my stupid questions and your great pedagogical skills helped me to start my work on the right track. I wish you the best in your new life as a physics teacher. The second person is of course Bruno Taketani. More than a simple collaborator, your became over the months a friend. You implication and your advises, on both scientific and political levels, have been very precious to me. I'm very grateful to you to have shared with me your big knowledge on quantum entanglement and quantum information processing during our "ten minutes meetings", which became most of the time "one hour and a half meetings".
Of course I also acknowledge every people I met during my stay in Saarbrücken, and in particular my two office roommates, Susanne for her help on administrative stuff, and the crazy Irishman Mossy for is daily good mood.

Le dernier projet de ma thèse a été réalisé en collaboration avec Thierry Platini. Je le (re)remercie donc pour son implication dans ce travail, pour sa disponibilité et pour avoir répondu à mes questions concernant les systèmes en interactions répétées. Merci également de m'avoir accueilli lors de mon séjour à Coventry.

J'ai eu la chance d'avoir pu enseigner durant cette thèse. Je remercie donc mes collègues de mécanique du point, Sacha Ourjoumtsev, Xavier Glad et Thierry Reveillé, ce dernier m'ayant particulièrement aidé en répondant à chacune de mes questions concernant l'enseignement. Merci également à Virginie Pichon avec qui j'ai enseigné en PACES durant ma dernière année. Qui dit contrat DCCE dit forcément formations et stages résidentiels... Je remercie donc mes compagnons d'infortune Thomas Drouot, Lucas Eichenberger, Marjorie Etique et Mylène Richard. Ces journées auraient été beaucoup, beaucoup plus longues sans votre présence.

Parce que pour arriver à l'étape "thèse" il faut d'abord passer par l'étape "cinq années de cours à l'université", je remercie tous mes camarades de promotion, en

particulier Guillaume, P-A et Pinpin, avec qui j'ai passé d'agréables moments.

Comme dit plus haut, le bon déroulement d'une thèse réside aussi dans le contact avec des personnes extérieures au monde la recherche universitaire. Je voudrais remercier deux secrétaires dont les compétences ne sont plus à prouver. Merci donc à Martine Gaulier pour son immense gentillesse et à Christine Sartori pour son dynamisme, son implication auprès des doctorants, et pour m'avoir sorti plus d'une fois d'imbroglios comme seule l'administration française sait en créer.
Merci aux gérants de la cafet', Philippe, Marie et leur fille Amélie pour leur bonne humeur quotidienne, pour m'avoir nourri toutes ces années et pour avoir accepté de mettre de la sauce salade dans mes sandwichs.
Je voudrais bien sûr remercier tous mes amis hors université, passés et présents. En particulier, je remercie Émile pour son amitié de presque deux décennies maintenant. Je ne compte plus le nombre de bons souvenirs en ta compagnie. J'ai également une pensée amicale pour Jessica et Jérémy Greco (il tenait au nom!). Merci pour toutes les invitations à Aumetz et pour continuer de jouer à Fifa avec moi malgré toutes tes défaites :).

Je tiens évidemment à remercier mes grands-parents, oncles, tantes et toute ma famille. En particulier ma sœur Sabrina, mon beau-frère Martial et surtout mes parents. Merci à eux pour leur soutien moral et financier [1], et pour m'avoir toujours laissé choisir mon chemin malgré le flou professionnel que peut représenter une thèse en physique théorique.

Ces remerciements ne sauraient être complets sans quelques lignes pour Aurélie. Merci de m'avoir accompagné pendant ces trois ans, cette thèse n'aurait définitivement pas été la même sans toi. Dans les moments difficiles, je savais que, même séparés par la distance, tu étais toujours un peu avec moi quand même. Merci pour ton soutien et tes conseils "d'ancienne thésarde". Ta présence m'aura permis de relativiser les difficultés, et de ne pas oublier l'essentiel. Merci à toi.

1. On oublie souvent de le préciser, mais ne pas avoir à se soucier de trouver de quoi payer son logement ou sa nourriture et un plus indéniable dans la réussite de ses études. Merci pour cela.

Contents

Résumé détaillé (en français)

Le concept d'intrication trouve ses origines dès les premiers temps du développement de la théorie quantique. Schrödinger est le premier à mettre un nom sur ce concept (*"Verschränkung"* en allemand), tandis qu'Einstein, Podolski et Rosen mentionnaient, dans leur célèbre article de 1935 [EPR35], *a spooky action at a distance* que l'on pourrait traduire par une action à distance fantomatique et effrayante. Si ce concept a, d'un point de vue théorique et philosophique, permis une meilleure compréhension des fondements de la mécanique quantique, l'intrication est devenue depuis les années quatre-vingt un ingrédient clé dans le développement de l'information quantique [NC00]. Ce domaine de recherche récent tente de surpasser les limites imposées par les concepts d'information classique. Une des premières applications modernes de l'intrication en tant que ressource technologique est la *"quantum key distribution"*, premier protocole de cryptographie quantique permettant des communications sécurisées. L'intrication quantique est également pressentie pour être d'une grande importance dans le développement d'ordinateurs quantiques, dans lesquels l'information n'est plus stockée dans des bits classiques, mais dans des bits quantiques, ou *"qubits"* [DV95]. Toutes ces nouvelles applications ont besoin d'un solide cadre théorique, c'est pourquoi de nombreux efforts ont été menés pour développer des définitions rigoureuses d'un état intriqué, introduire des critères de séparabilité [HHH96], ou des mesures d'intrication [PV07].
Ces méthodes développées en information quantique ont attiré la curiosité d'autres domaines de la physique, comme la physique de la matière condensée [Pre00, Sch13]. En effet, l'intrication d'un état quantique peut aider à la caractérisation de nouveaux états de la matière avec des corrélations à longue portée, comme les supraconducteurs à haute température [Ver04] ou l'effet Hall quantique [LH08]. L'étude de l'intrication est également un outil puissant dans la détection de transitions de phase quantiques à température nulle. Au point critique, le système présente des corrélations à longue portée à cause de l'intrication de l'état fondamental. Par exemple, les propriétés d'échelle d'états fondamentaux intriqués de systèmes critiques ont été analysées au travers du comportement de l'entropie d'intrication, une mesure utilisée lorsque le système est pur. Il a notamment été montré que l'entropie d'intrication de certaines théories critiques peut être reliée à la charge centrale de la théorie conforme correspondante [CC09, VLRK03, PS05]. Le concept de spectre d'intrication a été également introduit comme un outil puissant dans l'étude des phénomènes critiques. L'analyse du spectre de la matrice densité réduite d'une bipartition d'un système quantique et du gap de Schmidt (la différence entre les deux valeurs propres les plus élevées) a, par exemple, parfaitement décrit le comportement du paramètre d'ordre dans la région critique [DCLLS12].
Si tous ces travaux traitent de l'intrication de l'état fondamental, on peut se poser

la question quant au comportement de l'intrication dans des systèmes hors de l'équilibre. En effet, grâce aux nombreux progrès expérimentaux ces dernières années, la physique des systèmes hors de l'équilibre a connu un regain d'intérêt, spécialement dans des domaines comme la matière condensée, ou l'optique quantique. Malgré ces progrès expérimentaux, une théorie générale décrivant les systèmes quantiques hors équilibre est toujours manquante. La compréhension du comportement de ce genre de système est donc d'une grande importance dans la physique théorique moderne.

Les travaux exposés dans ce manuscrit sont consacrés à l'étude du comportement hors de l'équilibre de systèmes quantiques, et plus particulièrement de leurs propriétés d'intrication. Plusieurs protocoles peuvent être mis en œuvre pour amener un système hors de l'équilibre. On peut par exemple réaliser une trempe quantique [CG07, PSSV11] en variant plus ou moins rapidement un paramètre de contrôle dans l'hamiltonien. Le couplage d'un système à un environnement mène également à de très intéressantes dynamiques et propriétés d'intrication.
La chaîne de spins quantique constitue un très bon candidat pour cette étude. En effet, l'avantage de ce type de modèle réside dans sa faible dimensionnalité, nous autorisant la plupart du temps le développement de méthodes analytiques et numériques permettant de déduire leur principales propriétés [LSM61, BMD70, BM71a, BM71b, MBA71].

Cette thèse est divisée en cinq chapitres. Le **chapitre 1** est consacré à la présentation du cadre théorique et mathématique de cette thèse. On se consacre dans un premier temps à la description du phénomène d'intrication quantique. Un état quantique pur $|\Psi\rangle$ dans un espace de Hilbert composite $\mathcal{H} = \mathcal{H}_1 \otimes \mathcal{H}_2 \otimes \cdots \otimes \mathcal{H}_N$ est dit *séparable* s'il peut s'écrire sous la forme

$$|\Psi\rangle = |\phi_1\rangle \otimes |\phi_2\rangle \otimes \ldots |\phi_N\rangle, \tag{1}$$

où $|\phi_i\rangle \in \mathcal{H}_i$. S'il ne peut pas s'écrire sous la forme précédente, cet état est dit *intriqué*. Dans la suite de ce travail, nous nous limiterons au cas $N = 2$, et nous parlerons donc d'*intrication bipartite*. Si l'on considère deux spins 1/2, un état pur intriqué bien connu est par exemple l'un des états de Bell $|\Psi\rangle = \frac{1}{\sqrt{2}}(|\uparrow\downarrow\rangle + |\downarrow\uparrow\rangle)$, où l'état $|\uparrow\rangle$ (resp. $|\downarrow\rangle$) est état propre de l'opérateur σ^z avec la valeur propre 1 (resp. -1). Cet état possède une propriété intéressante lorsque l'on effectue une mesure sur l'un des deux spins, par exemple une mesure de sa polarisation. En effet, dû au principe de réduction du paquet d'onde, si on trouve que l'état du premier spin est $|\uparrow\rangle$ (resp. $|\downarrow\rangle$), cela veut dire que le deuxième spin a été instantanément projeté dans l'état $|\downarrow\rangle$ (resp. $|\uparrow\rangle$) bien qu'aucune mesure n'ait été effectuée sur ce spin.
Lorsque l'état considéré est un mélange statistique (cas des états thermiques par exemple), il ne peut être représenté par un vecteur de l'espace de Hilbert, et l'on doit faire appel au formalisme de la matrice densité. La notion d'intrication est alors généralisée de la manière suivante: un état ρ est dit séparable s'il peut s'écrire comme

$$\rho = \sum_i p_i \rho_i^A \otimes \rho_i^B, \quad \text{avec } \sum_i p_i = 1,\ p_i \geq 0\ \forall i, \tag{2}$$

et est intriqué autrement. Ici, ρ_i^A et ρ_i^B sont des matrices densité réduites associées aux

partitions A et B. Nous introduisons ensuite la notion de critère de séparabilité, qui nous permet de connaître le caractère intriqué ou non d'un état. Si cet état est pur, un de ces critères est basé sur la décomposition de Schmidt [Scho6, EK95]. Si un seul coefficient apparaît dans cette décomposition, alors l'état considéré est séparable. Pour un mélange statistique, l'un des critères les plus fréquemment utilisé est le critère PPT [Per96], pour *positive partial transpose* (transposée partielle positive en français). Si l'on obtient un spectre positif après avoir effectué la transposée partielle de la matrice de densité, alors l'état est séparable. Dans la pratique, la seule connaissance de l'intrication ou non d'un état quantique est souvent insuffisante. En effet, ces critères ne nous donnent pas accès à la quantité d'intrication présente, et il est alors judicieux de définir une mesure d'intrication [PV07]. Une mesure d'intrication est une application de la matrice densité vers un nombre réel qui nous indique si l'état est plus ou moins intriqué. Dans ce travail, nous avons utilisé deux mesures différentes. La première de ces mesures est l'entropie d'intrication, utile quand l'état est pur. Elle est définie comme l'entropie de von Neumann de la matrice densité réduite d'une des deux partitions

$$E\left(|\psi\rangle\right) = \mathcal{S}(\rho_A) = -\operatorname{Tr}\{\rho_A \ln \rho_A\} = \mathcal{S}(\rho_B). \tag{3}$$

Cette mesure étant incapable de discerner les corrélations classiques des corrélations quantiques dans le cas d'un mélange statistique, nous introduisons également *l'intrication de formation* [HW97, Woo98, Wooo1, PV07], définie comme l'intrication moyenne minimum sur toutes les décompositions possibles de l'état sur une base d'états purs:

$$E_f(\rho) = \min_{\{|\psi_i\rangle\}} \sum_i p_i E(|\psi_i\rangle). \tag{4}$$

Dans la pratique, cette minimisation est très difficile, mais il a cependant été montré que dans le cas où le système considéré est constitué de deux spins $1/2$ (ce qui sera majoritairement notre cas dans la suite), l'intrication de formation peut s'écrire en fonction d'un nombre $C \in [0:1]$, appelé *la concurrence*, et défini comme

$$C(\rho) = \max\{0, \lambda_1 - \lambda_2 - \lambda_3 - \lambda_4\}. \tag{5}$$

Ici, les λ_i sont les valeurs propres en ordre décroissant de la matrice $R = \sqrt{\sqrt{\rho}\tilde{\rho}\sqrt{\rho}}$ où $\tilde{\rho}$ est définie par $\tilde{\rho} = (\sigma^y \otimes \sigma^y)\rho^*(\sigma^y \otimes \sigma^y)$. L'intrication de formation étant une fonction monotone croissante de C, la concurrence peut être utilisée comme mesure en elle-même. Plus ce nombre est grand, plus les deux spins sont intriqués.

Après cette brève présentation de l'intrication quantique, nous nous focalisons sur les deux modèles utilisés, le modèle XY et le modèle de Bose-Hubbard. Le premier de ces modèles décrit une assemblée de spins en interaction. Son hamiltonien est

$$H^{XY} = -\frac{J}{2}\sum_n \left(\frac{1+\kappa}{2}\sigma_n^x\sigma_{n+1}^x + \frac{1-\kappa}{2}\sigma_n^y\sigma_{n+1}^y\right) - \frac{h}{2}\sum_n \sigma_i^z, \tag{6}$$

où les σ_n^α sont les matrices de Pauli dans la direction α ($\alpha = x, y, z$) associées au site n, h est un champ magnétique transverse, J est le couplage entre deux spins premiers voisins, et κ est un paramètre d'anisotropie. Le cas isotrope ($\kappa = 0$) correspond au modèle XX, tandis que la limite anisotrope ($\kappa = 1$) correspond au modèle d'Ising. Cet hamiltonien prend une forme fermionique quadratique après introduction de la

transformation de Jordan-Wigner qui associe aux opérateurs de montée et descente de spin des opérateurs de Clifford

$$\Gamma_n^1 = \prod_{i=1}^{n-1} (-\sigma_i^z)\, \sigma_n^x, \quad \Gamma_n^2 = \prod_{i=1}^{n-1} (-\sigma_i^z)\, \sigma_n^y, \tag{7}$$

et il devient

$$H = \frac{1}{4} \mathbf{\Gamma}^\dagger \boldsymbol{T} \mathbf{\Gamma}, \tag{8}$$

où $\boldsymbol{T}$ est la matrice hamiltonienne et $\mathbf{\Gamma}$ un vecteur contenant les opérateurs de Clifford. L'introduction des opérateurs fermioniques diagonaux η_q et $\eta_q^\dagger$, reliés aux opérateur de Clifford par une transformation de Bogoliubov permet l'écriture de l'hamiltonien sous une forme diagonale

$$H = \sum_q \varepsilon_q \left(\eta_q^\dagger \eta_q - \frac{1}{2} \right), \tag{9}$$

où ε_q est l'énergie de l'excitation fermionique q. L'analyse de ε_q nous permet d'avoir accès au diagramme de phase du modèle XY [Karo6] qui est discuté dans la section 1.3.2.

Après cela, nous nous intéressons à la dynamique des opérateurs de Clifford dans la représentation de Heisenberg, qui s'écrit

$$\mathbf{\Gamma}(t) = \boldsymbol{R}(t) \mathbf{\Gamma}(0), \tag{10}$$

avec $\boldsymbol{R}(t) = e^{-it\boldsymbol{T}}$, et nous dérivons une formule pour l'entropie d'intrication d'une partition A d'un système dans le cas du modèle XX. Nous rappelons qu'elle peut être reliée aux valeurs propres ξ_q de la matrice de corrélation, $C_A = \langle c_i^\dagger c_j \rangle$ où les indices i et j sont restreints au sous-espace A.

Finalement, le deuxième modèle que nous avons considéré est le modèle de Bose-Hubbard. Ce modèle décrit de façon simple la dynamique de bosons sur un réseau unidimensionnel. Son hamiltonien est ici

$$H_{BH} = -t \sum_i \left(b_i^\dagger b_{i+1} + b_i b_{i+1}^\dagger \right) - \mu \sum_i n_i + \frac{U}{2} \sum_i n_i (n_i - 1), \tag{11}$$

ou les b_i et $b_i^\dagger$ sont des opérateurs bosoniques, et $n_i = b_i^\dagger b_i$ est un opérateur de densité locale. Le premier terme de l'hamiltonien est un terme cinétique décrivant le saut d'un boson sur le site voisin. Le deuxième terme est proportionnel au potentiel chimique qui fixe le nombre de bosons du système, et le dernier terme est un terme d'interaction locale entre bosons sur le même site. Cette interaction est répulsive pour $U > 0$ et attractive si $U < 0$. L'hamiltonien devient soluble dans les deux limites de paramètres $t/U \to 0$ et $t/U \to \infty$. Dans la limite où $t \to 0$, le terme d'interaction domine et le système est caractérisé par une densité n_0 constante sur tous les sites, fixée par la minimisation de l'énergie. L'état fondamental est dit *état de Mott* et est donné par le produit tensoriel

$$|\Psi\rangle = \prod_i (b_i^\dagger)^{n_0} |0\rangle, \tag{12}$$

où $|0\rangle$ est l'état vide de boson. Dans la limite opposée, le terme cinétique est dominant, et le système est dans une *phase superfluide* où les bosons sont délocalisés sur tout le réseau. L'état fondamental est dans ce cas donné par

$$|\Psi\rangle = \left(\sum_i b_i^\dagger\right)^N |0\rangle. \tag{13}$$

Le diagramme de phase de ce modèle est présenté sur la figure 1.2.

Les quatre chapitres suivants contiennent les principaux résultats de la thèse. Le **chapitre** 2 est consacré à l'étude de la dynamique de trempe d'une condensat de bosons initialement piégé sur un réseau optique unidimensionnel par un potentiel de confinement harmonique. Le condensat de particules est initialement piégé entre les positions $x = A < 0$ et $x = 0$. En fonction de la valeur du paramètre de contrôle du potentiel, nous avons travaillé avec deux types d'états initiaux. Dans le premier cas, tout le condensat est dans une phase superfluide, avec une variation spatiale de la densité. Dans le deuxième cas, deux phases superfluides entourent une phase de Mott, centrée en $x = A/2$, où la densité locale reste constante et égale à un.
Dans la limite d'une répulsion infinie entre bosons sur un même site (limite bosons de cœur dur), nous avons développé une théorie hydrodynamique qui reproduit parfaitement le comportement des bosons. Cette théorie repose essentiellement sur une hypothèse d'équilibre local avec le potentiel. Dans le cadre de cette théorie, les particules sont émises vers la gauche et vers la droite le long de trajectoires d'énergie $\varepsilon_q = V(x) - \cos(q)$ constante. Les densités de particules dans l'espace des phases (x, q) se déplaçant vers la gauche (*left movers*, signe $-$) et vers la droite (*right movers*, signe $+$) sont données par

$$\rho^\pm(x, q, t) = \frac{1}{2}\int\int dx_0 dq_0 \rho_0(x_0, q_0)\delta(x - x^\pm(x_0, q_0, t))\delta(q - q^\pm(x_0, q_0, t)), \tag{14}$$

et la densité totale par $\rho(x, q, t) = \rho^+(x, q, t) + \rho^-(x, q, t)$. Dans l'expression précedente, $x^\pm(x_0, q_0, t)$ et $q^\pm(x_0, q_0, t)$ sont les équations d'évolution d'une particule initialement située en (x_0, q_0).
Nous avons considéré deux types de trempe différents. Le premier consiste à soudainement supprimer le potentiel de confinement. Après la trempe, l'équation d'évolution d'une particule initialement en (x_0, q_0) est celle d'une particule libre $x^\pm(x_0, q_0) = x_0 \pm v_{q_0} t$ où v_{q_0} est la vitesse de la particule ne dépendant que de son énergie initiale. Comme le potentiel est nul, les particules sont libres d'aller explorer tout l'espace, et le condensat s'étale vers la droite et la gauche jusqu'à ce que les particules atteignent les deux bords du système. Les prédictions données par la théorie hydrodynamique permettent de parfaitement décrire l'évolution temporelle du profil de densité, ainsi que l'évolution du nombre de particules présentes dans la région initiale du piège.
Le second protocole de trempe considéré consiste au passage d'un potentiel harmonique à un potentiel linéaire d'équation $V(x) = -Fx\ \Theta(-x)$ où la fonction de Heaviside assure que le potentiel n'est différent de zéro que dans la partie négative de l'axe. Le condensat présente un comportement plus riche que dans le cas précédent. En effet, on observe dans ce cas une séparation du condensat en deux

parties: les particules d'énergie initiale comprise entre -1 et 1 quittent la rampe et se propagent vers la droite de l'axe, tandis que les autres restent piégées par le potentiel en effectuant des oscillations de Bloch. En fonction de l'état initial et de la force F, plusieurs régimes d'oscillations sont observés:

- Pour un état initial complètement superfluide, toutes les particules quittent la rampe pour une force $F < F_{esc}^{Sf}$, où F_{esc}^{Sf} est la force telle que le point le plus énergétique du condensat initial soit égale à 1. Pour des valeurs de forces intermédiaires, on observe un régime d'oscillations où le condensat piégé se sépare en deux parties, une partie correspondant aux left movers, qui commencent leur mouvement vers la gauche, et une partie correspondant aux right movers, qui commencent leur mouvement vers la droite. Pour des forces élevées, tout le condensat commence son mouvement dans la même direction, et il oscille comme un tout.

- Lorsque l'état initial est un mélange Mott/superfluide, la seule force qui permet à toutes les particules de s'échapper du piège est $F = 0$. On observe pour cet état initial des oscillations de part et d'autre d'un plateau où la densité reste constante au cours du temps, et égale à sa valeur initiale. Trois régimes d'oscillations différents sont observés: Pour des faibles valeurs de force, les deux côtés oscillants du plateau commencent leurs oscillations dans des directions opposées (vers la gauche sur le côté gauche, et vers la droite sur le côté droit), menant à un *breathing regime*. Pour des valeurs de force intermédiaires, le côté gauche du plateau se sépare en deux parties, correspondant aux left et right movers, oscillant en sens contraire, alors que le mouvement du côté droit est inchangé. Finalement, pour des valeurs de force importantes, les deux côtés du condensat oscillent en phase, c'est à dire dans la même direction à un instant donné.

Un diagramme de phase décrivant les différents régimes d'oscillations est présenté figure 2.13. Finalement, on mentionne que nous avons également étudié la densité de particules s'échappant du piège, le courant de particules, ainsi que l'évolution temporelle de l'entropie d'intrication entre les particules piégées et celles s'échappant du piège.

Les trois chapitre suivant sont consacrés à l'étude de systèmes quantiques ouverts sur un environnement (ou bain). Dans le **chapitre 3**, nous focalisons notre attention sur la dynamique de deux spins "défauts", localement couplés de manière symétrique à un environnement modélisé par une chaîne de $2N$ spins avec interaction d'Ising, et dans un état thermique. Les deux défauts sont initialement préparés dans un état séparable (c'est à dire désintriqués), et l'on se pose la question de savoir si de l'intrication peut être créée entre ces deux spins par l'intermédiaire du couplage à un environnement commun. Dans la suite, la chaîne de spins a été transformée en une chaîne de bosons en interactions par la transformation d'Holstein-Primakoff. Nous avons choisi de travailler dans la limite où le champ magnétique transverse du bain est très supérieur au couplage intra-chaîne, rendant tous les spins de l'environnement presque parfaitement polarisés dans la direction du champ, et de plus, la tempéra-

ture de l'environnement est supposée très faible. Ces approximations nous amènent finalement à une chaîne d'Ising transformée en une assemblée d'oscillateurs harmoniques en interaction.
La symétrie d'échange des bosons $-n$ et n dans la chaîne nous pousse à l'introduction de nouvelles coordonnées pour la description du bain: les coordonnées de centre de masse (symétriques) et les coordonnées relatives (antisymétriques). L'introduction de ces nouvelles variables a pour effet de découpler la chaîne de taille $2N$ en deux chaînes de N oscillateurs contenant respectivement les coordonnées symétriques et antisymétriques. De la même manière, nous introduisons une base d'états non locaux symétriques et antisymétriques pour la description des deux spins défauts. Cette nouvelle base mène à nouveau à un découplage: les états symétriques ne sont couplés qu'au bain composé des variables symétriques, et de même pour les états antisymétriques. Ce découplage est brisé par l'introduction de l'hamiltonien Zeeman des deux défauts. En effet, cet hamiltonien, une fois écrit dans la nouvelle base, couple les sous-espaces symétrique et antisymétrique, et il devient donc impossible d'écrire l'opérateur d'évolution total comme un produit de deux opérateurs agissant dans les espaces symétrique et antisymétrique respectivement. Pour pouvoir écrire l'opérateur d'évolution de cette manière (et donc découpler la dynamique), nous avons fait appel à l'approximation suivante: la dynamique est analysée pour des temps très inférieurs au temps caractéristique microscopique des défauts donné par l'inverse de leur gap en énergie. Dans ce régime temporel, l'hamiltonien Zeeman n'influence pas la dynamique des défauts, et il peut être en conséquence négligé dans l'hamiltonien total. Dans la pratique, nous avons considéré des spins défauts dégénérés (c'est à dire que nous avons posé le champ transverse des défauts égal à zéro), ce qui nous autorise à étudier la dynamique pour des temps arbitrairement longs.
Grâce à l'approximation précédente, nous avons pu établir l'évolution temporelle des éléments de la matrice densité réduite des spins défauts (équation (3.52)), ce qui nous a permis de suivre l'évolution temporelle de la concurrence. Nous avons dans un premier temps analysé le cas de deux défauts couplés à la même position dans la chaîne, puis le cas de deux spins défauts couplés à deux endroits différents. Dans les deux cas, nous avons observé une création d'intrication entre les deux spins défauts. La concurrence associée oscille au cours du temps, avec des oscillations dépendant fortement des paramètres du système. La différence principale entre les deux cas précédemment mentionnés est que lorsque les spins sont couplés au même endroit, l'intrication est créée instantanément alors qu'un temps d'établissement est nécessaire lorsqu'ils sont séparés par une distance non nulle. Ce temps d'établissement d'intrication croît exponentiellement avec la distance entre les spins défauts. La période d'oscillation augmente lorsque les couplages intra-chaîne et défauts-chaîne sont augmentés, et le maximum atteint par la concurrence ne dépend lui que du couplage entre le défauts et la chaîne, ainsi que de l'état initial des défauts. En effet, l'intrication est créée pour tous les état initiaux, sauf lorsque l'un ou les deux défauts sont préparés initialement dans un état propre de l'hamiltonien d'interaction.

Dans le **chapitre 4**, nous étudions un modèle similaire au modèle étudié dans le chapitre précédent, à savoir deux spins défauts localement couplés aux positions 0 et d d'une chaîne d'Ising en champ transverse avec des conditions de bord péri-

odiques. La différence vient du fait que les défauts sont ici initialement préparés dans un état de Bell, c'est à dire que l'intrication est maximum. De plus, le champ transverse de l'environnement est soudainement trempé d'une valeur initiale h_i à une valeur finale h_f, le forçant à évoluer dans un régime hors de l'équilibre. Le but est ici d'étudier l'influence de la trempe de l'environnement sur l'intrication initiale des défauts par rapport à la situation d'équilibre (c'est à dire lorsqu'aucune trempe n'est effectuée) déjà traitée dans la littérature [CPo8b]. La concurrence s'exprime dans ce cas de manière très simple en fonction de l'écho de Loschmidt $\mathcal{L}(t)$, qui est lui même relié à l'évolution temporelle de la matrice de corrélation fermionique initiale des deux défauts. Cette évolution temporelle a été étudiée numériquement par diagonalisation exacte.
Nous nous sommes dans un premier temps penchés sur l'influence de la valeur du couplage ε entre les défauts et l'environnement. Nous avons identifié deux régimes différents, correspondant à un couplage faible et à un couplage fort. Dans le régime de couplage faible l'écho décroit lentement et de manière monotone. Lorsque le couplage est augmenté, la décroissance de l'écho est plus rapide et, pour de fortes valeurs de ε, l'écho développe des oscillations dont la fréquence est fonction de la valeur du couplage. Ces oscillations sont contenues dans une enveloppe indépendante de ε.
Nous avons ensuite étudié plus attentivement l'effet de la trempe sur les propriétés de désintrication. Il apparaît que la trempe est toujours néfaste du point de vue de la cohérence du système, dans le sens où elle accélère toujours la désintrication.
Nous avons également mis en évidence que l'écho reflète les propriétés critiques de l'environnement. En effet, la dérivé de l'écho par rapport au champ initial à un temps fixé présente une anomalie lorsque le champ initial est proche de la valeur $h_i = 1$. Le système étant de taille fini dans nos simulations numériques, l'anomalie observée est un pic et non une divergence totale de la dérivée. Une analyse d'effets de taille finie nous a permis de trouver la loi gouvernant la position du pic ainsi que sa valeur maximale en fonction de la taille de l'environnement:

$$|h_c - h_{max}| \sim N^{\gamma}, \quad d_h \mathcal{L}|_{h_{max}} \sim \ln N, \tag{15}$$

où γ est un exposant qui peut être relié à l'exposant critique de la longueur de corrélation ν de la classe d'universalité du modèle d'Ising ($\nu = 1$).
Nous avons ensuite considéré la dynamique aux temps courts. Dans ce régime temporel, la décroissance de l'écho est gaussienne $\mathcal{L}(t) \sim \exp(-\alpha t^2)$, et on trouve finalement:

$$\mathcal{L}(t) = 1 - t^2 \left[\langle \widetilde{H}_I^2 \rangle - \langle \widetilde{H}_I \rangle^2 \right] + \mathcal{O}(t^3), \tag{16}$$

où $\langle \widetilde{H}_I \rangle$ est la valeur moyenne de l'hamiltonien d'interaction dans l'état initial de l'environnement. Il apparaît donc que la trempe n'influence pas le début de l'évolution de l'écho, puisque c'est la variance de l'hamiltonien d'interaction dans l'état intial qui gouverne la dynamique de l'echo aux temps courts. En terme de fonction de corrélation spin-spin, le paramètre gaussien α est donné par

$$\alpha = 2\varepsilon^2 \left(1 + \langle \sigma_0^z \sigma_d^z \rangle_c - \langle \sigma_0^z \rangle^2 \right). \tag{17}$$

Loin du point critique, ce paramètre sature lorsque la distance devient grande. Au contraire, lorsque le champ transverse de l'environnement est proche du point critique $h_i = 1$, cette saturation n'existe pas. En effet, le corrélateur connecté $\langle \sigma_0^z \sigma_d^z \rangle_c$

décroit exponentiellement hors du point critique, menant à la saturation à grandes distances, alors que la décroissance est algébrique au point critique.
La taille finie de l'environnement dans nos simulations numériques induit un changement significatif de l'écho pour des temps de l'ordre de N. Ce phénomène de *revival* est dû au transport des quasi-particules le long de la chaîne. Une des différences majeures par rapport à la situation d'équilibre réside dans le fait que ce *revival* apparaît à des temps deux fois plus courts que lorsque l'environnement n'est pas trempé. En effet, dans le cas de la trempe globale considérée ici, tous les sites de la chaîne sont émetteurs d'excitations, ces dernières n'ont donc besoin de parcourir que la moitié de la chaîne pour reconstruire l'état initial. Au contraire, dans la situation d'équilibre, ces excitations ne sont émises qu'aux positions où les défauts sont couplés. Il leur est donc nécessaire de parcourir la chaîne entière afin de reconstruire la cohérence initiale.
Enfin, la dernière partie de cette étude tente d'identifier la part de la désintrication venant directement du couplage avec l'environnement, et celle venant de l'interaction mutuelle des deux défauts au travers de la chaîne. Pour cela, nous avons étudié la différence entre l'écho dans la situation où les défauts sont couplés à un environnement commun et l'écho dans la situation limite où les deux défauts sont couplés à des environnements différents. Lorsque le champ magnétique initial est loin de la valeur critique, l'évolution de l'écho est la même dans les deux situations jusqu'à ce que les spins soient corrélés par l'intermédiaire des quasi-particules parcourant l'environnement. Au contraire, pour une chaîne critique, la différence entre les échos est non nulle à $t = 0^+$, reflétant la corrélation initiale des deux défauts au travers de la longueur de corrélation critique.

Finalement, le **chapitre 5**, dernier chapitre de cette thèse, est consacré à la dynamique d'un système quantique couplé à un environnement décrit par un processus d'interactions répétées [AP06, AJ07, AD10]. L'environnement joue le rôle de réservoir d'intrication, et nous étudions le transfert de cette intrication au système considéré. Nous commençons ce chapitre par une introduction détaillée du processus d'interactions répétées. L'environnement est, dans ce contexte, modélisé par une assemblée de "copies" identiques et indépendantes et l'interaction avec le système se fait de manière répétée, c'est à dire que le système interagit avec toutes les copies, l'une après les autres, pendant un temps caractéristique τ. Notons que cela est équivalent à rafraîchir l'état initial de l'environnement après chaque temps $t = n\tau$. Si l'on ne s'intéresse qu'à l'évolution temporelle du système, on peut montrer que sa matrice densité réduite après la nième interaction est donnée par

$$\rho_s(n\tau) = Tr_n \left\{ U_i^{(n)} \left[\rho_s((n-1)\tau) \otimes \rho_n^b \right] U_i^{(n)\dagger} \right\}, \tag{18}$$

où $U_i^{(n)}$ est l'opérateur d'évolution couplant le système à la nième copie de l'environnement. Dans la limite continue où le temps d'interaction τ tend vers zéro, ρ_s obéit à l'équation de Lindblad

$$\partial_t \rho_s(t) = \mathcal{L}\{\rho_s\}, \tag{19}$$

avec

$$\mathcal{L}\{X\} = -i[H_s, X] - \frac{1}{2} \sum_i \left(\left\{ L_i L_i^\dagger, X \right\} - 2 L_i X L_i^\dagger \right). \tag{20}$$

Lorsque les hamiltoniens considérés peuvent s'écrire sous une forme quadratique d'opérateurs fermioniques, et que l'état initial total est Gaussien, il est possible de montrer que l'évolution temporelle préserve le caractère gaussien de l'état [Peso3]. Il s'en suit donc, d'après le théorème de Wick, que toutes les observables décrivant le système peuvent s'écrire en fonction des corrélateurs fermioniques à deux points. Dans la limite continue, la matrice de corrélation fermionique évolue selon l'équation

$$\partial_t G^S = -i[T_S, G^S] - \frac{1}{2}\left(\left\{G^S, \Theta\Theta^\dagger\right\} - 2\Theta G^B \Theta^\dagger\right) \tag{21}$$

où G^S et G^B sont les matrices de corrélation restreintes au système et à une copie du bain respectivement, et Θ est une matrice contenant le couplage système-bain.
Dans le reste de cette étude, les copies constituant le bain sont supposées être formées d'une paire de spins 1/2, non couplés entre eux, et préparés dans un état de Bell maximalement intriqué. Nous avons dans un premier temps étudié un modèle trivial, pour lequel la dynamique a pu être déterminée analytiquement. Il consiste en deux spins 1/2, chacun de ces spins étant couplé à un des constituants de la paire de Bell formant une copie de l'environnement (voir la figure 5.2 pour une représentation du modèle). Ces deux spins sont préparés dans un état thermique séparable paramétré par leur aimantation. Afin d'évaluer la concurrence dans le système, la matrice densité réduite est reconstruite à l'aide des fonctions de corrélation spin-spin, elles mêmes déterminées grâce à l'évolution temporelle de la matrice de corrélation fermionique. Nous trouvons que la concurrence évolue en suivant

$$\begin{aligned}\mathcal{C}(t) = \max\Bigg\{0, 1 - e^{-\gamma^2 t} - \frac{1}{2}\Bigg(\left[2e^{-\gamma^2 t} + (m_1^0 m_4^0 - 1)e^{-2\gamma^2 t}\right]^2, \\ -(m_1^0 + m_4^0)^2 e^{-2\gamma^2 t}\Bigg)^{1/2}\Bigg\}.\end{aligned} \tag{22}$$

où m_1^0 and m_4^0 sont les aimantations initiales des spins 1 et 4 respctivement. Dans l'état stationnaire, la concurrence atteint la valeur $\mathcal{C}_{14}(t \to \infty) = 1$, indiquant une intrication maximale entre les spins du système, bien qu'ils n'aient jamais interagi directement.
Après ce modèle trivial, nous avons considéré un système plus compliqué, où les deux spins sont remplacés par deux chaînes identiques de spins avec interactions de type XX. Chacune des chaînes est couplée sur un bord à un des spins constituant la paire de Bell (voir figure 5.7). Nous avons étudié la dynamique du système sur deux régimes temporels différents: un régime de temps courts par rapport à la longueur des chaînes $1 < t \ll N$, et un régime de temps longs $t \gg N$. La vitesse des excitations étant normalisée à $v = 1$, le temps $t = N$ correspond au temps nécessaire à la première excitation injectée pour atteindre le bord opposé du point d'interaction avec l'environnement. L'étude du premier de ces régimes nous renseigne sur le comportement d'un système semi-infini. Dans ce cas, le système atteint un état stationnaire hors équilibre, ou NESS (pour *non-equilibrium-steady-state* en anglais) caractérisé par un courant stationnaire traversant les deux chaînes. On étudie ce NESS au travers du comportement d'observables telles que l'aimantation locale et le courant. On s'intéresse également à deux types d'intrication: l'intrication longitudinale, mesurée entre deux spins consécutifs dans une chaîne, et la concurrence croisée, mesurée

entre un spin de la première chaîne et son équivalent dans la deuxième (voir les doubles flèches de la figure 5.7). En particulier, nous avons mis en évidence le comportement d'echelle de l'aimantation, du courant et de la concurrence longitudinale. La concurrence croisée, quant à elle, décroit exponentiellement avec la distance au point d'interaction de la paire de spins p considérée, $\mathcal{C}^{(p)} \sim \exp\left(-p/\xi_{ent}\right)$. On peut extraire de cette décroissance une longueur d'intrication typique ξ_{ent}, qui semble se comporter proportionnellement à l'inverse du courant stationnaire s'établissant dans les chaînes.
Finalement, pour des temps $t \gg N$, le système atteint un état stationnaire d'équilibre où le courant s'annule. Cet état est caractérisé par un produit d'états de Bell sur les spins se faisant face dans les deux chaînes, décrivant une intrication croisée maximale. On peut finalement noter que cet état stationnaire d'équilibre est indépendant de l'état initial du système.

Enfin, trois appendices viennent conclure ce manuscrit.
Dans **l'appendice A**, nous présentons en détail l'établissement de la formule d'évolution temporelle des éléments de la matrice densité réduite utilisée dans le chapitre 3.
Nous montrons dans **l'appendice B** que la matrice densité associée à chacune des paires de Bell peut s'écrire comme la limite basse température d'une matrice de densité thermale.
Enfin, dans **l'appendice C**, nous déduisons la fonction de corrélation spin-spin stationnaire entre spins se faisant face dans le cadre des interactions répétées.

Deux articles scientifiques directement en lien avec cette thèse ont été publiés, et deux autres sont actuellement en préparation:

- *Hydrodynamic description of Hard-core Bosons on a Galileo ramp*
  P. Wendenbaum, M. Collura and D. Karevski
  Physical Review A **87** 023624 (2013).

- *Decoherence of Bell states by local interactions with a suddenly quenched spin environment*
  P. Wendenbaum, B.G. Taketani and D. Karevski
  Physical Review A **90** 022125 (2014).

- *Entanglement creation between two spins embedded in a single spin chain*
  P. Wendenbaum, B.G. Taketani, E. Kajari, G. Morigi and D. Karevski
  En préparation.

- *Entanglement replication via quantum repeated interactions*
  P. Wendenbaum, T. Platini and D. Karevski
  En préparation.

General introduction

The concept of entanglement takes its origin in the early times of the development of quantum theory. Schrödinger is the first one to give it its name (*"Verschränkung"* in German), whereas, in their famous article of 1935 [EPR35], Einstein, Podolsy and Rosen mentioned it as a *"spooky action at a distance"*. If it has, from a purely theoretical and philosophical point of view, allowed a better understanding of the foundations of quantum mechanics, quantum entanglement became, since the eighties, a technological key ingredient with the development of quantum information processing [NC00]. This recent field of research tries to surpass the limits imposed by the concepts of classical information using quantum physics. One of the first concrete modern application of entanglement used as a resource is the quantum key distribution [BB84], first protocol of quantum cryptography, allowing secure communications. Quantum entanglement is also supposed to be of primary importance for the building of quantum computers, where information is no longer stored into classical bits, but into quantum bits, or "qubits" [DV95]. All these applications need a strong theoretical background, that's why a lots of efforts have been made to develop rigorous definitions of an entangled state, and introduce separability criteria [HHH96] or entanglement measures [PV07].
These methods developed in quantum information processing have attracted the curiosity of other areas of physics like condensed matter theory [Pre00, Sch13]. Indeed, the entanglement present in a quantum many-body state can help to the characterization of new states of matter with strong long-range correlations, like superconductivity [Ver04] or quantum Hall effect [LH08]. The study of entanglement is also a very powerful tool for the detection of quantum phase transitions at zero temperature. At the quantum critical point, the system exhibits long-range correlations due to the entanglement present in the many-body ground state. For example, scaling properties of ground state entanglement of quantum many-body critical systems have been analyzed through the scaling of entanglement entropy [VLRK03], an entanglement measure used when the state of the system is pure. For example, the entanglement entropy of certain critical theories can be related to the central charge of the corresponding conformal field theory [CC09, VLRK03, PS05]. The concept of entanglement spectrum has also been introduced as a powerful tool for the study of critical phenomena. The analyze of the spectrum of the reduced density matrix of a bipartition of a quantum system, together with the Schmidt gap (the difference between the two largest eigenvalues) has, for instance, perfectly reproduced the critical scaling behavior of order parameter close to criticality [DCLLS12].
If all these works deal with ground state entanglement, one may ask the question of entanglement behavior of system out of equilibrium. Indeed, thanks to experimental progresses during the few past decades, the physics of non equilibrium systems knows an impulse of interest, especially in the area of condensed matter physics

and quantum optics. Despite these experimental progresses, there is still a lack of a good general theoretical framework for the description of non-equilibrium quantum phenomena. Understanding the behavior of such phenomena is then one of the most challenging issues of modern theoretical physics.

The work presented in this thesis is devoted to the study of the non equilibrium behavior of one-dimensional strongly interacting quantum systems, with a special focus on their entanglement dynamics. Several protocols can drive the system under consideration into an out of equilibrium regime. For example, on can more or less suddenly vary one control parameter of the Hamiltonian, realizing the so-called quantum quench [CG07, PSSV11, MDDS07, RSMS09, CEF12a, CEF12b, Rou09, BRK11]. The coupling of the system to a biggest environment leads also to very interesting dynamics [KPS13, PKS13] and entanglement properties.
The quantum spin chains are a very good candidate for this study. Indeed, the big advantage of such models is their low dimensionality, allowing most of the time the development of analytical or numerical methods to extract their main properties [LSM61, BMD70, BM71a, BM71b, MBA71].

This thesis is divided in five chapters. The first one is devoted to the introduction of the theoretical and mathematical framework of the work. We give a general description of the concept of entanglement, and we turn to the presentation of the models used, namely the quantum XY and the Bose-Hubbard models.
The second chapter treats the effects of a sudden quench on the potential of a Bose cloud initially trapped in a certain region of an optical lattice. Two different initial states are considered, depending on the initial trapping potential. In the infinite repulsion regime (hard-core regime), we develop an hydrodynamical theory which perfectly catch the main features of the dynamics. The results obtained with this theory are confronted with numerical data given by exact diagonalization.
The two following chapters deal with the study of the dynamics of a small system (typically two spins 1/2) coupled to an environment modeled by a chain of interacting spins. In the third chapter, the two "defect" spins are initially prepared into a separable state and we ask if the coupling with the environment can create an effective interaction leading to entanglement. The reduced dynamics of the two defects is analyzed after performing a bosonization of the environment, and we look in particular to the dependence of the entanglement on the parameters of the system.
In chapter four, we start in the opposite situation where the two defect spins are initially maximally entangled, and we look at the effects of the coupling with the environment on this initial entangled state. In addition to the coupling, we also perform a sudden quench in the environment, forcing it to evolve in an out-of-equilibrium regime. We focus here on the influence of the degree of out-of-equilibrium on the disentanglement dynamics.
Finally, in a last chapter of this thesis, we analyze the dynamics of an open quantum system coupled to an environment by means of the repeated interactions process [AP06, AJ07, AD10]. The environment plays the role of a reservoir of entanglement, and we analyze if this entanglement can be transfered to the system. After a general description of the repeated interactions process, we study a simple toy model for which the entanglement properties can be completely determined analytically, and

we move afterward to a more general case analyzed for times shorter than the system size $t < N$, and times much larger than N.

Two articles have been published in link with this thesis, and two others are currently in preparation:

- *Hydrodynamic description of Hard-core Bosons on a Galileo ramp*
  P. Wendenbaum, M. Collura and D. Karevski
  Physical Review A **87** 023624 (2013).

- *Decoherence of Bell states by local interactions with a suddenly quenched spin environment*
  P. Wendenbaum, B.G. Taketani and D. Karevski
  Physical Review A **90** 022125 (2014).

- *Entanglement creation between two spins embedded in a single spin chain*
  P. Wendenbaum, B.G. Taketani, E. Kajari, G. Morigi and D. Karevski
  In preparation.

- *Entanglement replication via quantum repeated interactions*
  P. Wendenbaum, T. Platini and D. Karevski
  In preparation.

Quantum Entanglement and Models

1

In this chapter, we introduce the basic concepts used in this thesis. The first section is devoted to the presentation of a key ingredient of this work, namely quantum entanglement. We first give the basic concepts and introduce separability criteria for both pure and mixed states. Afterward, we introduce two measures of entanglement, necessary to know the amount of entanglement present in a quantum state. We also present the close relation between entanglement and quantum phase transitions, and the quantum teleportation is introduced as a direct application where entanglement is used as a resource. Afterward, we move to the description of the two models of quantum systems used in this work, namely the quantum XY and the Bose-Hubbard models. For the first of these models, we sketch in details the canonical diagonalization procedure by means of the Jordan Wigner transformation, and briefly discuss its phase diagram. The phase diagram of the Bose-Hubbard model is presented through two limits of the system's parameters.

1.1 Quantum entanglement

1.1.1 Definitions and separability criteria

Consider a quantum pure state $|\Psi\rangle$ living in a composite Hilbert space $\mathcal{H}$ given by

$$\mathcal{H} = \mathcal{H}_1 \otimes \mathcal{H}_2 \otimes \ldots \otimes \mathcal{H}_N, \tag{1.1}$$

where the $\mathcal{H}_i$ ($i = 1, \ldots, N$) are the N partitions of the total space. If the state $|\Psi\rangle$ can be written like

$$|\Psi\rangle = |\phi_1\rangle \otimes |\phi_2\rangle \otimes \ldots |\phi_N\rangle, \tag{1.2}$$

where $|\phi_i\rangle \in \mathcal{H}_i$, then this state is said to be *separable*. On the contrary, if it can not be written in the previous form, the state is said to be *entangled*. If the full Hilbert space $\mathcal{H}$ is compose by only two partitions (i.e $N = 2$ in the previous expression), we will then speak about *bipartite entanglement*.

As an example, let us consider the quantum state of two spins 1/2 labeled A and B. The state $|\Psi_1\rangle = \frac{1}{\sqrt{2}}(|\uparrow\uparrow\rangle + |\uparrow\downarrow\rangle)$ can be written like $|\Psi_1\rangle =$

$|\uparrow\rangle_A \otimes \frac{1}{\sqrt{2}}(|\uparrow\rangle + |\downarrow\rangle)_B = |\phi_A\rangle \otimes |\phi_B\rangle$ and is, as a consequence, separable. On the other hand, for the state $|\Psi_2\rangle = \frac{1}{\sqrt{2}}(|\uparrow\downarrow\rangle + |\downarrow\uparrow\rangle)$, it is impossible to find two states belonging to the subspaces A and B respectively such that it can be written in the form (1.2), this state is then entangled.
The entanglement has an interesting consequence when one makes a measurement on state $|\Psi_2\rangle$. Suppose that an experimentalist wants to know the state of the spin A by measuring its polarization. He will find the spin in one of the two states $|\uparrow\rangle_A$ or $|\downarrow\rangle_A$ with the same probability 1/2. If he finds the spin A in the state $|\uparrow\rangle_A$ (resp. $|\downarrow\rangle_A$), it means that the spin B, which can be arbitrary far from A, will instantaneously collapse into the state $|\downarrow\rangle_B$ (resp. $|\uparrow\rangle_B$) although no measurement has been done on it.

Given a certain quantum state, it is not always an easy task to know if this state is entangled or not. One criterion for separability is based on the *Schmidt decomposition* [Scho6, EK95]. Suppose a bipartite quantum state $|\psi\rangle$ leaving on a Hilbert space $\mathcal{H} = \mathcal{H}_A \otimes \mathcal{H}_B$ where we set, without loss of generality, $\dim(\mathcal{H}_A) = \dim(\mathcal{H}_B) = N$. Then, the state $|\psi_{AB}\rangle$ can be decomposed like

$$|\psi_{AB}\rangle = \sum_{i=1}^{N} \sqrt{p_i}|u_i^A\rangle \otimes |v_i^B\rangle, \tag{1.3}$$

where the $\{|u_i^A\rangle\}$ and $\{|v_i^B\rangle\}$ are the eigenvectors of the reduced density matrices $\rho_A = \mathrm{Tr}_B\{\rho\}$ and $\rho_B = \mathrm{Tr}_A\{\rho\}$ respectively, with the same eigenvalues p_i

$$\rho_A|u_i^A\rangle = p_i|u_i^A\rangle, \tag{1.4}$$
$$\rho_B|v_i^B\rangle = p_i|v_i^B\rangle. \tag{1.5}$$

To prove this, we expend the state $|\psi_{AB}\rangle$ on the base formed by the eigenstates of the reduced density matrices ρ_A and ρ_B

$$|\psi_{AB}\rangle = \sum_{ij} d_{ij}|u_i^A v_j^B\rangle, \quad \text{with } |u_i^A v_j^B\rangle \equiv |u_i^A\rangle \otimes |v_j^B\rangle, \tag{1.6}$$

and where the coefficients d_{ij} are given by the overlap $d_{ij} = \langle u_i^A v_j^B|\psi_{AB}\rangle$. Now we write down the reduced density matrices of the part A by tracing the part B from the full density matrix $\rho_{AB} = |\psi_{AB}\rangle\langle\psi_{AB}|$:

$$\begin{aligned}
\rho_A &= \mathrm{Tr}_B\{\rho_{AB}\} \\
&= \mathrm{Tr}_B\Big\{\sum_{ij}\sum_{i'j'} d_{ij}d_{i'j'}|u_i^A v_j^B\rangle\langle u_{i'}^A v_{j'}^B|\Big\} \\
&= \sum_{ij}\sum_{i'j'}\sum_{k} d_{ij}d_{i'j'}\langle v_k^B|u_i^A v_j^B\rangle\langle u_{i'}^A v_{j'}^B|v_k^B\rangle \\
&= \sum_{ij}\sum_{i'} d_{ij}d_{i'j}|u_i^A\rangle\langle u_{i'}^A|.
\end{aligned} \tag{1.7}$$

This expression (1.7) can be compared to the decomposition of ρ_A into its eigenstates

$$\rho_A = \sum_i p_i|u_i^A\rangle\langle u_i^A|, \tag{1.8}$$

giving the condition

$$\sum_j d_{ij} d_{i'j} = \delta_{ii'} p_i \tag{1.9}$$

such that (1.6) reduces to (1.3). The non negative numbers $\sqrt{p_i}$ are called the Schmidt coefficients, and the number of $p_i \neq 0$ is the Schmidt rank. The expression (1.3) together with the definition of an entangled state give us a criterion for the separability of a pure state: the state $|\psi_{AB}\rangle$ is separable if only one of its Schmidt coefficient is different from zero. Indeed, the only way to write (1.3) in the form (1.2) is to have only one non zero $\sqrt{p_i}$. Let us suppose that more than one p_i are different from zero. Because $p_i < 1 \ \forall i$, we have $p_i^2 < p_i$, and then it follows

$$\mathrm{Tr}\, \rho_A^2 = \mathrm{Tr}\, \rho_B^2 = \sum_i p_i^2 < 1. \tag{1.10}$$

It follows that the reduced density matrix of one part of a pure bipartite entangled state is a *mixed state*. In other words, when a pure state is entangled, we do not have all the information about one part by tracing out the full state over the second part, reflecting quantum correlations existing between parts A and B.

The previous definition of an entangled state and the separability criterion based on Schmidt decomposition held when the state of the quantum system is pure. What happens if the system is in a statistical mixture ? The notion of entanglement is generalized to mixed state in the following way: a mixed bipartite quantum state ρ is separable if it can be written in the form

$$\rho = \sum_i p_i \rho_i^A \otimes \rho_i^B, \quad \text{with } \sum_i p_i = 1, \ p_i \geq 0 \ \forall i, \tag{1.11}$$

and is entangled otherwise. In other words, ρ is separable if it is a convex sum of separable states belonging to subspaces A and B. The criterion based on the Schmidt decomposition does not hold anymore in this case. For mixed state, it exists an other criterion, the Positive Partial Transpose (PPT), also called Peres-Horodecki criterion [Per96]. Suppose a generic bipartite quantum state ρ acting on the Hilbert space $\mathcal{H}_A \otimes \mathcal{H}_B$

$$\rho = \sum_{ijmn} \rho_{ijmn} |i\rangle\langle j| \otimes |m\rangle\langle n|, \tag{1.12}$$

a necessary condition for its separability is that the partial transpose taken with respect to one part only, let's say the part B

$$(\rho)^{T_B} = \sum_{ijmn} \rho_{ijnm} |i\rangle\langle j| \otimes |n\rangle\langle m|, \tag{1.13}$$

has only non negative eigenvalues. More formally, the partial transposition of a separable state ρ has to be positive

$$(\rho)^{T_B} = (\mathbb{1}_A \otimes T)\rho > 0, \tag{1.14}$$

where T is the transposition operator. Indeed, if the state ρ is separable, it can be written in the form (1.11). After the partial transposition, it becomes

$$(\rho)^{T_B} = \sum_i p_i \rho_i^A \otimes (\rho_i^B)^{T_B}. \tag{1.15}$$

The partial transposition conserving the eigenvalues, it follows that the spectra of $(\rho)^{T_B}$ and ρ are identical. The latter operator being positive semidefinite, this proves the necessity of the criterion. The subsystem transposed is not important here since $(\rho)^{T_A} = (\rho^{T_B})^T$. This criterion is necessary when we deal with arbitrary size of Hilbert space $\mathcal{H}_A$ and $\mathcal{H}_B$, but it has been shown in [HHH96] that it becomes *sufficient* when the full Hilbert space has the structure $\mathcal{H} = \mathcal{H}^2 \otimes \mathcal{H}^2$, $\mathcal{H} = \mathcal{H}^3 \otimes \mathcal{H}^2$ or $\mathcal{H} = \mathcal{H}^2 \otimes \mathcal{H}^3$.

To illustrate this criterion, let us consider Werner state [Wer89]. A Werner state is a $N \times N$ state invariant under any unitary transformation of the form $U \otimes U$. Considering two spins 1/2, a Werner state can be defined assuming the spins in a fraction f of the entangled singlet state $|\psi\rangle = \frac{1}{\sqrt{2}}(|\uparrow\downarrow\rangle - |\downarrow\uparrow\rangle)$ with an impurity fraction $\frac{1}{4}(1-f)\mathbb{1}$. In the canonical base, the density matrix of such a state is

$$\rho^W = \frac{1}{4}\begin{pmatrix} 1-f & 0 & 0 & 0 \\ 0 & 1+f & -2f & 0 \\ 0 & -2f & 1+f & 0 \\ 0 & 0 & 0 & 1-f \end{pmatrix}. \tag{1.16}$$

Its partial transpose with respect to the second spin becomes

$$(\rho^W)^{T_B} = \frac{1}{4}\begin{pmatrix} 1-f & 0 & 0 & -2f \\ 0 & 1+f & 0 & 0 \\ 0 & 0 & 1+f & 0 \\ -2f & 0 & 0 & 1-f \end{pmatrix}, \tag{1.17}$$

and the diagonalization of the last matrix gives three eigenvalues equals to $(1+f)/4$ and one equal to $(1-3f)/4$. This last eigenvalue is the smallest one and gives a threshold value of the fraction $f^* = \frac{1}{3}$ such that the state is separable if $f > \frac{1}{3}$ and entangled if $f \leq \frac{1}{3}$.

1.1.2 Entanglement measures

So far, we have introduced entanglement criteria which tell us if a quantum state is entangled or not. But these criteria are unable to give how strong are these quantum correlations. Then, we need to introduce the notion of *entanglement measure* which gives us access to the amount of entanglement present in a given quantum state. It does not exist a unique definition of a measure of entanglement, but it is generally admitted that a measure $E(\rho)$ has to fulfill some requirements [Horo1, PV07]:

- A measure is a mapping between the density matrix and a real number.

$$\rho \to E(\rho) \in \mathbb{R}. \tag{1.18}$$

- $E(\rho)$ has to be zero for separable state.

$$\rho \text{ separable} \Leftrightarrow E(\rho) = 0. \tag{1.19}$$

- $E(\rho)$ does not increase under LOCC (Local Operation and Classical Communication).

- $E(\rho)$ has to reduce to the entanglement entropy, that we will define below, when the state is pure.

In the rest of this work, we will use two different measures of entanglement, namely the entanglement entropy and the concurrence.

1.1.2.1 Entanglement entropy

The entanglement entropy is an entanglement measure used when the system is pure. It is based on the von Neumann entropy defined by

$$\mathcal{S}(\rho) = -\operatorname{Tr}\{\rho \ln \rho\}, \tag{1.20}$$

and quantifying the classical mixing degree of a quantum state. Obviously, the von Neumann entropy of a pure state vanishes $\mathcal{S}(|\psi\rangle\langle\psi|) = 0$. As we saw in the previous section, the reduced density matrix of a bipartite entangled pure state $|\psi\rangle$ is a mixed state. Therefor, a way to quantify the entanglement present in $|\psi\rangle$ is to measure how this reduced density matrix is mixed by the introduction of the entanglement entropy, which is nothing else but the von Neumann entropy of one of the reduced density matrices ρ_A or ρ_B

$$E\left(|\psi\rangle\right) = \mathcal{S}(\rho_A) = -\operatorname{Tr}\{\rho_A \ln \rho_A\} = \mathcal{S}(\rho_B), \tag{1.21}$$

that can be rewritten using the spectral decomposition (1.8) of ρ_A like

$$\mathcal{S}(\rho_A) = -\sum_{i=1}^{N} p_i \ln p_i. \tag{1.22}$$

The value of $E\left(|\psi\rangle\right)$ is equal to zero when the state is separable and reaches its maximum value $E\left(|\psi\rangle\right) = \ln N$ when $p_i = 1/N \ \forall i$, where N is the dimension of ρ_A. To prove this last feature, we are looking for the extremum of the function $\mathcal{S}$ using the constraint $\sum_i p_i = 1$. Imposing this last constraint, we have

$$\mathcal{S}(\rho_A) = -\sum_{i=1}^{N-1} p_i \ln p_i - \left(1 - \sum_{i=1}^{N-1} p_i\right) \ln \left(1 - \sum_{i=1}^{N-1} p_i\right). \tag{1.23}$$

The derivative $\frac{\partial \mathcal{S}}{\partial p_j}$ gives

$$\frac{\partial \mathcal{S}}{\partial p_j} = -\ln p_j + \ln \left(1 - \sum_{i=1}^{N-1} p_i\right) \quad \forall j = 1, \cdots, N-1. \tag{1.24}$$

Setting this derivative to zero is equivalent to have

$$p_j = 1 - \sum_{i=1}^{N-1} p_i = p_N \quad \forall j = 1, \cdots, N-1, \tag{1.25}$$

that is fulfill only when $p_j = 1/N \ \forall j$. Now we know the probability distribution leading to the maximum entropy, we can easily compute $\mathcal{S}$ for this distribution

$$\mathcal{S}^{max} = -\sum_{i=1}^{N} \frac{1}{N} \ln \frac{1}{N} = \ln N. \tag{1.26}$$

When the entanglement entropy is maximum, the state is said to be *maximally entangled*. To illustrate this, consider two spins in the pure state $|\psi_{AB}\rangle = \frac{1}{\sqrt{2}}(|\uparrow\downarrow\rangle + |\downarrow\uparrow\rangle)$. The reduced density matrix ρ_A of the spin A obtained by tracing $\rho = |\psi\rangle\langle\psi|$ over the part B is, in the canonical base

$$\rho_A = \begin{pmatrix} 1/2 & 0 \\ 0 & 1/2 \end{pmatrix} = \frac{1}{2}\mathbb{1} \tag{1.27}$$

and the entanglement entropy becomes $E(|\psi_{AB}\rangle) = \ln 2$, as expected.

The entanglement entropy is a good measure when the system is in a pure state, but it becomes useless when the state is mixed. Indeed, this measure is unable to make the distinction between quantum and classical correlations. For example, if the two previous spins are in the classical separable mixed state $\rho_{AB} = \frac{1}{4}\mathbb{1}$, the reduced density matrix ρ_A yields to an entanglement entropy of $\mathcal{S} = \ln 2$, although the spins are in a separable state.

1.1.2.2 Entanglement of formation and concurrence

The entanglement entropy failing to detect entanglement of a mixed state, we need to introduce a proper measure able to distinguish quantum from classical correlations. The entanglement of formation [HW97, Woo98, Woo01, PV07] of a mixed state ρ is defined like

$$E_f(\rho) = \min_{\{|\psi_i\rangle\}} \sum_i p_i E(|\psi_i\rangle), \tag{1.28}$$

where the minimization is taken over all the possible pure-state decompositions $\{p_i, |\psi_i\rangle\}$ of ρ, and $E(\rho)$ is the entanglement entropy defined in the previous section. In other words, it is the minimal average entanglement over the pure state decomposition of the state ρ.
The decomposition of a mixed state into pure states being not unique, the minimization procedure appearing in the definition of $E_f(\rho)$ is in practice a difficult task. However, an exact expression of the entanglement of formation has been established for systems composed of two levels systems, like $1/2$ spins. For this kind of systems, the entanglement of formation has been found to be [HW97, Woo98]

$$E_f(\rho) = \mathcal{E}(C(\rho)), \tag{1.29}$$

where $\mathcal{E}(C)$ is the function

$$\mathcal{E}(C) = h\left(\frac{1}{2} + \frac{1-\sqrt{1-C^2}}{2}\right), \tag{1.30}$$

and $h(x) = -x\ln x - (1-x)\ln(1-x)$ is the binary entropy function. The number C appearing in the equation (1.30), ranging from 0 to 1, is called the *concurrence* and is defined by

$$C(\rho) = \max\{0, \lambda_1 - \lambda_2 - \lambda_3 - \lambda_4\}, \tag{1.31}$$

where the λ_i's are the eigenvalues in decreasing order of the Hermitian matrix $R = \sqrt{\sqrt{\rho}\tilde{\rho}\sqrt{\rho}}$ where $\tilde{\rho}$ is the flipped density matrix defined by

$$\tilde{\rho} = (\sigma^y \otimes \sigma^y)\rho^*(\sigma^y \otimes \sigma^y), \tag{1.32}$$

and the conjugate is taken in the standard base. Alternatively, the λ_i's can be seen as the square roots of the generally non Hermitian matrix [1] $R = \rho\tilde{\rho}$. The entanglement of formation E_f being a monotonically increasing function of C, the concurrence can be taken as an entanglement measure by itself. More the value of C is important, more the state is entangled. In particular, if $C = 0$, the two spins are in a separable state, whereas if $C = 1$, they are maximally entangled. In the rest of this work, we will use the concurrence as soon as we will have to determine the entanglement between two spins 1/2.

1.1.3 Entanglement and quantum phase transitions

While a classical phase transition occurs at non zero temperature, quantum phase transitions can only be observed at zero temperature [Sac00] when a physical parameter is varied in the Hamiltonian. In the first case, the transition is driven by the thermal fluctuations, whereas the quantum fluctuations are responsible of the transition in the quantum case. One example of such a transition will be given in section 1.3 where we will present the quantum XY model. The Ising point $\kappa = h = 1$ is the critical point separating the ferromagnetic phase from the paramagnetic one. At this point, the ground and first excited states cross and the energy gap Δ closes according to

$$\Delta \sim |h - h_c|^{z\nu}, \tag{1.33}$$

where z is the dynamical exponent and ν is the exponent of the correlation length ξ. This correlation length diverges at the critical point

$$\xi \sim |h - h_c|^{-\nu}, \tag{1.34}$$

whereas it is finite far from the critical region, and leads to exponentially damped correlations.

The quantum phase transition is characterized by a significant change in the ground state properties of a quantum many-body system. Then, if this ground state is an entangled state, it must exist a signature of this criticality in the entanglement properties. A big number of works has been devoted to the study of ground state entanglement in the vicinity or at the critical point (see for example the review [AFOV08]). One of the seminal work has been done by Osterloh *et al.* in [OAFF02], where they study the concurrence between pairs of spins in the one dimensional Ising chain in a transverse magnetic field. Entanglement is found only between nearest and next nearest neighbour spins. The nearest neighbour concurrence vanishes for $h = 0$ and in the limit $h \to \infty$ since the many-body ground state is a tensor product of single states. Between these two limits the concurrence is non zero and behaves smoothly.

1. Note that even if this matrix is non Hermitian, its eigenvalues are guaranteed to be non negative, the matrix R being the product of two positive definite matrices [Woo01].

It presents a maximum occurring close but, surprisingly, not at the critical point. One argument justifying this feature has been proposed in [ON02]. The fact that the concurrence is not maximum exactly at the critical point comes from the monogamy property of entanglement [CKW00], limiting the amount of entanglement that one system can share with two or more others. At the critical point, as the correlations increase, the *global* entanglement is maximum over the lattice. As a consequence of the aforementioned monogamy property, the pairwise entanglement decreases.
The signature of the second order phase transition is not encoded in the concurrence directly, but in its first derivative with respect to the magnetic field. This derivative shows a logarithmic divergence in the vicinity of the critical point in the thermodynamic limit. For finite systems, one observes rather a peak whose position is shifted with respect to the critical value. The position of the peak h_{max} and its maximum $\partial_h \mathcal{C}|_{h_{max}}$ obey to the finite size scaling

$$|h_c - h_{max}| \sim N^{-\mu}, \quad \partial_h \mathcal{C}|_{h_{max}} \sim c \ln(N) + cst, \tag{1.35}$$

where N is the number of spins in the chain. Note that the same kind of scaling of the entanglement entropy has been observed in [SSG06, Che07] where the local entanglement between two spins and the rest of the chain is analyzed in the quantum Ising model.

The entanglement properties of other models exhibiting quantum phase transition have been studied. For example the XXZ model [GLL03, GTL06] or the Lipkin-Meshkov-Glick model [VMD04, VPM04], which is a generalization of the Ising model where all spins are interacting together. The corresponding Hamiltonian is

$$H^{LMG} = -\frac{J}{N} \sum_{i<j} \left(\sigma_i^x \sigma_j^x + \gamma \sigma_i^y \sigma_j^y \right) - h \sum_i \sigma_i^z. \tag{1.36}$$

The nature of the phase transition of this model depends of the sign of the microscopic coupling J. Indeed, in the antiferromagnetic case $(J < 0)$, the phase transition is of the first order whereas it is of the second order in the ferromagnetic case $(J > 0)$. Obviously, any pair of spins will be entangled in the same way due to the symmetry of the Hamiltonian. It is then necessary to rescale the pair concurrence by multiplying it by the coordination number, $C_R = (N-1)C$, in order to have a finite value when $N \to \infty$. In the second order phase transition, it is shown [VPM04] that the concurrence is maximal at the critical point and its first derivative presents a divergence close to $h_c = 1$ like in the Ising case. Nevertheless, the divergence is not logarithmic but obeys to a power law, reflecting the fact that the two models belong to two different universality classes. In the antiferromagnetic case where the transition is of the first order at the transition point $h = 0$, the discontinuity occurs directly in the pair concurrence, and not in its derivative [VMD04].

From the previous observations, it seems that there is a deep relation between the nature of the quantum phase transition and the discontinuity observed (in the entanglement measure for a first order phase transition or in its derivative for a second order phase transition). Wu *et. al* have established in [WSL04] a theorem stating that, under certain conditions, a divergence of the concurrence (resp. its first derivative)

is a necessary and sufficient signal of the presence of a first order (resp. second order) phase transition. The basic idea behind this theorem is that a quantum phase transition is associated to a divergence of at least one of the elements of the reduced density matrix, or of one of its derivative. The conditions aforementioned guaranty that no accidental or artificial divergence occurs in the entanglement measure (or its derivative) used, or in the elements of the reduced density matrix (or its derivative). If one of these conditions is not fulfilled, one can for example find discontinuity in the derivative of the pair concurrence associated with no phase transition, or to a first order phase transition [Yano5].

Finally, we point out some works about thermal entanglement at low but non zero temperature [ABV01, Wano1, GKVB01, ONo2, APo7], where quantum effects are competing with thermal fluctuations.

1.1.4 Quantum teleportation

As mentioned in the introduction, entanglement can be use as a resource to build quantum technologies, opening the world of quantum communication [GTo7]. One of the most famous example of such a technology is the quantum teleportation. The teleportation protocol as been first described by Bennett *et al.* in [BBC$^+$93]. Here, we briefly sketch the principal steps of this protocol.
Suppose that Alice has a qubit in her hands, and she wants to transfer it to Bob, spatially separated from her. The communication between them can only be performed using classical channel, like phone or internet. The qubit of Alice is labeled by 1, and is in the state $|\phi_1\rangle = a|\uparrow\rangle + b|\downarrow\rangle$, with the usual normalization $|a|^2 + |b|^2 = 1$. The first step is to construct a pair of qubits in the entangled Bell state $|\psi_{23}^-\rangle = \frac{1}{\sqrt{2}}(|\uparrow_2\rangle|\downarrow_3\rangle - |\downarrow_2\rangle|\uparrow_3\rangle)$, and to give the qubit 2 to Alice, and the qubit 3 to Bob. Alice has then the qubit she wants to send and her constituent of the Bell pair, whereas Bob has only the second constituent. At this point, the full state of the three qubits systems is given by

$$|\Psi_{123}\rangle = \frac{a}{\sqrt{2}}\left(|\uparrow_1\rangle|\uparrow_2\rangle|\downarrow_3\rangle - |\uparrow_1\rangle|\downarrow_2\rangle|\uparrow_3\rangle\right) + \frac{b}{\sqrt{2}}\left(|\downarrow_1\rangle|\uparrow_2\rangle|\downarrow_3\rangle - |\downarrow_1\rangle|\downarrow_2\rangle|\uparrow_3\rangle\right). \tag{1.37}$$

We can rewrite this state using the Bell base for the spin 1 and 2

$$|\psi_{12}^\pm\rangle = \frac{1}{\sqrt{2}}\left(|\uparrow_1\rangle|\downarrow_2\rangle \pm |\downarrow_1\rangle|\uparrow_2\rangle\right), \tag{1.38}$$

$$|\phi_{12}^\pm\rangle = \frac{1}{\sqrt{2}}\left(|\uparrow_1\rangle|\uparrow_2\rangle \pm |\downarrow_1\rangle|\downarrow_2\rangle\right), \tag{1.39}$$

and we see easily that $|\Psi_{123}\rangle$ becomes

$$\begin{aligned}|\Psi_{123}\rangle = \frac{1}{2}\Big[&|\phi_{12}^+\rangle\left(a|\downarrow_3\rangle - b|\uparrow_3\rangle\right) + |\phi_{12}^-\rangle\left(a|\downarrow_3\rangle + b|\uparrow_3\rangle\right)\\ &+ |\psi_{12}^+\rangle\left(-a|\uparrow_3\rangle + b|\downarrow_3\rangle\right) + |\psi_{12}^-\rangle\left(-a|\uparrow_3\rangle - b|\downarrow_3\rangle\right)\Big].\end{aligned} \tag{1.40}$$

Now, Alice performs a joint measurement on the spins 1 and 2 she has on her side. According to the decomposition (1.40), the outcome of the measurement will be one of the four states composing the Bell base $|\psi_{23}^{\pm}\rangle$ or $|\phi_{23}^{\pm}\rangle$ with the same probability 1/4. Because the quantum channel was initially made of two entangled qubits, the qubit 3 of Bob will instantaneously be projected into one of the pure states appearing in eq.(1.40) parameterized by a and b. Once Alice knows the result of her measurement, she sends it to Bob by the classical channel, and he will perform a unitary transformation on his qubit $|\phi_3\rangle$ according to this result in order to reconstruct the initial state of the qubit of Alice. For example, if he receives that the result is $|\psi_{12}^{-}\rangle$, then his qubit is already in the desired state, up to a trivial phase factor, and no transformation is done. For the three other outcomes, he has to use the transformations

$$|\phi_{12}^{+}\rangle : |\phi_3\rangle \longrightarrow \begin{pmatrix} 0 & 1 \\ -1 & 0 \end{pmatrix} |\phi_3\rangle = i\sigma^y|\phi_3\rangle, \tag{1.41}$$

$$|\phi_{12}^{-}\rangle : |\phi_3\rangle \longrightarrow \begin{pmatrix} 0 & 1 \\ 1 & 0 \end{pmatrix} |\phi_3\rangle = \sigma^x|\phi_3\rangle, \tag{1.42}$$

$$|\psi_{12}^{+}\rangle : |\phi_3\rangle \longrightarrow \begin{pmatrix} -1 & 0 \\ 0 & 1 \end{pmatrix} |\phi_3\rangle = -\sigma^z|\phi_3\rangle, \tag{1.43}$$

to reconstruct the initial state of the qubit of Alice $|\phi_3\rangle = a|\uparrow_3\rangle + b|\downarrow_3\rangle$. Note that the state of the qubit of Alice has been destroyed during the measurement, the final state of the qubit of Bob does not result from a copy, and then, the teleportation protocol is not in contradiction with the non cloning theorem [WZ82].
Quantum teleportation has been achieved experimentally, for example in [BPM+97, MDRT+03, UJA+04, MHS+12] . In these experiments, the quantum channel is made by two photons prepared in an entangled state by parametric down conversion, and the polarization state of a photon is teleported from a place to another.

1.2 Quantum decoherence

The linearity of the Hilbert space used to describe a quantum system leads to the principle of quantum superposition. More precisely, if $|\Psi_1\rangle$ and $|\Psi_2\rangle$ are both accessible states of a quantum system, then a linear superposition $a|\Psi_1\rangle + b|\Psi_2\rangle$ is an accessible state as well. This principle is the origin of purely quantum effects like quantum interferences or entanglement, introduced just before. But this principle seems to be in contradiction with the vision we have of our macroscopic world, where all objects are in a definite state. Relevant questions are then: How the classical world emerges from the quantum world ? Is there a clear boundary between classic and quantum ? These questions lies in the heart of the *measurement problem* [Sch05, BR13]. It exists several theories aiming to answer these questions, but the most accepted one by the physicist community is the theory of decoherence[2] [Zur82, Zur02, Zur03, PZ01, Sch07]. In this theory, the classicality of a quantum state comes from the unavoidable interaction of the system under consideration with an environment. Indeed, a quantum system is never really isolated, and always interacts with the surrounding environment made of a big number of degrees of freedom.

2. For an alternative theory, see for example the many worlds interpretation [Eve57].

This interaction will have for consequence to kill the coherence (i.e the ability to do interferences) and then to destroy the quantum features. The off diagonal elements of the reduced density matrix of the system decay (until zero if the decoherence is total), and the state, which was initially a quantum superposition of pure states, is brought into a classical statistical mixture.

Let us illustrate the decoherence by the example of a simple system, taken from [Zur03]. The system under consideration is a single spin $\mathcal{S}$, coupled to a spin environment $\mathcal{E}$. The two states of the system are $\{|\Uparrow\rangle, |\Downarrow\rangle\}$, and it is moreover assumed that local Hamiltonians vanishes. The interaction between the system and the environment is

$$\begin{aligned}\mathcal{H}^{\mathcal{SE}} =& (|\Uparrow\rangle\langle\Uparrow| - |\Downarrow\rangle\langle\Downarrow|) \otimes \sum_k g_k \left(|\uparrow\rangle\langle\uparrow| - |\downarrow\rangle\langle\downarrow|\right)_k \\ =& \sigma^z_{\mathcal{S}} \otimes \sum_k g_k \sigma^z_k. \end{aligned} \tag{1.44}$$

The whole system spin plus environment is initially prepared into the state

$$|\Psi(0)\rangle = (a|\Uparrow\rangle + b|\Downarrow\rangle) \otimes \prod_k (\alpha_k|\uparrow\rangle_k + \beta_k|\downarrow\rangle_k), \tag{1.45}$$

which will be at a latter time t, under the dynamics set by the interaction Hamiltonian, in the state

$$|\Psi(t)\rangle = a|\Uparrow\rangle|\mathcal{E}_{\Uparrow}(t)\rangle + b|\Downarrow\rangle|\mathcal{E}_{\Downarrow}(t)\rangle, \tag{1.46}$$

where

$$|\mathcal{E}_{\Uparrow}(t)\rangle = \prod_{k=1}^{N} \left(\alpha_k e^{ig_k t}|\uparrow\rangle_k + \beta_k e^{-ig_k t}|\downarrow\rangle_k\right) = |\mathcal{E}_{\Downarrow}(-t)\rangle. \tag{1.47}$$

If one is interested only in the properties of the spin system, the partial trace has to be taken from the whole density matrix to have access to the reduced density matrix. After this operation, we get

$$\rho_{\mathcal{S}}(t) = |a|^2|\Uparrow\rangle\langle\Uparrow| + |b|^2|\Downarrow\rangle\langle\Downarrow| + ab^* f(t)|\Uparrow\rangle\langle\Downarrow| + ba^* f^*(t)|\Downarrow\rangle\langle\Uparrow| \tag{1.48}$$

where the function $f(t)$ encodes all the properties of the environment,

$$f(t) = \prod_k^N \left[\cos 2g_k t + i\left(|\alpha_k|^2 + |\beta_k|^2\right)\sin 2g_k t\right], \tag{1.49}$$

which behaves at large times and for big number of environmental spins like $|f(t)|^2 \sim 2^{-N}$. One clearly see here that the off diagonal elements of the reduced density matrix of the system are dramatically affected by the coupling with the environment. In the large times limit, the coherence is totally lost, and the system is in a classical mixture $\rho_{\mathcal{S}}(t) = |a|^2|\Uparrow\rangle\langle\Uparrow| + |b|^2|\Downarrow\rangle\langle\Downarrow|$ where the quantum effects have been suppressed. A model of decoherence will be studied in chapter 4.

1.3 The XY model

1.3.1 Presentation and canonical diagonalization

The quantum XY model is a model describing the behavior of interacting spins 1/2 on a one dimensional lattice. It has been first introduced without external magnetic field and solved by Lieb, Schultz and Mattis in 1961 [LSM61]. In 1970, Pfeuty solved the anisotropic case corresponding to the Ising model with a transverse magnetic field [Pfe70], and, one year latter, Barouch and McCoy solved the general XY model in a transverse field, established the critical behavior of the correlations functions and derived the phase diagram of the model [BMD70, BM71a, BM71b, MBA71]. In this section, we will sketch in details the canonical diagonalization procedure of this model [Kar06, Pla08, Col12]. The Hamiltonian of a the generic quantum XY model is given by

$$H^{XY} = -\frac{1}{2}\sum_n \left(\frac{1+\kappa}{2}\sigma_n^x\sigma_{n+1}^x + \frac{1-\kappa}{2}\sigma_n^y\sigma_{n+1}^y \right) - \frac{h}{2}\sum_n \sigma_i^z, \tag{1.50}$$

where $\sigma_n^\alpha, (\alpha = x, y, z)$ are the Pauli matrices in the α direction associated to the site n, and we consider first neighbor interactions with coupling constant J. Here, κ is a parameter fixing the anisotropy. The value $\kappa = 0$ corresponds to the isotropic case, called the XX model. On the other hand, the value $\kappa = 1$ describes the most anisotropic case, the Ising model. The main properties of theses models will be discussed in the next section, where the phase diagram is presented.

The Hamiltonian can be mapped into a chain of non interacting fermions by means of the Jordan-Wigner transformation [JW28]. Let us first introduce the spin ladder operators $\sigma_n^\pm = (\sigma_n^x \pm i\sigma_n^y)/2$ satisfying the anticommutative algebra $\{\sigma_n^+, \sigma_n^-\} = 1$, whereas they commute on different sites. The idea behind this transformation is to associate to these ladder operators creation and annihilation fermionic operators. This is done by the introduction of the Clifford operators

$$\begin{aligned} \Gamma_n^1 &= \prod_{i=1}^{n-1}(-\sigma_i^z)\,\sigma_n^x, \\ \Gamma_n^2 &= \prod_{i=1}^{n-1}(-\sigma_i^z)\,\sigma_n^y, \end{aligned} \tag{1.51}$$

satisfying Clifford algebra $\{\Gamma_n^\mu, \Gamma_m^\nu\} = 2\delta_{nm}\delta_{\mu\nu}$. Note that $\Gamma_n^\mu = \left(\Gamma_n^\mu\right)^\dagger$, so they can be seen as not properly normalized Majorana fermions. Using these new operators, the different terms of the Hamiltonian (1.50) become

$$\sigma_n^z = i\Gamma_n^1\Gamma_n^2, \tag{1.52}$$

$$\sigma_n^x\sigma_{n+1}^x = -i\Gamma_n^2\Gamma_{n+1}^1, \tag{1.53}$$

$$\sigma_n^y\sigma_{n+1}^y = i\Gamma_n^1\Gamma_{n+1}^2. \tag{1.54}$$

Introducing the $2N$ dimensional row vector

$$\mathbf{\Gamma}^\dagger = \left(\mathbf{\Gamma}^{1\dagger}, \mathbf{\Gamma}^{2\dagger}\right), \quad \text{with} \quad \mathbf{\Gamma}^{\nu\dagger} = \left(\Gamma_1^{\nu\dagger}, \ldots, \Gamma_N^{\nu\dagger}\right), \tag{1.55}$$

the Hamiltonian can be rewritten like

$$H = \frac{1}{4}\mathbf{\Gamma}^\dagger \boldsymbol{T} \mathbf{\Gamma}, \tag{1.56}$$

where $\boldsymbol{T}$ is a hermitian matrix

$$\boldsymbol{T} = \begin{pmatrix} 0 & \boldsymbol{C} \\ \boldsymbol{C}^\dagger & 0 \end{pmatrix}, \tag{1.57}$$

with the $N \times N$ matrix $\boldsymbol{C}$

$$\boldsymbol{C} = -i \begin{pmatrix} h & J_y & & & \\ J_x & \ddots & \ddots & & \\ & \ddots & \ddots & \ddots & \\ & & \ddots & \ddots & J_y \\ & & & J_x & h \end{pmatrix}, \tag{1.58}$$

and where we have introduced the notation

$$J_x = \frac{1+\kappa}{2}, \quad J_y = \frac{1-\kappa}{2}. \tag{1.59}$$

Now, we define the unitary matrix $\boldsymbol{V}$ containing the eigenvectors V_q of the matrix T

$$\boldsymbol{V} = (V_1, V_2, \dots V_N), \tag{1.60}$$

where the eigenvectors are parameterized like

$$V_q = \frac{1}{\sqrt{2}} \begin{pmatrix} \phi_q \\ -i\psi_q \end{pmatrix}. \tag{1.61}$$

The eigenvalue equation $\boldsymbol{T}V_q = \varepsilon_q V_q$ leads to two coupled equations

$$-i\boldsymbol{C}\psi_q = \varepsilon_q \phi_q, \tag{1.62}$$

$$\boldsymbol{C}^\dagger \phi_q = -i\varepsilon_q \psi_q. \tag{1.63}$$

We remark that the two equations (1.62) and (1.63) are invariant under the simultaneous changes $\varepsilon_q \to -\varepsilon_q$ and $\psi_q \to -\psi_q$. It follows that to each eigenvalue $\varepsilon_q \geq 0$ is associated an other one $\varepsilon'_q \leq 0$ with a corresponding eigenvector given by

$$V'_q = \frac{1}{\sqrt{2}} \begin{pmatrix} \phi_q \\ i\psi_q \end{pmatrix}. \tag{1.64}$$

Thanks to the symmetry of the $\boldsymbol{T}$ matrix, the eigenvalues are obtained by the singular value decomposition $\mathbf{\Lambda} = \boldsymbol{V}^\dagger \boldsymbol{T} \boldsymbol{V}$ with

$$\mathbf{\Lambda} = \begin{pmatrix} \boldsymbol{E} & \\ & -\boldsymbol{E} \end{pmatrix}, \qquad \boldsymbol{E} = \begin{pmatrix} \varepsilon_1 & & \\ & \ddots & \\ & & \varepsilon_N \end{pmatrix}. \tag{1.65}$$

Now, taking advantage that the $\boldsymbol{V}$ matrix is unitary ($\boldsymbol{V}\boldsymbol{V}^\dagger = \mathbb{1}$), we get

$$\begin{aligned} H =& \frac{1}{4}\boldsymbol{\Gamma}^\dagger \boldsymbol{V}\boldsymbol{V}^\dagger \boldsymbol{T}\boldsymbol{V}\boldsymbol{V}^\dagger \boldsymbol{\Gamma} \\ =& \frac{1}{2}\boldsymbol{\eta}^\dagger \boldsymbol{\Lambda}\boldsymbol{\eta}, \end{aligned} \tag{1.66}$$

where we have introduced the diagonal creation and annihilation operators η

$$\boldsymbol{\eta} = \begin{pmatrix} \eta_1 \\ \vdots \\ \eta_N \\ \eta_1^\dagger \\ \vdots \\ \eta_N^\dagger \end{pmatrix} = \frac{1}{\sqrt{2}}\boldsymbol{V}^\dagger \boldsymbol{\Gamma}, \tag{1.67}$$

satisfying the canonical anticommutative algebra $\{\eta_q^\dagger, \eta_{q'}\} = \delta_{qq'}$. More explicitly, they are given by the Bogoliubov decomposition

$$\eta_q = \frac{1}{2}\sum_{n=1}^{N}\left(\phi_q(n)\Gamma_n^1 + i\psi_q(n)\Gamma_n^2\right) \tag{1.68}$$

$$\eta_q^\dagger = \frac{1}{2}\sum_{n=1}^{N}\left(\phi_q(n)\Gamma_n^1 - i\psi_q(n)\Gamma_n^2\right). \tag{1.69}$$

These relations that can be inverted to express the Clifford operators as a function of the diagonal ones

$$\Gamma_n^1 = \sum_{q=1}^{N}\phi_q(n)\left(\eta_q + \eta_q^\dagger\right) \tag{1.70}$$

$$\Gamma_n^2 = \sum_{q=1}^{N} -i\psi_q(n)\left(\eta_q - \eta_q^\dagger\right). \tag{1.71}$$

$$\tag{1.72}$$

Using the explicit expression of the matrix Λ, the Hamiltonian is recast in the form

$$\begin{aligned} H =& \frac{1}{2}(\eta_1^\dagger, \ldots, \eta_N^\dagger, \eta_1 \ldots, \eta_N)\begin{pmatrix} \boldsymbol{E} & \\ & -\boldsymbol{E} \end{pmatrix}\begin{pmatrix} \eta_1 \\ \vdots \\ \eta_N \\ \eta_1^\dagger \\ \vdots \\ \eta_N^\dagger \end{pmatrix} \\ =& \frac{1}{2}\sum_{q=1}^{N}\varepsilon_q\eta_q^\dagger\eta_q - \varepsilon_q\eta_q\eta_q^\dagger \\ =& \sum_{q=1}^{N}\varepsilon_q\left(\eta_q^\dagger\eta_q - \frac{1}{2}\right), \end{aligned} \tag{1.73}$$

where we have used the anticommutation relation $\{\eta_q^\dagger, \eta_q\} = 1$. The ground state is thus given by the product of the $\eta's$ vacuum states $|0\rangle$:

$$|GS\rangle = |0\rangle^{\otimes N}, \tag{1.74}$$

with the property $\eta_q|0\rangle = 0, \langle 0|\eta_q^\dagger = 0 \ \forall q = 1, \cdots, N$. The associated ground state energy is given by $E_0 = -\frac{1}{2}\sum_{q=1}^{N} \varepsilon_q$.

1.3.2 Phase diagram

The dispersion relation of the XY model is [LSM61, Karo6, Plao8]

$$\varepsilon_q = \sqrt{(h + \cos q)^2 - \kappa^2 \sin^2 q}, \tag{1.75}$$

where the quasi momentum q is restricted to the range $[0 : \pi]$, and the ε_q exhibits the symmetry $\varepsilon_{q+\pi} = -\varepsilon_q$. This dispersion relation allows us to build the phase diagram, as shown in figure 1.1.

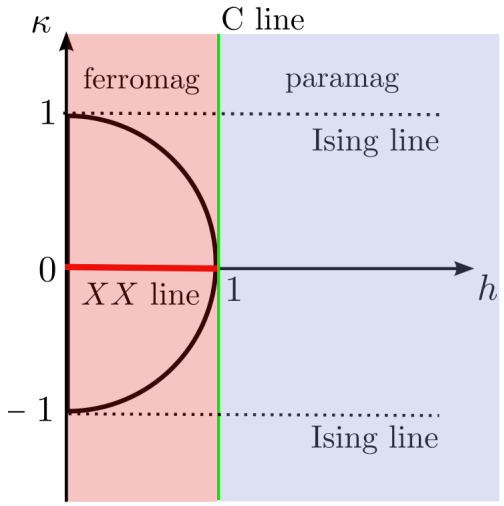

Figure 1.1 – *Phase diagram of the XY model in the (κ, h) plan. Note that this phase diagram is symmetric with respect to the change $h \to -h$.*

Thanks to the aforementioned symmetry, the XY model is gapless if it exists a value of the quasi momentum q^* such that $\varepsilon_{q^*} = 0$.
The C line of equation $h = 1$, represented in green, is a critical line separating a ferromagnetic phase from an paramagnetic one. On this line, one can see from the dispersion relation that the gap closes, and consequently, the correlation length diverges. Moreover, the correlation functions present an algebraic decay with the distance. This line is carachterized by the critical exponent $\nu = 1$ (correlation length) and a dynamical exponent $z = 1$. For $h < 1$, the system is in a ferromagnetic phase where the spins prefer to align in the direction of the microscopic coupling. On the contrary, for $h > 1$, the system is in the paramagnetic phase where it is more favorable for the spins

to align along the direction of the magnetic field. In order to distinguish these two phases, one can introduce an order parameter, which is different from zero only in the ordered phase. In this case, this role will be played by the average $\lim_{n\to\infty}\langle\sigma_i\sigma_{i+n}\rangle$. The two dashed lines represent the Ising lines corresponding to a anisotropy parameter $\kappa = \pm 1$. The value $+1$ corresponds to a coupling to the x direction, whereas the value -1 to a coupling of the y components.
The C_{XX} line, plotted in red in figure 1.1, represents a continuous critical transition. On this line and for any value of $h \leq 1$, the system is gapless and presents a critical behavior, with diverging correlation length and a slow decay of correlation functions. Finally, the region inside the circle of equation $|h|^2 + |\kappa|^2 = 1$, represents an oscillatory ferromagnetic phase. This phase is characterized by a wave vector modulating the exponential decay of the correlation functions, making them oscillate [Hen99].

1.3.3 Dynamics

Two different, but equivalent, representations are possible to describe the dynamics of a quantum system. The first one is the Schrödinger representation where the time dependence is carried by the state $|\psi\rangle(t)$ through the differential equation

$$\frac{d|\psi(t)\rangle}{dt} = -iH|\psi\rangle(t). \tag{1.76}$$

If the Hamiltonian is time independent, the quantum state $|\psi\rangle$ is given at a time t by the application of a unitary operator, the time evolution operator $U(t)$, on an initial state $|\psi(0)\rangle$

$$|\psi(t)\rangle = U(t)|\psi(0)\rangle, \tag{1.77}$$

where $U(t) = \exp(-iHt)$. If the system is initially in a statistical mixture and its state is described by the density matrix ρ, the state evolves following the von Neumann equation [BP02]

$$\frac{d\rho(t)}{dt} = -i[H, \rho(t)], \tag{1.78}$$

and the density matrix at a time t is

$$\rho(t) = U(t)\rho(0)U^\dagger(t). \tag{1.79}$$

In the Heisenberg representation, the time dependence is no longer carried by the state, but by the operators. An operator $\mathcal{O}(t)$ will then evolve through the Heisenberg equation of motion

$$\frac{d\mathcal{O}(t)}{dt} = i[H, \mathcal{O}(t)]. \tag{1.80}$$

The average of the operator $\mathcal{O}$ is given by

$$\langle\mathcal{O}\rangle(t) = \mathrm{Tr}\{\rho(t)\mathcal{O}\} = \mathrm{Tr}\{\rho\mathcal{O}(t)\}, \tag{1.81}$$

which defines the Heisenberg evolution of the operator $\mathcal{O}$

$$\mathcal{O}(t) = U^\dagger(t)\mathcal{O}(0)U(t). \tag{1.82}$$

Using this last representation, the operators η_q diagonalizing the XY Hamiltonian evolve through

$$\eta_q(t) = U^\dagger(t)\eta_q(0)U(t), \tag{1.83}$$

and with $U_q(t) = \exp(-it\varepsilon_q\eta_q^\dagger\eta_q)$, one has

$$\eta_q(t) = U_q^\dagger(t)\eta_q(0)U_q(t), \tag{1.84}$$

leading to

$$\eta_q(t) = e^{-it\varepsilon_q}\eta_q(0), \quad \eta_q^\dagger(t) = e^{it\varepsilon_q}\eta_q^\dagger(0), \tag{1.85}$$

or, in a matrix form

$$\boldsymbol{\eta}(t) = e^{-it\boldsymbol{\Lambda}}\boldsymbol{\eta}(0). \tag{1.86}$$

With this, on can write the time evolution of the Clifford operators using the linear transformation

$$\frac{1}{\sqrt{2}}\boldsymbol{\Gamma}(t) = \boldsymbol{V}\boldsymbol{\eta}(t) \tag{1.87}$$

and equation (1.86) to arrive at

$$\boldsymbol{\Gamma}(t) = \boldsymbol{R}(t)\boldsymbol{\Gamma}(0), \tag{1.88}$$

with $\boldsymbol{R}(t) = \boldsymbol{V}e^{-it\boldsymbol{\Lambda}}\boldsymbol{V}^\dagger = e^{-itV\boldsymbol{\Lambda}V^\dagger} = e^{-it\boldsymbol{T}}$, where $\boldsymbol{T}$ is the matrix (1.57).

1.3.4 Entanglement entropy of the XX chain

Here we establish a general expression for the entanglement entropy of the XX model, and we show that it can be related to the eigenvalues of the reduced correlation matrix [Col12]. Instead of using the Clifford operators as we did in section 1.3, we can use the lattice fermionic creation and annihilation operators $c_i^\dagger$ and c_i defined by

$$c_i = \prod_{j=1}^{i-1}(-\sigma_j^z)\sigma_i^-, \quad c_i^\dagger = \prod_{j=1}^{i-1}(-\sigma_j^z)\sigma_i^+, \tag{1.89}$$

leading to the following expression of the XX Hamiltonian

$$H^{XX} = \boldsymbol{c}^\dagger T\boldsymbol{c}. \tag{1.90}$$

The eigenfunctions of the Hamiltonian being Slater determinant, and defining the two-point correlation matrix as $C_{ij} = \langle c_i^\dagger c_j\rangle$, it follows that, according Wick theorem, all the correlators of higher order are expressed in terms of this two-point correlation function [Peso3]. By definition, any average of local operator acting on the subsystem A has to be expressed in terms of the reduced density matrix ρ_A. As a consequence, we must have

$$C_{ij} = \mathrm{Tr}\{\rho_A c_i^\dagger c_j\}, \quad i,j \in A, \tag{1.91}$$

and all the correlations of highest order must factorize. It can be shown [Peso3, CP01] that the previous property is valid if the reduced density matrix ρ_A is written as the exponential of a quadratic form in terms of fermionic operators, i.e

$$\rho_A = \frac{1}{Z}\exp\left(-\sum_{ij} c_i^\dagger B_{ij} c_j\right), \tag{1.92}$$

where Z is a normalization constant ensuring the unity of the trace. The expression (1.92) can be rewritten

$$\rho_A = \frac{1}{Z} \exp\left(- \sum_k \varepsilon_k \eta_k^\dagger \eta_k \right) \tag{1.93}$$

by the introduction of the diagonal operators related to the original ones by the relation

$$c_i = \sum_k \phi_k(i) \eta_k, \quad c_i^\dagger = \sum_k \phi_k^*(i) \eta_k^\dagger. \tag{1.94}$$

Using the fact that

$$\langle \eta_k^\dagger \eta_{k'} \rangle_\rho = \frac{\delta_{kk'}}{1 + e^{\varepsilon_k}}, \tag{1.95}$$

the elements of the reduced correlation matrix C_{ij} of the subsystem A become

$$C_{ij} = \sum_k \phi_k(i) \phi_k^*(j) \frac{1}{1 + e^{\varepsilon_k}}. \tag{1.96}$$

This last expression gives a relation between the eigenvalues ξ_k associated to the C matrix and those associated to the B matrix

$$\xi_k = \frac{1}{1 + e^{\varepsilon_k}}. \tag{1.97}$$

Let us come back to the entanglement entropy, which takes the expression, using $n_k = \eta_k^\dagger \eta_k$

$$\begin{aligned} \mathcal{S}(\rho_A) &= - \operatorname{Tr}\{\rho_A \ln \rho_A\} \\ &= - \operatorname{Tr}\left\{ \rho_A \ln \left(\frac{1}{Z} \exp\left(- \sum_k \varepsilon_k n_k \right) \right) \right\} \\ &= - \sum_k \varepsilon_k \operatorname{Tr}\{\rho_A n_k\} + \ln Z. \end{aligned} \tag{1.98}$$

The normalization constant Z is given by

$$Z \equiv \operatorname{Tr}\{e^{-\sum_k \varepsilon_k n_k}\} = \prod_k (1 + e^{-\varepsilon_k}). \tag{1.99}$$

Using this last expression together with equations (1.95) and (1.97), we obtain the final expression

$$\mathcal{S}(\rho_A) = \sum_k \left[-\xi_k \ln \xi_k - (1 - \xi_k) \ln (1 - \xi_k) \right]. \tag{1.100}$$

The entanglement entropy of a block A is then completely determined by the eigenvalues of the two-point correlation matrix of the block. This form of the entanglement entropy of a XX chain will be used in the chapter 2.

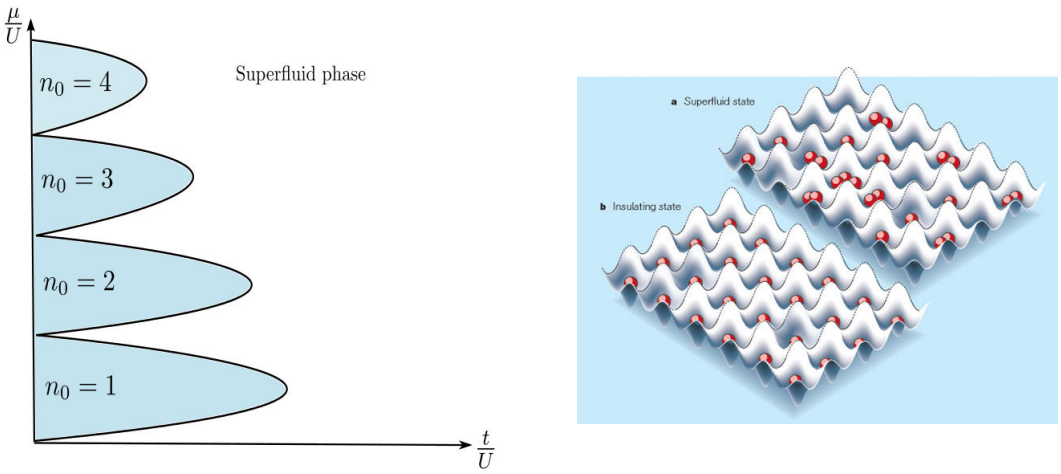

Figure 1.2 – *(left) Phase diagram of the Bose-Hubbard model. Inside the blue lobes, the system is in a Mott phase where the particle density is constant, whereas outside, the system is in a superfluid phase with delocalized particles over the lattice. (right) Pictural representation of the transition between the Mott insulator and the superfluid states of the Bose-Hubbard model (picture taken from* `http://www.lorentz.leidenuniv.nl/~pjhdent/`*).*

1.4 The Bose-Hubbard model

We finish this chapter by the presentation of the Bose Hubbard model. The Hubbard model has been introduced in 1963 for the description of the behavior of electrons in a low temperature solid [Hub63]. The extension of this model to bosonic fields is called the Bose-Hubbard model. This is a simple model describing interacting bosons on a lattice. The corresponding Hamiltonian in one dimension is

$$H_{BH} = -t\sum_i \left(b_i^\dagger b_{i+1} + b_i b_{i+1}^\dagger\right) - \mu\sum_i n_i + \frac{U}{2}\sum_i n_i(n_i-1), \tag{1.101}$$

where the $b_i^\dagger$ and b_i are creation and destruction bosonic operators on site i satisfying the bosonic algebra $[b_i^\dagger, b_j] = \delta_{ij}$, and $n_i = b_i^\dagger b_i$ is the occupation number operator. The bosons are allowed to jump from site i to site $i+1$ with an amplitude t. The second term is proportional to the chemical potential μ controlling the number of bosons in the system. Finally, the last term is local bosonic pair interaction term repulsive for $U > 0$ and attractive for $U < 0$.
This Hamiltonian is analytically solvable in the two limits $t/U \to 0$ and $t/U \to \infty$ [FWGF89]. In the first case, the on-site interaction term is dominant and the Hamiltonian reduces to $H_i = -\mu\sum_i n_i + \frac{U}{2}\sum_i n_i(n_i-1)$. The system is characterized by a constant density of particles n_0 on each site fixed by the minimization constraint

$$\left.\frac{\partial\varepsilon}{\partial n}\right|_{n_0} = 0, \tag{1.102}$$

where $\varepsilon(n) = -\mu n_0 + \frac{1}{2}Un_0(n-1)$ is the on-site energy. The ground state is given by the product of states with n_0 density

$$|\Psi\rangle = \prod_i (b_i^\dagger)^{n_0}|0\rangle, \tag{1.103}$$

where $|0\rangle$ is the vacuum state with no boson. The state is said to be incompressible in the sense that $d\langle\hat{N}\rangle/d\mu = 0$ where $\hat{N}$ is the total occupation number $\hat{N} = \sum_i n_i$. This ground state corresponds in consequence to a *Mott insulator* state. In the other limit, the kinetic part of the Hamiltonian dominates and the system is in a *superfluid* phase. The ground state is given by

$$|\Psi\rangle = \left(\sum_i b_i^\dagger\right)^N |0\rangle, \tag{1.104}$$

and all the particles are completely delocalized over the whole lattice.

The pictural phase diagram in the $(t/U) - (\mu/U)$ plane of the Bose-Hubbard model is presented on figure 1.2. The Mott insulator phases are confined in lobes inside which the number of bosons on each site is constant. In this phase, it exists an energy gap between the ground and the first excited states. Considering non exactly integer values of μ/U to avoid degeneracy [3], the ground state will move adiabatically without level crossing when the hopping amplitude t is tuned to a small value. Additionally, the Mott ground state (1.103) is an eigenstate of the total particle number operator $\hat{N}$ with eigenvalue Nn_0. The small perturbation brought by a small t commuting with the Hamiltonian, it results that the ground state remains an eigenstate of $\hat{N}$ with the same eigenvalue, explaining the survival of the Mott phase with fixed density even for non zero hopping [Sacoo]. The Mott to superfluid transition is of second order, and the phase boundary can be determined using standard Landau theory of phase transitions. One can define a Landau free energy

$$L = r|\Psi_B|^2 + q|\Psi_B|^4 + \mathcal{O}(|\Psi_B|^6), \tag{1.105}$$

where $|\Psi_B|^2$ acts as order parameter. The parameter r can be found using second order perturbation theory

$$r = \xi(\mu/U)\left(1 - zt\xi(\mu/U)\right), \tag{1.106}$$

where z is the coordination number, and

$$\xi(\mu/U) = \frac{n_0(\mu/U)+1}{Un_0(\mu/U)-\mu} + \frac{n_0(\mu/U)}{\mu - Un_0(\mu/U) - 1}. \tag{1.107}$$

The transition occurs at $r = 0$ giving the phase boundary $\frac{\mu}{U} = \frac{\mu}{U}\left(\frac{t}{U}\right)$.

3. If μ/U is integer, there is two degenerate ground states on each lattice site with occupation number differing by one [Sacoo].

Self-trapping of Hard Core bosons on optical lattice

2

Experimental progresses have relaunched the interest of physicists for one dimensional many-body systems. Among these systems, one can cite for example ultra cold quantum gases on optical lattices, which is the subject of many experiments [Blo05, BDZ08, PSSV11]. Among all the interesting phenomenon observed in such a systems, one is particularly relevant for our study, namely the Bloch oscillations [Blo28, Zen34, DPR+96, KK04]. These oscillations occur when a constant force F is applied to a quasi-particle on a lattice, leading to a periodic motion with period $2\pi/|F|$. Some works have been devoted to the studies of the out of equilibrium dynamics of bosonic systems in a lattice after the release of the confining trap [HMMR+09, MG05, RM05], and recently, studies have considered the dynamics of Hard core bosons on tilted optical lattices [CCW11, CARK12].
In this work, we propose to extend the work done in [CARK12] by considering an initial inhomogeneous distribution of particles set by an harmonic trapping potential. Depending on the value of the harmonic potential, two different kinds of initial states are possible. The system can be completely in a superfluid state, or it can be composed by a Mott phase surrounded by two superfluid phases. In the following, we propose two different kinds of quench, the sudden release of the trapping potential, and the release of the trap and the loading of a linear ramp with constant force F on the negative part of the real axe. We develop an hydrodynamical theory that allows us to explain the main features of the behavior of the particles.

The chapter is organized as follow: In a first part, we present the Bose Hubbard Hamiltonian, describing bosons on a lattice, and we introduce the Hard Core limit. After that, the main features of the hydrodynamical theory are sketched, and the two kind of initial states used in this chapter are presented. Afterward, in section 2.4, we turn to the description of the out of equilibrium dynamics after the quench of the trapping potential, starting with the free expansion case and finishing with the tilted potential case. Finally, the different results are summarized in section 2.5.

2.1 Bose-Hubbard model and Hard-Core limit

Our model consist of bosons loaded on a one dimensional lattice. It is described by the Bose-Hubbard Hamiltonian

$$\mathcal{H}_{BH} = -J\sum_{i=1}^{N-1}\left(b_i^\dagger b_{i+1} + H.c\right) + \frac{U}{2}\sum_{i=1}^{N} n_i(n_i-1) + \sum_{i=1}^{N} V_i n_i, \tag{2.1}$$

where the $b_i^\dagger$ and b_i are the creation and destruction bosonic operators, and $n_i = b_i^\dagger b_i$ is the density operator counting the particle on site i. The first term is the kinetic term modeling the hopping of one particle from the site i to the next one $i+1$ with amplitude J. The second one, with $U > 0$, introduces a local pair repulsive interaction between bosons located at the same site. Finally, the last term is an inhomogeneous potential over the lattice.
The phase diagram of this model has been briefly discussed in section 1.4. It presents two different phases, a Mott insulator phase, where the particles are well localized on each site, leading to a constant integer value of the particle density $n_0 = 1, 2, 3\ldots$, and a superfluid phase, where all the particles are completely delocalized over the lattice. The Hamiltonian is not integrable and then not analytically solvable. Nevertheless, we can consider the limit of an infinite repulsion between bosons on one site $U \to \infty$, namely the Hard Core boson limit. In this case, the particle density is then restricted to the two values $n_0 = 0$ or $n_0 = 1$, and the system is sent to the origin of the phase diagram (see figure 1.2). The second term of the Hamiltonian disappears and we end up with the Hard Core boson Hamiltonian

$$\mathcal{H}^{hc} = -J\sum_{i}\left(b_i^\dagger b_{i+1} + H.c\right) + \sum_{i} V_i n_i. \tag{2.2}$$

The Hard Core boson model becomes analytically solvable and can be mapped into free fermions model. The first step is done by the introduction of the transformation between bosonic creation and destruction operators and Pauli operators

$$\begin{aligned}
\sigma_i^x &= b_i^\dagger + b_i = \sigma_i^+ + \sigma_i^- \\
\sigma_i^y &= i(b_i - b_i^\dagger) = \sigma_i^+ - \sigma_i^- \\
\sigma_i^z &= 2b_i^\dagger b_i - 1 = \sigma_i^+\sigma_i^- - 1.
\end{aligned} \tag{2.3}$$

Plugging this transformation into equation (2.2), one gets the Hamiltonian of interacting spins 1/2:

$$\mathcal{H} = -\frac{J}{2}\sum_{i=1}^{N-1}\left(\sigma_i^x\sigma_{i+1}^x + \sigma_i^y\sigma_{i+1}^y\right) + \frac{1}{2}\sum_{i=1}^{N} V_i\sigma_i^z. \tag{2.4}$$

The usual procedure to treat this Hamiltonian is to use the Jordan Wigner transformation between spin operators and lattice fermionic ones

$$c_i^\dagger = \prod_{j<i}(-\sigma_j^z)\sigma_i^+, \quad c_i = \prod_{i<j}(-\sigma_j^z)\sigma_i^-, \tag{2.5}$$

in order to map the Hamiltonian (2.4) into free fermionic model

$$\begin{aligned}\mathcal{H} =& -J\sum_{i=1}^{N-1}(c_i^\dagger c_{i+1} + c_{i+1}^\dagger c_i) + \sum_{i=1}^{N} V_i c_i^\dagger c_i \\ =& \boldsymbol{c}^\dagger \mathcal{T} \boldsymbol{c}.\end{aligned} \tag{2.6}$$

The $c_i^\dagger$ and c_i are fermionic creation and destruction operators satisfying anticommutative algebra $\{c_i^\dagger c_j\} = \delta_{ij}$. We have introduced the N components row vector $\boldsymbol{c}^\dagger = (c_1^\dagger, c_2^\dagger, \ldots, c_N^\dagger)$ and the tridiagonal matrix $(\mathcal{T})_{ij} = V_i\delta_{ij} - J(\delta_{j,i+1} + \delta_{j,i+1})$. This last Hamiltonian can be diagonalized through Bogoliubov transformation, by the introduction of the diagonal operators η_q related to the lattice ones by

$$\eta_q = \sum_i \phi_q^*(i) c_i, \quad \eta_q^\dagger = \sum_i \phi_q(i) c_i^\dagger, \tag{2.7}$$

leading to the diagonal form

$$\mathcal{H} = \sum_q \varepsilon_q \eta_q^\dagger \eta_q, \tag{2.8}$$

where the ε_q are the excitation energies associated to the free Fermi particles created by $\eta_q^\dagger$ and destroyed by η_q. For general inhomogeneous potential V_i, the spectrum ε_q has to be computed numerically. But if the potential becomes homogeneous, i.e $V_i = V\ \forall i$, the spectrum can be obtained analytically, and one gets

$$\varepsilon_q = V - 2J\cos(q), \tag{2.9}$$

associated to the eigenvector

$$\phi_q(i) = \sqrt{\frac{2}{N+1}}\sin(qi), \tag{2.10}$$

with the quasi momentum $q_n = n\pi/(N+1) \in [0:\pi]$. In the rest of the chapter, the value of the hopping strength J will be set to $J = 1/2$, leading to a dispersion relation equal to $\varepsilon_k = V - \cos(q)$ and to a band width $\Delta = 2$.
From the dispersion relation, all the quasi energies ε_k are positives for $V > 1$ leading to the vacuum state $|0\rangle$ with a particle number $n_0 = 0$. On the contrary, if $V < -1$, all the excitations are negatives, and the system is in a Mott phase with a particle number equal to $n_0 = 1$ on each site. For intermediate values of the potential $-1 < V < 1$, the system is in a superfluid phase with a density given by

$$\rho_0 = \frac{q_F}{\pi}, \tag{2.11}$$

where q_F is the Fermi level associated to the Fermi energy fixed by the constraint $\sum_q \eta_q^\dagger \eta_q = N$ on the total number of particles.

2.2 Continuum limit and local equilibrium hypothesis

The behavior of the Hard Core bosonic system can be well understood by considering an hydrodynamical description, as already introduced in [CARK12, Col12],

based on a local equilibrium hypothesis. Here we briefly sketch the main features of this description [Col12].
Suppose an one dimensional bosonic system with lattice spacing $a \ll 1$. Using continuous variable $x = na$, one can split the real line into intervals $[x, x + \Delta x]$ with $\Delta x = aM$, where M is the number of sites. Suppose moreover that we keep the interval Δx small enough such that the potential keep an almost constant value over this interval, that is $V(ja) \approx V(x)\ \forall ja \in [x, x + \Delta x]$. Taking the continuums limit $a \to 0$ and $\Delta x \to 0$ keeping the ratio $\Delta x/a = M \gg 1$, the Hamiltonian can be rewritten,

$$\mathcal{H} = \int_{-\infty}^{\infty} dx \mathcal{H}(x), \tag{2.12}$$

with

$$\mathcal{H}(x) = \frac{1}{a\Delta x} \int_0^{\Delta x} dy \left[\frac{1}{2} \Psi^\dagger(x+y)\Psi(x+y-a) + H.c + \Psi^\dagger(x+y)V(x)\Psi(x+y) \right], \tag{2.13}$$

where we have introduced the creation and annihilation Fermi field operators $\Psi^\dagger(x)$ and $\Psi(x)$. This local Hamiltonian density can be diagonalized using the mapping

$$\Psi(x+y) = \int_0^{\pi} dq \Phi_q(x+y)\eta(x,q), \tag{2.14}$$

$$\Psi^\dagger(x+y) = \int_0^{\pi} dq \Phi_q(x+y)\eta^\dagger(x,q), \tag{2.15}$$

where the $\eta^\dagger(x,q)$ and $\eta(x,q)$, satisfying the anti commutation relation $\{\eta^\dagger(x,q), \eta(x',q')\} = \delta(q-q')\delta(x-x')$, respectively create and annihilate a particle with momentum q in the region $[x, x + \Delta x]$. The $\phi_q(u)$ entering into the mapping are the Bogoliubov functions, whose exact expression depends essentially on the boundary conditions. Using these field operators, the Hamiltonian is recast into the diagonal form

$$\mathcal{H} = \int_{-\infty}^{\infty} dx \int_0^{\pi} dq \left(V(x) - \cos q\right) \eta^\dagger(x,q)\eta(x,q). \tag{2.16}$$

The corresponding ground state is then given by adding to the vacuum state $|0\rangle$ all the quasi particles, starting from the lowest energy up to the Fermi level ε_F . In the grand canonical ensemble, where the number of particles can fluctuate, the Fermi level has to be set to $\varepsilon_F = 0$. Hence, the ground state is given by adding to the vacuum $|0\rangle$ the quasiparticles with negative energy

$$|GS\rangle = \prod_{V(x)-\cos q<0} \eta^\dagger(x,q)|0\rangle, \tag{2.17}$$

and the density profile is given by

$$\rho(x) = \begin{cases} 0 & \text{if } V(x) > 1 \\ \frac{1}{\pi}\arccos(V(x)) & \text{if } |V(x)| < 1 \\ 1 & \text{if } V(x) < -1 \end{cases}. \tag{2.18}$$

Now, introducing a region $\Delta x \Delta q$ around a point (x, q) of the phase space, we can define the coarse grained density

$$\rho(x,q) = \frac{1}{\Delta x \Delta q} \int_{x-\Delta x/2}^{x+\Delta x/2} \int_{q-\Delta q/2}^{q+\Delta q/2} |\Phi_p(y)|^2 dp dy, \tag{2.19}$$

and state that this coarse grained density is almost constant leading to an almost homogeneous distribution in the phase space

$$\rho(x,q) = \frac{1}{\pi}\Theta(q)\Theta(q_F - q)\Theta(-x)\Theta(x+A), \tag{2.20}$$

where $\Theta(x)$ is the Heaviside function, and $A < 0$ fix the spacial extension of the condensate. The spacial density profile is given by integrating the previous expression over the momentum

$$\rho(x) = \frac{q_F}{\pi}\Theta(-x)\Theta(x+A), \tag{2.21}$$

with $q_F = \arccos(V(x))$.

2.3 Initial states

In the following, we fix the initial state of the system with an harmonic trap. This harmonic potential $V(x)$ is parameterized like

$$V(x) = \alpha \left[x - \frac{A}{2}\right]^2 - \mu_0, \quad \alpha = \frac{4}{A^2}(1+\mu_0), \tag{2.22}$$

with $A < 0$ and $\mu_0 > -1$. This last form ensures that the bosons are loaded between positions $x = A$ and $x = 0$ with a condensate centered in $x = A/2$. Depending on the value of the parameters, two distinct situations are possible, controlled by μ_0 (see figure 2.1 for a pictural representation of the different cases).

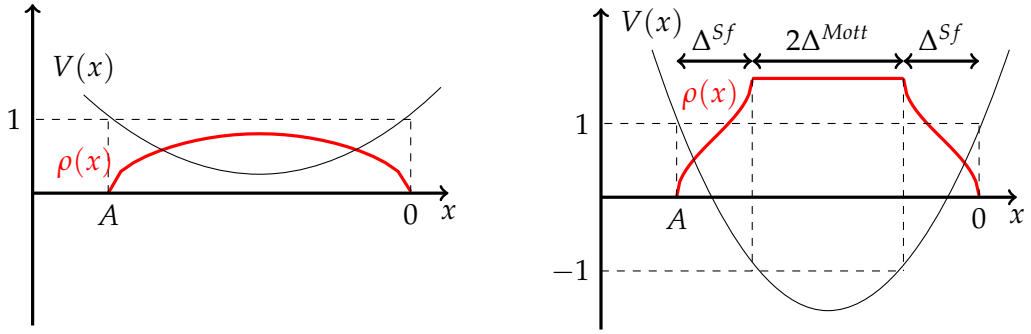

Figure 2.1 – *Two different possible initial states depending on the value of the parameter μ_0. On the left, μ_0 is smaller than 1, leading to a condensate initially completely in a superfluid phase. On the right, μ_0 is greater than 1, leading to a Mott phase of extension Δ^{Mott} surrounding by two superfluid phases of extension Δ^{Sf}.*

If μ_0<1, the potential $V(x)$ is never smaller than -1 and the full condensate is then in a superfluid phase. Integrating the phase space density, we get the following particle density

$$\rho_0(x) = \frac{\theta(x)\theta(x+A)}{\pi} \arccos(V(x)). \tag{2.23}$$

On the other hand, when $\mu_0 > 1$, it exists a spacial region where the potential is smaller than -1 leading to a Mott phase with $\rho_0 = 1$ surrounded by two superfluid phases. The Mott phase extends over the spacial region $x \in [\frac{A}{2} - \Delta^{Mott}, \frac{A}{2} + \Delta^{Mott}]$, where Δ^{Mott} is given by

$$\Delta^{Mott} = \frac{|A|}{2}\sqrt{\frac{\mu_0 - 1}{\mu_0 + 1}}, \tag{2.24}$$

and is surrounded by a superfluid phase of extension

$$\Delta^{Sf} = \frac{|A|}{2}\left(1 - \sqrt{\frac{1-\mu_0}{1+\mu_0}}\right), \tag{2.25}$$

with a density profile given by the equation 2.23. We plot in figure 2.2 the density profiles corresponding to a superfluid initial state (left) and a mixture Mott/superfluid initial state (right) for different values of μ_0. We see that the hydrodynamical predictions fit perfectly the numerical results obtained by exact diagonalization.

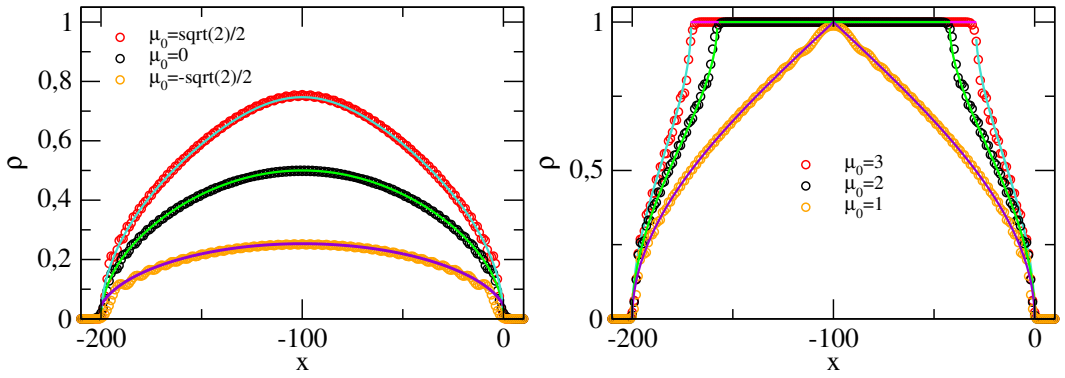

Figure 2.2 – *Initial density profiles for an initial state in the superfluid phase (left) and in a mixture Mott/superfluid (right) for different values of the parameter μ_0. The spacial extension of the condensate is $A = -200$. The hydrodynamical predications are given by the full lines whereas the dots represent the numerical data obtained by exact diagonalization.*

2.4 Dynamics after the sudden quench

The quantum quench is realized by suddenly changing the value of the trapping potential at $t = 0^+$, resulting in an out of equilibrium dynamics. Using the fact that the dynamics is unitary, and that all the quasiparticles are non interacting, they are emitted to the right and to the left on trajectories with constant energy.

2.4.1 Free expansion of the condensate

The first kind of quench we have considered is the sudden release of the trap at time $t = 0^+$, the potential passing from a non zero value to a vanishing one, i.e

$$\begin{aligned} V(x) &= \alpha\left[x - \frac{A}{2}\right]^2 - \mu_0 && \text{if } t < 0 \\ V(x) &= 0 && \text{if } t > 0. \end{aligned} \tag{2.26}$$

The Evolution of the density profile obtained numerically by exact diagonalization is shown in figure 2.3 for the two initial states presented above.

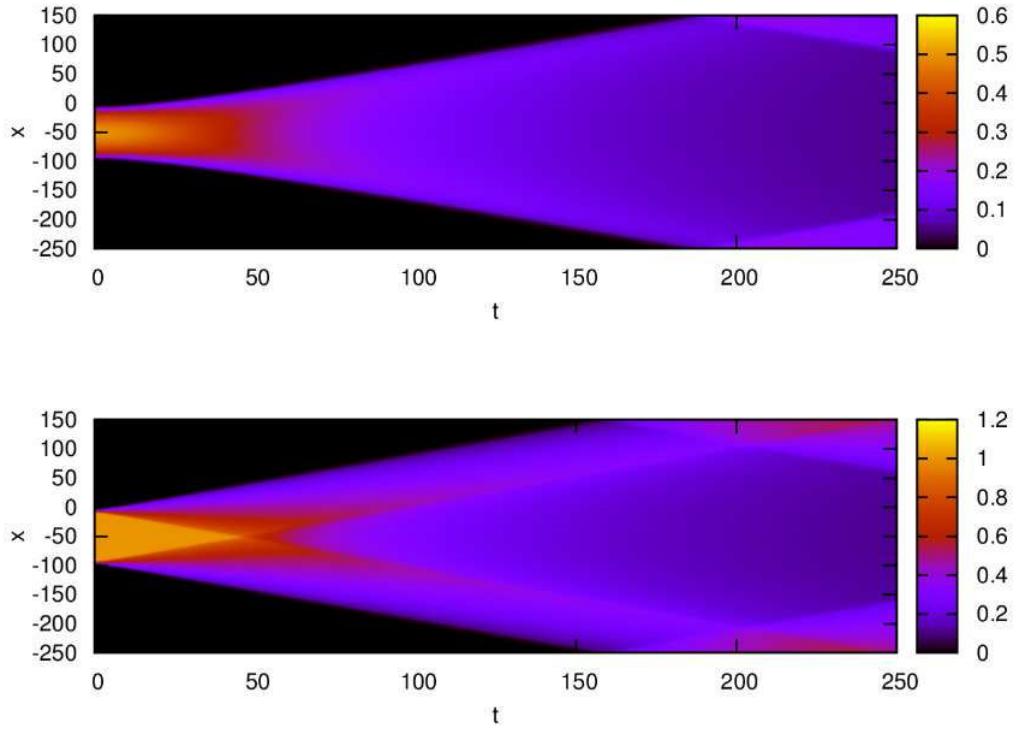

Figure 2.3 – *Evolution of the density profile obtained numerically by exact diagonalization. The up snapshot represents an initial condensate in a superfluid phase with $\mu_0 = 0$, whereas the down snapshot is for a initial state in a mixture Mott/superfluid with $\mu_0 = 3$. In both cases, the spacial extension of the condensate is $|A| = 100$.*

After the quench, the potential being zero, the condensate is allowed to explore spacial regions that were forbidden in the presence of the trapping potential. One can see that the condensate is spreading to the right and to the left over the whole lattice. Notice that since the numerical results are obtained with finite system size, the particles are reflected when they reach the two boundaries.

After the quench, the energy of the quasiparticles is simply given by the kinetic part

$$\varepsilon = -\cos(q) \quad \in [-1, 1]. \tag{2.27}$$

The movement of the quasiparticles being ballistic, their velocity is given by the derivative of the energy with respect to the momentum

$$v^{\pm} = \pm \left| \frac{\partial \varepsilon}{\partial q} \right|, \tag{2.28}$$

where the $+$ sign (resp. $-$) counts for the right (resp. left) movers. Using the expression 2.27 for the energy, we find that the velocity is given by

$$v_q^{\pm} = \pm\sqrt{1-\varepsilon^2} = \pm\sqrt{1-\cos^2 q}, \tag{2.29}$$

and depends only on the initial energy of the quasiparticles. Since the potential vanishes, the dynamics of the quasiparticles is free. As a consequence, a quasiparticle initially located at the point (x_0, q_0) at $t = 0$ will be at a latter time $t > 0$ moved at the point

$$x^{\pm}(x_0, q_0, t) = x_0 \pm t\sqrt{1-\varepsilon^2} = x_0 \pm t\sqrt{1-\cos^2 q_0}. \tag{2.30}$$

The density at a point (x, q) of the phase space associated to the right and left movers is given by [CARK12, Col12]

$$\rho^{\pm}(x, q, t) = \frac{1}{2\pi}\int_A^0 dx_0 \int_0^{q_F(x_0)} dq_0 \delta(x - x^{\pm}(x_0, q_0, t))\delta(q - q^{\pm}(x_0, q_0, t)). \tag{2.31}$$

In other words, we are looking in the initial distribution all the points (x_0, q_0) that will be at time t at the point (x, t) under the effect of the quench dynamics. The spacial density is simply given by integrating (2.31) over the momentum q, and we get

$$\rho^{\pm}(x, t) = \frac{1}{2\pi}\int_A^0 dx_0 \int_0^{q_F(x_0)} dq_0 \delta(x - x^{\pm}(x_0, q_0, t)). \tag{2.32}$$

The total density at a point x and time t is obtained by summing the right and left movers contributions

$$\rho(x, t) = \rho^{+}(x, t) + \rho^{-}(x, t). \tag{2.33}$$

We present on figure 2.4 the density profile for different times for the two types of initial states. The numerical evaluation of the integral (2.32) reproduce perfectly the exact diagonalization results.

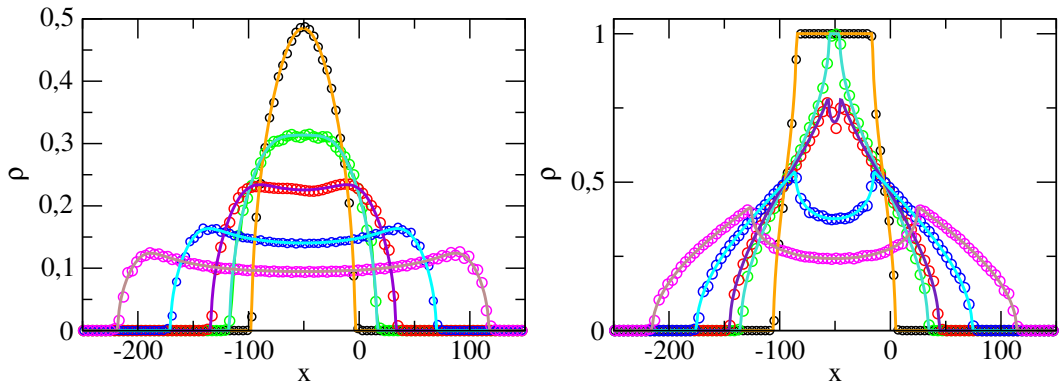

Figure 2.4 – *Density profile for different times. In the left plot, the condensate is initially in a superfluid phase with* $\mu_0 = 0$ *and the times are, from top to bottom* $t = 10$, $t = 40$, $t = 60$, $t = 100$ *and* $t = 150$. *In the right plot, the initial state is a mixture Mott/superfluid with* $\mu_0 = 3$ *and the times are, from top to bottom,* $t = 10$, $t = 40$, $t = 50$, $t = 80$ *and* $t = 120$. *In both case, we have* $|A| = 100$. *The numerical calculation of the expression (2.32) is given by the full lines, whereas the symbol are the exact diagonalization results.*

It is interesting to look at the number of particles N_t present in the initial trapping region of the condensate as a function of time. This number is obtained by integrating the density $\rho(x, t)$ between positions A and 0

$$N_t(t) = N_t^{+}(t) + N_t^{-}(t), \tag{2.34}$$

with

$$N_t^{\pm} = \frac{1}{2\pi}\int_A^0 dx \int_A^0 dx_0 \int_0^{q_F(x_0)} dq_0 \delta(x - x^{\pm}(x_0, q_0, t)). \tag{2.35}$$

The system possessing the mirror symmetry with respect to the middle of the condensate in the point $x = \frac{A}{2}$, the contributions associated to the right and left movers are equals, and $N_t^+ = N_t^-$. Using this symmetry and the properties of the delta function, one arrives at

$$N_t(t) = \frac{1}{\pi}\int_A^0 dx_0 \int_0^{q_F(x_0)} dq_0 \Pi_{[A:0]}(x^-(x_0, q_0, t)), \tag{2.36}$$

where $\Pi_{[a,b]}(x)$ is the door function defined by

$$\Pi_{[a,b]}(x) \quad = \quad \begin{cases} 1 & \text{if } x \in [a,b] \\ 0 & \text{if } x \notin [a,b]. \end{cases} \tag{2.37}$$

The dots in figure 2.5 represent, for the two initial states, the number of particles present in the initial trapped region as a function of time obtained by exact diagonalization, whereas the full lines give the hydrodynamical predictions using numerical evaluation of the integral (2.36). Interestingly, one can see, after a transient time where N_t is constant, two different regimes for an initial Mott/superfluid state, where the behavior is linear at the beginning of the evolution and turns to a power law after a time $t \approx |A|$, whereas the initial superfluid case presents only the second regime.

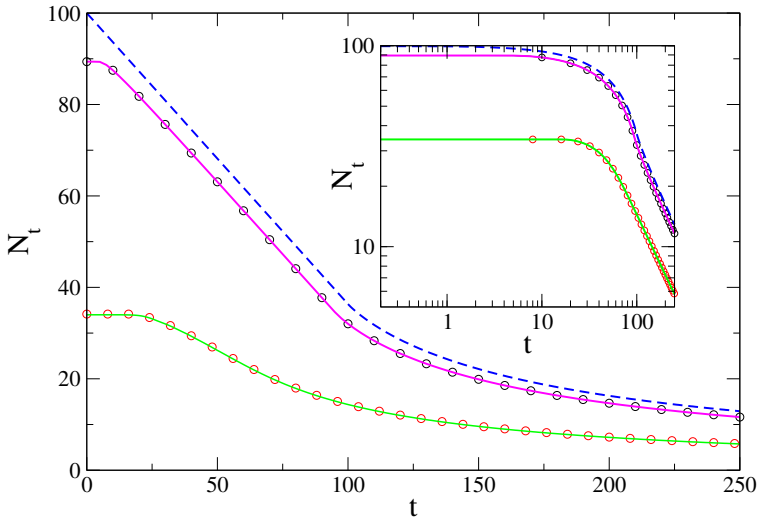

Figure 2.5 – *Number of particles N_t, present in the initial trapping region as a function of the time for an initial Mott/superfluid state (up curves) and an initial fully superfluid condensate (down curves). The dots are obtained with exact diagonalization, whereas the full lines give the hydrodynamical predictions using equation (2.56). The full blue line is the expression (2.41), corresponding to an initial state completely in a Mott phase (case $\mu \to \infty$). On the insert is shown the same plot in log scale.*

The analytical evaluation of the integral (2.36) is difficult for the two initial states, but we can nevertheless understand this change of behavior by considering the case $\mu_0 \to \infty$. This case corresponds to an initial state completely in a Mott phase with $q_0(x_0) = \pi \ \forall x_0$ and $\rho_0 = 1 \ \forall x_0$. In this case, the condition imposed by the door function in equation (2.36) is fulfilled for all $q_0 \in [0 : \pi]$ considering initial positions

$x_0 > A + t$. For values of $x_0 < A + t$, this condition is fulfilled in the interval $q_0 \in [0 : q^+(x_0, t)]$ and $q_0 \in [q^-(x_0, t) : \pi]$ where $q_0^\pm(x_0, t)$ are solutions of the equation $x^-(x_0, q_0, t) = A$ and given by

$$q_0^\pm(x_0, t) = \arccos\left(\pm\sqrt{1 - \frac{(x_0 - A)^2}{t^2}}\right). \tag{2.38}$$

The integral (2.36) can then be rewritten

$$N_t(t) = \frac{1}{\pi}\left(\int_A^{\tilde{x}(t)} dx_0 \left(\int_0^{q^+(x_0,t)} dq_0 + \int_{q^-(x_0,t)}^{\pi} dq_0\right) + \Theta(|A| - t)\int_{\tilde{x}(t)}^{0} dx_0 \int_0^{\pi} dq_0\right), \tag{2.39}$$

where $\tilde{x}(t) = (A + t)\Theta(|A| - t)$. Using the property $\arccos(x) + \arccos(-x) = \pi$ of the arccosinus function, one arrives to

$$N_t(t) = \frac{1}{\pi}\int_A^{\tilde{x}(t)} dx_0 2\arccos\left(\sqrt{1 - \frac{(x_0 - A)^2}{t^2}}\right) - \Theta(|A| - t)(A + t). \tag{2.40}$$

Performing the integral, we finally find

$$\begin{aligned} N_t(t) = &- A - \frac{2}{\pi}t\,\Theta(|A| - t) \\ &+ \left(-A + \frac{2A}{\pi}\left(\arctan\left(\sqrt{\frac{t^2}{A^2} - 1}\right) - t + \sqrt{t^2 - A^2}\right)\right)\Theta(t - |A|), \end{aligned} \tag{2.41}$$

which behaves, for $t \to \infty$, like $N_t(t) \sim 1/t$. We recover here the linear behavior for $t < |A|$ and the power law decay for $t > |A|$. The expression (2.41) is plotted in dashed line in figure 2.5, and we can see that the slope in the linear regime and the exponent in the power law decay are the same in the pure Mott and mixture Mott/superfluid cases.

2.4.2 Self Trapping with a linear potential

In this section, we turn to the second quench considered in this study. Starting from the two initial states mentioned previously, the trapping potential is suddenly released at time $t = 0^+$ and a linear ramp of equation

$$V(x, t > 0) = -Fx\,\Theta(-x) \tag{2.42}$$

is loaded in the negative part of the x axe. Just after the quench, the energy of a particle in position x is shifted by the quantity $-Fx$, as shown in the figure 2.6 where we present a pictural representation of the energy band of a Mott/superfluid initial state just after the loading of the ramp.
Like in the previous case treated, the sudden quench leads to an out-of-equilibrium unitary dynamics, whose main features are perfectly caught by the hydrodynamical theory developed above. We present in figure 2.7 the dynamics of the density profile just after the quench for the two initial states and for different forces of the linear potential. One can see from this picture that the initial condensate is splitting into

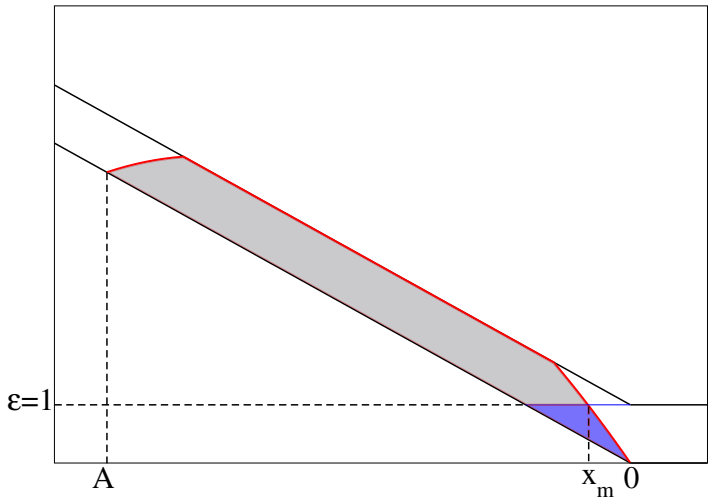

Figure 2.6 – *The particles in the blue region leave the trap. The position x_m corresponds to the most right position of the initial condensate with energy $\varepsilon = 1$.*

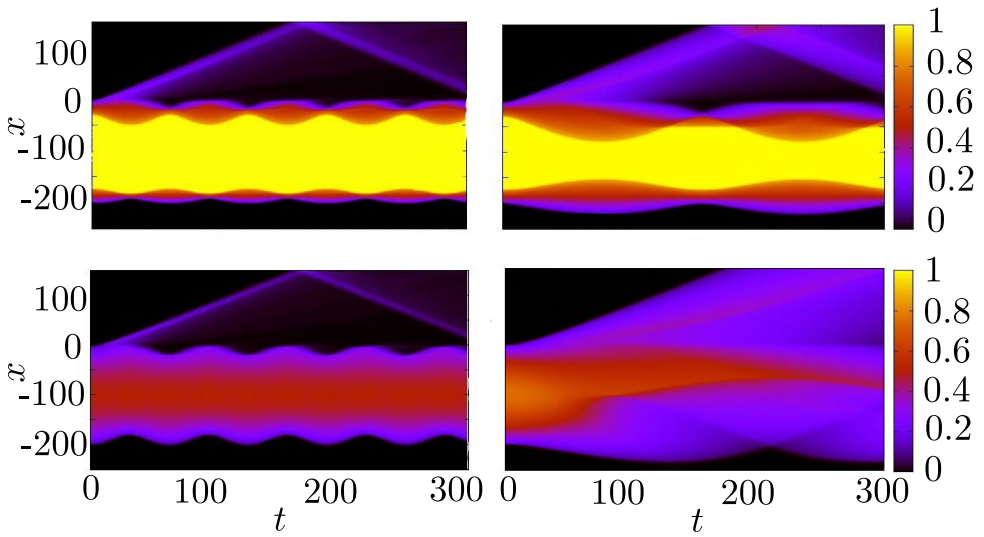

Figure 2.7 – *Snapshot of the time evolution of the density profile obtained numerically by exact diagonalization starting from the two initial states and for different forces. Up/left: Mott/superfluid state with $\mu_0 = 3$ and $F = 0.1$, top/right: Mott/superfluid state with $\mu_0 = 3$ and $F = 0.04$, bottom/left: superfluid state with $\mu_0 = 0$ and $F = 0.1$, and bottom/right: superfluid state with $\mu_0 = \sqrt{2}/2$ and $F = 0.015$. For all cases, we set $|A| = 200$.*

two parts: a first part of the condensate leaves the initial region and spreads in time toward the right of the x axis, whereas a second part stays trapped into the region $x \in [A, 0]$ and performs Bloch oscillations. Note that like in the previous case, the escaping particles are reflected into the right boundary since the system is numerically finite.

The reason why a part of the condensate escapes the initial region can be understood

in the following way: the particles with an energy in the range $\varepsilon \in [-1,1]$ are connected with the propagative band starting at position $x = 0$ with zero potential, and then can escape toward the right side of the system. On the contrary, particles with an energy higher than $\varepsilon = 1$ stay trapped inside the initial region due to the energy conservation.

The number of escaping particles N_{esc} is then given by summing all the particles with an energy ε between -1 and 1 in the initial density distribution. Using energy variable, it yields

$$N_{esc} = \frac{1}{F\pi}\int_{-1}^{1} d\varepsilon \int_{\mathcal{Q}(\varepsilon)} dq_0, \tag{2.43}$$

where $\mathcal{Q}(\varepsilon)$ is the integration contour shown in blue in figure 2.6. In particular, if the most energetic locus of the initial distribution has an energy smaller than $\varepsilon = 1$, the region connected to the propagative band covers the complete condensate, and, as a consequence, $N_{esc} = N$, meaning that all the particles are living the trap and are escaping to the right. Of course, if the system is initially in a Mott/superfluid state, the highest energy is always $\varepsilon = 1$ and then the only value of the force leading to $N_{esc} = N$ is $F = 0$. On the contrary, if the system is in a pure superfluid state, the most energetic point just after the quench is given by the solution of the equation $\partial\varepsilon/\partial x = 0$, that is

$$x_{max} = \begin{cases} \frac{A}{2} - \frac{FA^2}{8(1+\mu_0)} & \text{if } F < F_2, \\ A & \text{if } F > F_2, \end{cases} \tag{2.44}$$

where $F_2 = -\frac{4}{A}(1+\mu_0)$ is the force making the most energetic point located in $x = A$. The force below which all the particles escape has then to fulfill the equation $-Fx_{max} - \cos q_F(x_{max}) = 1$. We finally find the values

$$F_{esc}^{M/sf} = 0 \tag{2.45}$$

$$F_{esc}^{Sf} = \begin{cases} \frac{4}{A}(1+\mu_0)\left(1-\sqrt{\frac{2}{\mu_0+1}}\right) & \text{if } F < F_2 \\ -\frac{2}{A} & \text{if } F > F_2. \end{cases} \tag{2.46}$$

We plot in figure 2.8 N_{esc} as a function of the force F obtained numerically for the two initial states and for several values of μ_0. As predicted, we see that N_{esc} is constant to N for forces smaller than F_{esc}. Once this force crossed, the number of escaping particles decreases when the force is increased. We find a power law $N_{esc} \propto F^{\gamma}$ where the exponent γ increases with the value of μ_0 until a saturation value $\gamma = 1$ for $\mu_0 \to \infty$. Indeed, in this case, the spacial extension of the superfluid phase tends to zero, and the system is initially in a fully Mott phase, leading to the behavior $N_{esc} \propto \frac{1}{F}$ found in [Col12, CARK12].

2.4.2.1 Dynamics of the trapped particles

We focus in a first time our attention on the dynamics of the trapped particles. These particles with energy $\varepsilon > 1$ perform Bloch oscillations due to the constant force F acting on them.
For an initial Mott/superfluid state, one observes two oscillatory regions, located at

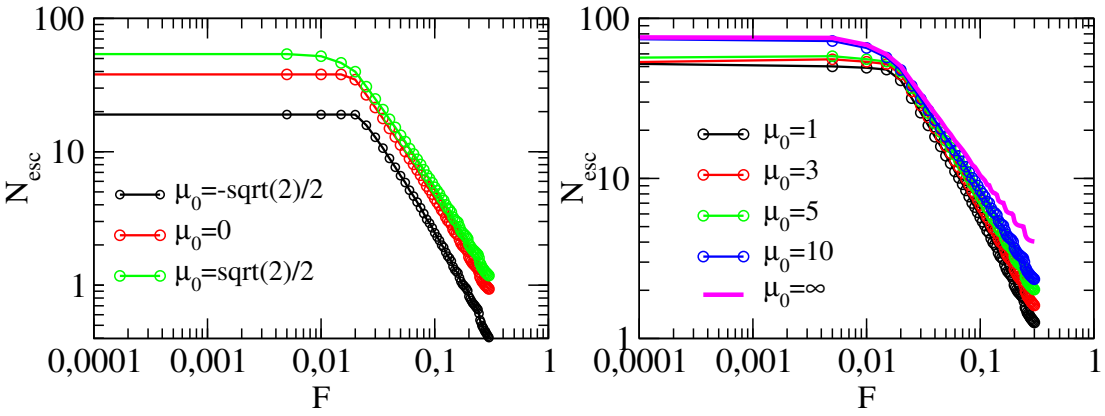

Figure 2.8 – *Number of escaping particles N_{esc} as a function of the force F for different values of μ_0. The system is initially in a pure superfluid state in the left plot, whereas it is in a Mott/Superfluid mixture on the right one. The full pink line represents the case of $\mu_0 = \infty$, corresponding to a condensate initially in a fully Mott phase.*

the two edges, surrounding a plateau region where the density stays constant and equal to the initial value of the Mott phase $\rho_0 = 1$. We can also note different regimes of oscillations, depending of the value of the applied force. Indeed, by looking figure 2.7, we can see that at high forces, the two regions surrounding the plateau oscillate in phase, in the sense that they start to move both to the right. On the contrary, at lower forces, these two regions oscillate in opposite direction, the left side of the plateau starting to move to the left, and the right side to the right, leading to a breathing regime.
When the initial state is fully superfluid, the oscillations concern now the complete condensate. The distinction between high and low force discussed above still holds for this initial state. Indeed, for high forces, all the condensate oscillates as whole whereas at low forces, it splits into two parts, one part starting to move to the left and the other one to the right.
One can finally note that, for both initial states and at low forces, the leftmost locus of the condensate can explore spacial region located at the left of the position $x = A$ delimiting the initial position of the condensate. All these last features can be explained by to the hydrodynamical theory, as we will now see.

The dynamics being unitary, the particles evolve along trajectories of constant energy. We then obtain

$$\frac{d\varepsilon}{dt} = \frac{d}{dt}\left(V(x) - \cos q\right) = 0, \tag{2.47}$$

giving

$$-F\frac{dx}{dt} + \frac{dq}{dt}\sin q = 0. \tag{2.48}$$

Using the expression (2.28) of the velocity

$$v^{\pm} = \pm\left|\frac{\partial\varepsilon}{\partial q}\right| = \pm\sin q, \tag{2.49}$$

we find

$$\pm F + \frac{dq}{dt} = 0, \tag{2.50}$$

leading, after integration, to the evolution equation of the momentum $q^{\pm}(t)$

$$q^{\pm}(t) = \pm q_0 + Ft. \tag{2.51}$$

This last equation describes the conversion of the potential energy $V(x)$ into kinetic one $-\cos q(t)$. We remind that the density corresponding to the right and left movers is given at a time t by

$$\rho^{\pm}(x,q,t) = \frac{1}{2\pi}\int_A^0 dx_0 \int_0^{q_F(x_0)} dq_0 \delta(x - x^{\pm}(x_0,q_0,t))\delta(q - q^{\pm}(x_0,q_0,t)), \tag{2.52}$$

and the spacial density by the integration over the momentum q:

$$\rho^{\pm}(x,t) = \frac{1}{2\pi}\int_A^0 dx_0 \int_0^{q_F(x_0)} dq_0 \delta(x - x^{\pm}(x_0,q_0,t)). \tag{2.53}$$

Now, we use the fact that

$$dx_0 \delta(x - x^{\pm}(x_0,q_0,t)) = -\frac{1}{F} d\varepsilon \delta(x - x^{\pm}(\varepsilon,q_0,t)) \tag{2.54}$$

with

$$x^{\pm}(\varepsilon,q_0,t) = -\frac{1}{F}(\varepsilon + \cos(\pm q_0 + Ft)) \tag{2.55}$$

together with the energy at the initial time $\varepsilon = -Fx_0 - \cos(q_0)$, and we find that the right and left densities can be rewritten

$$\rho^{\pm}(x,t) = \frac{1}{2\pi}\int_0^{\pi} dq_0 \int dx_0 \delta(x_0 - g^{\pm}(x,q_0,t)) \tag{2.56}$$

where the function $g^{\pm}(x,q_0,t)$ is given by

$$g^{\pm}(x,q_0,t) = x - \frac{1}{F}\left[\cos(q_0) - \cos(\pm q_0 + Ft)\right]. \tag{2.57}$$

Finally, performing the integration, we get the expression

$$\rho^{\pm}(x,t) = \frac{1}{2\pi}\int_{q_{inf}}^{\pi} dq_0 \Pi_{[f_2(q_0),f_1(q_0)]}(g^{\pm}(x,q_0,t)), \tag{2.58}$$

where we have used to properties of the delta distribution, and the functions $f_1(q_0)$ and $f_2(q_0)$ are respectively given by

$$f_1(q) = \begin{cases} -\dfrac{1+\cos q_0}{F} & q_0 \in [q_{inf}, \tilde{q_0}] \\ \dfrac{A}{2} + \sqrt{\dfrac{\cos q_0 + \mu_0}{\alpha}} & q_0 \in [\tilde{q_0}, \pi] \end{cases} \tag{2.59}$$

$$f_2(q) = \frac{A}{2} - \sqrt{\frac{\cos q_0 + \mu_0}{\alpha}} \tag{2.60}$$

with $\tilde{q}_0$ satisfying the equation $-Fx_m + \cos\tilde{q}_0 = 1$ where x_m is the rightmost locus of the condensate with energy $\varepsilon = 1$ (see figure 2.6), and the lower bound q_{inf} of the integral is equal to

$$q_{inf} = \begin{cases} 0 & \text{if } F > -\frac{2}{A} \\ \arccos(1 - Fx^*) & \text{if } F < -\frac{2}{A}. \end{cases} \tag{2.61}$$

The reason why the expression on the function $f_1(q_0)$ depends of the range of q_0 is to take into account the escaping particles. Indeed, these particles have left the trap by the propagating band, and then they do not contribute to the oscillating behavior. It is then necessary to remove them from the initial density profile when the integration is performed.

In figures 2.9 and 2.10, we plot the time evolution of the density profile of the self trapped particles over a half period of oscillations for the two initial states Mott/superfluid and superfluid, both numerical (full lines) and theoretical (dashed lines), together with a pictural representation of the energy band just after the quench. The first observation that can be made is that the hydrodynamical predictions perfectly reproduce the oscillatory behavior of the density profile. Secondly, the different oscillatory regimes corresponding to low and high forces are clearly visible for the two kinds of initial states. We can also see that the condensate extents beyond the position $x = A$ in the low forces case. The key point to understand these features is to look at the position of the most energetic locus of the condensate x_{max}. We find

$$x_{max}^{M/sf} = \begin{cases} \dfrac{A}{2}\left(1 - \sqrt{\dfrac{\mu_0 - 1}{\mu_0 + 1}}\right) & \text{if } F < F_1 = -\dfrac{4}{A}\sqrt{\mu_0^2 - 1} \\ \dfrac{A}{2} - \dfrac{FA^2}{8(1+\mu_0)} & \text{if } F_1 < F < F_2 \\ A & \text{if } F > F_2 \end{cases} \tag{2.62}$$

for the case of a initial Mott/superfluid state, and

$$x_{max}^{sf} = \begin{cases} \dfrac{A}{2} - \dfrac{FA^2}{8(1+\mu_0)} & \text{if } F < F_2 \\ A & \text{if } F > F_2 \end{cases} \tag{2.63}$$

for a fully superfluid initial state. Here, F_1 is the force making the most energetic position in the separating position $x = x_{[M-Sf]}$ between Mott and superfluid phases. If the most energetic position is located at $x_{max} > A$, i.e for forces $F < F_2$, the condensate can explore spacial region on the left of the point $x = A$ thanks to the unitary evolution. The leftmost location of the condensate may extend until the position x_L (see down plot of figure 2.9) defined by the equation

$$-Fx_L - 1 = -Fx_{max} - \cos(q_F(x_{max})), \tag{2.64}$$

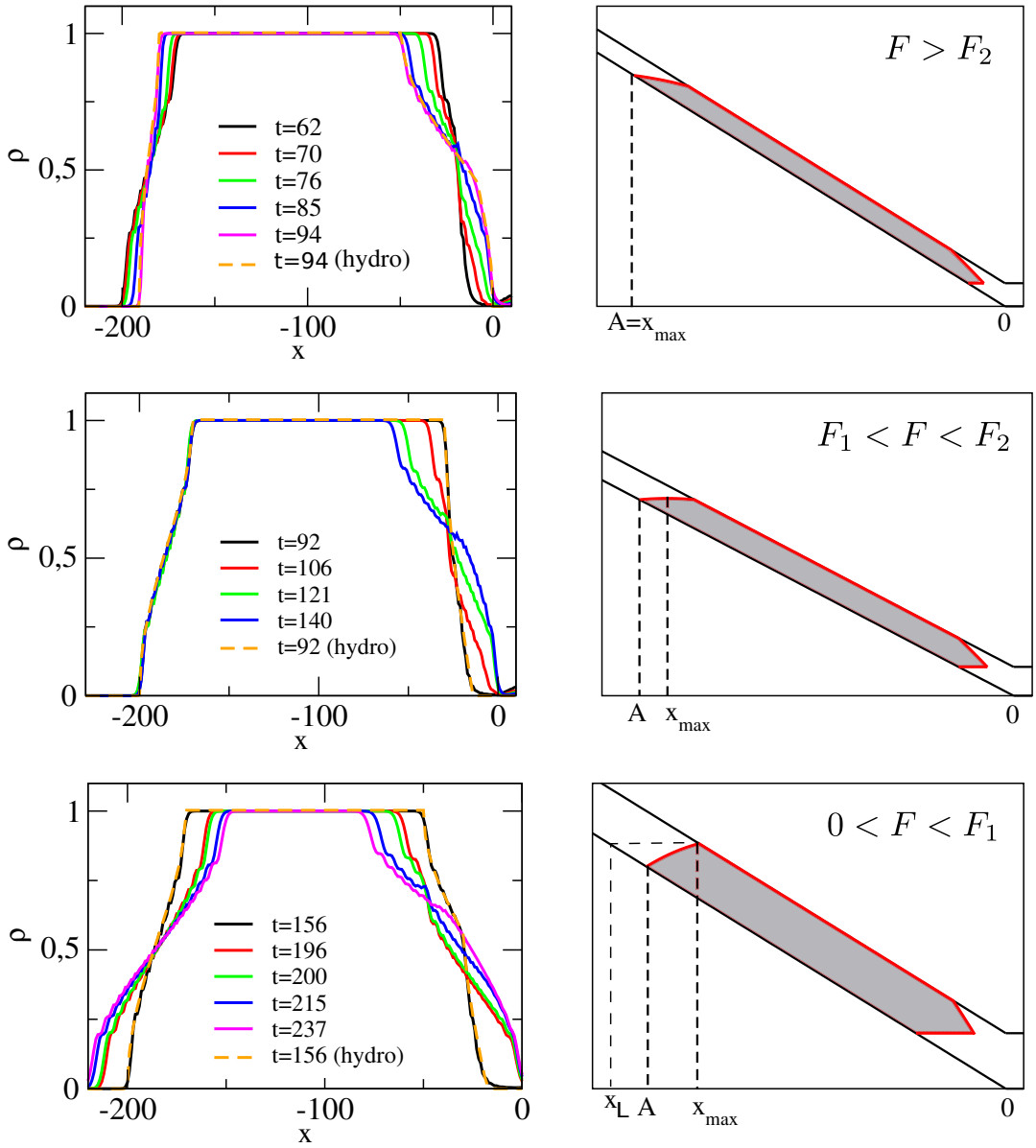

Figure 2.9 – *Top: Self-trapped density profile for an initial SF-Mott state with* $\mu_0 = 3$ *at different times for* $F = 0.1$. *Middle: Same as top for* $F = 0.068$.. *Down: Same as top for* $F = 0.04$. *In each cases, we set* $A = -200$, *and the hydrodynamical predictions are represented in each case by the orange dashed lines.*

giving

$$x_L^{M/sf} = \begin{cases} \dfrac{A}{2}\left(1 - \sqrt{\dfrac{\mu_0 - 1}{\mu_0 + 1}}\right) - \dfrac{2}{F} & \text{if } 0 < F < F_1 \\ \dfrac{A}{2} - \dfrac{FA^2}{16(1+\mu_0)} - \dfrac{1+\mu_0}{F} & \text{if } F_1 < F < F_2 \end{cases} \tag{2.65}$$

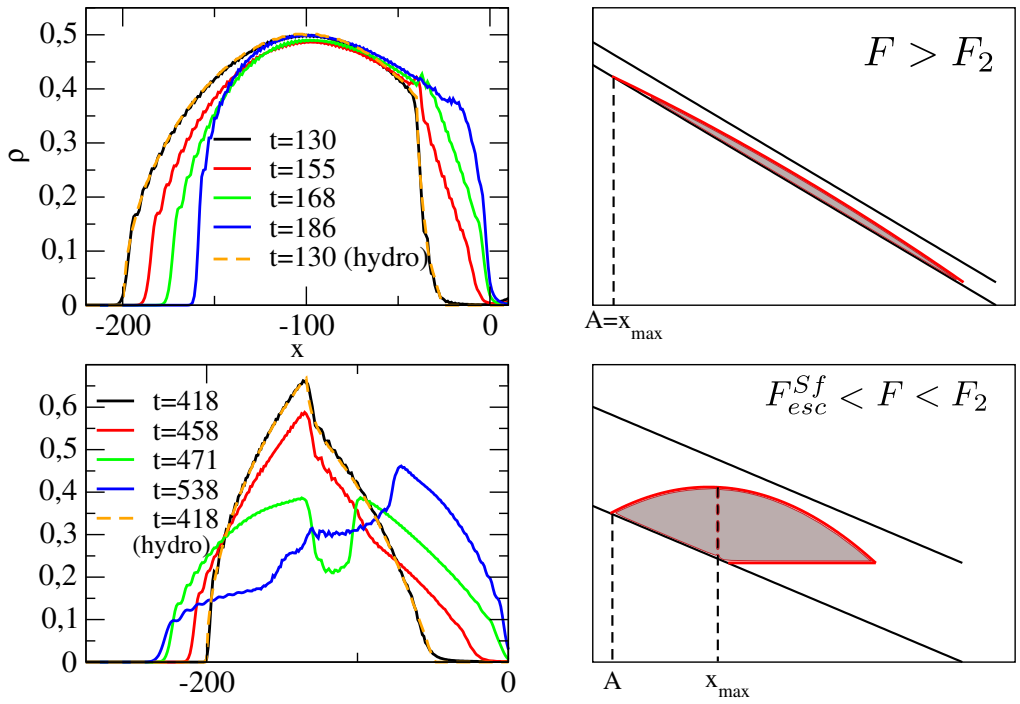

Figure 2.10 – *Top: Self-trapped density profile for an initial superfluid state with* $\mu_0 = 0$ *at different times for* $F = 0.01$*. Down: Same as top for* $\mu_0 = \sqrt{2}/2$ *and* $F = 0.015$*. In each cases, we set* $A = -200$*, and the hydrodynamical predictions are represented in each case by the orange dashed lines.*

and

$$x_L^{sf} = \frac{A}{2} - \frac{FA^2}{16(1+\mu_0)} - \frac{1+\mu_0}{F} \quad \text{if } F_{esc}^{Sf} < F < F_2. \tag{2.66}$$

In this range of forces, the energy of the point x_{max} is greater than the energy of the point $x = A$. As a consequence, there is accessible region on the left and on the right of the point $x = x_{max}$ (see for instance down plot of figure 2.10), and the trapped density of the initial superfluid condensate splits into two parts, one starts to move to the left, whereas the other one starts to move to the right. This dynamics will be called the *splitting regime*. For an initial Mott/superfluid state, one has to make the distinction between the two force regimes $F < F_1$ and $F_1 < F < F_2$. Indeed, in the first case, the most energetic point is the separating point $x_{[M-sf]}$ between the Mott and superfluid phase, and is then located on the right tilted edge (see down plot in figure 2.9). Therefore, the part of the condensate located on the left of the plateau starts to move to the left whereas the right side of the plateau starts to move to the right, leading to a *breathing regime*. In the other case $F_1 < F < F_2$, one recovers the splitting

regime but only in the region on the left of the plateau. Indeed, this part of the initial condensate splits into two parts moving in opposite direction, whereas the movement of the right side is unchanged. We can note that in this case, the oscillations in the left part of the condensate are weak. This feature is due to the fact that the energy in the three points $x = A$, $x = x_{max}$ and $x = x_{[M-sf]}$ are close to each other, and then the part of the condensate participating to the oscillation is small, leading to almost no oscillations.
In the strong forces regime $F > F_2$, the most energetic point is $x_{max} = A$ and is then located on the left tilde band. In this case, and whatever the initial state, the condensate *oscillates in phase*. Indeed, in the superfluid case, the condensate oscillates as a whole, and in the Mott/superfluid case, the two sides of the plateau move in the same direction at a given time. Note finally that the two boundaries x_{p1} and x_{p2} of this plateau are also force dependent, and given by

$$x_{p1} = \begin{cases} A + \frac{2}{F} & \text{if } F < F_2 \\ \frac{A}{2}\left(1 + \sqrt{\frac{\mu_0 - 1}{\mu_0 + 1}}\right) & \text{if } F > F_2 \end{cases} \tag{2.67}$$

$$x_{p2} = \frac{A}{2}\left(1 - \sqrt{\frac{\mu_0 - 1}{\mu_0 + 1}}\right) - \frac{2}{F}. \tag{2.68}$$

The oscillatory behavior of the density profile is associated to a flow of particles giving rise to a current density $j(x,t)$. This current is defined through the continuity equation

$$\frac{dn_k}{dt} = -i[H, n_k] = -\nabla j_k = j_{k-1} - j_k, \tag{2.69}$$

where n_k is the occupation number at site k. The explicit calculation of the commutator gives

$$j_k = \frac{1}{2}\left(c_k^\dagger c_{k+1} - c_{k+1}^\dagger c_k\right), \tag{2.70}$$

and its average reads

$$\langle j_k \rangle = -\mathrm{Im}\left(\langle c_k c_{k+1}^\dagger \rangle\right). \tag{2.71}$$

We present in figure 2.11 snapshots of the time evolution of the current profile, obtained numerically, for a superfluid initial state, and for a Mott/superfluid initial state at different forces.
In all the cases, we clearly see the oscillatory behavior of the particles in the trapped region. For an initial superfluid state at high forces, we observe a strip structure of the oscillations showing that all the condensate is oscillating as a whole, as already observed in the density profile. For low forces, there are two regions in the trapped profile of opposite sign current at the beginning of the evolution, indicating movement in opposite direction (see second plot of figure 2.11). In the Mott/superfluid case, the current vanishes in the plateau region $x \in [x_{p1}, x_{p2}]$ where the density stays constant at the initial value $\rho_0 = 1$ and where no oscillations of the density is observed. At high forces $F > F_2$, the two sides of the condensate oscillate in phase, and the sign of the current is the same on both sides of the plateau at a given time, whereas at low forces $F < F_1$, the two sides surrounding the plateau

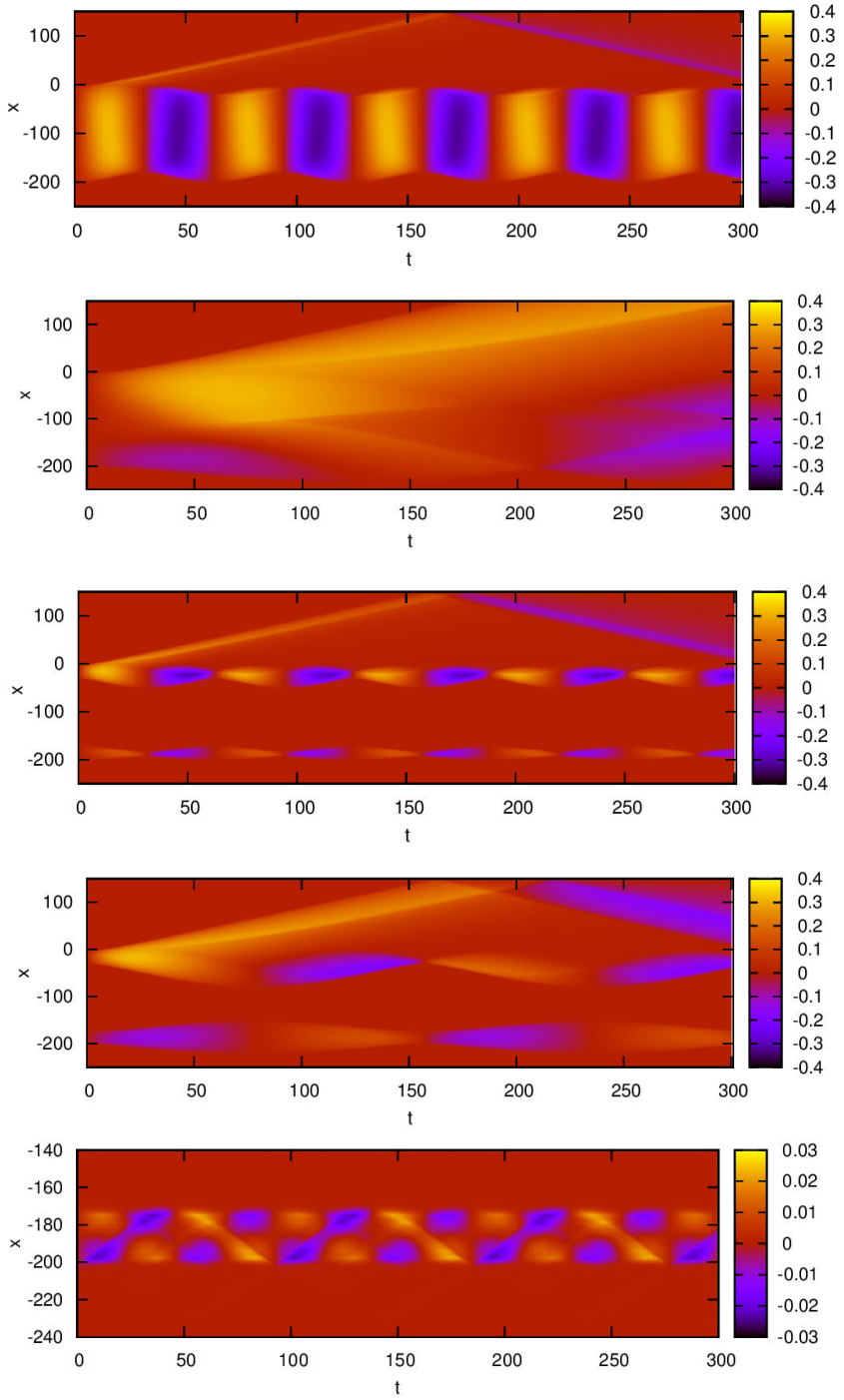

Figure 2.11 – *Snapshot of the time evolution of the current density profile. In the two first plots starting from the top the initial states are superfluid with* $\mu_0 = 0$ *and* $F = 0.1$ *and* $\mu_0 = \sqrt{2}/2$ *and* $F = 0.015$ *respectively. In the two following, the initial states are a Mott/superfluid mixture with* $\mu_0 = 3$ *and* $F = 0.1$ *and* $F = 0.04$ *respectively. The last plot is a zoom in the left part of the plateau for a Mott/superfluid initial state with* $\mu_0 = 3$ *and* $F = 0.068$*. In the three cases,* $A = -200$*.*

oscillate in opposite direction leading to current of opposite sign at a given time. For intermediate forces $F_1 < F < F_2$, we see the perfect alternation of currents with different sign on both sides of the middle of the superfluid phase reflecting the splitting regime taking place on the left side of the plateau (see last plot of figure 2.11).

In the framework of the hydrodynamical theory, the current density is obtained by summing the current contributions of all the particles $j(q) = \rho(q)v(q)$ with velocities $v^{\pm}(q) = \pm\sin(\pm q_0 + Ft)$. Then the current is given by adding a factor $\pm\sin(\pm q_0 + Ft)$ to the integral (2.56), leading to

$$\begin{aligned} j(x,t) = &\int_{q_{inf}}^{\pi} \frac{dq_0}{2\pi} \sin(q_0 + Ft)\Pi_{[f_2(q_0),f_1(q_0)]}(g^+(x,q_0,t)) \\ &- \int_{q_{inf}}^{\pi} \frac{dq_0}{2\pi} \sin(q_0 - Ft)\Pi_{[f_2(q_0),f_1(q_0)]}(g^-(x,q_0,t)) \ . \end{aligned} \tag{2.72}$$

We plot in figure 2.12 the behavior of the current for different situations.
The hydrodynamical predictions fit perfectly the numerical data for all the plots except the case of a initial superfluid state at low forces where the curves are different at the beginning of the evolution. The reason for that comes from the escaping particles. Indeed, in the theoretical development, these particles are removed from the initial density profile in order to not take them into account during the Bloch oscillations of the trapped particles. Because the force is small, some of the escaping particles contribute to the current until they leave the trap. Once these particles far in the right region (at $t \approx 200$), the predictions match the numerical data.
We can remark a perfect sinusoidal time evolution in the middle of the condensate $x = A/2$ in the case of a initial pure superfluid state. In this case, the condition given by the door function in equation (2.72) is fulfilled for $q_0 \in [0 : \pi/2]$ leading to

$$\begin{aligned} j^{SF}(A/2,t) =& \frac{1}{2\pi}\int_0^{\pi/2} dq_0 \left(\sin(q_0 + Ft) - \sin(q_0 - Ft)\right) \\ =& \frac{1}{\pi}\sin(Ft) \end{aligned} \tag{2.73}$$

On the contrary, for a Mott/superfluid, the middle of the condensate is located in the plateau region and the condition is always fulfilled, leading to a vanishing current.

Finally, on figure 2.13 we resume all the different features we have observed previously in a phase diagram in the $(F|A|, \mu_0)$ plan.

2.4.2.2 Dynamics of the escaping particles

Here we describe the dynamics of the escaping particles. We remind that these particles are those with an energy $\varepsilon \in [-1, 1]$, and that the evolution equation leads to a drift of the momentum according to $q^{\pm}(t) = q_0 \pm Ft$. The right movers moving to the right, they will leave directly the trap, whereas the left movers will be first reflected on the left tilde band edge before escaping. When a particle reaches the position $x = 0$, all the potential energy has been converted into kinetic one, and the dynamics becomes free, like in the case treated in section 2.4.1. If we call $t^{\pm}$ the time

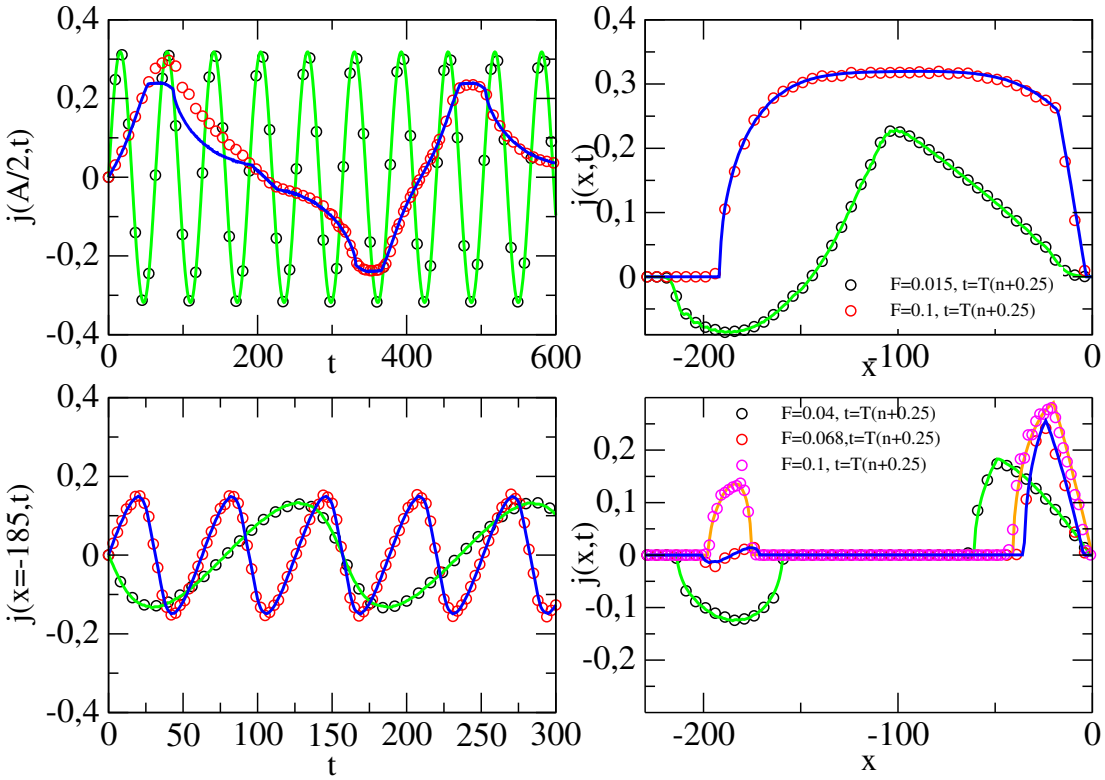

Figure 2.12 – *(Top) Current in a initial superfluid state as a function of the time (left) in the middle of the condensate in two different cases ($\mu_0 = 0$ and $F = 0.1$ in black dots and $\mu_0 = \sqrt{2}/2$ and $F = 0.015$ in red ones) and as a function of the position (right) at quarter of the period T for two different forces corresponding to the different oscillations regime. (Bottom) Current in a initial mixture Mott/superfluid as a function of the time (left) at position $x = -185$ (corresponding to the middle of the left superfluid phase) for two forces ($F = 0.04$ in black dots and $F = 0.1$ in red ones) and as a function of the position (right) at quarter of the period T for three different forces corresponding to the different oscillations regimes. The dots are the numerical data obtained by exact diagonalization, and the full lines are the predictions given by the integral (2.72).*

needed for a particle to reach the position $x^{\pm} = 0$, we find that $t^{\pm}$ is equal, thanks to equation (2.55), to

$$t^{\pm} = \frac{1}{F}\left(\mp q_0 + \arccos(-\epsilon)\right). \tag{2.74}$$

The potential being zero in the region $x > 0$, we then find

$$x^{\pm} = \sqrt{1-\varepsilon^2}(t - t^{\pm}), \tag{2.75}$$

that can be rewritten as a function of x_0 and q_0 like

$$x^{\pm}(x_0, q_0, t) = \sqrt{1-(Fx_0 + \cos q_0)^2}\left(t - \frac{1}{F}\left(\mp q_0 + \arccos(Fx_0 + \cos q_0)\right)\right). \tag{2.76}$$

The density is then given by $\rho_{esc}(x,t) = \rho^{+}_{esc}(x,t) + \rho^{-}_{esc}(x,t)$, where the right and left contributions are given by, using energy variable

$$\rho^{\pm}_{esc}(x,t) = \int_{-1}^{1} \frac{d\varepsilon}{F} \int_{\mathcal{Q}(\varepsilon)} \frac{dq_0}{2\pi} \delta(x - x^{\pm}(\varepsilon, q_0, t)), \tag{2.77}$$

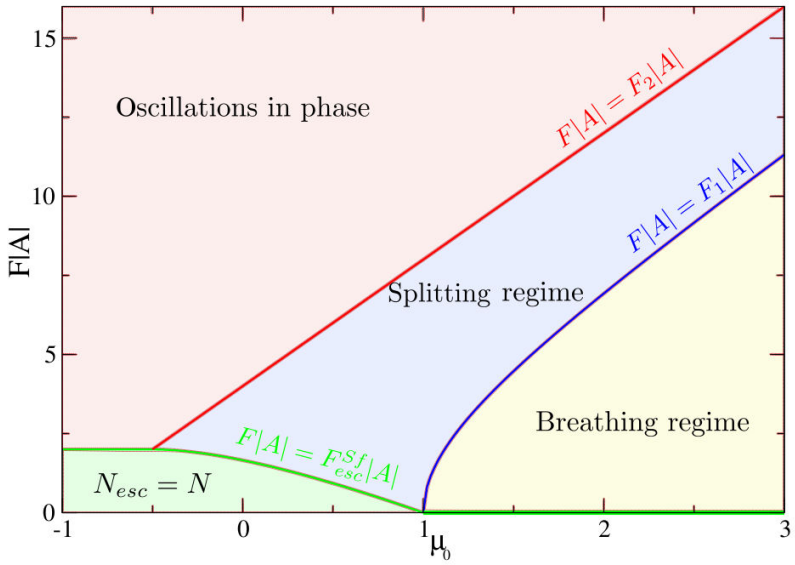

Figure 2.13 – *Phase diagram showing the different behaviors of the trapped part of the condensate in the* $(F|A|, \mu_0)$ *plan. In the green region, all the particles are leaving the trap because the most energetic point has an energy smaller than* $\varepsilon = 1$*. In the red region, the condensate oscillates in phase, the most energetic point is the left-most locus* $x_{max} = A$*. In the blue region, the position of the most energetic point is force dependent, and the splitting dynamics takes place. Finally, in the yellow region, concerning only the Mott/superfluid case, the condensate oscillates with a breathing regime where the left and right sides of the plateau start to move in opposite direction.*

and the integration domain $\mathcal{Q}(\varepsilon)$ is represented in dashed blue in figure 2.6. We show in figure 2.14 the comparison of the escaping density at different times between numerical exact diagonalization and hydrodynamical predictions given by equation (2.77). We see a good agreement between the hydrodynamical predictions and numerical results, up to interferences which disappear in the continuum limit.
It is interesting to note that the right propagating front of the escaping density profile has a stair like structure (the phenomenon is well observable for time $t = 156$ in figure 2.14). The integration of the density over each stair being equal to 1, they represent an ejected particle moving ballistically with a velocity $v(\varepsilon) = \sqrt{1-\varepsilon^2}$. Note that this stair like structure of propagating front has already been observed in different contexts [HRS04, PK05].

2.4.2.3 Entanglement dynamics

As we saw previously, the quench will have for consequence the splitting of the initial condensate into an escaping part and a trapped one. It results from the correlations presents in the initial state an entanglement between these two parts. This entanglement between escaping particles and trapped ones is quantified by the entanglement entropy introduced in chapter 1, which is completely determined by the eigenvalues of the reduced correlation matrix (see equation (1.100)). We present the

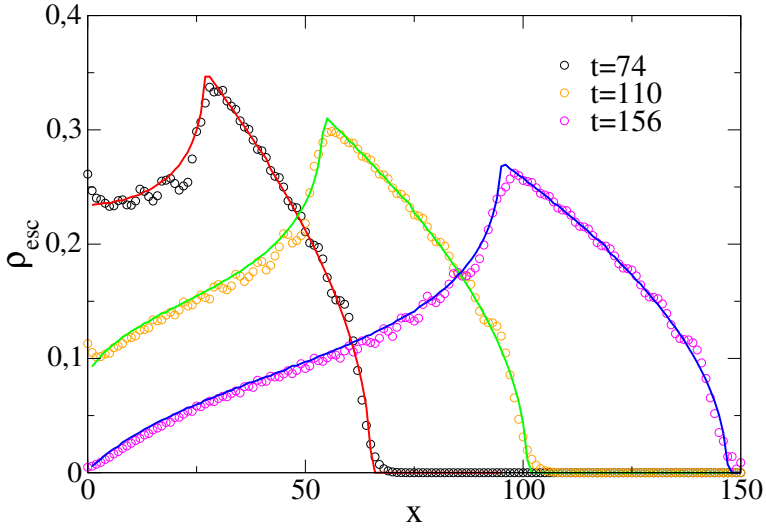

Figure 2.14 – *Density profile of the escaping particles for an initial Mott/superfluid state. The dots correspond to the numerical data, whereas the full line are the results of the integral* (2.77).

time evolution of the entanglement profile in figure 2.15 for the two different initial states with $A = -50$. In both cases, we clearly see the entanglement growth between the trapping region and the propagative band by the ballistic movement of the escaping particles. Inside the trapped region, one has to distinguish between the two initial states. In the case of a pure superfluid state, the entanglement is non zero in the complete zone and it exhibits the same kind of oscillation already observed in the dynamics of the density profile. In the Mott/superfluid initial state, the entanglement vanishes in the plateau region. Indeed, in this region, the whole state of the system can be written as a direct product of single-occupancy local states and is, as a consequence, separable. Interestingly, the entanglement present initially within the self trapped condensate is conserved in time, indicating that no entanglement is created or lost in this region. Indeed, we can see in figure 2.16, where the entanglement entropy is plotted at integer multiple of the period and of the half period, the perfect superposition of the profiles, indicating that the entanglement shows a trivial time evolution simply related to the Bloch oscillations of the trapped particles.

2.5 Conclusion

In this chapter, we have studied the behavior of hard core bosons after the sudden quench of the trapping potential. The use of the hydrodynamical description, based on a local equilibrium hypothesis, gave us access to observable like density or current, and perfectly explain the main features of the dynamics. Two different kinds of initial states, depending on the value of μ_0 have been considered : an initial state completely in a superfluid phase, and a initial state showing a mixture between superfluid and Mott phases.
We first studied the case of a quench consisting in the release of the trapping potential. We observed a spreading of the condensate to the left and the right, and we derived the number of particles within the initial trapping region in the case $\mu_0 \to \infty$.

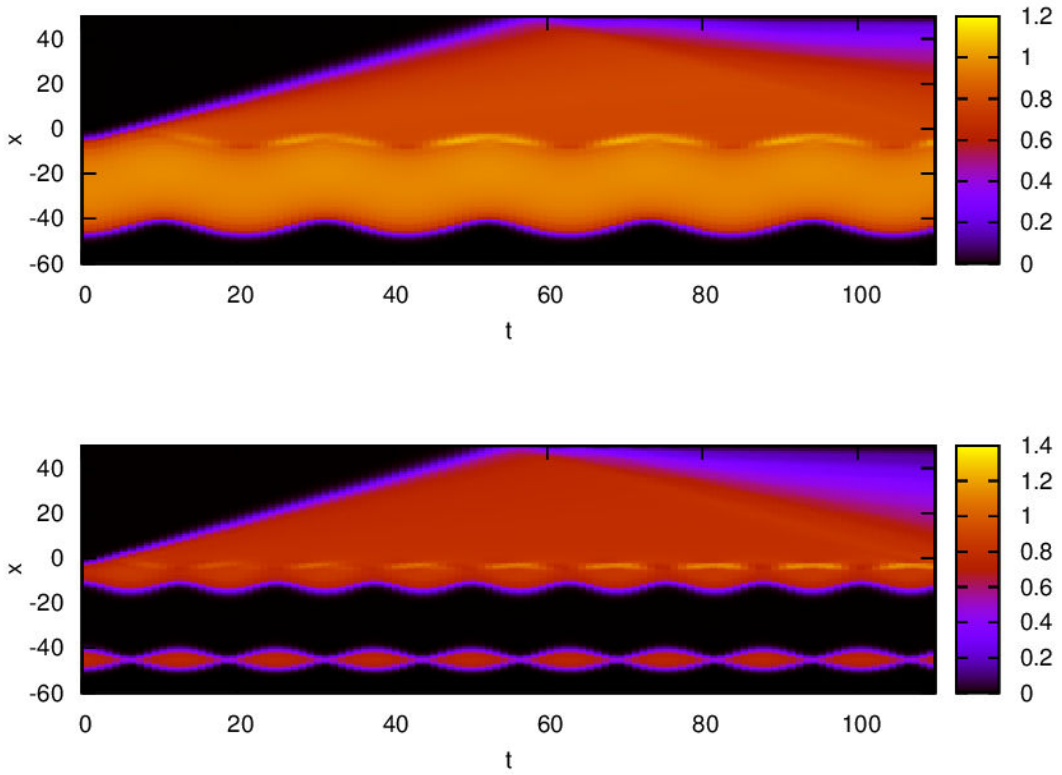

Figure 2.15 – *Time evolution of the entanglement entropy profile obtained numerically by using* (1.100) *for an initial superfluid state with* $F = 0.3$ *and* $\mu_0 = 0$ *(top) and an initial Mott/superfluid state (bottom) with* $F = 0.5$ *and* $\mu_0 = 2$*. In both cases, we set the spacial extension of the condensate to* $A = -50$*.*

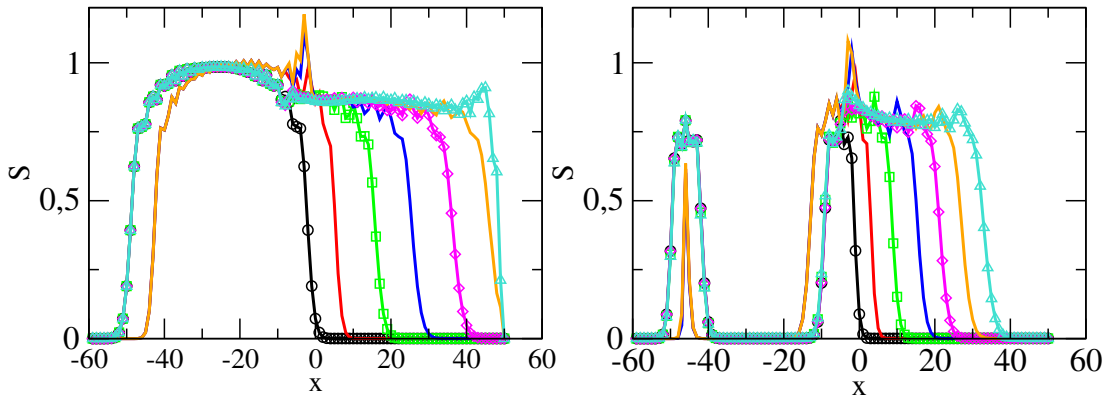

Figure 2.16 – *Entanglement entropy at integer multiples of the Bloch period and of the half period for an initial superfluid state with* $\mu_0 = 0$ *and* $F = 0.1$ *(left) and for an initial mixture Mott/superfluid with* $\mu_0 = 2$ *and* $F = 0.5$*. In both case, the times multiple of the period are plotted with symbols, and those multiple of the half period with full lines, and* A *is set to* -50*.*

Secondly, we considered the case of the release of the initial potential and the loading of a linear ramp in the negative side of the real axe. As already observed in the case of an initial homogeneous distribution of particles, the condensate splits into a escaping

part leaving the region $[A : 0]$ and a part which stays trapped due to the unitary evolution. The trapped particles perform Bloch oscillations due to the constant force acting on them, We identified different scenario for these oscillations, depending of the initial state and the applied force. Finally, we have analyzed the entanglement entropy between the escaping part and the trapped one.

Entanglement creation between two spins embedded in an Ising chain

3

Since the development of quantum information processing [NC00], quantum entanglement is not only used for a better understanding of the foundation of quantum mechanics, but it becomes also the key ingredient of concrete applications, like quantum communication [GT07], quantum cryptography [GRTZ02, BB84] or teleportation [BBC+93]. Creating and manipulating entangled quantum states is then a major issue of modern physics. Since entanglement is related to strong correlations, the simplest way to entangle two parts of a quantum system is the direct interaction between them. However, from a quantum information point of view, it is better to create entanglement between parts located at finite distance.
Whereas it is commonly believed that interaction of a quantum system with an environment leads to a death of quantum features like entanglement, it has recently been shown that the coupling to a bath can endorse the creation of entanglement between two distant systems interacting with it [Bra02, CVDEBR06, CVGIZ07, CVDEBR07, PR08, PR09, WDCK+11, KWLM12, FKT+13, TFK+14]. The environment can be modeled by different physical systems, such as an assembly of harmonic oscillators, spin or ion chains. For instance, in [Bra02], D. Braun studied the creation of entanglement between two spins coupled at the same point to a chain of harmonic oscillators. He identified a decoherence free subspace which protects a part of the initial coherence and created entanglement. In [WDCK+11, KWLM12], the authors investigated the entanglement between two harmonic oscillators coupled to an harmonic crystal in the thermodynamic limit. Depending on the parameters, different scenarios have been found for the steady state entanglement: sudden death, no sudden death or sudden death and revivals.

In this chapter, we propose to extend the model studied in [Bra02] by considering the case of two non interacting defect spins 1/2 coupled at two different locations in a quantum Ising chain. The chapter is organized as follows: in a first section, we give the model and the theoretical treatment of the problem. We show how the spin bath can be mapped, in the high magnetization and low temperature limit, into a collection of interacting harmonic oscillators. Then we introduce a new set of coordinates leading to a natural decoupling of the systems, and we derive the time evolution of the reduced density matrix of the two defect spins, allowing us to have access to

their entanglement evolution. In the second section, we present the results concerning the entanglement dynamics, for both vanishing and non vanishing distance between the defects. The behavior of the concurrence as a function of the parameters of the systems is in particular analyzed.

3.1 Model and theoretical treatment

3.1.1 Hamiltonians and initial states

We consider in this study a chain of $2N$ spins with Ising interactions and transverse magnetic field described by the Hamiltonian

$$H_b = -\frac{J}{2}\sum_{<ij>}{}' \sigma_i^x \sigma_j^x - \frac{1}{2}\sum_i{}' \sigma_i^z, \tag{3.1}$$

where the ferromagnetic coupling ($J > 0$) runs over the first neighbors only. The prime in the sum symbol indicates that the label $i = 0$ has been removed for further convenience. Moreover, we assume periodic boundary conditions $\sigma_{N+1}^{\alpha} = \sigma_{-N}^{\alpha}$, with $\alpha = x, y, z$. The two spins $-l$ and l of this chain are locally coupled to "defect" spins, labeled A and B, thought the Hamiltonian

$$H_i = \gamma\left(\sigma_A^x \sigma_{-l}^x + \sigma_B^x \sigma_l^x\right), \tag{3.2}$$

with coupling strength γ. Moreover, the two defect spins are subject to a Zeeman term

$$H_d = -h(\sigma_A^z + \sigma_B^z). \tag{3.3}$$

The whole system being close, the dynamics is unitary and is set by the total Hamiltonian $H = H_b + H_d + H_i$. The spin chain will act as an environment for the two defect spins by mediating an effective interaction between them.

In the following, the chain is prepared into a thermal state at temperature T. Its density matrix is the Gibbs state

$$\rho_b = \frac{1}{Z} e^{-H_b/T}, \tag{3.4}$$

where $Z \equiv \mathrm{Tr}\{e^{-H_b/T}\}$ is the normalization constant. The two defect spins are initially supposed to be in a pure separable state

$$|\Psi_{AB}\rangle = |\psi\rangle_A \otimes |\psi\rangle_B, \tag{3.5}$$

where $|\psi\rangle_{A,B} = \alpha_{A,B}|\uparrow\rangle_{A,B} + \beta_{A,B}|\downarrow\rangle_{A,B}$ with the usual normalization $|\alpha_{A,B}|^2 + |\beta_{A,B}|^2 = 1$ and $|\uparrow\rangle_{A,B}$ and $|\downarrow\rangle_{A,B}$ the eigenstates of the operator $\sigma_{A,B}^z$ with eigenvalues 1 and -1 respectively.

3.1.2 High magnetization limit

As illustrated in [CVDEBR06, CVGIZ07, GI10, SG09], bath-mediated entanglement between the boundary spins of a finite spin chain is found in the ground state of highly symmetric Hamiltonians where the reservoir presents long-range correlations. A major limitation faced in these systems is the vanishing energy gap between the ground state and the excited ones [GI10] as the chain size is increased. End-to-end entanglement is therefore very sensitive to attenuation of long-range correlations due to thermal fluctuations. In the case we consider here, decreasing the correlation length in the chain will decrease the correlations between spins $-l$ and l. This will naturally lead to a drastic attenuation of the entanglement between the defects. In order to avoid this decrease of correlations, we opt for the low temperature and the paramagnetic regime $J \ll 1$ where the spin of the environment are highly polarized along the direction of the transverse field.
This limit allows us to perform a bosonization of the spins of the environment by means of the Holstein-Primakoff transformation [HP40]. The idea of the transformation is to introduce a mapping between the spin operators and bosonic operators $a_n^\dagger$ and a_n:

$$\sigma_n^+ = \sqrt{1 - a_n^\dagger a_n}\, a_n, \tag{3.6}$$

$$\sigma_n^- = a_n^\dagger \sqrt{1 - a_n^\dagger a_n}, \tag{3.7}$$

$$\sigma_n^z = 1 - 2a_n^\dagger a_n. \tag{3.8}$$

Here, σ_n^+ and σ_n^- are the spin ladder operators, and $a_n^\dagger$ and a_n are creation and annihilation bosonic operator respectively, satisfying the algebra $[a_n, a_m^\dagger] = \delta_{nm}$. Note that the average in the operator $a_n^\dagger a_n$ counting the number of bosons in the mode n represents the deviation of the projection of the spin polarization with respect to its maximal value. From our previous requirement of a high polarization of the spins and a low temperature, it follows then that the average $\langle a_n^\dagger a_n \rangle$ is small. The expressions (3.6)-(3.8) can in consequence be truncated up the to zeroth order, leading to

$$\sigma_n^- \approx a_n^\dagger, \tag{3.9}$$

$$\sigma_n^+ \approx a_n. \tag{3.10}$$

Their is then a direct correspondence between lowering (resp. rising) spin operators and creation (resp. destruction) bosonic operators.
Plugging this transformation into the total Hamiltonian, we get a system of $2N$ interacting bosons

$$\begin{aligned} H = &- \frac{J}{2} {\sum_n}' \left(a_n a_{n+1} + a_n^\dagger a_{n+1} + a_n a_{n+1}^\dagger + a_n^\dagger a_{n+1}^\dagger \right) + {\sum_n}' a_n^\dagger a_n \\ &\gamma \left(\left(a_{-l} + a_{-l}^\dagger \right) \sigma_A^x + \left(a_l + a_l^\dagger \right) \sigma_B^x \right) - \left(\sigma_A^z + \sigma_B^z \right), \end{aligned} \tag{3.11}$$

where we have dropped an irrelevant constant. For further convenience, we introduce

the position and momentum operators x_n and p_n defined by

$$a_n = \frac{1}{\sqrt{2}}\left(x_n + ip_n\right), \tag{3.12}$$

$$a_n^\dagger = \frac{1}{\sqrt{2}}\left(x_n - ip_n\right), \tag{3.13}$$

and satisfying the canonical algebra $[x_n, p_m] = i\delta_{nm}$. Using these operators, the Hamiltonian is recast into

$$H = -J{\sum_n}' x_n x_{n+1} + \frac{1}{2}{\sum_n}'(x_n^2 + p_n^2) - \sqrt{2}\gamma(x_{-l}\sigma_A^x + x_l\sigma_B^x) - h(\sigma_A^z + \sigma_B^z). \tag{3.14}$$

One can see from the previous expression that the bath has been mapped into a set of linearly coupled harmonic oscillators. The two defects spins are now locally coupled to the position variables of the $-l$ and l oscillators. One can note that this system is close to the model studied in [KWLM12] where, instead of spins, the two defects are also of harmonic oscillator nature.

3.1.3 Characterization of the bath

In this section, we focus our attention to the description of the bath Hamiltonian H_b. To determine the time evolution of the spin defects, we first need to write the bath Hamiltonian is terms of its normal modes. Let us first introduce the position and momentum vectors

$$\mathbf{x}^\dagger = (x_{-N}, \ldots, x_{-1}, x_1, \ldots, x_N), \quad \mathbf{p}^\dagger = (p_{-N}, \ldots, p_{-1}, p_1, \ldots, p_N), \tag{3.15}$$

such that the bath Hamiltonian is written into a matrix form

$$\begin{aligned} H_b &= -J\sum_n x_n x_{n+1} + \frac{1}{2}\sum_n (x_n^2 + p_n^2) \\ &= \frac{1}{2}\mathbf{p}^\dagger\mathbf{p} + \frac{1}{2}\mathbf{x}^\dagger V_b \mathbf{x} = \frac{1}{2}p^2 + \frac{1}{2}\mathbf{x}^\dagger V_b \mathbf{x}, \end{aligned} \tag{3.16}$$

where we have introduced the potential matrix

$$V_b = \begin{pmatrix} 1 & -J & 0 & \ldots & \ldots & 0 & -J \\ -J & \ddots & \ddots & & & & 0 \\ 0 & \ddots & \ddots & \ddots & & & \vdots \\ \vdots & & \ddots & \ddots & \ddots & & \vdots \\ \vdots & & & \ddots & \ddots & \ddots & 0 \\ 0 & & & & \ddots & \ddots & -J \\ -J & 0 & \ldots & \ldots & 0 & -J & 1 \end{pmatrix} \in \mathbb{R}^{2N\times 2N}. \tag{3.17}$$

This potential matrix can be rewritten into a block matrix form

$$V_b = \begin{pmatrix} A & B \\ B & A \end{pmatrix}, \tag{3.18}$$

where the A and B matrices assume the expression

$$A = \begin{pmatrix} 1 & -J & & \\ -J & \ddots & \ddots & \\ & \ddots & \ddots & -J \\ & & -J & 1 \end{pmatrix}, \qquad B = \begin{pmatrix} & & & -J \\ & & 0 & \\ & \iddots & & \\ 0 & & & \\ -J & & & \end{pmatrix} \in \mathbb{R}^{N\times N}. \tag{3.19}$$

The bath Hamiltonian H_b is invariant under the exchange of the two bosons $-n$ and n. With this in mind, we describe the bath using symmetric (center-of-mass) and antisymmetric (relative) variables by the introduction of

$$x_n^{S,A} = \frac{x_n \pm x_{-n}}{\sqrt{2}}, \qquad p_n^{S,A} = \frac{p_n \pm p_{-n}}{\sqrt{2}}, \tag{3.20}$$

where the upperscript S (A) refers to center-of-mass (relative) coordinates. This transformation can be written into a vectorial form

$$\boldsymbol{\xi} = R\mathbf{x}, \quad \boldsymbol{\pi} = R\mathbf{p}, \tag{3.21}$$

where we have introduced the vectors

$$\boldsymbol{\xi}^\dagger = \left(\mathbf{x}^{S\dagger}, \mathbf{x}^{A\dagger}\right) = \left(x_1^S, \ldots, x_N^S, x_1^A, \ldots, x_N^A\right), \tag{3.22}$$

$$\boldsymbol{\pi}^\dagger = \left(\mathbf{p}^{S\dagger}, \mathbf{p}^{A\dagger}\right) = \left(p_1^S, \ldots, p_N^S, p_1^A, \ldots, p_N^A\right), \tag{3.23}$$

together with the orthogonal ($R^{-1} = R^T$) transformation matrix R

$$R = \frac{1}{\sqrt{2}} \begin{pmatrix} \bar{\mathbb{1}} & \mathbb{1} \\ -\bar{\mathbb{1}} & \mathbb{1} \end{pmatrix}, \text{with} \quad \bar{\mathbb{1}} = \begin{pmatrix} & & 1 \\ & \iddots & \\ 1 & & \end{pmatrix} \in \mathbb{R}^{N\times N}. \tag{3.24}$$

Plugging the relation $R^T R = \mathbb{1}$ on both sides of the potential matrix, the interaction part of equation (3.16) becomes

$$\frac{1}{2}\mathbf{x}^\dagger V_b \mathbf{x} = \frac{1}{2}\boldsymbol{\xi}^\dagger \Lambda_b \boldsymbol{\xi} \tag{3.25}$$

where $\Lambda_b = RV_bR^T$ is the transformed potential matrix. Its explicit expression can be determined using the block representation (3.18)

$$\begin{aligned} \Lambda_b &= RV_BR^T \\ &= \frac{1}{2}\begin{pmatrix} \bar{\mathbb{1}} & \mathbb{1} \\ -\bar{\mathbb{1}} & \mathbb{1} \end{pmatrix}\begin{pmatrix} A & B \\ B & A \end{pmatrix}\begin{pmatrix} \bar{\mathbb{1}} & -\bar{\mathbb{1}} \\ \mathbb{1} & \mathbb{1} \end{pmatrix} \\ &= \frac{1}{2}\begin{pmatrix} \bar{\mathbb{1}}A\bar{\mathbb{1}} + B\bar{\mathbb{1}} + \bar{\mathbb{1}}B + A & -\bar{\mathbb{1}}A\bar{\mathbb{1}} - B\bar{\mathbb{1}} + \bar{\mathbb{1}}B + A \\ -\bar{\mathbb{1}}A\bar{\mathbb{1}} + B\bar{\mathbb{1}} - \bar{\mathbb{1}}B + A & \bar{\mathbb{1}}A\bar{\mathbb{1}} - B\bar{\mathbb{1}} - \bar{\mathbb{1}}B + A \end{pmatrix}. \end{aligned} \tag{3.26}$$

One can easily show that $\bar{\mathbb{1}}A\bar{\mathbb{1}} = A$ and $B\bar{\mathbb{1}} = \bar{\mathbb{1}}B$, leading to

$$\Lambda_b = \begin{pmatrix} V_b^S & 0 \\ 0 & V_b^A \end{pmatrix}, \tag{3.27}$$

with the two matrices

$$V_b^S = A + K, \quad V_b^A = A - K, \tag{3.28}$$

and $K_{ij} = (\bar{\mathbb{1}}B)_{ij} = -J(\delta_{i1}\delta_{j1} + \delta_{iN}\delta_{jN})$. The potential matrix in the new representation is block diagonal. The introduction of symmetric and antisymmetric coordinates leads then to a natural splitting of the initial bath into two independent baths composed of N particles and such that the Hamiltonian is $H_b = H_b^S + H_b^A$ with

$$H_b^{S(A)} = \frac{1}{2}(p^{S(A)})^2 + \frac{1}{2}\mathbf{x}^{S(A)\dagger} V_b^{S(A)} \mathbf{x}^{S(A)}. \tag{3.29}$$

For latter convenience, we write the bath Hamiltonian in term of its normal modes. Introducing the normal center-of-mass and relatives coordinates $\widetilde{x}^{S(A)}$ and $\widetilde{p}^{S(A)}$ defined by

$$\widetilde{\mathbf{x}}^{S(A)} = (O^{S(A)})^\dagger \mathbf{x}^{S(A)}, \quad \widetilde{\mathbf{p}}^{S(A)} = (O^{S(A)})^\dagger \mathbf{p}^{S(A)}, \tag{3.30}$$

where O^S and O^A diagonalize the potential matrices V_b^S and V_b^A respectively such that

$$D^{S(A)} = (O^{S(A)})^\dagger V_b^{S(A)} O^{S(A)}. \tag{3.31}$$

With theses coordinates, the two bath Hamiltonians are given by a set of independent oscillators

$$\begin{aligned} \widetilde{H}_b^{S(A)} =& \frac{1}{2}(\widetilde{p}^{S(A)})^2 + \frac{1}{2}(\widetilde{\mathbf{x}}^{S(A)})^\dagger D^{S(A)} \widetilde{\mathbf{x}}^{S(A)} \\ =& \sum_n \left(\frac{1}{2}(\widetilde{p}_n^{S(A)})^2 + \frac{1}{2}(\widetilde{\omega}_n^{S(A)})^2 \ (\widetilde{x}_n^{S(A)})^2 \right), \end{aligned} \tag{3.32}$$

where the normalfrequencies are given by

$$(\widetilde{\omega}_n^S)^2 = 1 - 2J\cos\left(\frac{n\pi}{N}\right), \quad n = 0, \cdots, N-1 \tag{3.33}$$

$$(\widetilde{\omega}_n^A)^2 = 1 - 2J\cos\left(\frac{n\pi}{N}\right), \quad n = 1, \cdots, N\,. \tag{3.34}$$

associated with the eigenvectors $Q_n^{S(A)}(k) = [O^{S(A)}]_{kn}$

$$\begin{cases} Q_n^S(k) = & \dfrac{1}{\sqrt{N}} \quad \text{for} \quad n = 0 \\ Q_n^S(k) = & \sqrt{\dfrac{2}{N}} \cos\left(\dfrac{n\pi}{2N}(2k-1)\right) \quad \text{for} \quad n = 1 \ldots N-1 \end{cases} \tag{3.35}$$

$$\begin{cases} Q_n^A(k) = & \sqrt{\dfrac{2}{N}} \sin\left(\dfrac{n\pi}{2N}(2k-1)\right) \quad \text{for} \quad n = 1 \ldots N-1 \\ Q_n^A(k) = & \dfrac{(-1)^k}{\sqrt{N}} \quad \text{for} \quad n = N. \end{cases} \tag{3.36}$$

3.1.4 Full Hamiltonian in normal coordinates

In the same spirit than the introduction of symmetric and antisymmetric coordinates for the bath variables, we also introduce a base composed by non local symmetric and antisymmetric states for the defect spins:

$$|\phi^{S(A)}\rangle = \frac{|\uparrow\uparrow\rangle + (-)|\downarrow\downarrow\rangle}{\sqrt{2}}, \tag{3.37}$$

$$|\psi^{S(A)}\rangle = \frac{|\uparrow\downarrow\rangle + (-)|\downarrow\uparrow\rangle}{\sqrt{2}}. \tag{3.38}$$

Note that these four states are the four maximally entangled Bell states. Defining the two operators

$$S_x^S = (|\psi^S\rangle\langle\phi^S| + |\phi^S\rangle\langle\psi^S|), \tag{3.39}$$

$$S_x^A = (|\psi^A\rangle\langle\phi^A| + |\phi^A\rangle\langle\psi^A|), \tag{3.40}$$

acting as spin flip operators in the symmetric and antisymmetric Hilbert space respectively, the interaction Hamiltonian H_i takes the form

$$H_i = -2\gamma\left(S_x^S x_l^S + S_x^A x_l^A\right). \tag{3.41}$$

As for the bath, the interaction Hamiltonian presents a clear decoupling, the operator in the symmetric (resp. antisymmetric) Hilbert space being coupled only to symmetric (resp antisymmetric) bath operators. By the introduction of the coupling vector

$$\boldsymbol{\gamma}^T = \left(0, \cdots, 2\sqrt{2}\gamma, \cdots, 0\right), \tag{3.42}$$

where the only non zero entry occupies the position l, the coupling Hamiltonian is recast in a more compact form

$$H_i = -(S_x^S \boldsymbol{\gamma}^T \mathbf{x}^S + S_x^A \boldsymbol{\gamma}^T \mathbf{x}^A). \tag{3.43}$$

Introducing the matrix $O^{S(A)}$, the Hamiltonian is written in terms of the normal modes of the baths by $\widetilde{H}_i = \widetilde{H}_i^S + \widetilde{H}_i^A$ where

$$\widetilde{H}_i^{S(A)} = -S_x^{S(A)} (\widetilde{\boldsymbol{\gamma}}^{S(A)})^T \widetilde{\mathbf{x}}^{S(A)} \tag{3.44}$$

with the new coupling vectors to the normal modes $\widetilde{\boldsymbol{\gamma}}^{S(A)} = (O^{S(A)})^T \boldsymbol{\gamma}$ explicitly given by

$$\widetilde{\boldsymbol{\gamma}}^S = \frac{2\gamma}{\sqrt{N}} \begin{pmatrix} 1 \\ \sqrt{2}\cos\left(\frac{\pi}{2N}(2l-1)\right) \\ \vdots \\ \sqrt{2}\cos\left(\frac{(N-1)\pi}{2N}(2l-1)\right) \end{pmatrix}, \widetilde{\boldsymbol{\gamma}}^A = \frac{2\gamma}{\sqrt{N}} \begin{pmatrix} \sqrt{2}\sin\left(\frac{\pi}{2N}(2l-1)\right) \\ \vdots \\ \sqrt{2}\sin\left(\frac{(N-1)\pi}{2N}(2l-1)\right) \\ (-1)^{N+1} \end{pmatrix}. \tag{3.45}$$

Note that $2l-1$ appearing in the expression of the coupling vectors is the distance d between the two defect spins. This situation is the starting point of the model studied in [Brao2] where the two defect spins are coupled to the same location in the bath.

The last step is to write down the local Zeeman term. It reads in the symmetric and antisymmetric base

$$\begin{aligned}\widetilde{H}_d =& -2h\left(|\phi^A\rangle\langle\phi^S| + |\phi^S\rangle\langle\phi^A|\right)\\ =& -2hS_z,\end{aligned} \tag{3.46}$$

where we have defined the operator $S_z = |\phi^A\rangle\langle\phi^S| + |\phi^S\rangle\langle\phi^A|$ [1].
Now that all our Hamiltonians are written in the proper bases, we can write the total Hamiltonian as $\widetilde{H} = \widetilde{H}^S + \widetilde{H}^A + \widetilde{H}_d$ with

$$\widetilde{H}^S = \frac{1}{2}(\widetilde{\mathbf{p}}^S)^2 + \frac{1}{2}(\widetilde{\mathbf{x}}^S)^T D^S \widetilde{\mathbf{x}}^S - S_x^S(\widetilde{\boldsymbol{\gamma}}^S)^T\widetilde{\mathbf{x}}^S, \tag{3.47}$$

$$\widetilde{H}^A = \frac{1}{2}(\widetilde{\mathbf{p}}^A)^2 + \frac{1}{2}(\widetilde{\mathbf{x}}^A)^T D^A \widetilde{\mathbf{x}}^A - S_x^A(\widetilde{\boldsymbol{\gamma}}^A)^T\widetilde{\mathbf{x}}^A. \tag{3.48}$$

Because they are acting in two different Hilbert spaces, the two Hamiltonians $\widetilde{H}^S$ and $\widetilde{H}^A$ represents two decoupled dynamics. On the contrary, the Zeeman term couples the two subspaces and breaks the independent dynamics since $[\widetilde{H}_d, \widetilde{H}^{S,A}] \neq 0$.

3.2 Time evolution of the spin defects

The fact that $\widetilde{H}_d$ and $\widetilde{H}^{S,A}$ do not commute renders the calculation of the time evolution of the spin defects difficult. However, at short time scales, the dynamics is easily derived. Indeed, for times smaller than the typical time scale of the defects given by the inverse of the energy gap $h/2$, the contribution of the local Hamiltonian $\widetilde{H}_d$ can be ignored in the total Hamiltonian and a decoupled solution of the form

$$\widetilde{U}(t) = \widetilde{U}^S(t)\widetilde{U}^A(t) \tag{3.49}$$

can be obtained in the lowest order in h.

In the following, we set the transverse magnetic field h of the defects to zero, leading to perfectly degenerate spins, allowing us to assess the dynamics for an arbitrary long time. Moreover, in all our numerical simulations of the dynamics, the number of harmonic oscillators in the bath will be fixed to $N = 10^4$, sufficiently big to avoid finite size effects. Finally, the temperature will be set to a low value to fulfill the high polarization limit, and we choose $T = 10^{-5}$.
We remind here that the two defect spins are initially prepared into a separable state $|\Psi_{AB}\rangle = |\psi_A\rangle \otimes |\psi_B\rangle$ and the bath into a thermal state $\rho_b = \exp(-H_b/T)/Z$. The defects and the bath are moreover supposed to be initially uncorrelated such that

$$\rho_{tot}(0) = \rho_b(0) \otimes \rho_d(0). \tag{3.50}$$

1. Note that if instead of the symmetric and antisymmetric base we would have used the singlet triplet base $|j, m_j\rangle$, the Zeeman Hamiltonian would have been $\widetilde{H}_d = -2h(|1,1\rangle\langle 1,1| - |1,-1\rangle\langle 1,-1|)$ and then introduces an energy gap between the two states $|1,1\rangle$ and $|1,-1\rangle$ of the triplet sector.

The time evolution of the elements of the reduced density matrix are written in the 4-dimensional common eigenbase $\{|s_i\rangle\}$ of the coupling operators $S_x^{S(A)}$ defined by $S_x^{S(A)}|s_i\rangle = s_i^{S(A)}|s_i\rangle$ with eigenvalues $s_i^{S(A)} = 0, \pm 1$. In this base, the elements the reduced density matrix

$$\rho_d(t) = \mathrm{Tr}_b\{\widetilde{U}(t)\rho_d(0)\widetilde{U}(t)^\dagger\} \tag{3.51}$$

evolve through (see appendix A for details of the calculations)

$$\begin{aligned}\langle s_i|\rho_d(t)|s_j\rangle = &\exp\Big\{-\big[f^S(t)(s_i^S - s_j^S)^2 + f^A(t)(s_i^A - s_j^A)^2\big] \\ &+ i\big[\varphi^S(t)((s_i^S)^2 - (s_j^S)^2) + \varphi^A(t)(s_i^A)^2 - (s_j^A)^2)\big]\Big\}\langle s_i|\rho_d(0)|s_j\rangle,\end{aligned} \tag{3.52}$$

where the four time dependent functions are given by

$$f^{S(A)}(t) = \sum_i \frac{\left(\widetilde{\gamma}_i^{S(A)}\right)^2 (2\widetilde{n}_i^{S(A)} + 1)}{2\left(\widetilde{\omega}_i^{S(A)}\right)^3}\left(1 - \cos\left(\widetilde{\omega}_i^{S(A)} t\right)\right), \tag{3.53}$$

$$\varphi^{S(A)}(t) = \sum_i \frac{\left(\widetilde{\gamma}_i^{S(A)}\right)^2}{2\left(\widetilde{\omega}_i^{S(A)}\right)^2}\left(t - \frac{\sin\left(\widetilde{\omega}_i^{S(A)} t\right)}{\widetilde{\omega}_i^{S(A)}}\right). \tag{3.54}$$

In the expression of the $f^{S(A)}(t)$ functions, $n_i^{S(A)} = \left(\exp\left(\widetilde{\omega}_i^{S(A)}/T\right) - 1\right)^{-1}$ is the thermal occupation of the bosonic mode i of the symmetric (antisymmetric) bath. Note that the dynamics is then completely set by the bath through these functions encoding all the properties of the environment like frequency or temperature. The elements of ρ_d have an oscillatory term depending on the $\varphi^{S(A)}$ function together with an exponential decay set by $f^{S(A)}(t)$. One can remark that the diagonal elements ($s_i^{S(A)} = s_j^{S(A)}$) do not evolve in time. In the base $\{|s_i\rangle\}$, the population elements are then constant in time and only the coherence elements are affected by the coupling to the bath. The spin chains constitutes then in this base a purely dephasing environment. The time evolution of the four functions $f^{S(A)(t)}$ and $\varphi^{S(A)}(t)$ is shown in figure 3.1 for two different distances.

One can remark that the linear part of both functions φ^S and φ^A are the same in the case $l = 5$, as well as the constant part of the f^S and f^A functions. We plot the slope of the $\varphi^{S(A)}$ and the constant part of the $f^{S(A)}$ functions as a function of the parameter l in figure 3.2. As we already guessed, the linear part of the φ and the constant part of the f functions become equal for the symmetric and antisymmetric baths when $l \approx 5$. Moreover, they become independent of the value of l for large distances.

Before turning to the entanglement dynamics of the defects, let us first study their dynamics for short times. The dynamics of one individual spin is obtained by tracing the density matrix $\rho_d(t)$ over the second one, for example $\rho_A(t) = \mathrm{Tr}_B\{\rho_d(t)\}$. If the two defects are, for instance, prepared in the state $|\uparrow\uparrow\rangle$, one can show that the

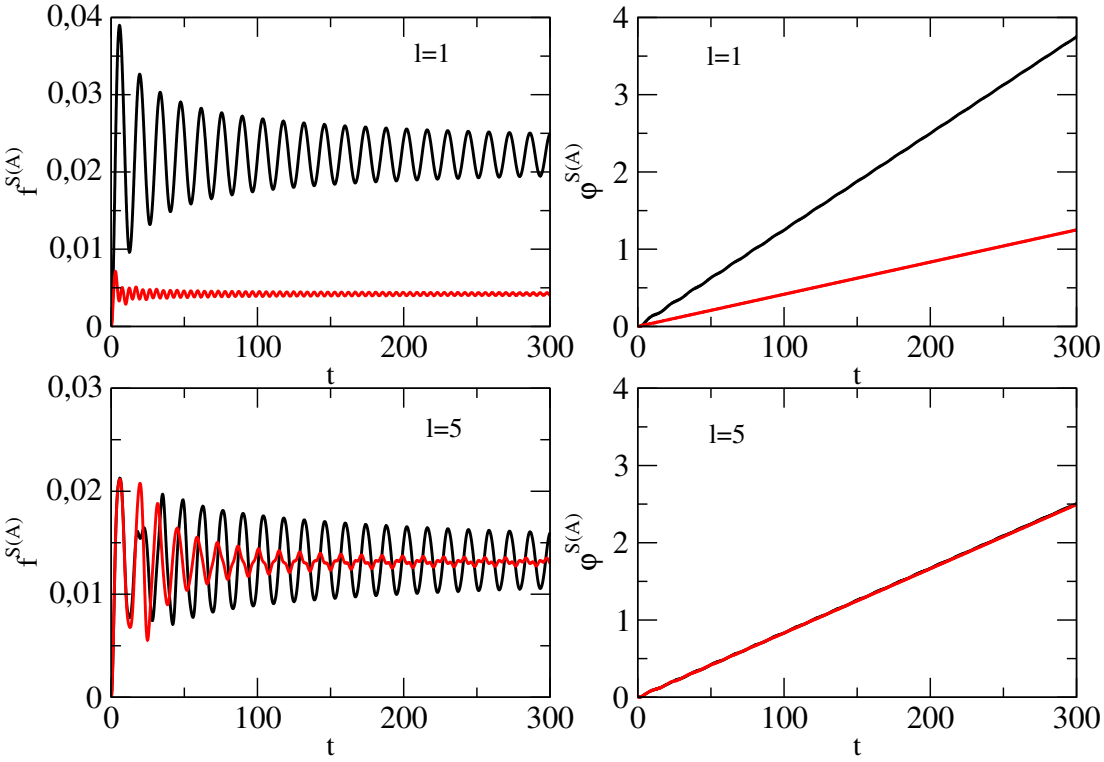

Figure 3.1 – *Time evolution of the four functions $f^{S(A)}$ (left panels) and $\varphi^{S(A)}$ (right panels) for $l = 1$ (up panels) and $l = 5$ (down panels). The black curves correspond to the symmetric bath whereas the red curves correspond to the antisymmetric bath. The others parameters are $\gamma = 0.05$, $J = 0.4$, $T = 10^{-5}$ and $N = 10^4$.*

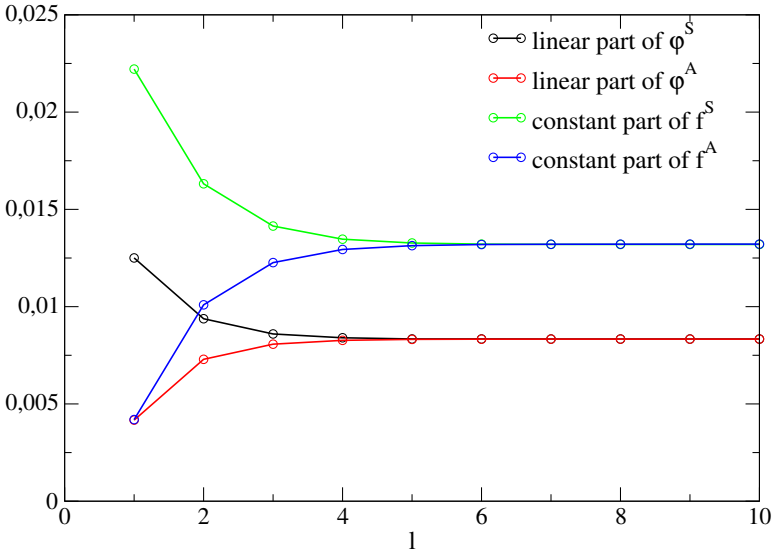

Figure 3.2 – *Linear part of the $\phi^{S,A}$ functions and constant part of the $f^{S,A}$ functions a function of the parameter l. The couplings are fixed to $\gamma = 0.05$, $J = 0.4$ and the temperature is $T = 10^{-5}$.*

population elements evolve as

$$\rho^A_{\uparrow\uparrow}(t) = \frac{1}{2}\left(1 + e^{-f^S(t)-f^A(t)}\cos\left(\varphi^S(t) - \varphi^A(t)\right)\right), \tag{3.55}$$

$$\rho^A_{\downarrow\downarrow}(t) = 1 - \rho^A_{\uparrow\uparrow}(t). \tag{3.56}$$

The exponential appearing in the previous expression depends on the sum $f^S(t) + f^A(t)$, which in the case of the coupling vector given by equation (3.45), is proportional to $\cos^2((2l-1)\frac{k_i}{2}) + \sin^2((2l-1)\frac{k_i}{2})$ and is as a consequence independent of the value of l. For short times and for sufficiently low temperature such that $\widetilde{n}_i^{S,A} = 0\ \forall i$, on can expend the functions $f^{S(A)}(t)$ and $\varphi^{S(A)}(t)$ around zero, and we find, taking the thermodynamic limit $N \to \infty$

$$f^S(t) + f^A(t) \approx \frac{2\gamma^2}{\pi}\frac{K\left(\frac{4J}{2J+1}\right)}{\sqrt{2J+1}}t^2, \tag{3.57}$$

$$\varphi^S(t) = \varphi^A(t) \approx \frac{\gamma^2}{3}t^3, \tag{3.58}$$

where $K(x)$ is the complete elliptic integral of the first kind. The sum $f^S(t) + f^A(t)$ is, as expected, independent of the value of l, but we also find that the $\varphi^{S(A)}$ functions are distance independent as well. For short times, the defect's dynamics does not dependent on the distance between them. The evolution of one spin does not influence the one of the second spin, and the dynamics comes only from the coupling with the bath through the decoherence process. This independent dynamics holds until the first excitation emitted in position $-l$ (resp. l) reaches the position l (resp. $-l$), that is until a time t^l_{ind} given by

$$t^l_{ind} = \frac{2l-1}{v_g}, \tag{3.59}$$

where $v_g = J$ is the group velocity along the chain in the limit $J < 1$. We compare in figure 3.3 the evolution of the populations $\rho_{\uparrow\uparrow}$ of the spin A in the case of two spins coupled to the same bath, obtained by tracing the reduced density matrix $\rho_d(t)$, and the evolution of the population $\rho^{ind}_{\uparrow\uparrow}$ of a single spin coupled to the bath. As expected, the curves collapse until a time given approximatively by t^l_{ind}, as shown in the inset, indicating that the spin evolution is only the consequence of the coupling with the bath. We also add the curve corresponding to the short time dynamics, obtained with expansions (3.57) and (3.58), which reproduces correctly the dynamics until a time $t \approx 0.5$.

3.3 Entanglement dynamics

In this section, we analyze the entanglement dynamics, measured by the concurrence, of the two defect spins as a function of the parameters of the system. We first start by the simplest case of two defects coupled to the same spin of the chain, and we turn to the general case of a non vanishing distance $d = 2l - 1$ afterward.

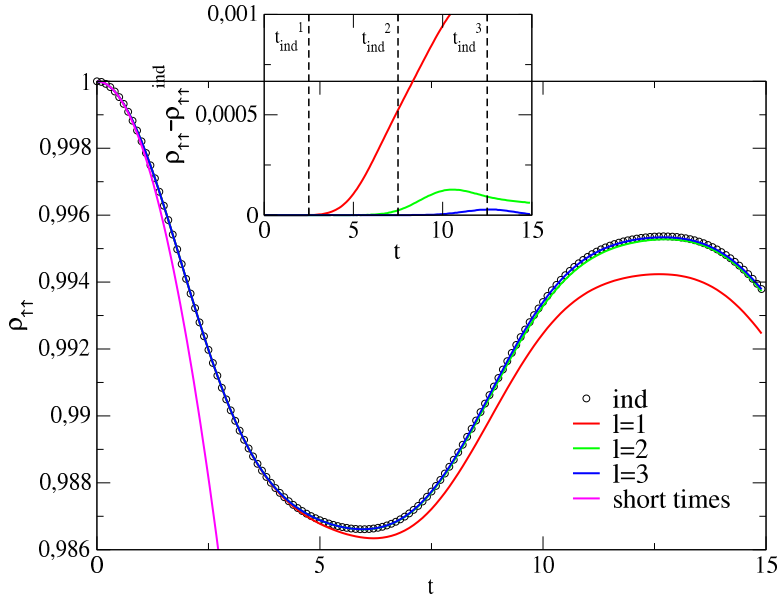

Figure 3.3 – *Evolution of the population $\rho_{\uparrow\uparrow}$ of the spin A for different distances (full lines) compared to the case of an individual spin (dots). In the inset is shown $\rho_{\uparrow\uparrow} - \rho_{\uparrow\uparrow}^{ind}$ for several distances. All the spins are initially prepared in the state $|\uparrow\rangle$.*

3.3.1 Spins coupled to the same point

Here, the defect spins are coupled to the same spin l of the chain. Note that this is the case treated in [Brao2], where the author used a phenomenological bath. In the case of a vanishing distance, the interaction Hamiltonian (3.41) is transformed into

$$\widetilde{H}_i = S_x^S(\widetilde{\gamma}^S\widetilde{\mathbf{x}}^S + \widetilde{\gamma}^A\widetilde{\mathbf{x}}^A). \tag{3.60}$$

Note that only the coupling operator in the symmetric space S_x^S appears now in the interaction Hamiltonian. The two antisymmetric states $|\psi^A\rangle$ and $|\phi^A\rangle$ are no longer involved in the dynamics. The coupling of the two defects in the same point has then for effect the creation of a two dimensional *decoherence free subspace* [LW03], composed by the two antisymmetric states, protected from the non unitary dynamics set by the coupling with the bath.

Using the same method developed in appendix A, the elements of the reduced density matrix of the defects in the eigenbase $\{|s_i\rangle\}$ of the coupling operators are given by

$$\begin{aligned}\langle s_i|\rho_d(t)|s_j\rangle =& \exp\Big\{-\big[(f^S(t)+f^A(t))(s_i^S-s_j^S)^2\big] \; + i\big[(\varphi^S(t)+\varphi^A(t))((s_i^S)^2-(s_j^S)^2)\big]\Big\} \\ & \times \langle s_i|\rho_d(0)|s_j\rangle.\end{aligned} \tag{3.61}$$

We show on figure 3.4 the time evolution of the concurrence between the two defects coupled to the same point for several values of γ (left plot) and J (right plot). One observes that the concurrence starts to grow at $t = 0$, indicating an instantaneous creation of entanglement between the two defects. The concurrence has an oscillatory

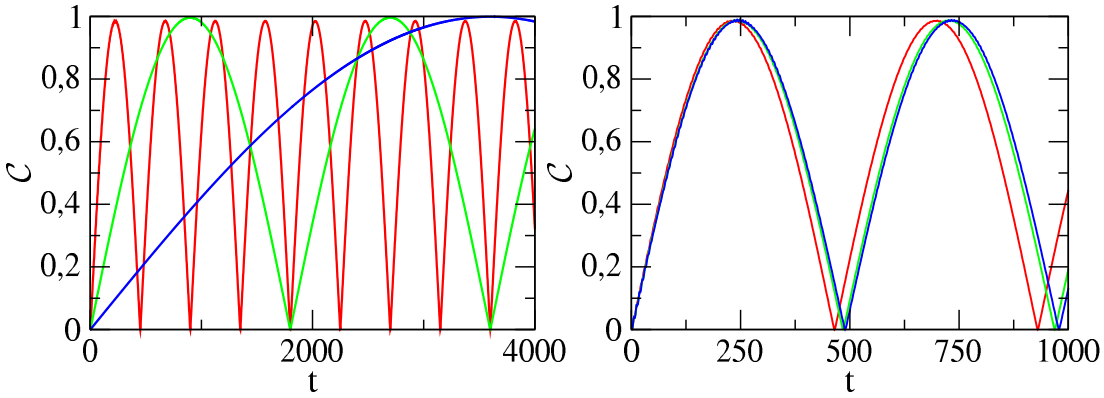

Figure 3.4 – *Entanglement dynamics for the two defect spins coupled to the same point. Parameters are* $l = 10$*, and (left)* $J = 0.4$*,* $\gamma = 0.04$ *(red),* $\gamma = 0.02$ *(green),* $\gamma = 0.01$ *(blue) and (right)* $\gamma = 0.04$ *(red),* $J = 0.32$ *(red),* $J = 0.16$ *(green),* $J = 0.08$ *(blue). In both plots the initial states is* $|\varphi_A\rangle \otimes |\varphi_B\rangle = |\uparrow\rangle_A \otimes |\uparrow\rangle_B$.

behavior which highly depends on the system's parameters. This dependence of the oscillation period will be analyzed in the next section when the defect are separated by a non vanishing distance d.
We can finally note that the entanglement dynamics is independent on the coupling position l since the boundary conditions are periodic which is reflected by the fact that the matrix elements of $\rho_d(t)$ depend only on the sum $(f^S + f^A)$ and $(\varphi^S + \varphi^A)$, which, as already seen in the previous section, are independent on the value of l.

3.3.2 Spins coupled at two different points

Now we increase the distance between the defects, setting the distance $d = 2l - 1$ between the defects. The decoherence free subspace created by the coupling to the same point in the chain disappears in this case, and the two states $|\phi^A\rangle$ and $|\psi^A\rangle$ are now participating in the dynamics. The reduced density matrix evolves in this case following the evolution equation (3.52).

We present in figure 3.5 the concurrence dynamics of the two defects when the parameters l is varied for coupling constant $J = 0.4$ and $\gamma = 0.04$. As in the case of a vanishing distance, we observe oscillations in the time evolution of the concurrence, with maxima close to unity. One of the main difference with the previous case is that now, entanglement does not start to grow a $t = 0$, but the defects need an establishment time t_{ent} to become entangled due to the finite distance between them (see right plot of figure 3.5). This time grows exponentially with the distance $t_{ent} \sim \exp(c_1 l)$, as shown in figure 3.6. This exponential increase indicates that the entanglement is not mediated by the fastest excitation travelling from one defect to the other. As the sound velocity does not change with the distance, this would rather lead to a linear growth. As in the case treated previously, the period P of the oscillations of the concurrence depends on the parameters of the system, as we can see in figure 3.7.

The decrease of the coupling strength γ leads to a reduction of the information transfer between the defects mediated by the chain, leading to an increase of the

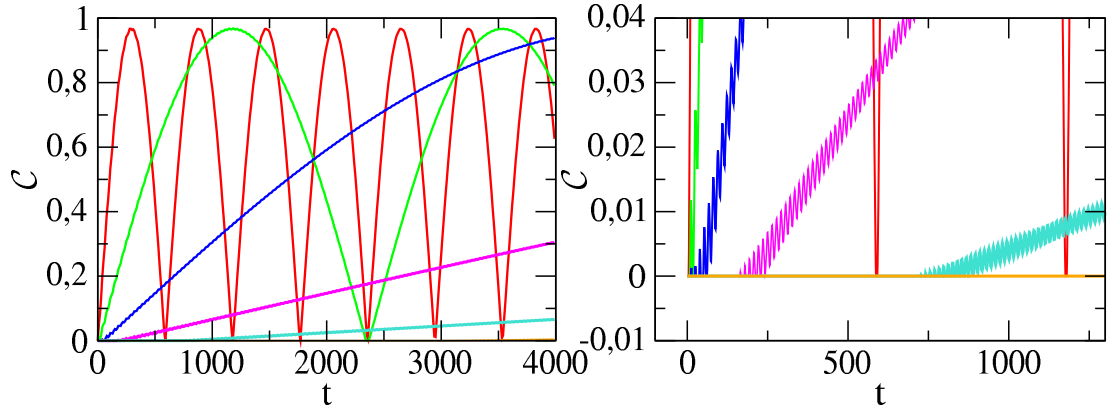

Figure 3.5 – *(left) Time evolution of the concurrence for* $J = 0.4$, $\gamma = 0.04$ *and* $l = 1$ *(red),* $l = 2$ *(green),* $l = 3$ *(blue),* $l = 4$ *(magenta),* $l = 5$ *(light blue) and* $l = 6$ *(orange). (right) Zoom at the beginning of the growth of* $\mathcal{C}(t)$*. Initial state is* $|\varphi_A\rangle \otimes |\varphi_B\rangle = |\uparrow\rangle_A \otimes |\uparrow\rangle_B$.

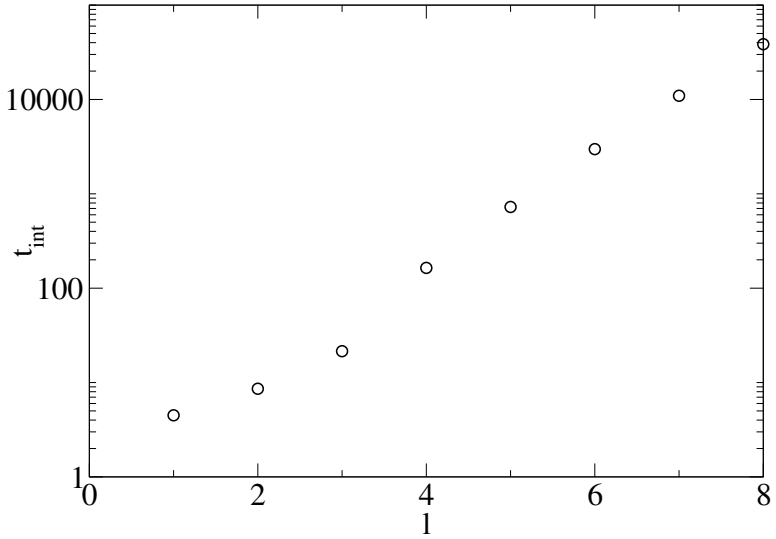

Figure 3.6 – *Establishment time* t_{ent} *of the entanglement as a function of the parameter* l*. The other parameters are* $\gamma = 0.04$*, and* $J = 0.4$.

period of the oscillation of $\mathcal{C}(t)$. We find numerically a power law scaling following

$$P(\gamma) \sim \gamma^{-2}. \tag{3.62}$$

On the other hand, the increase of the defect-chain coupling build more correlations (and then more entanglement) between the defects and the chain. Due to the monogamy property of the entanglement [CKW00], this has for effect to linearly decay the maximum of the concurrence $\mathcal{C}_{max}(\gamma)$, as we can see on the down left panel of figure 3.7. This last feature does not occur when the intra-chain coupling J is varied since it is only responsible of the transport of the information in the chain, and not on the of the build-up of correlations between the defects and the chain. The J parameters influences then only the period P by making the transport of the information easier. We found an exponential decay of this period when the coupling

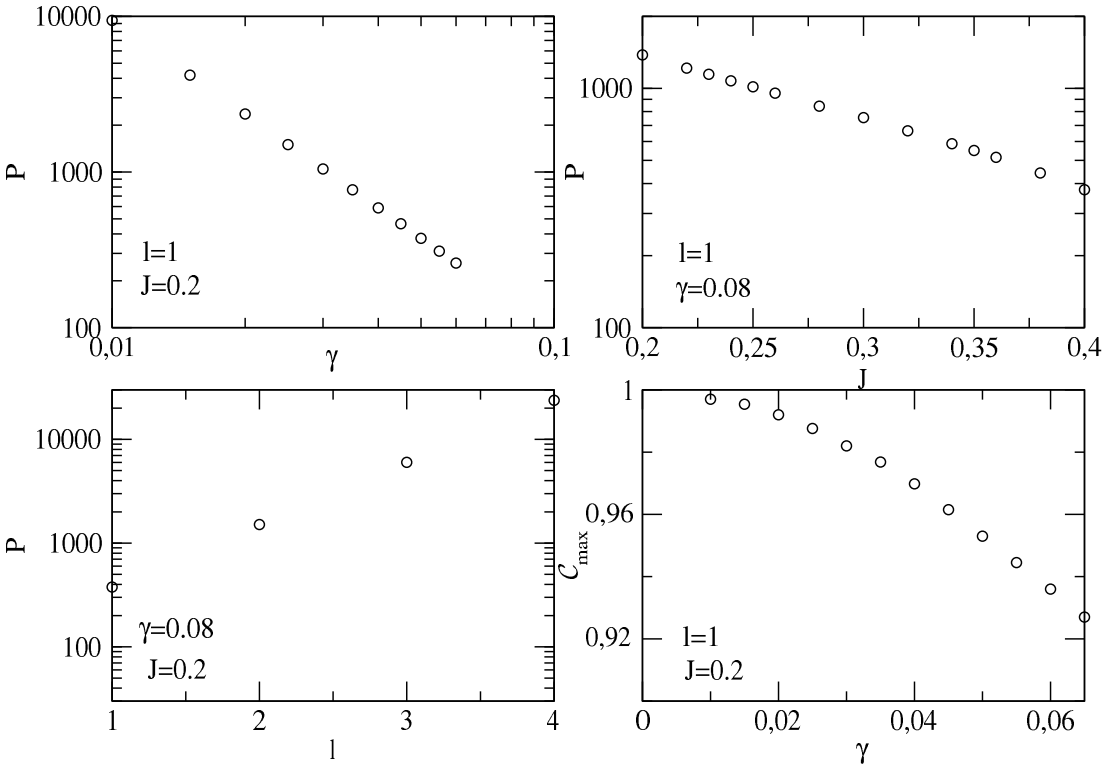

Figure 3.7 – *Variation of the oscillation period P of the concurrence as a function of γ (up left), J (up right), l (down left), and variations of the maximum of the concurrence C_{max} as a function of the coupling γ.*

J is increased.
As for the time needed for the growth of entanglement, we find that the period P of the oscillations increases exponentially with the distance $P(l) \sim \exp(c_2 l)$. Interestingly, for fixed coupling parameters, we find that the numerically fitted values of c_1 and c_1 are very close (1.36 and 1.38 respectively with the parameters of the figures 3.6 and 3.7). This would indicate a close relation between these two quantities.

The initial state of the defects is influencing the oscillatory behavior of the concurrence too. Changing this state has an effect in the maximum reached by the concurrence, but not on the period of the oscillations. We parameterize then the initial state of the defects as $|\Psi\rangle = |\psi\rangle_A \otimes |\psi\rangle_B$ with

$$|\psi\rangle_i = \cos\alpha_i |\uparrow\rangle_i + \sin\alpha_i |\downarrow\rangle_i, \quad i = A, B, \tag{3.63}$$

and we show the maximum of the concurrence as a function of $\tan\alpha_A$ and $\tan\alpha_B$ in the left panel of figure 3.8 for $J = 0.2$ and $\gamma = 0.04$. One can see that entanglement is found to be non zero for every initial state, except when one of the defects is prepared in the equal superposition

$$|\psi\rangle_i = \frac{1}{\sqrt{2}} \left(|\uparrow\rangle_i + |\downarrow\rangle_i \right), \quad i = A, B. \tag{3.64}$$

This state being an eigenstate of the coupling Hamiltonian, it will not evolve and

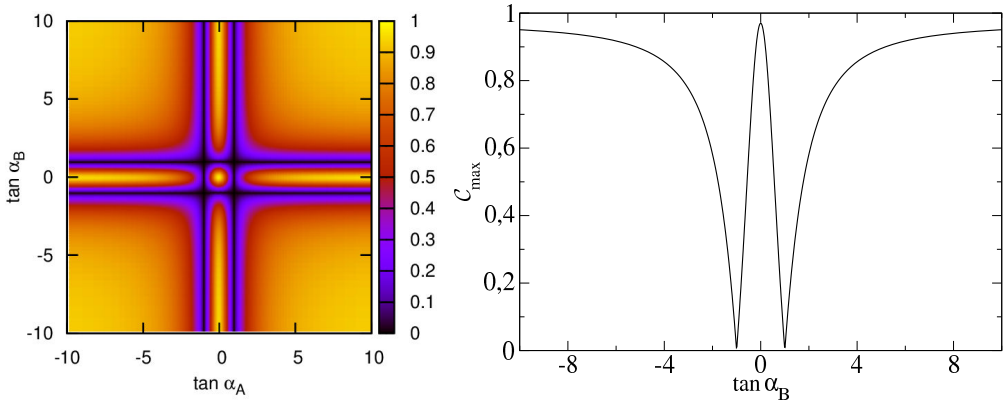

Figure 3.8 – *(left) Maximum of the concurrence as a function of* $\tan\alpha_A$ *and* $\tan\alpha_B$ *for* $J = 0.2$ *and* $\gamma = 0.04$*. (right) Maximum of the concurrence as a function of the state of the spin B when the state of the spin A is fixed to* $|\psi\rangle_A = |\uparrow\rangle$ *with the same parameters as the left plot.*

is then unable to develop correlations with the other defect. On the other hand, the concurrence reaches its biggest value when the two spins A and B are in one of the eigenstates of the σ^z operator $|\psi\rangle_i = \pm|\uparrow\rangle$ or $|\psi\rangle_i = \pm|\downarrow\rangle$.
The maximum of the concurrence is untouched by the exchange of the state of the two defects $|\psi\rangle_A \Leftrightarrow |\psi\rangle_B$, as we can see from the symmetry axe of equation $\tan\alpha_A = \tan\alpha_B$. The other axes correspond to the transformation $\cos\alpha_i|\uparrow\rangle_i + \sin\alpha_i|\downarrow\rangle_i \Leftrightarrow -\cos\alpha_i|\uparrow\rangle_i + \sin\alpha_i|\downarrow\rangle_i$ or $\cos\alpha_i|\uparrow\rangle_i + \sin\alpha_i|\downarrow\rangle_i \Leftrightarrow \cos\alpha_i|\uparrow\rangle_i - \sin\alpha_i|\downarrow\rangle_i$ with $i = A, B$.

3.4 Spectral density theory

The theory developed above is a feature of the degeneracy of the two states $|1,1\rangle$ and $|1,-1\rangle$ of the triplet sector, which come from the choice to work with a vanishing defect free Hamiltonian ($h = 0$). This approximation is usually not valid, and the free evolution of the defect spins has to be taken into account in the total dynamics.

Recently, it has been shown [WDCK+11, KWLM12, FKT+13] that environments may support decoherence free subspaces which can be used to generate correlations and entanglement between defects coupled to it. For the creation of the mentioned decoherence free subspace, it is necessary to tune the defect's frequencies in a value for which the modes of the environment interfere destructively, leading to an effective decoupling of the defects with the bath. These special frequencies are found by analyzing the spectral density of the bath [Wei99], which measures how strong the defects are coupled to the different modes of the environment. Its expression is given by [Wei99]

$$\mathcal{I}^{S(A)}(\widetilde{\omega}) = \frac{\pi}{2}\sum_n \frac{(\widetilde{\gamma}_n^{S(A)})^2}{\widetilde{\omega}_n^{S(A)}}\delta\left(\widetilde{\omega} - \widetilde{\omega}_n^{S(A)}\right). \tag{3.65}$$

Using the bath spectra (3.33) and (3.34) and taking the thermodynamic limit $N \to \infty$,

the continuous limit of $\mathcal{I}^{S(A)}$ is found to be

$$\mathcal{I}^{S}(\tilde{\omega}) = \frac{\gamma^2 \cos^2\left[\frac{1}{2}(2l-1)\arccos\left(\frac{1}{2J}(1-\tilde{\omega}^2)\right)\right]}{J\sqrt{1-\left(\frac{1}{2J}(1-\tilde{\omega}^2)\right)^2}}, \tag{3.66}$$

$$\mathcal{I}^{A}(\tilde{\omega}) = \frac{\gamma^2 \sin^2\left[\frac{1}{2}(2l-1)\arccos\left(\frac{1}{2J}(1-\tilde{\omega}^2)\right)\right]}{J\sqrt{1-\left(\frac{1}{2J}(1-\tilde{\omega}^2)\right)^2}}. \tag{3.67}$$

The figure 3.9 shows the spectral densities for different defect separations l for the

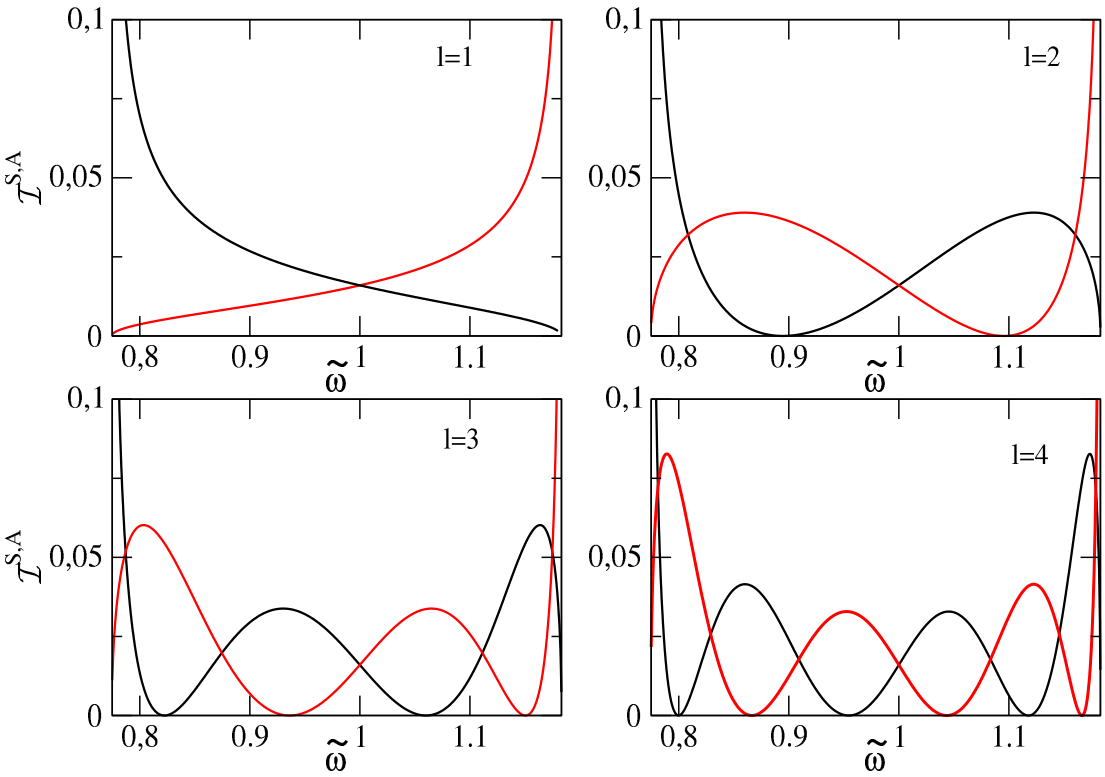

Figure 3.9 – *Spectral density associated to the-center-of mass (black) and relative coordinates (red) baths for several values of the distance. The parameters are* $\gamma = 0.04$, *and* $J = 0.2$.

center-of-mass and relative baths. The zeros in $\mathcal{I}_{S(A)}$ indicate the effective decoupling to the symmetric (antisymmetric) bath and the presence of the decoherence-free subspaces. For example for the relative bath, the zeros are found by vanishing the numerator of expression (3.67), leading to

$$\tilde{\omega}_0^A(p) = \sqrt{1 - 2J\cos\left(\frac{2p\pi}{2l-1}\right)}, \tag{3.68}$$

with $p = 0, \ldots, l-1$. We can note that the spectral density has l zeros for a distance $d = 2l-1$.

As mentioned previously, one has to tune the transition frequency of the defects to match one zero of the spectral densities $\mathcal{I}_{S(A)}(\widetilde{\omega})$ in order to recover the presence of a decoherence free subspace. For example, if the transition frequencies $2h$ is engineered to match one $\widetilde{\omega}_0^A(p)$, the two global states of the antisymmetric subspace $|\phi^A\rangle$ and $|\psi_A\rangle$ will be effectively decoupled from the antisymmetric bath, and then they will form the decoherence free subspace.

The definition (3.65) is valid for frequencies in the range $\widetilde{\omega} \in [\sqrt{1-2J}, \sqrt{1+2J}]$. On the other hand, the bosonization of the bath made in section 3.1.2 imposes $J \ll 1$ rending this interval confined around 1. The theory used in the previous section is valid for times shorter than the inverse of the energy gap $1/2h$, which turns to be close to 1 if the magnetic field is tuned to match a zero of the spectral density. As a consequence, the time evolution of the reduced density matrix (3.52) is not valid to determine the entanglement dynamics for times $t \ll 1$. Nevertheless, it can be used in order to determined the derivative of the concurrence at $t = 0$ $\partial_t \mathcal{C}(t)|_{t=0}$ in order to investigate the effect of the decoherence free subspace on the creation of entanglement between the two defect spins. The effective decoupling of the global states of the antisymmetric subspace $|\phi^A\rangle$ and $|\psi_A\rangle$ is equivalent to set the two corresponding functions $f^A(t)$ and $\varphi^A(t)$ to zero in the time evolution of the matrix elements of ρ_d. We show in figure 3.10 the derivative at $t = 0$ of the concurrence for different values of the two couplings J and γ.

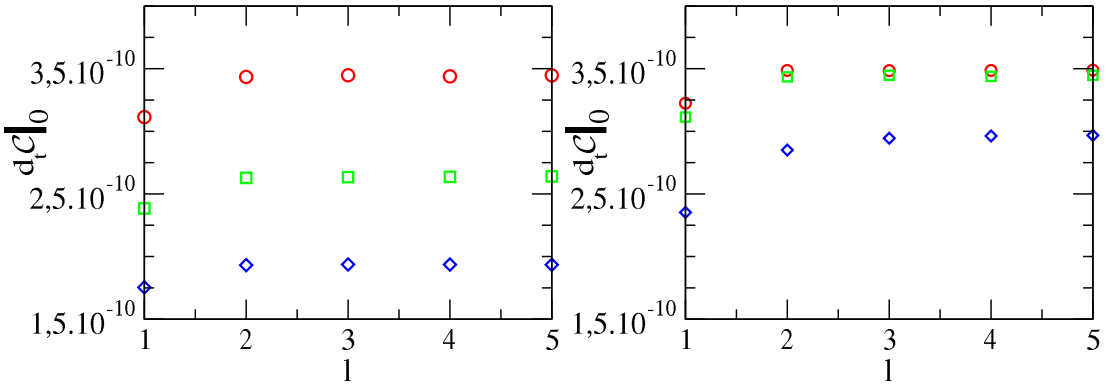

Figure 3.10 – *Derivative of the concurrence at $t = 0$ as a function of the distance. On the left plot, we set $J = 0.2$, and $\gamma = 0.08$ (red circles), 0.07 (green squares) and 0.06 (blue diamonds). On the right plot, we set $\gamma = 0.08$ and $J = 0.16$ (red circles), 0.2 (green squares) and 0.4 (blue diamonds). Initial state is $|\varphi_A\rangle \otimes |\varphi_B\rangle = |\uparrow\rangle_A \otimes |\uparrow\rangle_B$.*

We can see here a significant difference with the case of a vanishing magnetic field on the defect spins. Indeed, and as a direct consequence of the creation of the decoherence free subspace, the derivative of the concurrence is non zero even for finite distances, indicating an instantaneous creation of entanglement. At a given value of the parameters, the entanglement creation seems to be not very sensitive to the distance between the defects, the derivative of the concurrence reaching an almost constant value for $l > 2$. Once again, because we are looking at the dynamics over a small time scale, the two defect spins evolve independently for sufficiently large distance, leading the an independent value of the derivative of the concurrence

with respect to l.
We can finally note that, as we already observed in the previous section, an increase of γ or a decrease of J leads to a speed up of the establishment of the entanglement between the defects.

3.5 Conclusion

The entanglement dynamics between two defect spins locally coupled to an Ising chain has been studied in this chapter. After an Holstein-Primakoff transformation, the spin chain has been mapped into an assembly of interacting harmonic oscillators, and the introduction of new coordinates leads to a natural decoupling of the full dynamics. For a certain time regime, the dynamics of the two defect spins has been derived, and the entanglement evolution deduced from it. We analyzed the dependence of the concurrence on the parameters like the coupling constants, the distances between the defects, or their initial states. Finally, we used the spectral density and its zeros to create artificially a decoherence free subspace, which has for effect the instantaneous creation of entanglement between the defects, even at finite distances.

4 Disentanglement of Bell state by interaction with a non equilibrium environment

One of the main difficulties faced in the development of quantum information processing [NC00] comes from the unavoidable interaction of a quantum system with its surrounding environment. This phenomenon, the so-called decoherence process [Zur82, Zur02, Zur03, PZ01, Sch07], is detrimental for example for quantum computers, since it is responsible of the loss of quantum features such as entanglement or coherence, necessary for their achievement. It is in consequence of primary importance to understand the decoherence of a quantum system, and to try to limit its undesired effects. For example, dynamical control consisting in pulses applied to the systems have been proposed to limit the decoherence process [VL98, RFF+08]. With this in mind, a big number of studies have been realized about dynamics of open coherent quantum system interacting with an environment. A good candidate for the description of such an environment is quantum spin chain, since it describes many physical situations [dSDS03, KS06]. Models with one or two spins coupled globally or locally to spin baths have then be extensively studied in the literature [CPZ05, QSL+06, CFVP07, YZL07, RCG+07b, RCG+07a, CP08b, DQZ11, MSD12, SMD12, NDD12, FS13]. For example, a special focus has been set to the effects of the criticality of the environment on the decoherence dynamics [QSL+06], the latter being enhanced close to the critical point. Universal effects have also been pointed out in [CFVP07, CP08a], where it is shown that the decay of quantum correlations has an envelope independent of the strength of the system-environment coupling.
In Ref [CP08b], Cormick and Paz have studied the decoherence dynamics of two initially entangled spins coupled locally to a spin chain environment. In this work, and in most of the previously cited ones, the environment is initially "at equilibrium", since it is prepared in its ground state. In this chapter, we propose to look at what happens to the systems studied in [CP08b] when the environment is set out of equilibrium by a sudden change of one of its control parameters, realizing the so-called quantum quench [CC05, PSSV11]. The main objective of this work is to study the influence of the quench on the decoherence process with respect to the equilibrium situation treated in [CP08b].

The chapter is organized as follows: In a first section, we introduce the setup of our model, and we show that the decoherence dynamics of the system can be

completely determined by the Loschmidt echo, for which we give an expression in terms of the fermionic covariance matrix. Then, we turn to the description of non equilibrium disentanglement, starting with the rough description of the effect of the quench, with a focus of the case of an initial critical environment. It will be followed by the short time dynamics of the systems, and the comparison to the independent case. Finally, the chapter is ended by summary and conclusion.

4.1 Hamiltonian and dynamics

In the study, we consider then the same kind of system already introduced in the previous chapter, namely two non interacting defect spins locally coupled to a spin chain environment, see figure 4.1.

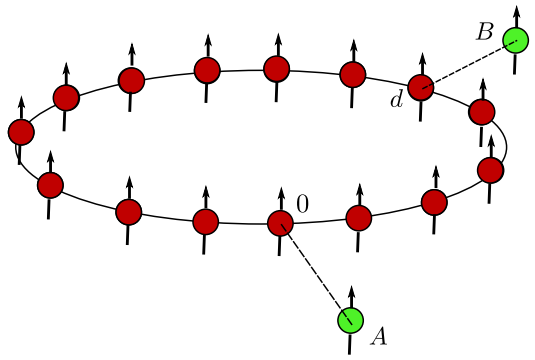

Figure 4.1 – *Two defect spins labeled A and B are locally coupled to two locations 0 and d of a spin chain environment.*

The total Hamiltonian governing the dynamics is $H_{tot} = H_E + H_I$ where H_E is the Hamiltonian of the Ising chain playing the role of the environment

$$H_E(h) = -J \sum_{j=0}^{N-1} \sigma_j^x \sigma_{j+1}^x - h \sum_{j=0}^{N-1} \sigma_j^z. \tag{4.1}$$

We choose here a positive nearest neighbor coupling J, and h is a transverse magnetic field. We assume periodic boundary conditions $\sigma_N^i = \sigma_0^i$ with $i = x, y, z$. The interaction between the defect spins and the environment is modeled by the interaction Hamiltonian H_I

$$H_I = -\varepsilon\big(|\uparrow\rangle\langle\uparrow|_A \otimes \sigma_0^z + |\uparrow\rangle\langle\uparrow|_B \otimes \sigma_d^z\big)\ , \tag{4.2}$$

where the state $|\uparrow\rangle_{A,B}$ is an eigenstate of the $\sigma_{A,B}^z$ operator satisfying $\sigma_{A,B}^z|\uparrow\rangle = |\uparrow\rangle$, and ε is the positive coupling constant which sets the strength of the interaction. Note that we work without local Hamiltonian for the defect spins. Indeed, due to the form of the coupling Hamiltonian, a Zeeman term turns to be uneffective on the disentanglement process.

The two spins forming the system are assumed to be initially in the maximally entangled Bell state $|\phi\rangle_{AB} = \frac{1}{\sqrt{2}}(|\uparrow\uparrow\rangle + |\downarrow\downarrow\rangle)$ and decoupled from the environment

such that the total state of the whole system can be written

$$|\psi(0)\rangle = |\phi\rangle_{AB} \otimes |G(h_i)\rangle_E, \tag{4.3}$$

where $|G(h_i)\rangle_E$ is the ground state of the spin chain environment $H_E(h_i)$ with initial magnetic field h_i. At time $t = 0^+$, in addition to the switch-on of the interaction, the transverse field of the environment is suddenly quenched from its initial value h_i to the final one h_f, forcing the chain to evolve in a non equilibrium regime.
In order to derive the dynamics of the defects, lets rewrite the total Hamiltonian like [YZL07]

$$H_{tot} = \sum_{k=1}^{4} |k\rangle\langle k| \otimes H_k(h_f), \tag{4.4}$$

where $|k\rangle$ is one of the four states $\{|\uparrow\uparrow\rangle, |\uparrow\downarrow\rangle, |\downarrow\uparrow\rangle, |\downarrow\downarrow\rangle\}$. One can see here that H_{tot} splits into four different channels governed by the effective Hamiltonians

$$H_{\uparrow\uparrow}(h_f) = H_E(h_f) - \varepsilon(\sigma_0^z + \sigma_d^z) \quad \text{if the defects are in the state } |\uparrow\uparrow\rangle, \tag{4.5}$$
$$H_{\uparrow\downarrow}(h_f) = H_E(h_f) - \varepsilon\sigma_0^z \quad \text{if the defects are in the state } |\uparrow\downarrow\rangle, \tag{4.6}$$
$$H_{\downarrow\uparrow}(h_f) = H_E(h_f) - \varepsilon\sigma_d^z \quad \text{if the defects are in the state } |\downarrow\uparrow\rangle, \tag{4.7}$$
$$H_{\downarrow\downarrow}(h_f) = H_E(h_f) \quad \text{if the defects are in the state } |\downarrow\downarrow\rangle. \tag{4.8}$$

The Hamiltonian $H_{\downarrow\downarrow}(h_f)$ is then equal to the environment Hamiltonian, whereas the three remaining are the environment Hamiltonian with a magnetic field acting at position 0 ($H_{\uparrow\downarrow}(h_f)$), d ($H_{\downarrow\uparrow}(h_f)$) or at both positions 0 and d ($H_{\uparrow\uparrow}(h_f)$) and taking the value $h_f + \varepsilon$ instead of h_f.
Since the total system is close and the Hamiltonians time independent, the initial state $|\psi\rangle(0)$ evolves according to

$$|\psi(t)\rangle = U(t)|\psi(0)\rangle, \tag{4.9}$$

with the evolution operator $U(t) = \exp(-iH_{tot}t)$. Using the expression (4.4) of the total Hamiltonian, one can easily show that the evolution operator takes the form

$$U(t) = \sum_{k=1}^{4} |k\rangle\langle k| \otimes U_k(t), \tag{4.10}$$

with

$$U_k(t) = e^{-iH_k(h_f)t}. \tag{4.11}$$

At a time t, giving the initial state of the defects, the global state becomes

$$|\psi\rangle(t) = \frac{1}{\sqrt{2}}\left[|\uparrow\uparrow\rangle \otimes |\varphi_{\uparrow\uparrow}(t)\rangle_E + |\downarrow\downarrow\rangle \otimes |\varphi_{\downarrow\downarrow}(t)\rangle_E\right], \tag{4.12}$$

with the evolved states

$$|\varphi_k(t)\rangle_E = e^{-iH_k(h_f)t}|G(h_i)\rangle_E, \tag{4.13}$$

where $k = \uparrow\uparrow, \downarrow\downarrow$. Since the initial state is a superposition of the two pure states $|\uparrow\uparrow\rangle$ and $|\downarrow\downarrow\rangle$, only the two corresponding channels appear in the evolved total state $|\psi\rangle(t)$.
The dynamics of the defect spins is encoded in their reduced density matrix obtained

by tracing out the environmental degrees of freedom from the total density matrix $\rho_s(t) = \mathrm{Tr}_E\{|\psi(t)\rangle\langle\psi(t)|\}$. We obtain

$$\rho_s(t) = \frac{1}{2}\sum_{k,k'} \langle G(h_i)|U_k^\dagger(t)U_k(t)|G(h_i)\rangle |k\rangle\langle k'|, \tag{4.14}$$

or, written in the computational base $\{|\uparrow\uparrow\rangle, |\uparrow\downarrow\rangle, |\downarrow\uparrow\rangle, |\downarrow\downarrow\rangle\}$

$$\rho_s(t) = \frac{1}{2}\begin{pmatrix} 1 & 0 & 0 & D_{\uparrow\uparrow,\downarrow\downarrow}(t) \\ 0 & 0 & 0 & 0 \\ 0 & 0 & 0 & 0 \\ D_{\downarrow\downarrow,\uparrow\uparrow}(t) & 0 & 0 & 1 \end{pmatrix}. \tag{4.15}$$

where

$$D_{\uparrow\uparrow,\downarrow\downarrow}(t) = \langle\varphi_{\downarrow\downarrow}(t)|\varphi_{\uparrow\uparrow}(t)\rangle = \langle G(h_i)|e^{iH_{\downarrow\downarrow}(h_f)t}e^{-iH_{\uparrow\uparrow}(h_f)t}|G(h_i)\rangle = D^*_{\downarrow\downarrow,\uparrow\uparrow}(t) \tag{4.16}$$

is the decoherence factor. One can remark that the populations do not evolve in time, whereas the coherence elements are affected by a factor between 0 and 1. In this base, the model describes a completely dephasing process. This decoherence factor, describing completely the dynamics of the defect spins, can be related to the so-called Loschmidt echo [GJPW12] via

$$\mathscr{L}_{\uparrow\uparrow,\downarrow\downarrow}(t) = \left|D_{\uparrow\uparrow,\downarrow\downarrow}(t)\right|^2 = \left|\langle G(h_i)|e^{iH_{\downarrow\downarrow}(h_f)t}e^{-iH_{\uparrow\uparrow}(h_f)t}|G(h_i)\rangle\right|^2. \tag{4.17}$$

Note that if we set $h_f = h_i$, meaning that we do not quench the transverse magnetic field of the chain, the initial state $|G(h_i)\rangle$ is an eigenstate of the Hamiltonian $H_{\downarrow\downarrow}$, and the echo reduces to $\mathscr{L}(t) = \left|\langle G(h_i)|e^{-iH_{\uparrow\uparrow}(h_i)t}|G(h_i)\rangle\right|^2$, which is the case treated by Cormick and Paz in [CP08b].

The decoherence process coming from the interaction with the bath leads to a loss of the entanglement initially present in the Bell state of the defects. In order to measure this disentanglement, we use the concurrence introduced in chapter 1. We remind that it is defined through the eigenvalues of the matrix $R = \rho\widetilde{\rho}$ with $\widetilde{\rho} = (\sigma^z \otimes \sigma^z)\rho^*(\sigma^z \otimes \sigma^z)$. In the case of the density matrix (4.15), one has $\rho = \widetilde{\rho}$, and then

$$R = \rho^2 = \frac{1}{4}\begin{pmatrix} 1+|D|^2 & 0 & 0 & 2D \\ 0 & 0 & 0 & 0 \\ 0 & 0 & 0 & 0 \\ 2D^* & 0 & 0 & 1+|D|^2 \end{pmatrix}, \tag{4.18}$$

leading to the eigenvalues $\varepsilon_1 = \frac{1}{4}(1+|D|)^2, \varepsilon_2 = \frac{1}{4}(1-|D|)^2, \varepsilon_3 = \varepsilon_4 = 0$. Finally, the concurrence is simply related to the Loschmidt echo via [1]

$$\mathcal{C}_{AB}(t) = \sqrt{\mathscr{L}(t)} = |D(t)|. \tag{4.19}$$

1. Note that if we would have worked with a Zeeman term for the defects $H_d = -\frac{h_d}{2}(\sigma_A^z + \sigma_B^z)$, this would have changed the density matrix element $\langle\uparrow\downarrow|\rho_s|\downarrow\uparrow\rangle$ to $\langle\uparrow\downarrow|\rho_s|\downarrow\uparrow\rangle = e^{-2ih_dt}D_{\uparrow\uparrow,\downarrow\downarrow} = \langle\downarrow\uparrow|\rho_s|\uparrow\downarrow\rangle^*$. But this phase factor disappears in the calculation of the concurrence, and the relation (4.19) still holds in that case.

The complete decoherence and disentanglement dynamics is then encoded in the Loschmidt echo, and our goal is to determined it.

4.2 Loschmidt Echo in the fermionic representation

In this section, we give the explicit expression of the Loschmidt echo in terms of fermionic operators. For later convenience, we use the fermionic representation for the description and the diagonalization of the environment. Indeed, as we mentioned previously, the two channels Hamiltonians are identical, except the two shifted magnetic fields in position 0 and d for $H_{\uparrow\uparrow}$, and they are then diagonalized in the same way, that is the Jordan-Wigner mapping followed by a Bogoliubov transformation. After the Jordan-Wigner transformation, the Hamiltonian rewritten in the relevant parity sector is

$$H = \sum_{i,j}(c_i^\dagger A_{ij} c_j + \frac{1}{2}(c_i^\dagger B_{ij} c_j^\dagger + h.c.)) \,, \tag{4.20}$$

where the Fermi operators satisfy the algebra $\{c_i, c_j^\dagger\} = \delta_{i,j}$, $\{c_i, c_j\} = \{c_i^\dagger, c_j^\dagger\} = 0$, and the symmetric A and antisymmetric B matrices are given by $A_{ij} = -2h_i\delta_{ij} - J[\delta_{i,j-1} + \delta_{i,j+1}]$ and $B_{ij} = J[\delta_{i,j+1} - \delta_{i,j-1}]$ where the indice N is identified with indices 0 in order to take into account the periodic boundary conditions. One can introduce the field operator

$$\mathbf{\Psi}^\dagger = (\boldsymbol{C}, \boldsymbol{C}^\dagger) = (c_0, \ldots, c_{N-1}, c_0^\dagger, \ldots, c_{N-1}^\dagger) \,, \tag{4.21}$$

to write the Hamiltonian in a more compact form

$$H = \frac{1}{2}\mathbf{\Psi}^\dagger \mathcal{H} \mathbf{\Psi}, \tag{4.22}$$

where the single particle Hamiltonian is given by

$$\mathcal{H} = \begin{pmatrix} -A & -B \\ B & A \end{pmatrix} \,. \tag{4.23}$$

The introduction of the unitary matrix

$$V = \begin{pmatrix} g & h \\ h & g \end{pmatrix} \tag{4.24}$$

diagonalizing the single particle Hamiltonian matrix $\mathcal{H}$: $\Lambda = V^\dagger \mathcal{H} V$ leads to the diagonalization of H through the normal modes $\boldsymbol{\eta} = V^\dagger \mathbf{\Psi}$

$$H = \frac{1}{2}\boldsymbol{\eta}^\dagger \Lambda \boldsymbol{\eta} \,. \tag{4.25}$$

These normal modes operators can be related to the original Fermi operators via the Bogoliubov coefficients g_{ij} and h_{ij}

$$\eta_k = \sum_i (g_{ik} c_i + h_{ik} c_i^\dagger), \tag{4.26}$$

with similar expressions for the adjoins $\eta_k^\dagger$. The inversion of these relations gives the original Fermi operators as a function of the normal modes

$$c_i = \sum_k (g_{ik}\eta_k + h_{ik}\eta_k^\dagger). \tag{4.27}$$

The Loschmidt echo (4.17) is nothing else but the square of the fidelity of the two evolved states

$$\begin{aligned} |\varphi_{\uparrow\uparrow}(t)\rangle =& e^{-iH_{\uparrow\uparrow}(h_f)t}|G(h_i)\rangle, \\ |\varphi_{\downarrow\downarrow}(t)\rangle =& e^{-iH_{\downarrow\downarrow}(h_f)t}|G(h_i)\rangle. \end{aligned}$$

This fidelity can be rewritten

$$|\langle\varphi_{\downarrow\downarrow}(t)|\varphi_{\uparrow\uparrow}(t)\rangle|^2 = \langle\varphi_{\uparrow\uparrow}(t)|\rho_{\varphi_{\downarrow\downarrow}}|\varphi_{\uparrow\uparrow}(t)\rangle \tag{4.28}$$

with $\rho_{\varphi_{\downarrow\downarrow}} = |\varphi_{\downarrow\downarrow}(t)\rangle\langle\varphi_{\downarrow\downarrow}(t)|$. Since the two Hamiltonians $H_{\uparrow\uparrow}$ and $H_{\downarrow\downarrow}$ are free fermionic, they are pure fermionic Gaussian states, and it has been shown in [KS10] that expression (4.28) can be evaluated by Gaussian Grassmann integrals involving the covariance matrices

$$C_k(t) = \langle\varphi_k(t)|\mathbf{\Psi}\mathbf{\Psi}^\dagger|\varphi_k(t)\rangle, \quad k = \uparrow\uparrow, \downarrow\downarrow, \tag{4.29}$$

and it reads [KS10, Cor09]

$$\mathscr{L}_{\uparrow\uparrow,\downarrow\downarrow}(t) = \sqrt{\left|\det\left(\mathbb{1} - C_{\downarrow\downarrow}(t) - C_{\uparrow\uparrow}(t)\right)\right|}, \tag{4.30}$$

where $\mathbb{1}$ is the $2N \times 2N$ identity matrix.
We need then the time evolution of the covariances matrices (4.29) in order to determine the Loschmidt echo. To derive the time dependence, it is better to switch into the Heisenberg representation. In this representation, the fermionic creation and annihilation operators obey to the evolution equation

$$\frac{dc_j}{dt} = i[H, c_j], \quad \frac{dc_j^\dagger}{dt} = i[H, c_j^\dagger], \tag{4.31}$$

leading to the differential equation

$$i\frac{d}{dt}\mathbf{\Psi}_k = \mathcal{H}_k\mathbf{\Psi}_k \tag{4.32}$$

for the fermionic fields $\mathbf{\Psi}_k$. In the last expression, the k indice referes to the two possible channels $\uparrow\uparrow$ and $\downarrow\downarrow$. Giving the initial conditions $\mathbf{\Psi}_k(0) = \mathbf{\Psi}_k$, these equations are easily integrated and one has

$$\mathbf{\Psi}_k(t) = e^{-it\mathcal{H}_k}\mathbf{\Psi}. \tag{4.33}$$

With this, on can write the time evolution of the covariance matrices like

$$C_k(t) = e^{-it\mathcal{H}_k}C(0)e^{it\mathcal{H}_k}, \tag{4.34}$$

with $C_k(0) = \langle G(h_i)|\mathbf{\Psi}_k\mathbf{\Psi}^\dagger{}_k|G(h_i)\rangle$ the matrices at time $t = 0$. Using the field operators $\boldsymbol{C}$ and $\boldsymbol{C}^\dagger$, these matrices are written

$$C(0) = \begin{pmatrix} \langle \boldsymbol{C}^\dagger \boldsymbol{C}\rangle & \langle \boldsymbol{C}^\dagger \boldsymbol{C}^\dagger\rangle \\ \langle \boldsymbol{C}\boldsymbol{C}\rangle & \langle \boldsymbol{C}\boldsymbol{C}^\dagger\rangle \end{pmatrix} , \tag{4.35}$$

where the brackets indicates the expectation value taken in the chain ground state $|G(h_i)\rangle$, and where we have dropped the indices k. The evolution of the Loschmidt echo is then derived using equation (4.30) together with (4.34) given the initial condition $C_k(0)$.

4.3 Quench dynamics

4.3.1 Weak and strong coupling regimes

We study first the influence of the coupling strength ε on the decoherence dynamics of the two defect spins. We show in figure 4.2 the time evolution of the Loschmidt echo for a quench from an initial transverse field $h_i = 1.5$ to a final one $h_f = 0.5$ and a distance $d = 1$ for different values of ε.

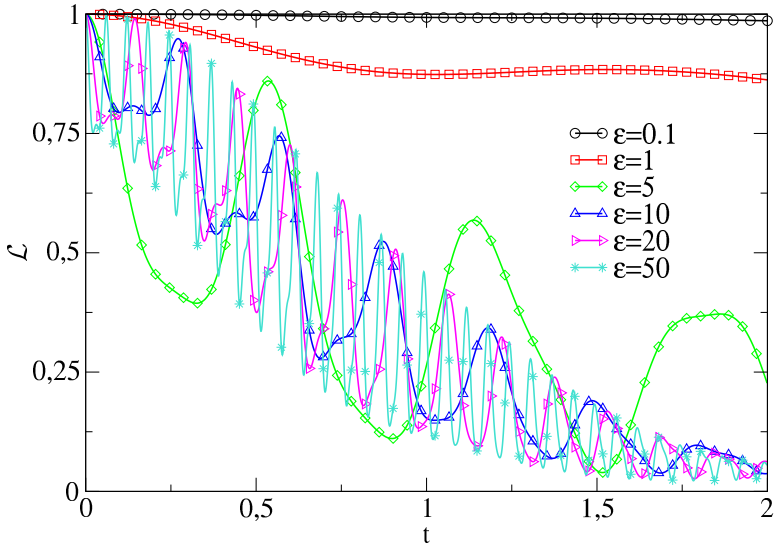

Figure 4.2 – *Time evolution of the Loschmidt echo after a quench from* $h_i = 1.5$ *to* $h_f = 0.5$ *for different values of the coupling strength* ε*. The distance is set to* $d = 1$ *and the size of the chain is* $N = 100$*.*

One can observe that the decoherence is faster as the coupling strength is increased. However the behavior of the echo is different depending on the strength of the coupling. Indeed, whereas the echo decreases slowly in the regime $\varepsilon \ll 1$, oscillations start to appear when the coupling is close to unity. When the coupling is increased further, $\varepsilon \gg 1$, the echo exhibits faster oscillations embedded inside an envelope which is independent of the coupling strength for sufficiently strong ε (see for instance the cases $\varepsilon = 20$ and $\varepsilon = 50$ in figure 4.2). Note that this change of behavior is not a consequence of the quench performed in the transverse field of the chain, since

it has been observed in the equilibrium situation $h_i = h_f$ as well [CPo8b]. The fast oscillations are the consequence of the introduction of two high frequencies by the coupling of the two defect spins, whereas the remaining frequencies, independent of ε, are responsible of the slow decay of the envelope.

4.3.2 Effect of the quench on the disentanglement dynamics

Let us now have a more precise look on the effect of the quench on the disentanglement properties of the two spins, through the time evolution of the Loschmidt echo obtained numerically by exact diagonalization using equations (4.30) and (4.34). The evolution of the echo in the weak and strong regimes ($\varepsilon = 0.1$ and $\varepsilon = 20$), $N = 100$ and $d = 1$ for different magnetic fields is shown in figures 4.3 and 4.4.

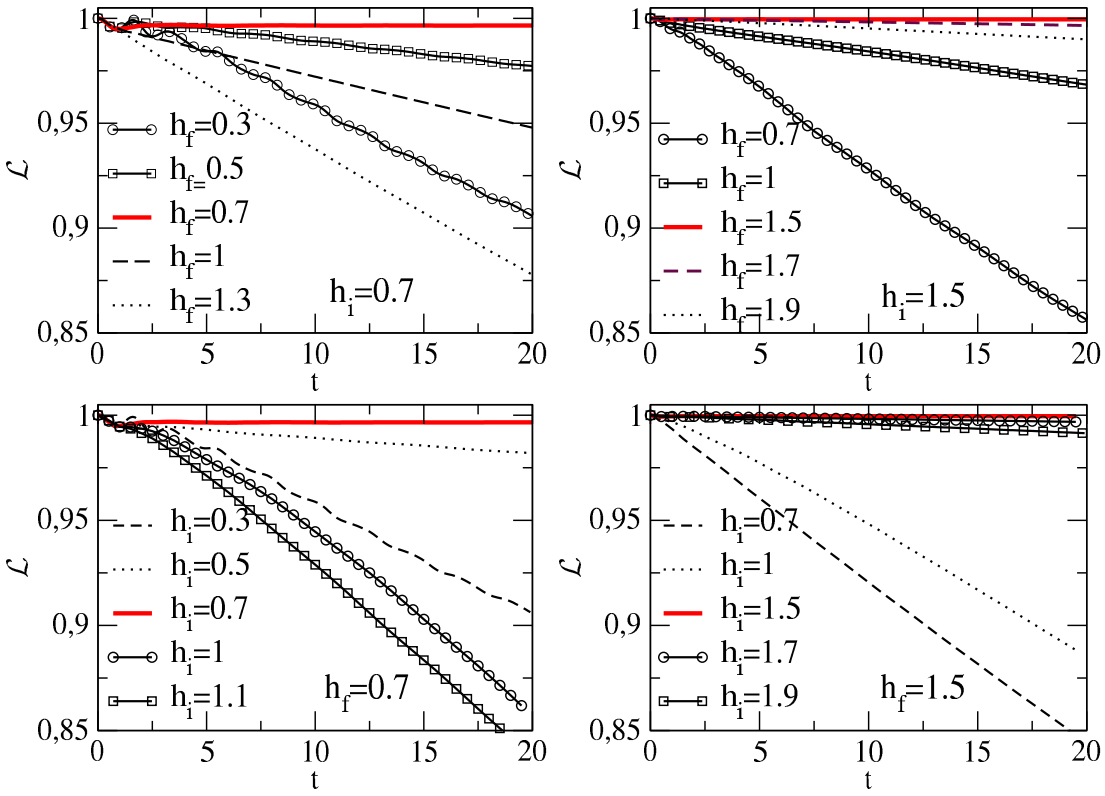

Figure 4.3 – *Time evolution of the echo for different quench protocols. For all plots, we choose* $N = 100$, $\varepsilon = 0.1$ *and keep fixed the distance to* $d = 1$. *The two up plots are a variation of the final magnetic field whereas the two down plots are a variation of the initial magnetic field. For all plots, the varied field is plotted with symbols for* $h_i > h_f$, *with dashed line for* $h_i < h_f$ *and in full line in the equilibrium case* $h_i = h_f$.

One can observe that the quench in the bath is always detrimental for the two system's spins, in the sense that it increases the decoherence, as we can see by comparaison to the equilibrium situation represented in red lines in figures 4.3 and 4.4. More the quench amplitude $|h_i - h_f|$ is important, more the decoherence is strong. Note that we observe such a behavior whatever the distance between the defect spins is. The behavior of the echo with the defect spins separation is opposite in weak and

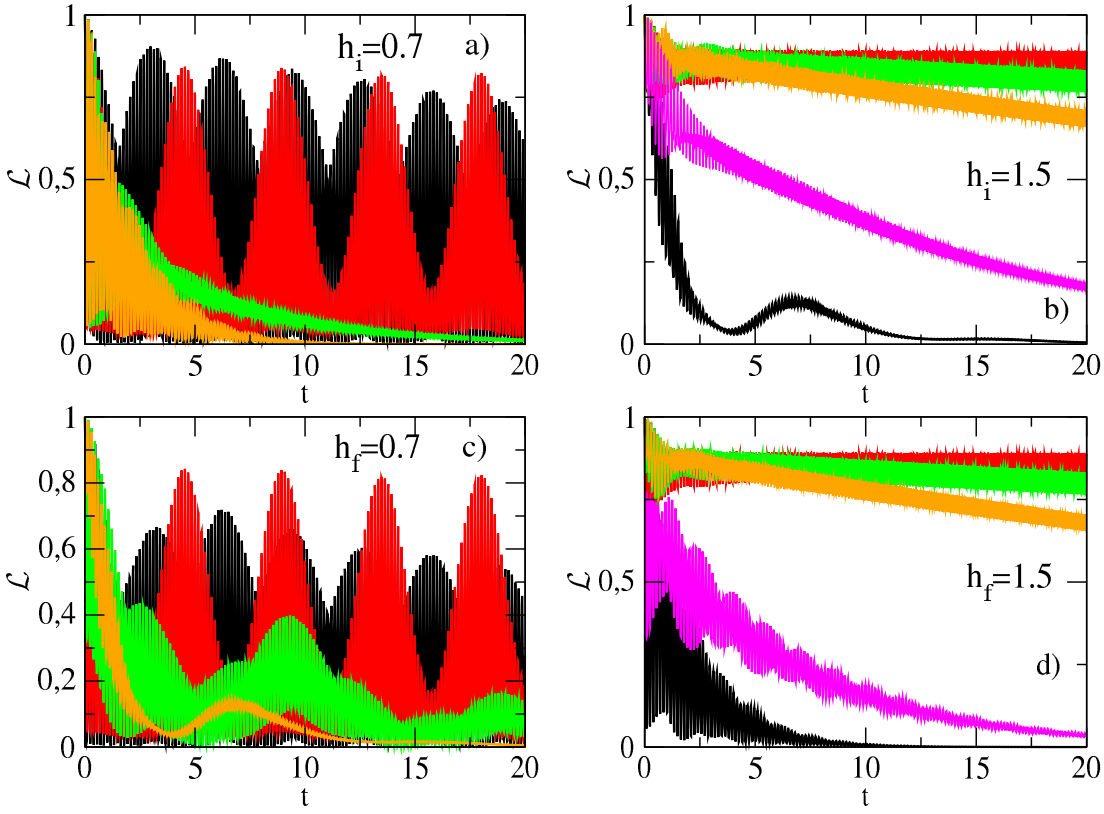

Figure 4.4 – *Time evolution of the echo in the strong coupling regime for different quench protocols. For all plots, we choose $N = 100$, $\varepsilon = 20$ and keep fixed the distance to $d = 1$. The two up plots are a variation of the final magnetic field whereas the two down plots are a variation of the initial one. For a) and c), the varied fields are $h_{i,f} = 0.5$ (black), $h_{i,f} = 0.7$ (red), $h_{i,f} = 1$ (green) and $h_{i,f} = 1.5$ (orange). For b) and d), the varied fields are $h_{i,f} = 0.7$ (black), $h_{i,f} = 1$ (magenta), $h_{i,f} = 1.5$ (red), $h_{i,f} = 1.7$ (green) and $h_{i,f} = 1.9$ (orange).*

strong coupling regimes. Indeed, in the weak coupling regime, the echo increases with the distance whereas it decrease with the distance in the strong coupling regime [CPo8b], as it is shown in figure 4.5 where, for a given quench protocol, we have plotted the echo for different distances and for the two coupling regimes.

In the strong coupling regime, one can observe beating of the envelope containing the fast oscillations, see for instance the red curves in plots a) and c) of figure 4.4. This feature, already observed in the equilibrium situation [CPo8b] can be explained in terms of the decomposition of the spectrum of the Hamiltonian. As we have already mentioned, the coupling of the defect spins to the chain brings two high frequencies, of the order of ε, in the spectrum. The remaining ones can be split into two different regions, namely the region lying between the two interaction points (at position 0 and d), and the one outside these points. When the transverse field is smaller than the critical value, it appears that the lowest energy level, belonging to the outside region, is the most populated [CPo8b]. This frequency is associated to the beating of the envelope. When the magnetic field is increased, more and more levels, with frequencies of the same order as the lowest energy level, start to be populated,

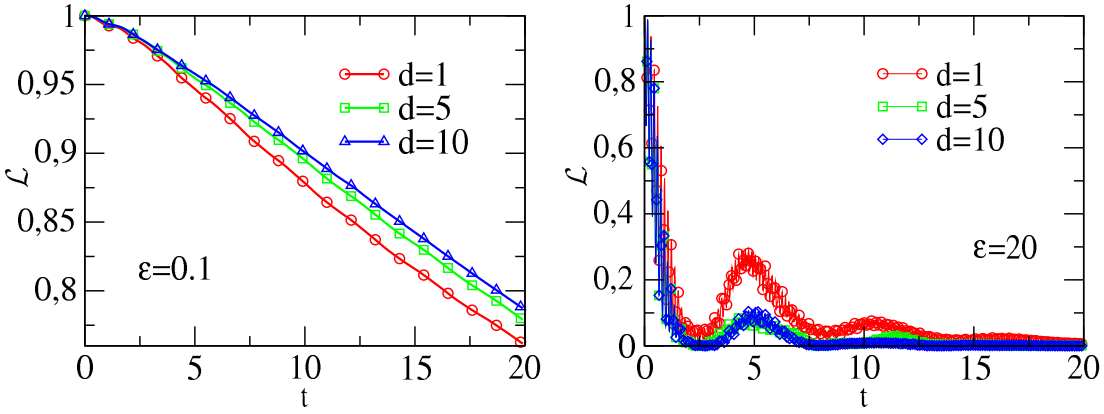

Figure 4.5 – *Time evolution of the Loschmidt echo in the weak (left) and strong (right) coupling regimes as a function of the distance for a quench from* $h_i = 1.5$ *to* $h_f = 0.5$*. The size of the environment is set to* $N = 100$*.*

resulting to the disappearance of the envelope beating.
In the weak coupling regime, the Loschmidt echo decrease monotonously during the time evolution, with some superimposed oscillations, whereas it tends to reach a constant value in the equilibrium case [CP08b, RCG+07b].

In order to check if our observations linking the amplitude of the quench with the strengh of the decoherence is correct, we study the dependence of the Loschmidt echo with the quench amplitude in the weak coupling case, where the decrease is monotonous. For this, we plot on figure 4.6 the echo at large time enough (we choose $t = 10$) as a function of the initial field when the final one is fixed (left panel), and as a function of the final field when the initial one is fixed (right panel).

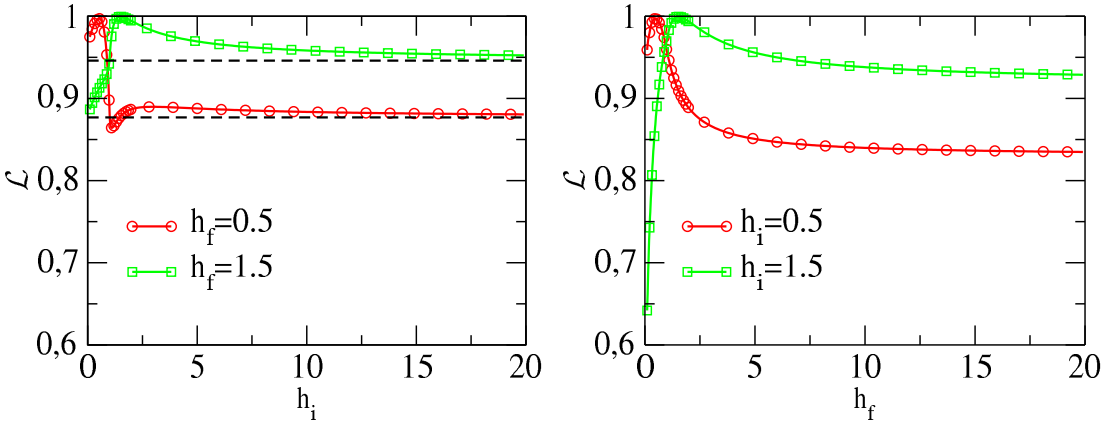

Figure 4.6 – *Loschmidt echo at time* $t = 10$ *as a function of the initial (final fixed) (left) and final (initial fixed) (right) magnetic field. The varied magnetic fields are* 0.5 *(red) and* 1.5 *(green). The dashed lines represent the limiting case of a completely polarized initial state (*$J = 0$*). Other parameters are* $d = 1$ *and* $\varepsilon = 0.1$*.*

The plots confirm our predictions, we clearly see that the echo increases until it

reaches its maximal value at the equilibrium point [2] $(h_i = h_f)$, and decreases once the equilibrium point, reflecting the fact that the quench situation is always unfavorable for the coherence dynamics. This last point can be explained by expending the initial ground state $|G(h_i)\rangle$ over the eigenstates $\{|\phi_n\rangle\}$ of the Hamiltonian $H_E(h_f)$ with eigenenergies $E_n(h_f)$

$$|G(h_i)\rangle = \sum_n a_n |\phi_n\rangle, \tag{4.36}$$

such that

$$e^{iH(h_f)t}|G(h_i)\rangle = \sum_n a_n e^{iE_n(h_f)t}|\phi_n\rangle. \tag{4.37}$$

Then, more the quench amplitude is important, more the number of oscillatory terms in the expansion (4.37) will be important, leading to a decrease of the Loschmidt echo [MSD12].
One can see in the curves of figure 4.6 that the echo saturates at constant value for very large initial or final fields. The saturation for initial strong field can be easily understood. Indeed, if h_i is very high, the initial state is close to the completely polarized state $|\uparrow\uparrow\cdots\uparrow\rangle$ where all the spins of the environment are pointing in the direction of the magnetic field. The initial covariance matrix associated to this state is then

$$C(0) = \begin{pmatrix} \mathbb{1} & 0 \\ 0 & 0 \end{pmatrix}, \tag{4.38}$$

which obviously does not depend on the value of the field, and as a consequence, the echo neither. The value of the echo of a completely polarized state, obtained by setting $J = 0$ in the initial Hamiltonian $H(h_i)$, is shown in dashed lines in the left panel of figure 4.6. One can check that, asymptotically, the echo converges to this limiting value.

The Loschmidt echo (and then the disentanglement) exhibits a clear signature of the quantum phase transition experienced by the Ising environment at the critical field $h = 1$. By looking at the left panel of figure 4.6, where the initial magnetic field is varied, one can see a jump in the curves when the field approaches the critical value. This behavior is better seen by analyzing the derivative with respect to the field h_i of the curves of figure 4.6. These derivatives are presented on figure 4.7 for two different final fields in the ordered and disordered phases.

In the two cases, we clearly see a singularity in $d_h\mathcal{L}$ at the critical value $h_i = 1$. One can note that the sign of the peak is different in the two cases. Indeed, for $h_f = 0.5$, the critical point is located after the equilibrium point $h_i = h_f = 0.5$, that is when the echo is decreasing with the field leading to a negative derivative. The opposite situation occurs for $h_f = 1.5$, the critical point being located before the equilibrium point $h_i = h_f = 1.5$, the derivative is positive since the echo is increasing with the field.
On the other hand, the derivative with respect to the final magnetic field h_f at fixed initial one are more smooth and does not show such singularity as we can see in the inset of the figure 4.7. The critical behavior of the Loschmidt echo is then completely set by the initial field h_i, whereas the final one is only responsible of dynamical effects

2. Note that at the equilibrium point, we recover the value of the echo obtained in [CPo8b].

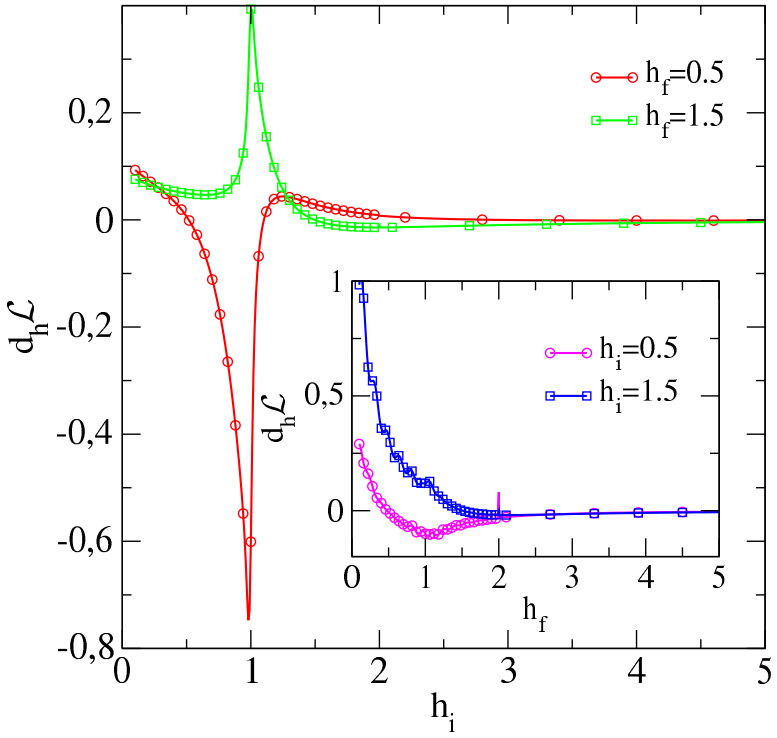

Figure 4.7 – *First derivative of the Loschmidt echo with respect to the initial field h_i for two final fields $h_f = 0.5$ (circles) and $h_f = 1.5$ (squares). In the inset is shown the first derivative of the Loschmidt echo with respect to the final field h_f for two initial fields $h_i = 0.5$ (circles) and $h_i = 1.5$ (squares). The other parameters are $N = 100$, $\varepsilon = 0.1$, $d = 1$ and $t = 10$.*

through the information transfer mediated by the chain.

Due to the finite size of the environment, the first derivative of the Loschmidt echo reaches a finite value and does not diverge. Indeed, the divergence of the correlation length in the thermodynamic limit is suppressed by finite size effects. In figure 4.8, we plot the derivative of the Loschmidt echo with respect to the initial field for several sizes of the chain. On can see that the maximum in the singularity of the derivative is rounded and appears at a value of the field h_{max} shifted from the infinite critical value $h_c = 1$. Numerical analyses show that the maximum value of the derivative of the Loschmidt echo diverges logarithmically with the environment size like

$$d_h \mathcal{L}|_{h_{max}} \sim \ln N, \tag{4.39}$$

whereas the position of the maximum h_{max} approaches the critical value as a power law of the environmental size :

$$|h_c - h_{max}| \sim N^{\gamma}, \tag{4.40}$$

with an exponent γ found numerically to be $\gamma \sim -1.1$, as shown in figure 4.9, where we plot the maximum reached by the derivative and the shift to the critical point both with respect to the environment size.

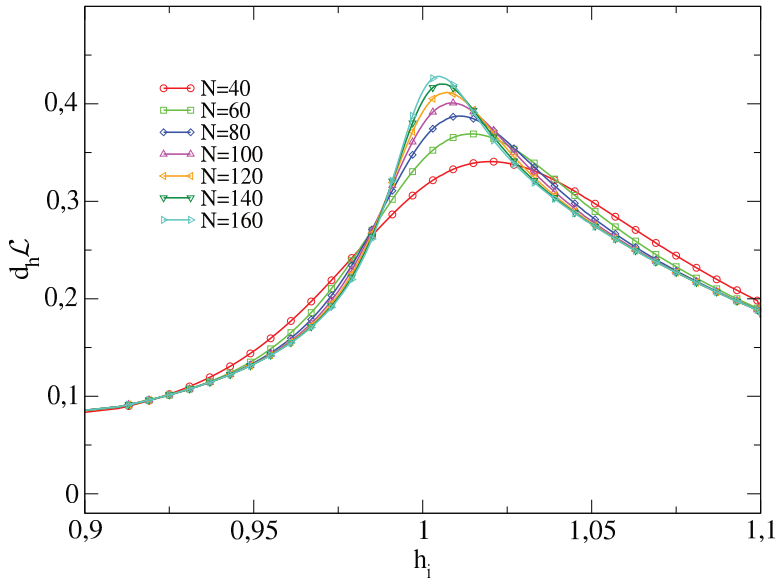

Figure 4.8 – *First derivative of the Loschmidt echo with respect to the initial field h_i for several sizes of the chain, from $N = 40$ to $N = 160$. The other parameters are $\varepsilon = 0.1$, $d = 1$, $h_f = 1.5$ and $t = 10$.*

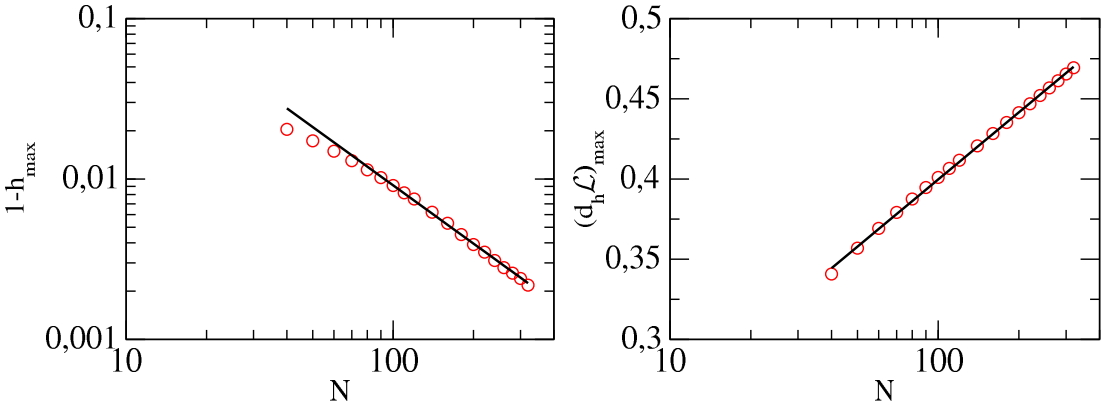

Figure 4.9 – *Left: Scaling of the position of the maximum h_{max} of the derivative as a function of the environment size. Right: Scaling of the maximum reached by the derivative $d_h\mathcal{L}|_{h_{max}}$ as a function of the environment size.*

Using arguments of critical scaling theory [Hen99], the γ exponent is expected to be related to the critical exponent ν of the correlation length like

$$\gamma = -\frac{1}{\nu} = -1. \tag{4.41}$$

The numerical departure of γ from the scaling theory prediction can be attributed to strong corrections to finite size scaling. These corrections are numerically compatible with a $1/N$ scaling correction :

$$N(h_c - h_{max}) \sim 1 + const.\frac{1}{N}. \tag{4.42}$$

Note that these scaling relations are coherent with those found in [OAFF02, ZZL08].

4.3.3 Short times dynamics

In this section, we focus our attention to the short time dynamics of the Loschmidt echo. For times shorter than the typical time of the system $t \ll t_{typ}$ given by

$$t_{typ} = 1 \quad \text{if } \varepsilon \ll 1$$
$$t_{typ} = \frac{1}{\varepsilon} \quad \text{if } \varepsilon \gg 1,$$

one can show that the decay is Gaussian [Per84, RCG+07b] $\mathscr{L}(t) \sim \exp(-\alpha t^2)$ where α is the Gaussian rate. The coefficient α can be determined by expending the two exponentials appearing in the echo up to the second order in t:

$$\begin{aligned} e^{iH_{\downarrow\downarrow}t}e^{-iH_{\uparrow\uparrow}t} &= 1 + it(H_{\uparrow\uparrow} - H_{\downarrow\downarrow}) - \frac{t^2}{2}(H_{\uparrow\uparrow}^2 + H_{\downarrow\downarrow}^2) + t^2 H_{\uparrow\uparrow}H_{\downarrow\downarrow} + \mathcal{O}(t^3) \\ &= 1 + i\widetilde{H}_I t - \frac{t^2}{2}\left(H_{\downarrow\downarrow}^2 + H_{\uparrow\uparrow}^2 - 2H_{\downarrow\downarrow}H_{\uparrow\uparrow}\right) + \mathcal{O}(t^3), \end{aligned} \tag{4.43}$$

where $\widetilde{H}_I = H_{\uparrow\uparrow} - H_{\downarrow\downarrow} = -\varepsilon(\sigma_0^z + \sigma_d^z)$. Remarking that we can write

$$\left(H_{\uparrow\uparrow} - H_{\downarrow\downarrow}\right)^2 = \left(H_{\downarrow\downarrow}^2 - 2H_{\downarrow\downarrow}H_{\uparrow\uparrow} + H_{\uparrow\uparrow}^2\right) + \left[H_{\uparrow\uparrow}, H_{\downarrow\downarrow}\right], \tag{4.44}$$

equation (4.43) becomes, taking the average over the ground state $|G(h_i)\rangle$,

$$\langle G(h_i)|e^{iH_{\downarrow\downarrow}t}e^{-iH_{\uparrow\uparrow}t}|G(h_i)\rangle = 1 - \frac{t^2}{2}\left(\langle \widetilde{H}_I^2\rangle - \langle\left[H_{\uparrow\uparrow}, H_{\downarrow\downarrow}\right]\rangle\right) + i\langle\widetilde{H}_I\rangle + \mathcal{O}(t^3). \tag{4.45}$$

The two Hamiltonians $H_{\uparrow\uparrow}$ and $H_{\downarrow\downarrow}$ being Hermitian, their commutator is antihermitian, $\left[H_{\uparrow\uparrow}, H_{\downarrow\downarrow}\right] = i\boldsymbol{C}$ with $\boldsymbol{C}^\dagger = \boldsymbol{C}$. It follows

$$\langle G(h_i)|e^{iH_{\downarrow\downarrow}t}e^{-iH_{\uparrow\uparrow}t}|G(h_i)\rangle = 1 - \frac{t^2}{2}\langle\widetilde{H}_I^2\rangle + i\left(\langle\widetilde{H}_I\rangle t + \frac{t^2}{2}\langle\boldsymbol{C}\rangle\right) + \mathcal{O}(t^3). \tag{4.46}$$

Finally, taking the square modulus, we obtain

$$\mathcal{L}(t) = 1 - t^2\left[\langle\widetilde{H}_I^2\rangle - \langle\widetilde{H}_I\rangle^2\right] + \mathcal{O}(t^3). \tag{4.47}$$

The Gaussian rate α depends only on the variance of the interaction Hamiltonian taken in the initial state of the bath $|G(h_i)\rangle$, and is as a consequence independent of the quench protocol, as we can see on figure 4.10 where the short time behavior of the echo is shown for several final magnetic fields for both weak and strong coupling regimes.

The variance α can be determined using the expression of the interaction Hamiltonian $\widetilde{H}_I$ in terms of the normal modes of the Hamiltonian $H_E(h_i)$. Using the relation $\sigma_i^z = 2c_i^\dagger c_i - 1$ and equation (4.27), one finds

$$\widetilde{H}_I = -2\varepsilon\sum_{kl}\left[(g_{0k}\eta_k^\dagger + h_{0k}\eta_k)(g_{0l}\eta_l + h_{0l}\eta_l^\dagger) + (g_{dk}\eta_k^\dagger + h_{dk}\eta_k)(g_{dl}\eta_l + h_{dl}\eta_l^\dagger)\right] + 2\varepsilon. \tag{4.48}$$

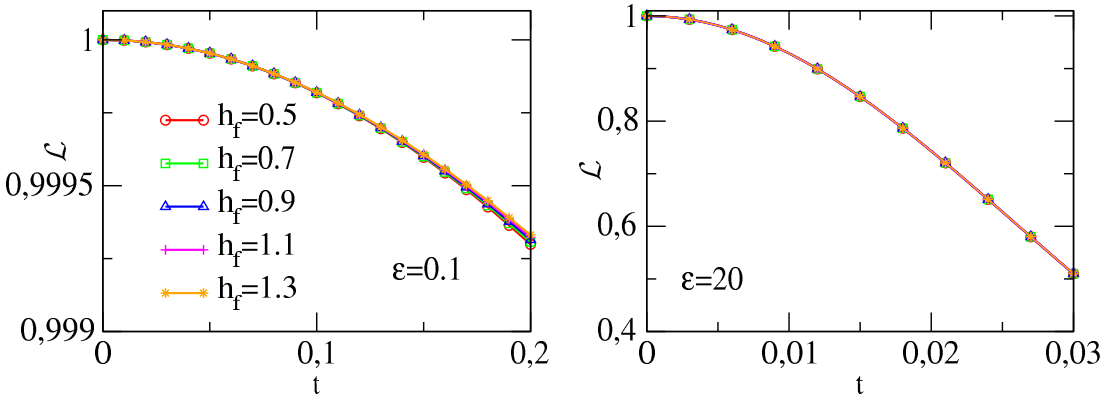

Figure 4.10 – *Short time evolution of the Loschmidt echo for different quench protocols in the weak (left) and strong coupling (right) regimes. Other parameters are* $N = 100$, $h_i = 1.5$ *and* $d = 1$.

Using the expectation values of the normal modes into the ground state $\langle \eta_k \eta_l \rangle = \langle \eta_k^\dagger \eta_l^\dagger \rangle = 0$ and $\langle \eta_k \eta_l^\dagger \rangle = \delta_{kl}$, on obtains

$$\langle \widetilde{H}_I \rangle^2 = 4\varepsilon^2 \left[\sum_k \left(|h_{0k}|^2 + |h_{dk}|^2 \right) - 1 \right]^2 , \tag{4.49}$$

and

$$\begin{aligned} \langle \widetilde{H}_I^2 \rangle =& 4\varepsilon^2 \Bigg\{ \left[\sum_k (|h_{0k}|^2 + |h_{dk}|^2) - 1 \right]^2 + \sum_{k \neq l} \Big[(g_{0k} h_{0l})^2 + (g_{dk} h_{dl})^2 \\ & + 2h_{dl} h_{0l} g_{dk} g_{0k} - 2h_{dk} h_{0l} g_{dl} g_{0k} - h_{0k} h_{0l} g_{0k} g_{0k} - h_{dk} h_{dl} g_{dk} g_{dk} \Big] \Bigg\} \end{aligned} \tag{4.50}$$

leading to the final expression for the variance α [3]

$$\begin{aligned} \alpha = 4\varepsilon^2 \sum_{k \neq l} \Big[& (g_{0k} h_{0l})^2 + (g_{dk} h_{dl})^2 + 2h_{dl} h_{0l} g_{dk} g_{0k} \\ & - 2h_{dk} h_{0l} g_{dl} g_{0k} - h_{0k} h_{0l} g_{0k} g_{0k} - h_{dk} h_{dl} g_{dk} g_{dk} \Big] . \end{aligned} \tag{4.51}$$

Notice that in terms of spin correlation functions, the variance α is nothing but

$$\alpha = 2\varepsilon^2 \left(1 + \langle \sigma_0^z \sigma_d^z \rangle_c - \langle \sigma_0^z \rangle^2 \right) , \tag{4.52}$$

where $\langle AB \rangle \equiv \langle AB \rangle - \langle A \rangle \langle B \rangle$ is the connected correlator, and where we have used the fact that $\langle \sigma_0^z \rangle = \langle \sigma_d^z \rangle$ due to the translational invariance.

In figure 4.11, α is plotted as a function of the initial field h_i for several distances and for $\varepsilon = 0.1$. On can see that the full lines given by equation (4.51) match perfectly the numerical fit of the echo represented by the symbols. For initial magnetic fields

3. We can note that if we set $d = 0$, meaning that the two spins are coupled to the same spin in the chain, we recover the formula obtained in [RCG+07b], but with a coupling constant ε two times stronger. Indeed, $\widetilde{H}_I = -\varepsilon(\sigma_0^z + \sigma_{d=0}^z) = -(2\varepsilon)\sigma_0^z$.

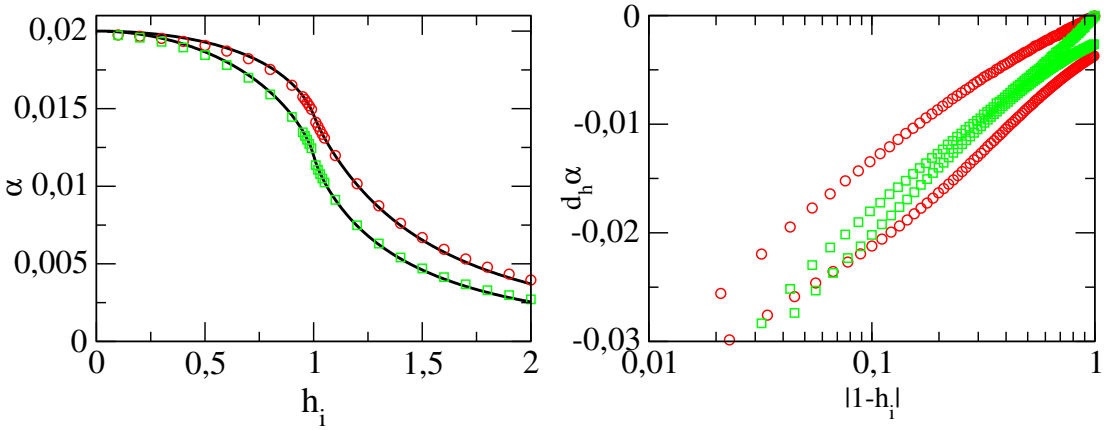

Figure 4.11 – *Gaussian rate α as a function of the initial magnetic field h_i (left). The symbols represent a numerical fit of the echo for $d = 1$ (dots) and $d = 5$ (squares) whereas the full line represents the numerical computation of equation (4.51). On the right panel are plotted the derivative of α with respect to $|h_c - h_i|$ for the two distances. The other parameters are $N = 100$, $h_f = 0.5$ and $\varepsilon = 0.1$.*

close enough to the critical value $h_i = 1$, the derivative of α with respect to the field exhibits a logarithmic divergence characteristic of the $2d$-Ising universality class.

For large distances compared to the correlation length of the ground state environment $d \gg \xi$, one expects a saturation of the Gaussian rate. Indeed, for large distances and because we look at short time scales, one defect spin evolves without influencing the other one, and the dynamics is independent, leading to the saturation. This can be seen by analyzing equation (4.52). For $d \gg \xi$, the connected correlator $\langle \sigma_0^z \sigma_d^z \rangle_c$ vanishes and the saturation values of α becomes

$$\alpha(d \gg 1) = 2\varepsilon^2 \left(1 - \langle \sigma_0^z \rangle^2\right). \tag{4.53}$$

On the other hand, when the environment approaches criticality $h \approx 1$, the situation is different since long-range correlations are present in the initial state, making the evolution not independent even for large distances. Close to the critical point, the decay of the connected correlator is algebraic with [Hen99]

$$\langle \sigma_0^z \sigma_d^z \rangle_c \sim d^{-2}, \tag{4.54}$$

leading to an algebraic decay of α toward the infinite value $\alpha(d \to \infty)$. The correlation functions and the local magnetization of the critical Ising model are known analytically [Pfe70]

$$\langle \sigma_0^z \sigma_d^z \rangle_c = \frac{4}{\pi^2} \frac{1}{4d^2 - 1}, \quad \langle \sigma_0^z \rangle = \frac{2}{\pi}, \tag{4.55}$$

leading to the critical value of α

$$\alpha^{crit} = 2\varepsilon^2 \left(1 - \frac{4}{\pi^2}\left(1 + \frac{1}{1 - 4d^2}\right)\right). \tag{4.56}$$

The correlators out of criticality are more complicated to determined analytically, and require the computation of Toeplitz determinants [LSM61, Pfe70]. We plot on the left

panel of figure 4.12 the Gaussian rate α as a function of the distance for several initial fields. The predictions given by equation (4.51) match the numerical fit of the echo, witch saturate in the value given by equation (4.53). On the right panel, we show the critical algebraic decay of α toward the infinite value with a power law with exponent -2, as expected from critical phenomena.

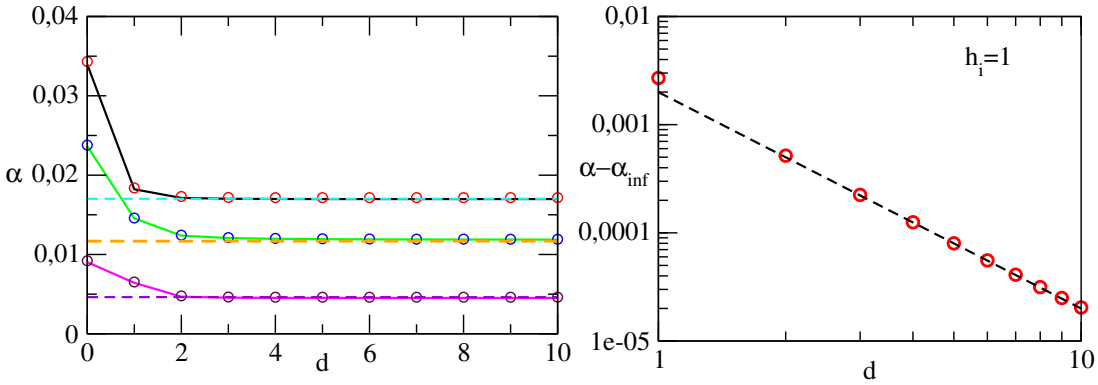

Figure 4.12 – *(left) Gaussian rate α as a function of the distance. The initial fields are, from top to bottom $h_i = 0.7$, $h_i = 1$ (critical environment) and $h_i = 1.5$. The dots are obtained by a numerical fit, the full lines are the calculation of the equation (4.51), and the dashed lines are the saturation values (4.53). On the right is shown on logarithmic scales the algebraic decay toward the infinite value of α in the critical case $h_i = 1$. The dashed line has a slope equal to -2. Other parameters are $N = 100$, $h_f = 0.7$ and $\varepsilon = 0.1$.*

4.3.4 Revival time

The dynamics described in the previous section referred to times shorter than a revival time. Indeed, depending on the separation d between the spins and the size N of the environment, we observe a significant change in the behavior of the Loschmidt echo at long times, as we can see on figure 4.13, where we plot the echo for different separation distances and two sizes of the environment ($N = 100$ and $N = 200$). Note that the following considerations will be exampled in the weak coupling case ($\varepsilon = 0.1$), but the phenomenology of the revival is the same in the strong coupling regime.
One can see in figure 4.13 that for $t < N/4$, the decay of the echo is basically linear for initial state far from criticality and its seems to be weakly dependent on the distance. At time $t \simeq N/4$, one clearly see that, for separation distances far from the symmetric position (i.e $d = N/2$), the echo turns to a linear increase indicating a recovering of the coherence between the spins. Note that this phenomenon appears every $t_n \simeq n \times N/4$.

On the other hand, when the distance between the spins gets close to the symmetric situation $d = N/2$, we observe a supplementary singularity following by a speed up of the linear decrease of the echo appearing at half the previous revival time $\tau^* \simeq t^*/2 \simeq N/8$. The maximum of the slope is reached when the two spins are facing each other, i.e when $d = N/2$. We plot on the left panel of figure 4.14 the

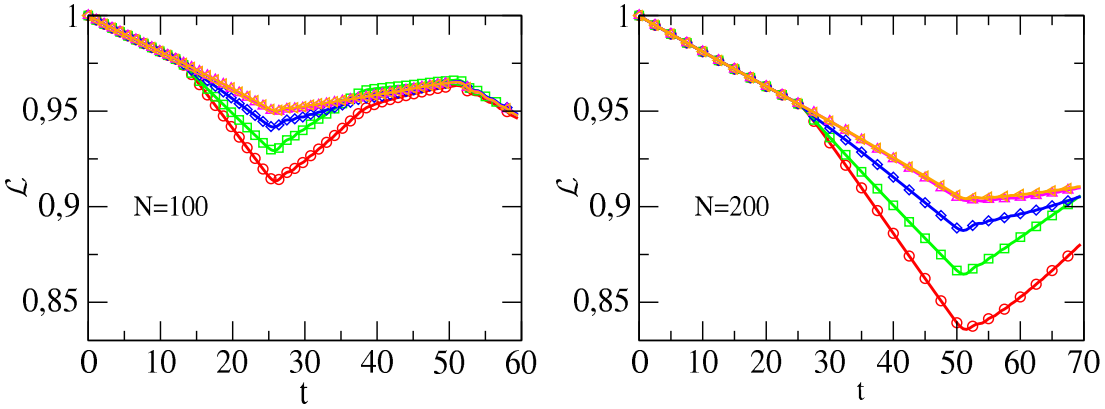

Figure 4.13 – *Loschmidt Echo for distances $N/2$ (red circles), $N/2-1$ (green squares), $N/2-2$ (blue diamonds), $N/2-5$ (magenta up triangles) and $N/2-15$ (orange left triangles) for $N=100$ (left) and $N=200$ (right). Note that due to their almost perfect matching, the two curves for $d=N/2-5$ and $d=N/2-15$ are nor distinguishable. The other parameters are set to $\varepsilon=0.1$, $h_i=1.5$ and h_f=0.99.*

derivative of the Loschmidt echo with respect to time at fixed quench protocol for different distances $N/2, N/2-1, N/2-2$ and $N/2-15$.

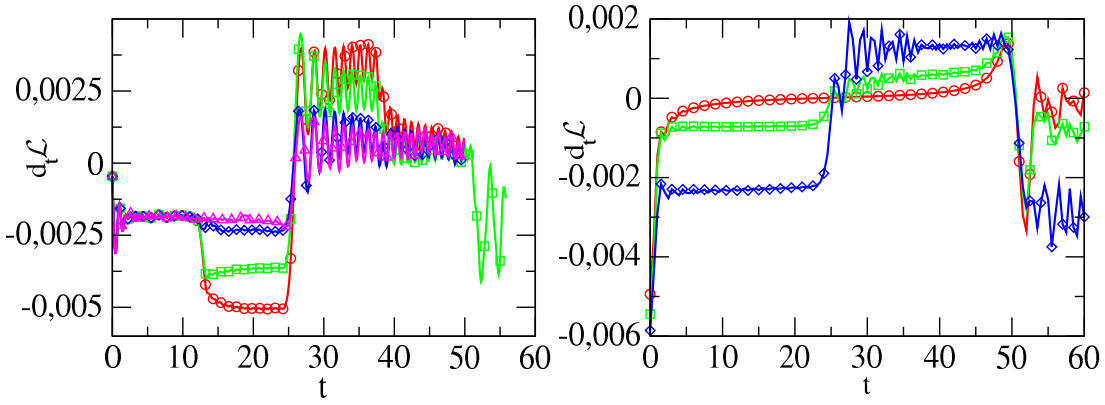

Figure 4.14 – *First derivative of the Loschmidt Echo with respect to time. In the left plot, we keep fixed $h_i=1.5$ and $h_f=0.99$ and we vary the distance. The different plots are $d=N/2$ (red circles), $d=N/2-1$ (green squares), $d=N/2-2$ (blue diamonds) and $N/2-15$ (magenta triangles) . In the right plot, the distance is $d=1$, $h_f=0.99$ and $h_i=0.99$ (red circles), $h_i=0.9$ (green squares), and $h_i=0.7$ (blue diamonds). The others parameters are $\varepsilon=0.1$ and $N=100$.*

One can clearly see the singularity in the derivative at $t=\tau^*$ for distances close to the symmetric situation. This singularity has already disappeared for the distance $d=N/2-15$, see the magenta triangles in figure 4.14. Note that whatever the distance between the spin is, we observe a singularity in the derivative at time $t=t^*\simeq 25$, reflecting the distance independent recovery of the coherence.

In the right panel of the figure 4.14 is plotted the time derivative of the echo at distance fixed to $d=1$ for different quench protocols, including the equilibrium situation $h_i=h_f$. As expected from the previous observation, we do not see any

effect at time $t = \tau^*$ because we are far from the symmetric situation. For the two out of equilibrium cases ($h_i = 0.7$ and $h_i = 0.9$ to $h_f = 0.99$), we only see the effect at time $t = t^*$. On the other hand, in the equilibrium situation, the revival occurs at a time t^*_{eq} that is twice the value of the non equilibrium situation, $t^*_{eq} = 2t^*$. This difference between equilibrium and non equilibrium in the revival time can be understood in terms of quasiparticles emission [CC05, SLRD13]. Indeed, the non equilibrium case corresponds to a global quench, where the transverse magnetic field is suddenly changed everywhere in the chain. As a consequence of this global change in the energy, a pair of quasiparticles with momentum $\pm k$ is emitted at every position in the chain. The fastest group velocity of these quasiparticles is given by

$$v_g = \max_k \left(\frac{\partial \varepsilon_k}{\partial k} \right) \Big|_k = \begin{cases} 2h_f & \text{if} \quad h_f < 1 \\ 2 & \text{if} \quad h_f \geq 1 \end{cases} , \tag{4.57}$$

and because every site in the chain acts as a local emitter, the quasiparticles need to travel only the half of the chain to start to reconstruct the initial state, leading to a revival time $t^* = N/2v_g$. On the contrary, the equilibrium case corresponds to a local quench occurring only at the positions where the two spins are coupled. As a consequence, the excitations are emitted only at these two positions, and they need to travel the complete chain to restore the initial state, leading to a revival time twice bigger than in the quenched case.
When the initial state is long range, that is for initial field close to the critical value $h_i = 1$, the situation is very close to what we observed for short range initial states, namely a revival at $t = t^*$, a singular behavior at $t = \tau^* = t^*/2$ for distances close to the symmetric situation and a doubling of t^* in the equilibrium case. The main difference between critical and non critical initial environment lies in the shape of the decay of the echo. Indeed, in the critical case, it is no longer linear as it were for the non critical environment, but it is rather a power law decay, as we can see on figure 4.15.

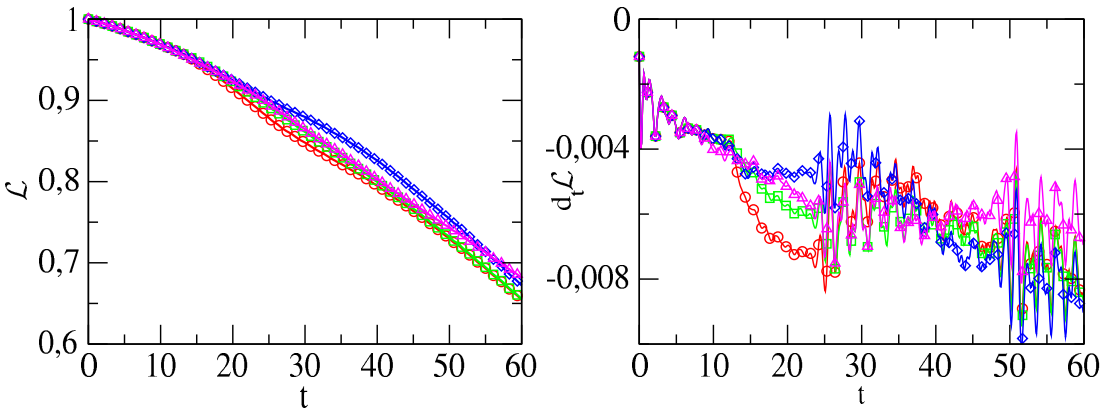

Figure 4.15 – *Left: Loschmidt echo for a critical initial environment for distances* $d = N/2$ *(red circles),* $d = N/2 - 1$ *(green squares),* $d = N/2 - 5$ *(blue diamond) and* $d = N/2 - 15$ *(magenta triangles). Right: Time derivative of the Loschmidt echo for the previous distances. Other parameters are* $N = 100$, $h_f = 1.5$ *and* $\varepsilon = 0.1$.

The almost linear decay of the time derivative of the echo in the right panel of the figure 4.15 suggests a parabolic decay of $\mathcal{L}$ in the critical initial state case.

4.3.5 Independent dynamics

A part of the decoherence dynamics between the two defect spins is a consequence of their direct coupling to the environment, whereas the remaining part comes from their mutual coupling mediated by the spin chain. In order to quantify the part of the decoherence which comes from the direct interaction with the chain, we compute the difference between the echos in the situation where the spins are coupled to a common environment and the case where the spins are coupled to two non interacting environments $\Delta\mathcal{L} = \mathcal{L} - \mathcal{L}_{ind}$. The results are presented in figure 4.16 where $\Delta\mathcal{L}$ is plotted for different initial and final fields and for several distances d.

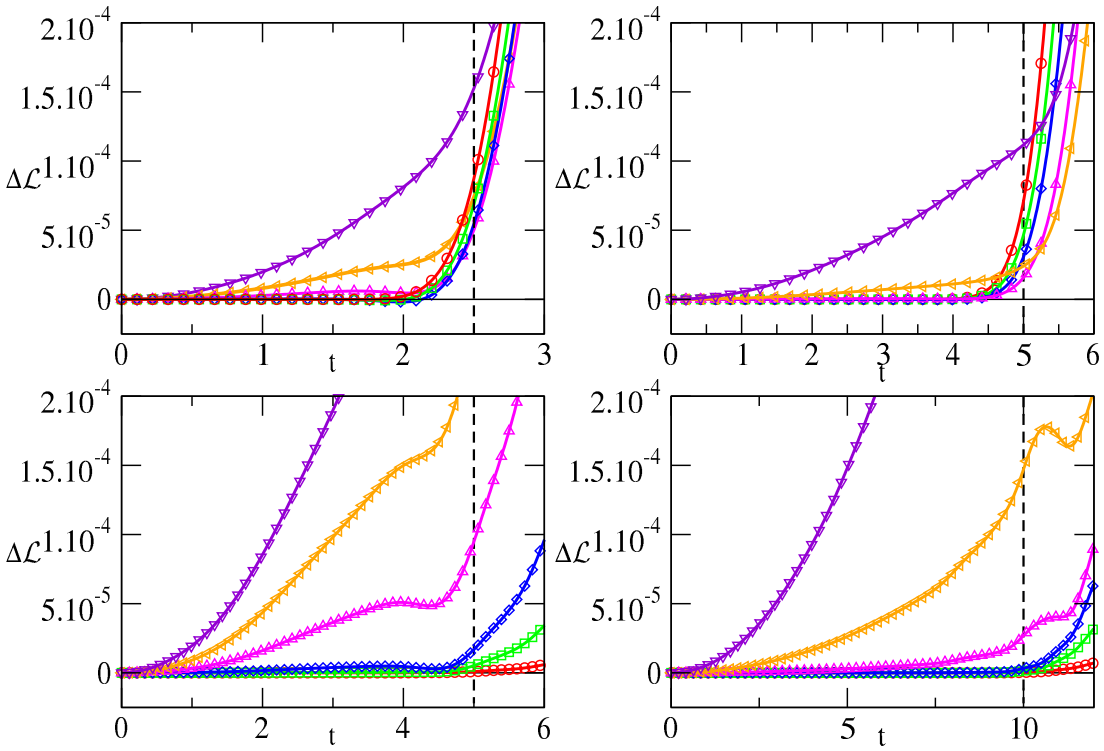

Figure 4.16 – *Difference between the Loschmidt echo $\Delta\mathcal{L}$ in the situation where the two spins are coupled to the same bath and to two independent baths as a function of time for different quench protocols and distances. Up left: $h_f = 1.5$ and $d = 10$, up right: $h_f = 1.5$ and $d = 20$, down left: $h_f = 0.5$ and $d = 10$ and down right: $h_f = 0.5$ and $d = 20$. The initial magnetic fields are: $h_i = 0.5$ (red circles for UR and UL), $h_i = 0.4$ (red circles curves for DR and DL), $h_i = 0.7$ (green squares), $h_i = 0.8$ (blue diamonds), $h_i = 0.9$ (magenta up triangles), $h_i = 0.95$ (orange left triangles) and $h_i = 1$ (indigo down triangles). In all plots, we also add in dashed line the theoretical value of $t_{ind} = d/(2v_g)$*

One can see in figure 4.16 that for initial fields far from the critical value $h_i = 1$, $\Delta\mathcal{L}$ is equal to zero at the beginning of the evolution until a time t_{ind} when it starts to grow (see for example red curves in figure 4.16). This means that, until this time t_{ind}, the two defect spins are evolving independently in the same way as if they were coupled to two non interacting environments. For $t > t_{ind}$, the dynamics of one spin is influenced by the second one through the chain, leading to a non independent dynamics. The physical meaning of t_{ind} can be understood following more or less the same reasoning than for the revival time, namely in term of the travel of the

quasi particle excitations. The two spins evolve in an independent way until a pair of entangled quasi particles created by the quenched environment in the middle of them creates correlations between them and, as a consequence, breaks the independent dynamics. The time t_{ind} needed for the excitations to reach the two positions where the spins are coupled is then given by half the distance between them divided by the sound velocity

$$t_{ind} = \frac{d}{2v_g}, \tag{4.58}$$

where v_g is given by equation (4.57). Note that this time depends only of the final value on the field and the distance, and is independent of the initial state. The theoretical prediction (4.58) of t_{ind} is shown in dashed lines in figure 4.16, where we see that it is in good agreement with the numerical data. Notice that in the equilibrium situation, due to the locality of the excitations emission, the quasi particles need to travel along the complete distance d to correlate the spins, leading to a t_{ind} twice bigger.

When the initial state is prepared with a magnetic field close to the critical value, the situation is different. Indeed, one can see in figure 4.16 that the departure from zero of $\Delta\mathcal{L}$ starts already at $t = 0^+$, indicating that the spins are never evolving independently. This is a consequence of the long-range correlations present in the critical initial state of the chain. When the correlation length ξ of the initial state, whose typical value is given in term of the initial field by $\xi = |\ln(h_i)|^{-1}$ [Pfe70], is bigger than the spin separation d, the defect are already correlated initially through this correlation length, leading the independent dynamics impossible even at short times. A pictural representation of the difference between short and long range situations is shown in figure 4.17

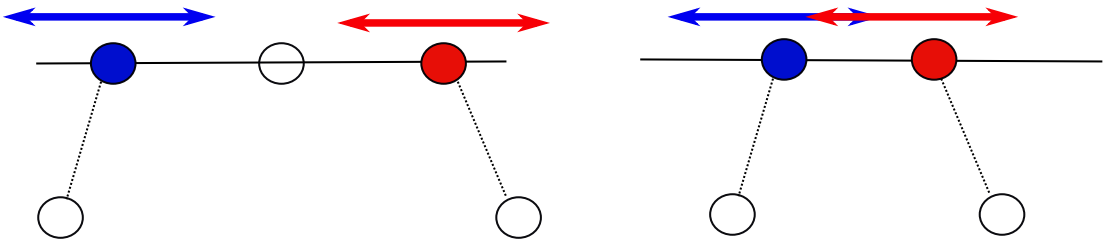

Figure 4.17 – *In the left situation, the distance between the two spins connected to the defect spins is larger than the initial correlation length (schematized by the blue and red arrow). Then, the two defect spins will evolve independently until the excitation created by the white spin correlated them. On the contrary, in the right plot, the two spins already feel each other at $t = 0$ because the distance is shorter than the correlation length. In this last situation, they will never evolve independently.*

More large is d, more we need to have a large initial correlation length (and then a magnetic field h_i close to criticality) in order to be in the regime where the independent dynamics is broken. For example, in the case of $h_f = 0.5$ and $d = 10$, this regime it already reached for $h_i = 0.8$, whereas it is not in the case $h_f = 0.7$, $d = 20$, because the initial correlations are not long range enough. Finally, we can note that, even in this long range initial correlations regime, the signature of the correlation between the defect spins through the emission of excitation by the spin in the middle of them

discussed for the initial field far from criticality is still present. Indeed, one clearly see an increase of $\Delta\mathcal{L}$ for $t > t_{ind}$ (see for example magenta curve in the down left panel).

4.4 Conclusion

In this chapter, we have studied the decoherence dynamics of two spins 1/2 locally coupled to an environment set out of equilibrium after the sudden change of its transverse magnetic field. This dynamics has been investigated through the time evolution of the Loschmidt echo, which gave us all the informations about the entanglement between the two spins. We identified in a first time two regimes of the coupling strength, a weak one, where the echo decrease monotonically, and a strong one when the echo performes fast oscillations depending on ε, embedded in an envelope independent of the coupling. We also observed that the decoherence at large time in both regimes is enhanced in the case of a quenched environment with respect to the equilibrium situation. When the environment is prepared at criticality, we observed clear signatures in the Loschmidt echo (at both short and long times) of the quantum phase transition experienced by the bath, signatures that where nonexistent when the final field was set to the critical value. At large enough times, the systems exhibits revivals, due to the final size of the environment, at time t^*, which is twice smaller than in the equilibrium case. This can be explained trough the global emission of quasiparticles, with velocity set by the final field, whereas the emission is local (at the defect positions) in the equilibrium situation. The quasiparticles need then to travel in the non equilibrium situation half the chain for the revival to appear. One also observe a singular change of the echo when the spins are coupled in opposite positions in the chain, which does not seem to be explained in terms of the quasiparticles propagation. We find then that the two magnetic fields setting the quench protocols have two distinct roles, the initial one sets the length of the correlations, whereas the final one is responsible of dynamical effect trough the excitations propagation.

5 Non Equilibrium and Equilibrium Steady State entanglement driven by quantum repeated interactions

In the two previous chapters, we have analyzed the behavior of a small quantum system interacting with an environment using a Hamiltonian approach [AJP06a]. In this kind of approach, the global system (small system+environment, both described by a Hamiltonian) is closed and its dynamics is unitary. The evolution equation governing the state of the small system is obtained by the trace over the environmental degrees of freedom of the complete state. The effects of the coupling to the environment are then encoded in the evolution equation governing ρ_S. An other description of open quantum system is the Markovian approach [AJP06b]. In this approach, it is unnecessary to give a description of the environment, since its effects are described by dissipative terms in the differential equation governing the small system dynamics, like Quantum Langevin [FK87] or Lindblad [Lin76] equations. In the last decade, the quantum repeated interactions process [AP06, AJ07, AD10, BJM14] has been introduced by Attal *et. al* to describe the interaction of a system with an environment. The studies based on this description are essentially mathematical [Dha08, BJM08, BJM10], but some results concerning physical systems exist. For instance, Karevski and Platini have studied the dynamics of an open XX chain coupled at both ends to two reservoirs at different temperatures via the quantum repeated interactions [KP09]. They derive the long time behavior of the system and found that its state reaches a non-equilibrium-steady-state with observables fixed by the reservoir's properties. More recently, entanglement properties of a bipartite quantum system subject to a repeated interaction with an environment has been studied [ADP14].
In a recent work, Zippilli *et. al* studied the steady state properties of two quantum systems coupled at one edge to a common entangled quantum field [ZPAI13, ZI14]. This coupling has for effect the perfect replication of the entanglement along the array by the creation of two-particles Bell states. In this chapter, we propose to study if the repeated interactions process can lead to the same kind of entanglement duplication over two non interacting arrays of spins.

The chapter is organized as follows: the first section is devoted to a detailed description of the repeated interactions process. We show in particular that, under cer-

tain conditions, the system can be described by means of the two-point fermionic correlators. After that, we introduce a toy model and solve completely its dynamics, focusing ourself to entanglement properties of the system. Finally, in the last section, we study the most general case of two arrays of size N, and show that there is very rich transient entanglement dynamics close to the boundary before the system reaches its steady state.

5.1 Quantum repeated interactions

In this section and in the following one, we describe in details the repeated interactions process [Plao8].

5.1.1 Description of the repeated interactions process

The repeated interactions process has recently been introduced to describe the interaction of a system with an environment (also called bath). This environment is assumed to be made of an infinite number of copies, all these copies being identical and independent. The dynamics of the system part is driven by the Hamiltonian H_S, leaving in the Hilbert space $\mathcal{H}_S$, whereas the Hamiltonian of the environment leaves in the Hilbert space $\mathcal{E} = \bigotimes_{\mathbb{N}^*} \mathcal{H}_j$, where the $\mathcal{H}_j$ are the Hilbert spaces of the individual copies. Because the constituents of the environment are all independent, the Hamiltonian of the environment is

$$H_B = \sum_{\mathbb{N}^*} H_n, \tag{5.1}$$

where the H_n are the Hamiltonians of the individual copies.
We suppose that the system and the environment are initially not correlated, such that the total density matrix $\rho(0)$ can be written

$$\rho(0) = \rho_S \otimes \rho_B, \tag{5.2}$$

where ρ_S is the density matrix of the system part, and

$$\rho_B = \bigotimes_{\mathbb{N}^*} \rho_j, \tag{5.3}$$

where the ρ_j are the density matrices of each copy. The idea of the repeated interactions is that the system interacts with every copy of the environment one after the other, over a time scale τ. Once the interaction time with one copy over, the coupling with this copy is suppressed, and an other one takes its place, and the process is repeated in this way. A physical picture of this process is given by a laser beam falling into a surface. Each photon interacts with the surface one after the other before being absorbed or reflected and not participating anymore to the dynamics of the system. A pictural representation of the repeated interactions process is shown in figure 5.1.
The whole dynamics is driven by the time dependant total Hamiltonian

$$H = H_S + H_B + H_I(t), \tag{5.4}$$

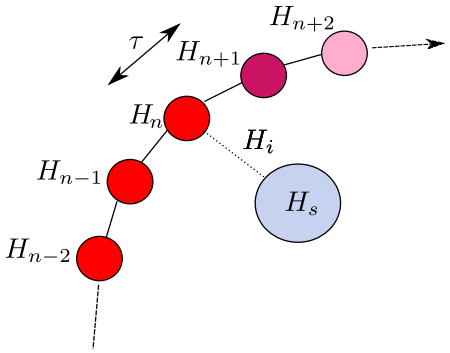

Figure 5.1 – *Pictural representation of the repeated interactions process. A system, described by a Hamiltonian H_s interacts with every copy of the environment over a time scale τ.*

where $H_I(t)$ is the interaction Hamiltonian. This interaction Hamiltonian is constant over the time interval $](n-1)\tau, n\tau]$, $H_I(t) = H_I^n$, describing the coupling between the system and the n^{th} copy of the bath. The temporal evolution is governed by the time evolution operator

$$K_n(\tau) = U_I^n(\tau) \otimes \prod_{\mathbb{N}^* \setminus n} U_k(\tau) \tag{5.5}$$

where

$$U_I^n(\tau) = e^{-i(H_S + H_n + H_I^n)\tau} \tag{5.6}$$

is the evolution operator coupling the system and the environment, and

$$U_k(\tau) = e^{-iH_k\tau}, \quad k \in \mathbb{N}^* \setminus n \tag{5.7}$$

is the time evolution operator of all the copies which are not interacting with the system. The total dynamics from time $t = 0$ until time $t = n\tau$ is then governed by the string

$$\mathbb{U}(n\tau) = K_n(\tau)K_{n-1}(\tau)\cdots K_1(\tau). \tag{5.8}$$

In the Schrödinger representation, the density matrix at time $t = n\tau$ is given by the Liouville equation

$$\rho(n\tau) = \mathbb{U}(n\tau)\rho(0)\mathbb{U}^\dagger(n\tau), \tag{5.9}$$

which can be rewritten using the expression (5.8) like an iterative equation

$$\rho(n\tau) = K_n(\tau)\rho((n-1)\tau)K_n^\dagger(\tau). \tag{5.10}$$

In the Heisenberg representation, where the time dependence is carried by the observable through

$$\langle \mathcal{O}(t) \rangle = \mathrm{Tr}\{\mathcal{O}\rho(t)\} = \mathrm{Tr}\{\mathcal{O}(t)\rho(0)\}, \tag{5.11}$$

we obtain

$$\mathcal{O}(n\tau) = \mathbb{U}^\dagger(n\tau)\mathcal{O}\mathbb{U}(n\tau) = K_n^\dagger(\tau)\mathcal{O}((n-1)\tau)K_n(\tau). \tag{5.12}$$

5.1.2 Time evolution of the system

Here, we focus our attention to the dynamics of the system part only. Its density matrix is obtained by tracing $\rho(t)$ over the environmental degrees of freedom

$$\rho_S(n\tau) = \mathrm{Tr}_B\{\rho(n\tau)\}. \tag{5.13}$$

Explicitly, the density matrix of the system during the interaction with the n^{th} copy of the environment is

$$\begin{aligned}\rho_S(n\tau) &= \mathrm{Tr}_B\left\{\mathbb{U}(n\tau)\rho_S\prod_{k\leq n}\rho_k\mathbb{U}^\dagger(n\tau)\prod_{k>n}\rho_k\right\}\\ &= \mathrm{Tr}_{k\leq n}\left\{\mathbb{U}(n\tau)\rho_S(0)\prod_{k\leq n}\rho_k\mathbb{U}^\dagger(n\tau)\right\}.\end{aligned} \tag{5.14}$$

After some algebra, we arrive to the fundamental equation of evolution of the reduced density matrix

$$\rho_S(n\tau) = \mathrm{Tr}_n\left\{U_I^n(\tau)\rho_S((n-1)\tau)\otimes\rho_n U_I^{n\dagger}(\tau)\right\}, \tag{5.15}$$

where the trace is now performed on the n^{th} copy of the environment only. To proceed further, lets introduce the diagonal base of the n^{th} copy of the environment

$$\rho_n|\phi_k^n\rangle = p_k|\phi_k^n\rangle, \quad k = 1,\cdots,\dim(\mathcal{H}_n) = \Omega. \tag{5.16}$$

In the base $|S_j\rangle\otimes|\phi_k^n\rangle$, where the vectors $|S_j\rangle$ form a base of the system's Hilbert space $\mathcal{H}_S$, the density matrix $\rho_($$(n-1)\tau)$ is written like

$$\rho_n\otimes\rho_S((n-1)\tau) = \begin{pmatrix} p_1\rho_S((n-1)\tau) & & & \\ & p_2\rho_S((n-1)\tau) & & \\ & & \ddots & \\ & & & p_\Omega\rho_S((n-1)\tau)\end{pmatrix}. \tag{5.17}$$

Introducing the decomposition

$$U_I^n(n\tau) = \begin{pmatrix} V_1^1 & V_1^2 & \cdots & V_1^\Omega \\ \vdots & \vdots & & \vdots \\ \vdots & \vdots & & \vdots \\ V_\Omega^1 & V_\Omega^2 & \cdots & V_\Omega^\Omega\end{pmatrix}, \tag{5.18}$$

where the V_i^j are operators living in $\mathcal{H}_S$, one can show that the density matrix at time $t = n\tau$ is given by the application of a super operator on the density matrix at previous time $t = (n-1)\tau$

$$\rho_S(n\tau) = \mathbb{L}(\rho_S((n-1)\tau)), \tag{5.19}$$

with

$$\mathbb{L}(X) = \sum_{ij}^{\Omega} p_i V_i^j X V_i^{j\dagger}. \tag{5.20}$$

Finally, because all the copies are identical and prepared in the same state, we obtain by successive iterations

$$\rho_S(n\tau) = \mathbb{L}^n(\rho_S(0)). \tag{5.21}$$

The adjoint of the super-operator $\mathbb{L}^\dagger$ is defined by the scalar product $(X, Y) = \mathrm{Tr}\{XY^\dagger\}$ through

$$(X, \mathbb{L}Y) = (\mathbb{L}^\dagger X, Y), \tag{5.22}$$

leading to the following average of an observable $\mathcal{O}$ in the Heisenberg representation

$$\mathcal{O}(n\tau) = \mathrm{Tr}_S\{\mathcal{O}(n\tau)\rho_S(0)\} = \mathrm{Tr}_S\{\mathbb{L}^{\dagger n}(\mathcal{O})\rho_S(0)\}, \tag{5.23}$$

with

$$\mathbb{L}^\dagger(\mathcal{O}) = \sum_{ij}^{\Omega} p_i V_i^{j\dagger} \mathcal{O} V_i^j. \tag{5.24}$$

The continuous limit of the evolution equation of an observable $\mathcal{O}$ is taken by letting the interaction time τ going to zero $\tau \to 0$. Here, we will not show the demonstration, but we just expose the result [APo6, Plao8] assuming that the environment is prepared in one of its eigenstate $|\alpha\rangle$. In this case, $p_i = \delta_{i,\alpha}$ and equation (5.24) simplifies to

$$\mathbb{L}^\dagger(\mathcal{O}) = \sum_{i}^{\Omega} V_i^{\alpha\dagger} \mathcal{O} V_i^\alpha. \tag{5.25}$$

It has been shown in [APo6] that the continuous limit of the evolution equation is described by the differential equation

$$\partial_t \mathcal{O}(t) = \mathcal{L}(\mathcal{O}), \tag{5.26}$$

where the Lindblad generator $\mathcal{L}(X)$ is defined like

$$\mathcal{L}(X) = i[H, X] + \frac{1}{2}\sum_i (2L_i^{\alpha *} X L_i^\alpha - \{L_i^{\alpha *} L_i^\alpha, X\}) \tag{5.27}$$

with the limits

$$L_\alpha^\alpha = \lim_{\tau\to 0} \frac{V_\alpha^\alpha - \mathbb{1}}{\tau}, \quad L_i^\alpha = \lim_{\tau\to 0} \frac{V_i^\alpha}{\sqrt{\tau}},\ i \neq \alpha. \tag{5.28}$$

5.2 XY MODEL

In the following, we consider that the system is a chain of N interacting spins with XY interactions. Its dynamics is governed by the Hamiltonian

$$H_S = -\frac{1}{2}\sum_{i=1}^{N-1}\left(\frac{1+\kappa}{2}\sigma_i^x\sigma_{i+1}^x + \frac{1-\kappa}{2}\sigma_i^y\sigma_{i+1}^y\right) - \frac{h}{2}\sum_{i=1}^{N}\sigma_i^z, \tag{5.29}$$

where κ is the anisotropy parameter. The environment is modeled by an infinite set of copies made by independent spins with Hamiltonian

$$H_B^n = -\frac{h_B}{2}\mu_n^z, \tag{5.30}$$

where the μ^i are the Pauli matrices in the bath Hilbert space. Moreover, we assume that only the first spin of the chain is interacting with the environment. This interaction is driven by the Hamiltonian

$$H_I = -\frac{\lambda_I}{2}\left(\frac{1+\kappa_I}{2}\mu^x\sigma_1^x + \frac{1-\kappa_I}{2}\mu^y\sigma_1^y\right). \tag{5.31}$$

5.2.1 Initial states

In the rest of this section, we will assume that the system and every copy of the bath are prepared into a Gibbs state at inverse temperature β_S and β_B

$$\rho_S = \frac{1}{Z_S}e^{-\beta_S H_S}, \quad \rho_n = \frac{1}{Z_B^n}e^{-\beta_B H_B^n}, \tag{5.32}$$

where $Z_{S,B}$ is a normalization constant. The initial state is then $\rho(0) = \rho_S \otimes \rho_B$ with

$$\rho_B = \bigotimes_{\mathbb{N}^*} \rho_n. \tag{5.33}$$

Here we can note that the states of the system and the bath are Gaussian, since they can be written as an exponential of a quadratic form in terms of fermionic operators.

5.2.2 Dynamics of the Clifford operators

We remind that in the time interval $](n-1)\tau, \tau]$, i.e when the system interacts with the n^{th} copy of the environment, the dynamics is governed by the total Hamiltonian

$$H = H_S + H_B^n + H_I, \tag{5.34}$$

which can be rewritten using Clifford operators Γ

$$\Gamma_k^1 = \prod_{j=1}^{k-1}(-\widetilde{\sigma}_j^z)\widetilde{\sigma}_k^x, \quad \Gamma_k^2 = -\prod_{j=1}^{k-1}(-\widetilde{\sigma}_j^z)\widetilde{\sigma}_k^y, \tag{5.35}$$

with $\Gamma^\dagger = \Gamma$, and where we have defined $\widetilde{\sigma}_{i=1,\cdots,N+1} = \{\mu, \sigma_{i=1,\cdots,N}\}$. The average of an operator written in terms of these Clifford operators $\mathcal{O} = f(\Gamma)$ will be at time $t = n\tau$

$$\begin{aligned}\langle\mathcal{O}\rangle(n\tau) &= \mathrm{Tr}_{S,n}\{\mathcal{O}U_I^n[\rho_S((n-1)\tau)\otimes\rho_n]U_I^{n\dagger}\} \\ &= \mathrm{Tr}_{S,n}\{\mathcal{O}(\tau)\rho_S((n-1)\tau)\otimes\rho_n\}.\end{aligned} \tag{5.36}$$

We see here that we adopt an "hybrid" representation for the dynamics of the average of the operator. Indeed, the time dependence is carried by the density matrix until the time $(n-1)\tau$, whereas the operator are evolving in the time interval $](n-1)\tau, \tau]$. We need then to know what is the dynamics of the Clifford operators. We remind that, for time independent Hamiltonian, the operators Γ evolve like

$$\mathbf{\Gamma} = R(t)\mathbf{\Gamma}(0) = e^{-i\boldsymbol{T}\tau}\mathbf{\Gamma}, \tag{5.37}$$

where $\boldsymbol{T}$ is the Hamiltonian matrix and

$$\boldsymbol{\Gamma} = \begin{pmatrix} \boldsymbol{\Gamma}^1 \\ \boldsymbol{\Gamma}^2 \end{pmatrix}, \quad \boldsymbol{\Gamma}^\alpha = \begin{pmatrix} \Gamma_1^\alpha \\ \Gamma_2^\alpha \\ \vdots \\ \Gamma_{N+1}^\alpha \end{pmatrix}. \tag{5.38}$$

5.2.3 Time evolution of the reduced density matrix

The initial state of the global system (5.32) can be written, using the fact that $[H_S, H_B] = 0$, like

$$\rho(0) = \frac{1}{Z_S Z_B} e^{-\beta_S H_S - \beta_B H_B} = \frac{1}{Z} e^{-H_0} \tag{5.39}$$

with $H_0 = \beta_S H_S + \beta_B H_B$. In terms of Clifford operators, it reads

$$H_0 = \frac{1}{4} \boldsymbol{\Gamma}^\dagger \boldsymbol{T} \boldsymbol{\Gamma}, \tag{5.40}$$

with

$$\boldsymbol{T} = \begin{pmatrix} 0 & 0 & \beta_S C_S & 0 \\ 0 & 0 & 0 & \beta_B C_B \\ \beta_S C_C^\dagger & 0 & 0 & 0 \\ 0 & \beta_B C_B^\dagger & 0 & 0 \end{pmatrix}, \tag{5.41}$$

and

$$C_S = -i \begin{pmatrix} h & J^y & & & \\ J^x & h & J^y & & \\ & \ddots & \ddots & \ddots & \\ & & J^x & h & J^y \\ & & & J^x & h \end{pmatrix}, \quad C_B = -ih, \tag{5.42}$$

where we have set $J^{x(y)} = (1 + (-)\kappa)/2$. After the interaction with the first copy of the environment, the density matrix is

$$\rho(\tau) = \frac{1}{Z_{0,1}} U_I^{(1)} e^{-H_{0,1}} U_I^{(1)\dagger} \prod_{\mathbb{N}^*/1} \rho_k, \tag{5.43}$$

where $H_{0,1} = \beta_S H_S + \beta_B H_B^{(1)}$ is the Hamiltonian of the system and the first copy. The density matrix can be rewritten

$$\rho(\tau) = \frac{1}{Z_{0,1}} e^{-H_{0,1}(\tau)} \prod_{\mathbb{N}^*/1} \rho_k = \frac{1}{Z_{0,1}} e^{\boldsymbol{\Gamma}^\dagger(-\tau) T_{0,1} \boldsymbol{\Gamma}(-\tau)} \prod_{\mathbb{N}^*/1} \rho_k, \tag{5.44}$$

where we have used the fact that $U_I^\dagger(\tau) = U_I(-\tau)$. Using the matrix representation (5.37), together with its adjoint, the Hamiltonian $H_{0,1}$ becomes

$$H_{0,1}(\tau) = \frac{1}{4} \boldsymbol{\Gamma}^\dagger \boldsymbol{T}_{0,1}(\tau) \boldsymbol{\Gamma}, \tag{5.45}$$

with $\boldsymbol{T}_{0,1}(\tau) = R(\tau)\boldsymbol{T}_{0,1}R^\dagger(\tau)$. Then, after the first interaction, the density matrix of the whole system is

$$\rho_{0,1}(\tau) = \frac{1}{Z_{S,B}} \exp\left(-\frac{1}{4}\boldsymbol{\Gamma}^\dagger \boldsymbol{T}_{0,1}(\tau)\boldsymbol{\Gamma}\right). \tag{5.46}$$

The state of the global system being a quadratic form of fermionic operators, it follows that the reduced density matrix associated with the system part $\rho_S(\tau) = \mathrm{Tr}_1\{\rho_{0,1}(\tau)\}$ is quadratic as well [Peso3], and can be written

$$\rho_S(\tau) = \frac{1}{K(\tau)} \exp\left(-\frac{1}{4}\boldsymbol{\Gamma}_S^\dagger \boldsymbol{T}_S(\tau)\boldsymbol{\Gamma}_S\right), \tag{5.47}$$

where the $\boldsymbol{\Gamma}_S$ belongs to the system part only, and where $\boldsymbol{T}_S(\tau)$ is the restriction of the matrix $\boldsymbol{T}_{0,1}(\tau)$ obtained after tracing over the bath degrees of freedom. The iteration of the process leads to

$$\rho_S(n\tau) = \frac{\exp\left(-\frac{1}{4}\boldsymbol{\Gamma}_S^\dagger \boldsymbol{T}_S(n\tau)\boldsymbol{\Gamma}_S\right)}{K(n\tau)}, \quad K(n\tau) = \mathrm{Tr}\left\{\exp\left(-\frac{1}{4}\boldsymbol{\Gamma}_S^\dagger \boldsymbol{T}_S(n\tau)\boldsymbol{\Gamma}_S\right)\right\}. \tag{5.48}$$

It is clear from the previous equation that the state of the system part is Gaussian. It follows that the Wick theorem applies, and the state can be completely described by the means of the two-point correlation functions. Indeed, using the Wick theorem, any string of an even number of Clifford operators factories into a product of two point correlators, for example

$$\langle \Gamma_i\Gamma_j\Gamma_k\Gamma_l\rangle = \langle \Gamma_i\Gamma_j\rangle\langle \Gamma_k\Gamma_l\rangle - \langle \Gamma_i\Gamma_k\rangle\langle \Gamma_j\Gamma_l\rangle + \langle \Gamma_i\Gamma_l\rangle\langle \Gamma_j\Gamma_k\rangle, \tag{5.49}$$

whereas the average of a string made by an odd number of operators vanishes, in particular $\langle \Gamma_i\rangle = 0$. Then, we just need to know how the correlation matrix of the system evolves to have access to the time evolution of the observables.

5.2.4 Time evolution of the two-point correlation matrix

The system being Gaussian, we can completely describe the state by means of the two-point correlation functions. We define the matrix G on the space formed by the system and the interacting copy by

$$G_{k,k'} = -i\langle \boldsymbol{\Gamma}_k\boldsymbol{\Gamma}_{k'}\rangle + i\delta_{kk'}, \quad k,k' = 1,\dots,N+1. \tag{5.50}$$

The time evolution of this matrix is given by the application of the $R(\tau)$ matrix

$$G^{0,n}(n\tau) = R(\tau)G^{(0,n)}((n-1)\tau)R^\dagger(\tau), \tag{5.51}$$

with, by definition

$$G^{(0,n)}_{kk'}((n-1)\tau) = -i\,\mathrm{Tr}_S\,\mathrm{Tr}_n\{\boldsymbol{\Gamma}_k\boldsymbol{\Gamma}_{k'}(\rho_S((n-1)\tau)\otimes\rho_n)\} + i\delta_{kk'}. \tag{5.52}$$

To go further, we reorganize the $\boldsymbol{\Gamma}$ operator like

$$\boldsymbol{\Gamma} = \begin{pmatrix}\boldsymbol{\Gamma}_B\\ \boldsymbol{\Gamma}_S\end{pmatrix}, \quad \boldsymbol{\Gamma}_S = \begin{pmatrix}\boldsymbol{\Gamma}_S^1\\ \boldsymbol{\Gamma}_S^2\end{pmatrix}, \tag{5.53}$$

and the same thing for $\mathbf{\Gamma}_B$. The system and the n^{th} copy of the environment being uncorrelated for times $t < (n-1)\tau$, it follows that, in the state $\rho_S((n-1)\tau) \otimes \rho_n$, all the correlators of type $\mathrm{Tr}_S \mathrm{Tr}_n\{\Gamma_B \Gamma_S(\rho_S((n-1)\tau) \otimes \rho_n)\}$ vanish, and the correlation matrix $G^{(0,n)}((n-1)\tau)$ assumes as a consequence the block diagonal structure

$$G^{(0,n)}((n-1)\tau) = \begin{pmatrix} G_B & 0 \\ 0 & G_S((n-1)\tau) \end{pmatrix}, \tag{5.54}$$

where

$$(G_S)_{kk'}((n-1)\tau) = -i\,\mathrm{Tr}_S\left\{\mathbf{\Gamma}_k \mathbf{\Gamma}_{k'} \rho_S((n-1)\tau)\right\} + i\delta_{kk'}. \tag{5.55}$$

Decomposing the rotation matrix $R(\tau)$ in the same way

$$R(\tau) = \begin{pmatrix} R_B(\tau) & R_{BS}(\tau) \\ R_{SB}(\tau) & R_S(\tau) \end{pmatrix}, \tag{5.56}$$

we obtain the fundamental evolution equation of the two-point correlation matrix

$$G_S(n\tau) = R_S(\tau) G_S((n-1)\tau) R_S^\dagger(\tau) + R_{SB}(n\tau) G_B R_{SB}^\dagger(n\tau). \tag{5.57}$$

The matrix at time $n\tau$ is then given by the application of a super operator on the matrix at time $(n-1)\tau$

$$G_S(n\tau) = \mathcal{L}(G_S((n-1)\tau)), \tag{5.58}$$

giving by successive iterations

$$G_S(n\tau) = \mathcal{L}^n(G_S(0)), \tag{5.59}$$

with

$$\mathcal{L}(X) = R_S X R_S^\dagger + R_{SB} G_B R_{SB}^\dagger. \tag{5.60}$$

5.2.5 Continuous limit of the evolution equation

The continuous limit is obtained by letting the interaction τ going to zero. In this limit, the matrix G_S obeys to the differential equation

$$\partial_t G_S = \lim_{\tau \to 0} \frac{\mathcal{L}(G_S(n\tau)) - G_S(n\tau)}{\tau}. \tag{5.61}$$

The continuous limit has to be taken carefully. Indeed, one needs to renormalize the coupling constant between the system and the environment. If one takes naively the limit $\tau \to 0$ without any rescaling of the coupling, this will lead to a decoupling of the system with the environment, and then to the trivial free evolution of the system without any influence of the bath.
It has been shown in [APo6, Plao8] that the the only possible rescaling leading to the correct continuum limit is to divide the coupling constant by the square root of the interaction time

$$\lambda_I \to \frac{\lambda_I}{\sqrt{\tau}}. \tag{5.62}$$

After this proper renormalization, we obtain the following fundamental evolution equation for the correlation of the system part [Plao8, KPo9]

$$\partial_t G_S(t) = -i[T_S, G_S(t)] - \frac{1}{2}\left(\left\{G_S(t), \Theta^\dagger \Theta\right\} - 2\Theta^\dagger G_B \Theta\right), \tag{5.63}$$

where T_S is the Hamiltonian matrix of the system part, and Θ is the interaction matrix containing the coupling between the system and the environment. Note that without the proper renormalization, the evolution equation will simply reduce to $\partial_t C_S(t) = -i[T_S, G_S(t)]$, and then to the trivial evolution.
Defining the super operator $\mathscr{L}(.) = -i[T_S, .] - \frac{1}{2}\{., \Theta^\dagger\Theta\}$ and the constant $C(G_B) = \Theta^\dagger G_B \Theta$, equation (5.62) can be rewritten

$$\partial_t G_S = -\mathscr{L}(G_S) + C(G_b), \tag{5.64}$$

with formal solution, given the initial condition $G_S(0)$

$$G_S(t) = e^{-\mathscr{L}t}(G_S(0) - \mathscr{L}^{-1}(C(G_B))) + \mathscr{L}^{-1}(C(G_B)), \tag{5.65}$$

where the matrix $\mathscr{L}^{-1}(C(G_B))$ contains all the informations about the steady state properties of the system.

5.3 Toy model

After the introduction of the general formalism of the quantum repeated interactions process, we will in this section investigate the case of a simple model, for which the dynamics can be completely determined analytically. Note that until the end of this chapter, we will use, except if the contrary is precised, the continuous limit $\tau \to 0$.

5.3.1 Model and shape of the reduced density matrix

The simplest model we can imagine consists of two non interacting spins, each of them coupled to one constituent of a pair of spins forming one copy of the bath, as shown in figure 5.2.

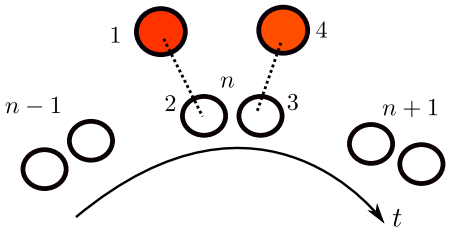

Figure 5.2 – *Pictural representation of our toy model. The two spins of the system (in red), labeled* 1 *and* 4 *are each coupled to one constituent of a pair of spin, labeled* 2 *and* 3 *forming the copy* n *of the environment.*

The unitary dynamics of the system+environment is driven by the time dependent Hamiltonian $H = H_S + H_B + H_I(t)$, where the local Hamiltonians of the system and the copies of the bath are simply given by a Zeeman term

$$H_S = -\frac{h}{2}(\sigma_1^z + \sigma_4^z), \tag{5.66}$$

$$H_B = \sum_{k=1}^{\infty} H_B^k, \tag{5.67}$$

where

$$H_B^k = -\frac{h}{2}(\sigma_{k,2}^z + \sigma_{k,3}^z), \tag{5.68}$$

is the Hamiltonian of the pair k. The time dependent interaction Hamiltonian is constant over one time step $[(k-1)\tau, k\tau[$ and is given by

$$H_I^{(k)} = -\frac{\gamma}{2}(\sigma_1^x\sigma_{k,2}^x + \sigma_1^y\sigma_{k,2}^y + \sigma_{k,3}^x\sigma_4^x + \sigma_{k,3}^y\sigma_4^y). \tag{5.69}$$

Here, because we work with XX type interactions, it is more judicious to use the Jordan-Wigner transformation in terms of c fermionic operators instead of Clifford ones, as we did in the presentation of the repeated interactions. After the mapping, we obtain

$$\begin{aligned} H_S =& h(c_1^\dagger c_1 + c_4^\dagger c_4), \\ H_B =& h(c_2^\dagger c_2 + c_3^\dagger c_3), \\ H_I =& -\gamma(c_1^\dagger c_2 + c_2^\dagger c_1 + c_3^\dagger c_4 + c_4^\dagger c_3), \end{aligned} \tag{5.70}$$

such that the total Hamiltonian H takes the matrix form, after the introduction of the row vector $\mathbf{\Psi}^\dagger = (\boldsymbol{c}_B^\dagger, \boldsymbol{c}_S^\dagger) = (c_2^\dagger, c_3^\dagger, c_1^\dagger, c_4^\dagger)$

$$H = \left(c_2^\dagger, c_3^\dagger, c_1^\dagger, c_4^\dagger\right) \begin{pmatrix} h & 0 & -\gamma & 0 \\ 0 & h & 0 & -\gamma \\ -\gamma & 0 & h & 0 \\ 0 & -\gamma & 0 & h \end{pmatrix} \begin{pmatrix} c_2 \\ c_3 \\ c_1 \\ c_4 \end{pmatrix} = \mathbf{\Psi}^\dagger \begin{pmatrix} T_B & \Theta \\ \Theta^\dagger & T_S \end{pmatrix} \mathbf{\Psi}. \tag{5.71}$$

In the following, we are interested in the dynamics of the two spins labeled 1 and 4, and more particularly to their entanglement properties. In order to have access to the concurrence between them, we need to know the density matrix $\rho_S = \mathrm{Tr}_{2,3}\{\rho_{tot}\}$. When the system into consideration is modeled by a spin chain with XY interaction, it has been shown [OW01, AOP+04] that, thanks to the parity symmetry of the XY Hamiltonian, the reduced density matrix of two constituents i and j of the chain assumes the structure

$$\rho_{ij} = \begin{pmatrix} a & 0 & 0 & c \\ 0 & x & z & 0 \\ 0 & z^* & y & 0 \\ c^* & 0 & 0 & b \end{pmatrix}. \tag{5.72}$$

With this simple structure, the concurrence reduces to

$$\mathcal{C} = 2\max\{0, |z| - \sqrt{ab}, |c| - \sqrt{xy}\}. \tag{5.73}$$

We are now left with the calculation of the matrix elements a, b, c, x, y, z to get the concurrence. These six elements can be expressed in terms of the spin-spin correlation

functions thanks to the definition $\langle \sigma_i^\alpha \sigma_j^\beta \rangle \equiv \mathrm{Tr}\{\rho_{ij}\sigma_i^\alpha \sigma_j^\beta\}$. We obtain

$$\begin{aligned}
a =& \frac{1}{4}\langle \sigma_i^z \rangle + \frac{1}{4}\langle \sigma_j^z \rangle + \frac{1}{4}\langle \sigma_i^z \sigma_j^z \rangle + \frac{1}{4}, \\
x =& \frac{1}{4}\langle \sigma_i^z \rangle - \frac{1}{4}\langle \sigma_j^z \rangle - \frac{1}{4}\langle \sigma_i^z \sigma_j^z \rangle + \frac{1}{4}, \\
y =& \frac{1}{4}\langle \sigma_j^z \rangle - \frac{1}{4}\langle \sigma_i^z \rangle - \frac{1}{4}\langle \sigma_i^z \sigma_j^z \rangle + \frac{1}{4}, \\
b =& -\frac{1}{4}\langle \sigma_i^z \rangle - \frac{1}{4}\langle \sigma_j^z \rangle + \frac{1}{4}\langle \sigma_i^z \sigma_j^z \rangle + \frac{1}{4}, \\
z =& \frac{1}{4}(\langle \sigma_i^x \sigma_j^x \rangle + \langle \sigma_i^y \sigma_j^y \rangle + i(\langle \sigma_i^x \sigma_j^y \rangle - \langle \sigma_i^y \sigma_j^x \rangle)), \\
c =& \frac{1}{4}(\langle \sigma_i^x \sigma_j^x \rangle - \langle \sigma_i^y \sigma_j^y \rangle - i(\langle \sigma_i^x \sigma_j^y \rangle + \langle \sigma_i^y \sigma_j^x \rangle)).
\end{aligned} \tag{5.74}$$

Note that another argument justifying the cross structure of the density matrix is to remark that all the vanishing elements in ρ_{ij} can be expressed as a function of $\langle \sigma_j^x \rangle$, $\langle \sigma_i^z \sigma_j^x \rangle$ or $\langle \sigma_i^z \sigma_j^y \rangle$, which, as soon as we are working with Gaussian states, vanish since they are written as a string of an odd number of fermionic operators.

5.3.2 Initial state

The system and the environment are initially uncorrelated such that the initial state is the product state $\rho(0) = \rho_S(0) \otimes \eta_B$. All the copies of the environment being independent, the initial density matrix of the bath is given by

$$\eta_B = \bigotimes_{k \in N^*} \eta. \tag{5.75}$$

We choose to prepare the system into a factorized state $\rho_S(0) = \rho_1 \otimes \rho_4$ where ρ_j ($j = 1, 4$) is the reduced density matrix associated to the spin j. We shall work with a thermal state for each system's spin

$$\rho_j = \frac{1 + m_j^0}{2} |\uparrow\rangle\langle\uparrow| + \frac{1 - m_j^0}{2} |\downarrow\rangle\langle\downarrow|, \quad j = 1, 4\,, \tag{5.76}$$

where m_j is the magnetization of the spin j given by $m_j \equiv \mathrm{Tr}\{\sigma_j^z \rho(0)\}$. The two spins forming the copies of the bath are supposed to be prepared into the maximally entangled Bell state

$$|\psi_B\rangle = \frac{1}{\sqrt{2}}(|\uparrow\downarrow\rangle + |\downarrow\uparrow\rangle). \tag{5.77}$$

As mentioned in the presentation section, in order to determine the evolution of the system in terms of the evolution of its two-point correlation matrix, the total system has to be prepared into a Gaussian state. For the two spins 1 and 4, this is obvious since

$$\rho_j = \frac{1}{Z} e^{-\beta_j h \sigma_z} \tag{5.78}$$

leading to $m_j = \tanh(\beta_j h/2)$. For the bath part, one has to check that the reduced density matrix of each pair

$$\eta = |\psi_B\rangle\langle\psi_B| = \frac{1}{2}\begin{pmatrix} 0 & 0 & 0 & 0 \\ 0 & 1 & 1 & 0 \\ 0 & 1 & 1 & 0 \\ 0 & 0 & 0 & 0 \end{pmatrix} \tag{5.79}$$

can be written as the low temperature limit ($\beta \to \infty$) of a thermal density matrix ρ_{th}

$$\eta = \lim_{\beta\to\infty} \rho_{th} = \lim_{\beta\to\infty} \frac{e^{-\beta\widetilde{H}}}{Z}, \tag{5.80}$$

with $\widetilde{H}$ a quadratic operator in terms of fermions. One can show (see appendix B for details) that the operator

$$\widetilde{H} = \frac{1}{2}\mathbb{1} - \frac{1}{4}(\sigma_2^x\sigma_3^x - \sigma_2^y\sigma_3^y), \tag{5.81}$$

which is well quadratic in terms of fermionic operators, leads to the correct density matrix in the limit $\beta \to \infty$.

Starting with the initial Bell state $|\psi_B\rangle$, the correlators of the bath's spins are given by

$$\langle\sigma_2^x\sigma_3^x\rangle = \langle\sigma_2^y\sigma_3^y\rangle = 1, \tag{5.82}$$
$$\langle\sigma_2^x\sigma_3^y\rangle = \langle\sigma_2^y\sigma_3^x\rangle = 0, \tag{5.83}$$
$$\langle\sigma_2^z\rangle = \langle\sigma_3^z\rangle = 0. \tag{5.84}$$

Using the Jordan-Wigner transformation, one can, from these correlators, reconstruct the initial fermionic two-point correlation function of the bath $(G_B)_{ij} = \langle c_i^\dagger c_j\rangle$ $(i,j = 2,3)$:

$$\begin{aligned} &\langle\sigma_2^x\sigma_3^x\rangle = \langle c_2^\dagger c_3 - c_2 c_3^\dagger\rangle = 2\Re e\langle c_2^\dagger c_3\rangle, \\ &\langle\sigma_2^x\sigma_3^y\rangle = i\langle c_2^\dagger c_3 + c_2 c_3^\dagger\rangle = -2\Im m\langle c_2^\dagger c_3\rangle, \\ &\langle\sigma_2^z\rangle = 2\langle c_2^\dagger c_2\rangle - 1, \\ &\langle\sigma_3^z\rangle = 2\langle c_3^\dagger c_3\rangle - 1, \end{aligned} \tag{5.85}$$

leading to

$$G_B(0) = \frac{1}{2}\begin{pmatrix} 1 & 1 \\ 1 & 1 \end{pmatrix}.$$

For the initial two-point correlation matrix of the system part $(G_S)_{ij} = \langle c_i^\dagger c_j\rangle$ $(i,j = 1,4)$, we obtain

$$G_S(0) = \begin{pmatrix} \dfrac{1+m_1^0}{2} & 0 \\ 0 & \dfrac{1+m_4^0}{2} \end{pmatrix}.$$

5.3.3 Time evolution of the correlation matrix

Here, we focus on the derivation of the time evolution of the two-point correlation matrix of the system. We remind that it evolves following the evolution equation

$$\partial_t G_S(t) = -i[T_S, G_S(t)] - \frac{1}{2}\left(\left\{G_S(t), \Theta^\dagger\Theta\right\} - 2\Theta^\dagger G_B \Theta\right). \tag{5.86}$$

In the simple case considered here, the T_S matrix is proportional to the identity $T_S = h\mathbb{1}_{2\times 2}$, then the first term of the r.h.s of equation (5.86) obviously vanishes

$$[T_S, G_S] = h[\mathbb{1}_{2\times 2}, G_S] = 0. \tag{5.87}$$

Using

$$\Theta^\dagger\Theta = \gamma^2\mathbb{1}_{2\times 2}, \quad \Theta^\dagger G_B \Theta = \gamma^2 G_B, \tag{5.88}$$

the equation governing the dynamics of G_S is found to be

$$\partial_t G_S(t) = -\gamma^2(G_B - G_S(t)), \tag{5.89}$$

leading to the following evolution equations of the fermionic correlators

$$\partial_t\langle c_1^\dagger c_1\rangle = -\gamma^2\langle c_1^\dagger c_1\rangle + \gamma^2\langle c_2^\dagger c_2\rangle, \tag{5.90}$$
$$\partial_t\langle c_4^\dagger c_4\rangle = -\gamma^2\langle c_4^\dagger c_4\rangle + \gamma^2\langle c_3^\dagger c_3\rangle, \tag{5.91}$$
$$\partial_t\langle c_1^\dagger c_4\rangle = -\gamma^2\langle c_1^\dagger c_4\rangle + \gamma^2\langle c_2^\dagger c_3\rangle. \tag{5.92}$$

The resolution of the two first equations gives the evolution of the local fermionic occupation

$$\langle c_j^\dagger c_j\rangle(t) = \frac{1}{2}\left(1 + m_j^0 e^{-\gamma^2 t}\right), \quad j = 1, 4, \tag{5.93}$$

whereas the off-diagonal equation leads to

$$\langle c_1^\dagger c_4\rangle(t) = \frac{1}{2}\left(1 - e^{-\gamma^2 t}\right). \tag{5.94}$$

Note that equation (5.93) is related to the local magnetization by $m_j(t) = 2\langle c_j^\dagger c_j\rangle(t) - 1$, giving

$$m_j(t) = m_j^0 e^{-\gamma^2 t}, \quad j = 1, 4. \tag{5.95}$$

We compare on figure 5.3 the magnetization on spin 1 and the fermionic correlators $\langle c_1^\dagger c_4\rangle$ obtained numerically by exact diagonalization, and the theoretical predictions given by equations (5.95) and (5.94). We see a very good agreement with the numerics.

5.3.4 Spin-spin correlation functions and evolution of the concurrence

As mentioned in the previous section, the reduced density matrix of spins 1 and 4 is reconstructed with the spin-spin correlation functions, see equations (5.74). To

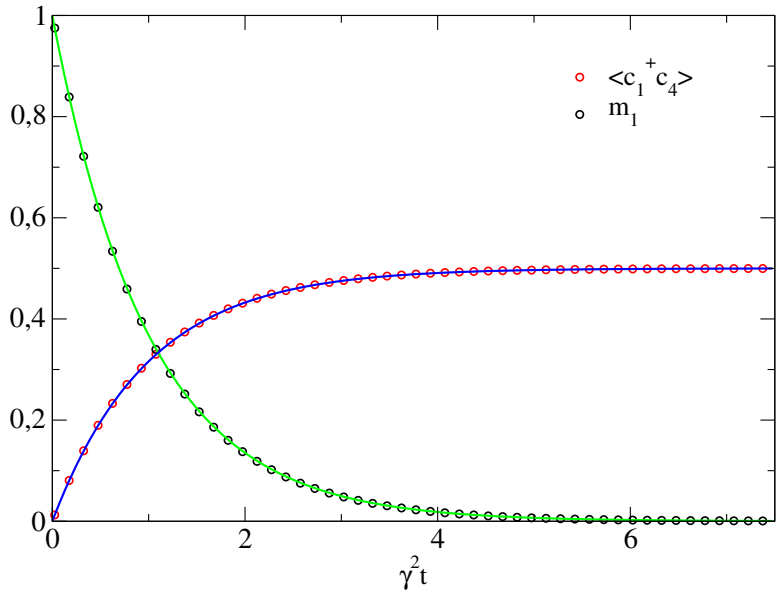

Figure 5.3 – *Magnetization of the first spin m_1 and fermionic correlators $\langle c_1^\dagger c_4\rangle$ as a function of the rescaled time $\gamma^2 t$. The dots are the numerical results obtained by exact diagonalization whereas the full lines are the formula (5.95) and (5.94). The two spins 1 and 4 are initially prepared in a state with $m^0 = 1$.*

proceed, we have to re-express all these correlators in terms of fermionic correlators using the Jordan-Wigner transformation. For example, considering $\langle \sigma_1^x \sigma_4^x\rangle$, we have

$$\begin{aligned}\langle \sigma_1^x \sigma_4^x\rangle =& -\langle (c_1^\dagger + c_1)\sigma_1^z \sigma_2^z \sigma_3^z (c_4^\dagger + c_4)\rangle \\ =&\langle (c_1^\dagger - c_1)\sigma_2^z \sigma_3^z (c_4^\dagger + c_4)\rangle \\ =&\langle (c_1^\dagger - c_1)(2c_2^\dagger c_2 - 1)(2c_3^\dagger c_3 - 1)(c_4^\dagger + c_4)\rangle. \end{aligned} \tag{5.96}$$

Since the Jordan-Wigner transformation is non local and the two system's spins are not consecutive, the sites belonging to the bath part are entering into the expression of the system's correlators. Using the fermionic commutation relations, and the fact that the matrices are Hermitian, it comes, after some algebra

$$\begin{aligned}&\langle \sigma_1^x \sigma_4^x\rangle = 2\Re e\langle c_1^\dagger c_4\rangle \left(1 - 2\left(\langle c_2^\dagger c_2\rangle + \langle c_3^\dagger c_3\rangle\right) + 4\langle c_2^\dagger c_2\rangle\langle c_3^\dagger c_3\rangle - 4|\langle c_2^\dagger c_3\rangle|^2\right) \\ &+ 4\Re e\left(\langle c_1^\dagger c_2\rangle\langle c_2^\dagger c_4\rangle\right)\left(1 - 2\langle c_2^\dagger c_2\rangle\right) + 4\Re e\left(\langle c_1^\dagger c_3\rangle\langle c_3^\dagger c_4\rangle\right)\left(1 - 2\langle c_3^\dagger c_3\rangle\right) \\ &+ 8\left(\Re e\left(\langle c_1^\dagger c_2\rangle\langle c_3^\dagger c_4\rangle\langle c_2^\dagger c_3\rangle\right) + \Re e\left(\langle c_1^\dagger c_3\rangle\langle c_2^\dagger c_4\rangle\langle c_2^\dagger c_3\rangle^*\right)\right). \end{aligned} \tag{5.97}$$

Here we recognize three types of fermionic correlators $\langle c_i^\dagger c_j\rangle$: those who describe correlations within the system ($i, j = 1, 4$), within the bath ($i, j = 2, 3$) and those who represent correlations between system and bath. In the repeated interactions process, the state of each pair interacting with the system is refreshed after the interaction time τ. Then, contrary to the "system-system" correlators, there is no cumulative effects concerning "bath-bath" and "system-bath" correlators and they stay close to their initial value during the evolution, for example $\langle c_2^\dagger c_2\rangle = 1/2 + \mathcal{O}(\tau)$ and $\langle c_1^\dagger c_2\rangle = 0 + \mathcal{O}(\tau)$.

In the continuous limit $\tau \to 0$, one can thus approximate equation (5.97) by

$$\langle \sigma_1^x \sigma_4^x \rangle(t) = 2\Re e \langle c_1^\dagger c_4 \rangle \left(1 - 2\left(\langle c_2^\dagger c_2 \rangle + \langle c_3^\dagger c_3 \rangle\right) + 4\left(\langle c_2^\dagger c_2 \rangle \langle c_3^\dagger c_3 \rangle\right) - 4|\langle c_2^\dagger c_3 \rangle|^2\right). \tag{5.98}$$

Using the initial values of the bath correlators $\langle c_2^\dagger c_2 \rangle = \langle c_3^\dagger c_3 \rangle = \langle c_2^\dagger c_3 \rangle = 1/2$, together with equation (5.94), we obtain finally

$$\langle \sigma_1^x \sigma_4^x \rangle(t) = e^{-\gamma^2 t} - 1. \tag{5.99}$$

Using the same reasoning for $\langle \sigma_1^y \sigma_4^y \rangle$, $\langle \sigma_1^x \sigma_4^y \rangle$ and $\langle \sigma_1^y \sigma_4^x \rangle$, we find

$$\langle \sigma_1^y \sigma_4^y \rangle(t) = \langle \sigma_1^x \sigma_4^x \rangle(t), \tag{5.100}$$

$$\langle \sigma_1^x \sigma_4^y \rangle(t) = \langle \sigma_1^y \sigma_4^x \rangle(t) = 0. \tag{5.101}$$

The last correlator to determined is $\langle \sigma_1^z \sigma_4^z \rangle(t)$. Its expression in terms of fermionic operators is

$$\langle \sigma_1^z \sigma_4^z \rangle = \langle (2c_1^\dagger c_1 - 1)(2c_4^\dagger c_4 - 1) \rangle. \tag{5.102}$$

Note that here, only operators acting on sites 1 and 4 are present, the Jordan-Wigner transformation of the σ^z operator being local. It becomes, using Wick theorem

$$\begin{aligned} \langle \sigma_1^z \sigma_4^z \rangle &= 4\left(\langle c_1^\dagger c_1 \rangle \langle c_4^\dagger c_4 \rangle - |\langle c_1^\dagger c_4 \rangle|^2\right) - 2\left(\langle c_1^\dagger c_1 \rangle + \langle c_4^\dagger c_4 \rangle\right) + 1 \\ &= m_1^0 m_4^0 e^{-2\gamma^2 t} - (1 - e^{-\gamma^2 t})^2 \end{aligned} \tag{5.103}$$

Now that all the spin-spin correlation functions are known, we are in position to write the matrix elements of $\rho_S(t)$ and determine the concurrence between spins 1 and 4. Taking expressions (5.74), the matrix elements of ρ_S are

$$a = \frac{1}{4}\left(1 + (m_1^0 + m_4^0)e^{-\gamma^2 t} + m_1^0 m_4^0 e^{-2\gamma^2 t} - (1 - e^{-\gamma^2 t})^2\right), \tag{5.104}$$

$$x = \frac{1}{4}\left(1 + (m_1^0 - m_4^0)e^{-\gamma^2 t} - m_1^0 m_4^0 e^{-2\gamma^2 t} + (1 - e^{-\gamma^2 t})^2\right), \tag{5.105}$$

$$y = \frac{1}{4}\left(1 + (m_4^0 - m_1^0)e^{-\gamma^2 t} - m_1^0 m_4^0 e^{-2\gamma^2 t} + (1 - e^{-\gamma^2 t})^2\right), \tag{5.106}$$

$$b = \frac{1}{4}\left(1 - (m_1^0 + m_4^0)e^{-\gamma^2 t} + m_1^0 m_4^0 e^{-2\gamma^2 t} - (1 - e^{-\gamma^2 t})^2\right), \tag{5.107}$$

$$c = 0, \tag{5.108}$$

$$z = \frac{1}{2}\left(e^{-\gamma^2 t} - 1\right), \tag{5.109}$$

leading to a concurrence of

$$\begin{aligned} \mathcal{C}_{14}(t) = \max\Bigg\{0, 1 - e^{-\gamma^2 t} - \frac{1}{2}\Bigg(&\left[2e^{-\gamma^2 t} + (m_1^0 m_4^0 - 1)e^{-2\gamma^2 t}\right]^2 \\ &- (m_1^0 + m_4^0)^2 e^{-2\gamma^2 t}\Bigg)^{1/2}\Bigg\}. \end{aligned} \tag{5.110}$$

One can see that if the two system's spins are each prepared in the state $|\uparrow\rangle$ with magnetization $m_{1,4}^0 = 1$ (resp. $|\downarrow\rangle$ with magnetization $m_{1,4}^0 = -1$), the matrix element

b (resp. a), corresponding to the probability to be in the state $|\downarrow\downarrow\rangle$ (resp. $|\uparrow\uparrow\rangle$), is zero during the evolution. The concurrence will be, as a consequence, always bigger for states with $|m^0_{1,4}| = 1$ than for states with $|m^0_{1,4}| \neq 1$. One can also remark that the concurrence is untouched by the simultaneous change $m^0_1 \to -m^0_1$ and $m^0_4 \to -m^0_4$.

For long times, and independently of the initial state of the system, the stationary concurrence reaches is maximal value

$$\mathcal{C}_{14}(t \to \infty) = 1, \tag{5.111}$$

reflecting the fact that $G_S(t \to \infty) = G_B$. This indicates a transfer and a replication of the entanglement present initially in the bath to the two non interacting system's spin. The steady state value of the matrix elements are $z = -1/2$, $x = y = 1/2$ and $a = b = c = 0$, leading to the density matrix

$$\rho^*_S = \frac{1}{2}\begin{pmatrix} 0 & 0 & 0 & 0 \\ 0 & 1 & -1 & 0 \\ 0 & -1 & 1 & 0 \\ 0 & 0 & 0 & 0 \end{pmatrix}. \tag{5.112}$$

The steady state of the spins 1 and 4 is then pure and given by the Bell state $|\psi^-\rangle = \frac{1}{\sqrt{2}}(|\uparrow\downarrow\rangle - |\downarrow\uparrow\rangle)$. Notice that the Bell state reached by the system is not the Bell state of the bath's copies $|\psi_B\rangle = \frac{1}{\sqrt{2}}(|\uparrow\downarrow\rangle + |\downarrow\uparrow\rangle)$. This difference comes from the microscopic coupling chosen to describe the interaction between the system and the bath. Indeed, by tuning the system-bath coupling properly, one can recover the Bell state $|\psi_B\rangle$ as steady state of the system, for example by setting the twisted interaction Hamiltonian

$$H_I = -\frac{\gamma}{2}\left(\sigma^x_1\sigma^y_2 - \sigma^y_1\sigma^x_2 + \sigma^x_3\sigma^y_4 - \sigma^y_3\sigma^x_4\right). \tag{5.113}$$

In this case, $G_S(t \to \infty) = (\mathbb{1} - \sigma^x)/2$, leading to $\langle\sigma^x_1\sigma^x_4\rangle = 1$ and then to

$$\rho^*_S = \frac{1}{2}\begin{pmatrix} 0 & 0 & 0 & 0 \\ 0 & 1 & 1 & 0 \\ 0 & 1 & 1 & 0 \\ 0 & 0 & 0 & 0 \end{pmatrix} = |\psi_B\rangle\langle\psi_B|. \tag{5.114}$$

We plot on the left panel of figure 5.4 the concurrence $\mathcal{C}_{14}(t)$ as a function of the rescaled time $\gamma^2 t$ for two different initial states.
One can see that the entanglement starts to grow directly at $t = 0$ in the case $m^0_1 = m^0_4 = 1$, corresponding to the pure state $|\uparrow\uparrow\rangle$, whereas their is a delay in the growth of $\mathcal{C}_{14}$ in the case $m^0_1 = -m^0_4 = 0.5$, corresponding to an initial mixed state. We plot in the right panel of figure 5.4 the time t_{ent}, defined by $\mathcal{C}_{14}(t) = 0, \forall t < t_{ent}$, as a function of the two initial magnetizations. This time is maximum for $|m^0_j| = 0$ corresponding to the state where the classical statistical mixing is the maximum, since it is prepared with an infinite temperature $\beta \to 0$.

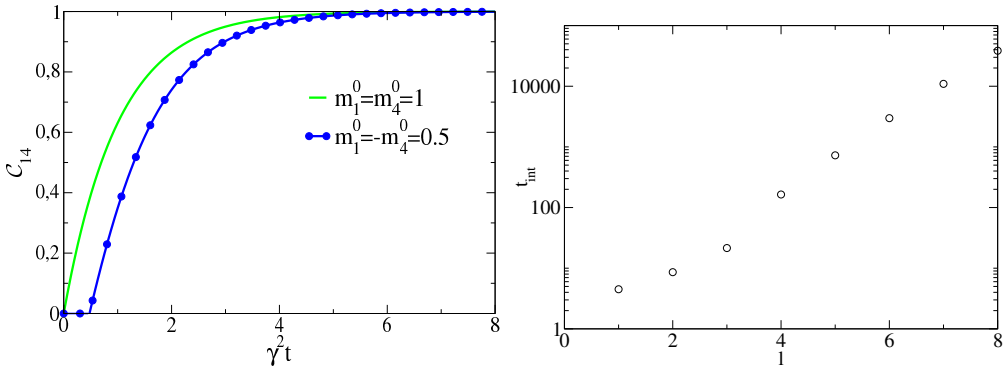

Figure 5.4 – *(Left) Concurrence $\mathcal{C}_{14}$ as a function of the rescaled time $\gamma^2 t$ for two different initial magnetizations. (Right) Time t_{ent} needed for the spins 1 and 4 to become entangled as a function of their initial magnetization m_1^0 and m_4^0.*

We can look in particular at the evolution of the entanglement for the two cases corresponding to identical magnetizations $m_1^0 = m_4^0 = m$ and to opposite magnetizations $m_1^0 = -m_4^0 = m$. In the first case, the concurrence reduces to

$$\mathcal{C}_{14}(t) = \max\left\{0, 1 - e^{-\gamma^2 t} - \frac{1}{2}\sqrt{e^{-2\gamma^2 t}\left(m^2 - 1\right)e^{-2\gamma^2 t} + 4\left(e^{-\gamma^2 t} - 1\right)}\right\}. \tag{5.115}$$

At large times, we can keep only terms of the order of $e^{-\gamma^2 t}$, and we obtain

$$\mathcal{C}_{14}(t) \approx \max\left\{0, 1 - e^{-\gamma^2 t}\left(1 + \sqrt{1 - m^2}\right)\right\}. \tag{5.116}$$

In the second case, the concurrence simplifies even more, and we get

$$\mathcal{C}_{14}(t) = \max\left\{0, 1 - 2e^{-\gamma^2 t} - \frac{1}{2}e^{-2\gamma^2 t}(1 - m^2)\right\}, \tag{5.117}$$

which becomes at large times

$$\mathcal{C}_{14}(t) \approx \max\left\{0, 1 - 2e^{-\gamma^2 t}\right\}. \tag{5.118}$$

In this last case, and contrary to the first one, the approach to the steady state value is independent of the initial magnetization m. The prefactor of the exponential in equation (5.116) lying between 1 and 2, the convergence of the concurrence toward the steady state value is always faster when the spins have the same magnetization than when they have an opposite one. We plot in the left panel of figure 5.22 $1 - \mathcal{C}_{14}$ as a function of $\exp(-\gamma^2 t)$ for different magnetizations.
One can check that the relaxation toward the stationary value is faster when the initial magnetization is $m = 1$, and becomes slower and slower when m is decreased, the slowest dynamics being for $m = 0$, mimicking the opposite magnetization case.

In the case of an opposite initial magnetization, thanks to the simple expression taken by the concurrence (5.117), we can get an analytical estimation of the rescaled

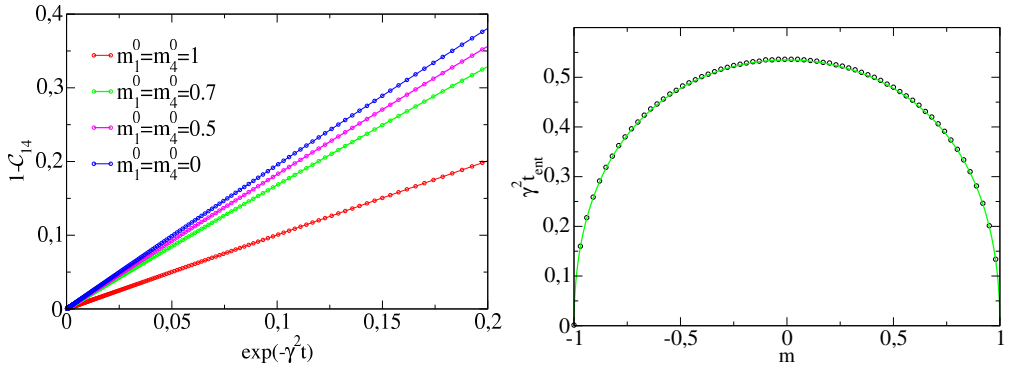

Figure 5.5 – *(Left)*$1-\mathcal{C}$ *as a function of* $\exp(-\gamma^2 t)$ *for different initial magnetizations of the system's spins. (Right) Rescaled time* $\gamma^2 t_{ent}$ *needed for the establishment of the entanglement in the case of opposite initial magnetization as a function of* m*. The dots are the values extracted from the numerical data whereas the full line is given by equation* (5.119).

time $\gamma^2 t_{ent}$ needed for the entanglement to be established. By solving the equation $\mathcal{C}_{14}(\gamma^2 t) = 0$, one finds

$$\gamma^2 t_{int} = \ln\left(1 + \sqrt{\frac{1-m^2}{2}}\right), \tag{5.119}$$

which vanishes with a square root singularity close to the pure state $|m| = 1$ like

$$\gamma^2 t_{int} \approx \sqrt{1-|m|}. \tag{5.120}$$

We compare on the right panel of figure 5.22 the estimation given by equation (5.119) with the numerical data, and we see a very good agreement.

5.3.5 Loss of entanglement in the environment

As we mentioned previously, one can consider that in the continuous limit $\tau \to 0$, the state of each spin of the environment is not affected by the coupling with the system, such that the fermionic correlators stay very close to their initial value. If we work now with a finite value of τ, this consideration does not hold anymore and the state of one copy can change after the interaction with the system. In particular, the coupling of each copy of the environment to the system may has for consequence a partial loss of entanglement between the spins of the Bell pairs.
For small but finite value of the interaction time τ, one can show that the difference between the fermionic correlation matrix describing the n^{th} copy after and before the interaction at time $t = n\tau$ is given by [Plao8]

$$\delta G_B = -\frac{\tau^2}{2}\left(\{G_B, \Theta^\dagger\Theta\} - 2\Theta^\dagger G_S(n\tau)\Theta\right), \quad \delta G_B = G_B((n+1)\tau) - G_B(n\tau). \tag{5.121}$$

After calculations, we obtain

$$\delta G_B = \tau^2\gamma^2(-G_B + G_S(n\tau)). \tag{5.122}$$

In order to compute this variation, one need the evolution of the fermionic correlation matrix of the system part. By solving the evolution equation of the system for finite interaction time (5.57), we find

$$\langle c_i^\dagger c_i\rangle(n\tau) = \frac{1}{2}\left(1 + m_i^0 \cos^{2n}(\gamma\tau)\right), \quad i = 1, 4, \tag{5.123}$$

$$\langle c_1^\dagger c_4\rangle(n\tau) = \frac{1}{2}\left(1 + \cos^{2n}(\gamma\tau)\right), \tag{5.124}$$

leading to the following values for the bath correlators of the copy n just after the interaction at time $t = n\tau$

$$\langle c_2^\dagger c_2\rangle((n+1)\tau) = \frac{1}{2}\left(1 + \gamma^2\tau^2 m_1^0 \cos^{2n}(\gamma\tau)\right) \tag{5.125}$$

$$\langle c_3^\dagger c_3\rangle((n+1)\tau) = \frac{1}{2}\left(1 + \gamma^2\tau^2 m_4^0 \cos^{2n}(\gamma\tau)\right) \tag{5.126}$$

$$\langle c_2^\dagger c_3\rangle((n+1)\tau) = \frac{1}{2}\left(1 - \gamma^2\tau^2 \cos^{2n}(\gamma\tau)\right). \tag{5.127}$$

We show on the left panel of figure 5.6 the value of the correlators $\langle c_2^\dagger c_2\rangle$ and $\langle c_2^\dagger c_3\rangle$ of the copy n after the interaction at time $t = n\tau$ for an interaction time $\tau = 0.25$. We can see that the theoretical predictions (full lines) perfectly match the data obtained by exact diagonalization (symbols).
After the calculation of the spin-spin correlation functions, we finally find that the concurrence of the copy n after the interaction at time $t = n\tau$ is given by

$$\mathcal{C}_B^{(n)} = 1 - \gamma^2\tau^2 \cos^{2n}(\gamma\tau)\left(1 + \frac{1}{2}\sqrt{\left(\gamma^2\tau^2\cos^{2n}(\gamma\tau)\left(m_1^0 m_4^0 - 1\right) + 2\right)^2 - \left(m_1^0 + m_4^0\right)^2}\right). \tag{5.128}$$

Since $\cos(\gamma\tau) < 1$, one can see from the previous equation that after many interactions, the copies do not loose any entanglement after the coupling with the system. Indeed, for long time, the two spins of the system have reached a steady state and consequently, they do not evolve anymore, as well as the copies of the environment. In the right panel of figure (5.57), we plot the concurrence after the interaction at time $t = n\tau$ for $\tau = 0.25$, $m_1^0 = m_4^0 = 0.5$. On can check that the concurrence goes to the initial value $\mathcal{C}_B = 1$ after many interactions, reflecting the fact that the spins of the system have reached the steady state.

5.4 General case: System of two chains of size N

5.4.1 Model an initial states

We now turn to the study of the most general case of two non interacting chains made by N spins. The spins of the first chain are labeled from 1 to N, and those of the second one from $N + 3$ to $2N + 2$. The environment will be modeled exactly as it was in the previous section, and the interaction will be done in the following way: the last spin of the first chain interacts with the first spin of the environmental pair, whereas the first spin of the second chain is coupled to the second one. A picture of the system is presented in figure 5.7.

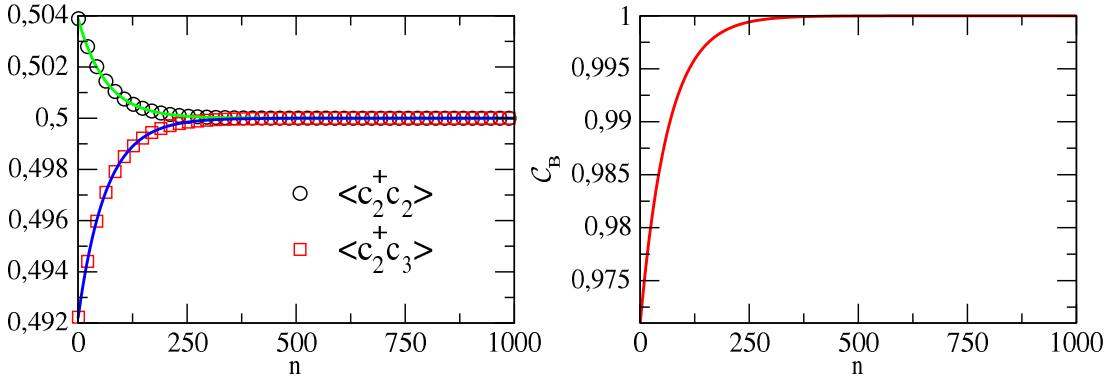

Figure 5.6 – *Values of the correlators $\langle c_2^\dagger c_2\rangle$ and $\langle c_2^\dagger c_3\rangle$ (left) and concurrence (right) of the copy n just after the interaction at time $t = n\tau$. In the left panel, the symbols are the numerical data whereas the full lines are given by equations (5.126) and (5.127). We used $\gamma = 0.5$, $m_1^0 = m_4^0 = 0.5$, and the interaction time is fixed to $\tau = 0.25$.*

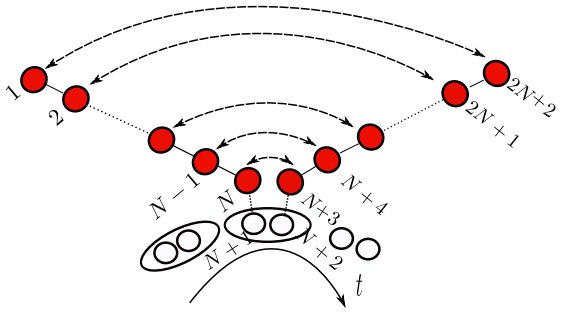

Figure 5.7 – *The repeated interactions process in the case of two chains made of N spins. The last spin of the first chain interacts with the first spin of the environmental pair, whereas the first spin of the second chain is coupled to the second one.*

The Hamiltonian of the system formed by the two chains is

$$H_S = -\frac{h}{2}\sum_{n\in\mathbb{S}}\sigma_n^z - \frac{J}{2}\sum_{n\in\mathbb{S}^*}\left(\sigma_n^x\sigma_{n+1}^x + \sigma_n^y\sigma_{n+1}^y\right), \tag{5.129}$$

with $\mathbb{S} = \{1,2,\ldots,N\}\cup\{N+3,N+4,\ldots,2N+2\}$ and $\mathbb{S}^* = \mathbb{S}\backslash\{N,2N+2\}$, whereas

$$H_B^k = -\frac{h}{2}(\sigma_{k,N+1}^z + \sigma_{k,N+2}^z), \tag{5.130}$$

and

$$H_I^{(k)} = -\frac{\gamma}{2}(\sigma_N^x\sigma_{k,N+1}^x + \sigma_N^y\sigma_{k,N+1}^y + \sigma_{k,N+2}^x\sigma_{N+3}^x + \sigma_{k,N+2}^y\sigma_{N+3}^y). \tag{5.131}$$

are the Hamiltonian of the copy k of the environment and the coupling Hamiltonian respectively. After the introduction of fermionic operators by the Jordan-Wigner transformation, the total Hamiltonian takes the form $H = \mathbf{\Psi}^\dagger \boldsymbol{T}\mathbf{\Psi}$ with $\mathbf{\Psi}^\dagger = (\boldsymbol{c}_S^\dagger, \boldsymbol{c}_B^\dagger)$ where $\boldsymbol{c}_S^\dagger = (c_1^\dagger,\ldots,c_N^\dagger,c_{N+3}^\dagger,\ldots,c_{2N+2}^\dagger)$ and $\boldsymbol{c}_B^\dagger = (c_{N+1}^\dagger, c_{N+2}^\dagger)$. The $(2N+2)\times(2N+2)$ matrix $\boldsymbol{T}$ is given by

$$T = \begin{pmatrix} T_S & \Theta \\ \Theta^\dagger & T_B \end{pmatrix}, \quad T_S = \begin{pmatrix} A & 0 \\ 0 & A \end{pmatrix} \tag{5.132}$$

with $A_{ij} = -h\delta_{ij} - J(\delta_{i,j+1} + \delta_{i,j-1})$ of size $N \times N$, $T_B = -h\mathbb{1}_{2\times 2}$, and the $2N \times 2$ coupling matrix Θ is given by $\Theta_{ij} = -\gamma(\delta_{i,N}\delta_{j,1} + \delta_{i,N+1}\delta_{j,2})$.

The whole system is initially prepared into an uncorrelated state such that

$$\rho(0) = \rho_S(0) \otimes \eta_B, \tag{5.133}$$

with $\eta_B = \bigotimes_{k\in N^*} \eta$, and

$$\eta = |\psi_B\rangle\langle\psi_B|, \quad |\psi_B\rangle = \frac{1}{\sqrt{2}}\left(|\uparrow\downarrow\rangle + |\downarrow\uparrow\rangle\right). \tag{5.134}$$

The two XX chains are prepared into a fully factorized thermal mixture

$$\rho_S(0) = \bigotimes_{n\in S} \rho_n \tag{5.135}$$

with

$$\rho_n = \frac{1+m_n^0}{2}|\uparrow\rangle\langle\uparrow| + \frac{1-m_n^0}{2}|\downarrow\rangle\langle\downarrow|, \tag{5.136}$$

with $m_n^0 = \mathrm{Tr}\{\rho(0)\sigma_n^z\}$ the initial magnetization of the spin n.
The initial state of the system and the bath being Gaussian, one can, as we did for the toy model, describe completely the system by means of its $2N \times 2N$ fermionic correlation matrix $(G_S)_{ij}(t) = \langle(\boldsymbol{c}_S^\dagger)_i(\boldsymbol{c}_S)_j\rangle(t)$. We remind that this correlation matrix evolves, in the continuous limit $\tau \to 0$ following the evolution equation

$$\partial_t G_S(t) = -i[T_S, G_S(t)] - \frac{1}{2}\left(\left\{G_S(t), \Theta^\dagger\Theta\right\} - 2\Theta^\dagger G_B \Theta\right), \tag{5.137}$$

where

$$G_B = \frac{1+\sigma^x}{2} \tag{5.138}$$

is the correlation matrix of the bath.

In the following, we are interested in the cross entanglement between two spins facing each other in the chains, as represented by the dashed double arrows in figure 5.7. We call $\mathcal{C}^{(p)}$ the associated concurrence between the spins $N-p$ (belonging to the left chain) and $N+3+p$ (belonging to the right chain), with $p = 0, \ldots, N-1$. The value $p = 0$ corresponds for example to the pair formed by the two spins in contact with the environment. Moreover, we introduce the longitudinal concurrence $\mathcal{C}_L^{(p)}$, measuring the entanglement between to neighboring sites p and $p-1$ in a given chain. These two concurrences are, as for the toy model, computed thanks to the reconstruction of the reduced density matrix using the spin-spin correlation functions, themselves obtained with the time evolved fermionic correlators. Concerning the cross concurrence, the fact that the two spins under consideration are not first neighbors in the chain renders the analytical determination of the spin-spin correlation functions very difficult. For a given p, it requires the calculation of a Pfaffian of size $4p+2$ [AOP+04]. This step will therefor be realized numerically.

We assume in the following that all spins of the two chains are prepared with the same initial magnetization, i.e $m_j^0 = m_0\ \forall j$. Moreover, the value of the intra-chain coupling J will be set to $J = 1/2$ in order to fix the sound velocity in the chains to 1.

5.4.2 Study for times $t < 2N$: NESS

We start our study by focusing our attention to the time regime $t < 2N$. This time corresponds to the time needed for an excitation introduced in the system at the coupling point to travel forward along the chain, be reflected on the opposite edge, and come back into the injection point.
Then, for sufficiently large system size N, and times $t \ll N$, the sites close to the boundary where the interaction takes place will experience a semi-infinite situation.

Before turning to the description of the dynamics of the system in this time regime, let's first mention an interesting and important feature: the dynamics of correlators belonging to one chain only is independent of the dynamics of the correlators belonging to the other chain. To prove that, lets decompose the matrix G_S like

$$G_S = \begin{pmatrix} G_S^1 & G_S^{12} \\ G_S^{21} & G_S^2 \end{pmatrix}, \tag{5.139}$$

where the matrices G_S^i contain the correlations within the chain i, with $i = 1, 2$, whereas the matrix $G_S^{12} = (G_S^{21})^\dagger$ contains the correlations between the two chains. Remarking that we can also split the other matrices into blocks

$$\Theta\Theta^\dagger = \begin{pmatrix} L_1 & \\ & L_2 \end{pmatrix} \quad \Theta G_B \Theta^\dagger = \frac{1}{2}\begin{pmatrix} L_1 & K_{12} \\ K_{21} & L_2 \end{pmatrix}, \tag{5.140}$$

with $L_1 = \mathrm{diag}(0, \cdots, 0, \gamma^2) \in \mathbb{R}^{N\times N}$, $L_2 = \mathrm{diag}(\gamma^2, 0, \cdots, 0) \in \mathbb{R}^{N\times N}$ and $(K_{12})_{ij} = \gamma^2\delta_{iN}\delta_{j1} = (K_{21})_{ji}$ the evolution equation of G_S becomes

$$\begin{aligned}\partial_t \begin{pmatrix} G_S^1 & G_S^{12} \\ G_S^{21} & G_S^2 \end{pmatrix} = &- i \begin{pmatrix} [G_S^1, A] & [G_S^{12}, A] \\ [G_S^{21}, A] & [G_S^2, A] \end{pmatrix} - \begin{pmatrix} \{G_S^1, L_1\} & G_S^{12}L_1 + L_2 G_S^{12} \\ L_2 G_S^{21} + G_S^{21} L_1 & \{G_S^2, L_2\} \end{pmatrix} \\ &+ \frac{1}{2}\begin{pmatrix} L_1 & K_{12} \\ K_{21} & L_2 \end{pmatrix}.\end{aligned} \tag{5.141}$$

where A is the matrix appearing in equation (5.132). We obtain thus two independent equations governing G_S^1 and G_S^2. As a consequence, the dynamics of the fermionic correlators belonging to the left chain and those belonging to the right one are decoupled. More precisely, because the spins of the two chains are prepared in the same initial state, we have

$$\langle c_i^\dagger c_j \rangle = \langle c_{2N+3-i}^\dagger c_{2N+3-j} \rangle, \quad i, j = 1, \ldots, N. \tag{5.142}$$

It appears then that local observables (like local magnetization for instance) evolve exactly in the same way in the two chains. Thus, if we are interested in such an observable, we can restrict the system to only one chain coupled at one of its boundary to a single spin with zero magnetization, which greatly improve the numerical calculation time.

The evolution equation (5.137) is difficult to solve analytically. As a consequence, the dynamics of the systems will be described numerically using exact diagonalization. We describe here the system through the evolution of observables like local

magnetization, currents, fermionic correlations and cross and longitudinal concurrences.
We plot in figure 5.8 the time evolution of the local magnetization (left) and the current (right) in the first 30 spins of a chain of $N = 150$ coupled at position N to a single spin with zero magnetization.

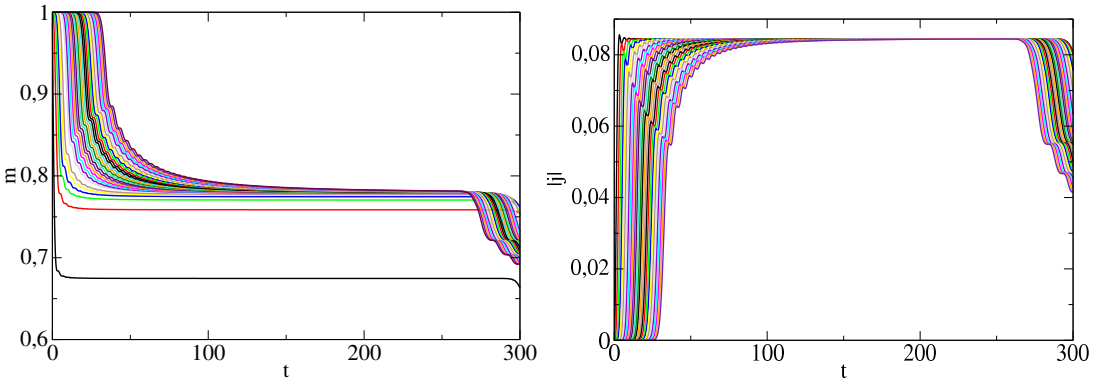

Figure 5.8 – *Magnetization (left) and current (left) in the* 30 *first spin of a chain of* $N = 150$ *in the time regime* $t < 2N$. *The initial magnetization is* $m_0 = 1$ *and the coupling parameters is fixed to* $\gamma = 0.5$.

The magnetization at a given spin at position $x = N - p$ is equal to the initial value m_0 until the time $t = x$ at which the first excitation injected has reached the position x. After this time, the magnetization decreases until a stationary value, which seems to be minimum for the spin in contact with the environment, and constant in the bulk. Once the fastest excitation comes back at position x at time $2N - x$ after being reflected on the opposite edge, this stationary regime is broken. The transport of excitations is associated with a current of quasiparticles. The behavior of the current is similar to the magnetization. Indeed, it starts to be non zero when the first excitation reaches the position x at time $t = x$, and increases until a stationary value. Contrary to the magnetization, the current is homogeneous in the chain.
In the time regime $t \ll N$ with N sufficiently large, the sites localized close to the interaction point are then in a non equilibrium steady state (ness) characterized by a non evolving magnetization on each spin and a stationary current traveling along the chain.
For both magnetization and current, the relaxation toward the non-equilibrium-steady-state value m^∞ and j^∞ is algebraic, as shown in figure 5.9.
We find

$$m - m^\infty \sim t^{-2} \tag{5.143}$$

$$|j - j^\infty| \sim t^{-3}. \tag{5.144}$$

The difference of exponent can be understood using hydrodynamical argument, the current being simply given by $j = nv$, where $v \sim t^{-1}$ is the velocity and n the local density proportional to the magnetization.
In order to have a good approximation of what is the steady state of the semi-infinite system, we look at magnetization and current profiles at time $t = N$. Indeed, for sufficiently large value of N, the state of the spins close to the interaction point has

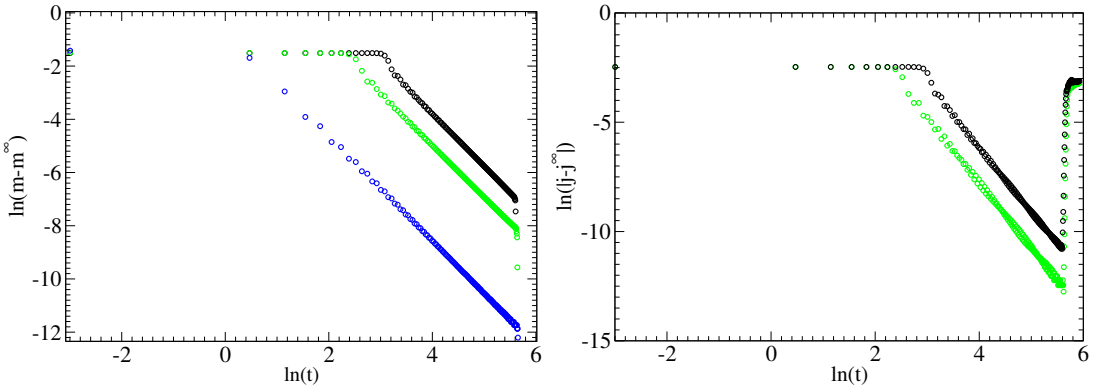

Figure 5.9 – *Left: relaxation of the magnetization to the asymptotic value of the spins $p = 0$ (blue), $p = 9$ (green) and $p = 19$ (black). Right: relaxation of the current of the spins $p = 1$ (green) and $p = 9$ (black). The initial magnetization is $m_0 = 1$ and the coupling is fixed to $\gamma = 0.5$.*

converged to the steady state, whereas the spins close to the opposite edge are still into a transient dynamics with observables evolving in time. We plot in figure 5.10 the magnetization and current profiles taken at $t = N$ for sizes of the chain $N = 100$, $N = 150$ and $N = 500$.

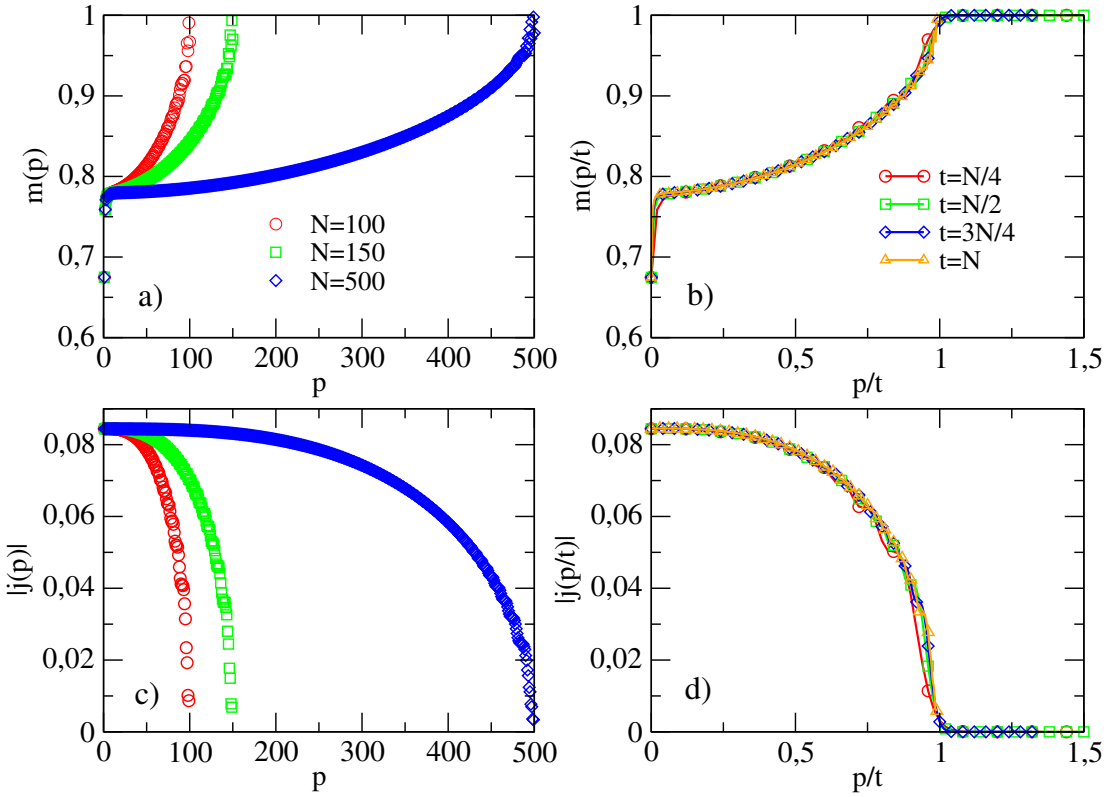

Figure 5.10 – *Magnetization (a) and current (c) profiles measures at $t = N$ for different sizes of the chains. Graphs (b) and (d) show the profiles at different times using the rescaled variable p/t. The size of the chain is in this case $N = 300$. For all plots, the initial magnetization is $m_0 = 1$ and γ is fixed to $1/2$. Since $m_0 = 1$, the plots of graph (d) give directly access to the scaling function $g(p/t)$.*

We can check that magnetization profile is bent at the interface with the environment ($p = 0$) whereas the deviation from the stationary value in the bulk is algebraic following

$$m(p) - m(p \to \infty) = a\left(\left(\frac{p}{t}\right)^2 - \frac{1}{(bp)^2}\right), \tag{5.145}$$

where a and b are parameters depending on the coupling constants. On the contrary, no interface is observed for the current profile, which tends to a homogeneous value along the complete chain. In the scaling region, the system is scale invariant such that we can introduce the rescaled variable p/t and write the magnetization and current profiles like [Plao8]

$$m\left(\frac{p}{t}\right) = m_0\left(1 - f\left(\frac{p}{t}\right)\right), \quad j\left(\frac{p}{t}\right) = m_0 g\left(\frac{p}{t}\right), \tag{5.146}$$

where $f(p/t)$ and $g(p/t)$ are two scaling functions which vanish in the non-causal region $p/t > 1$. We plot on the right panels of figure 5.9 the two profiles as a function of the variable p/t at different times for a chain of size $N = 300$. All the curves collapse into a single curve in the bulk, indicating that the system is well scale invariant. We can have access to the $f(p/t)$ function by evaluating numerically $1 - m(p/t)/m_0$. The results are shown in figure 5.11 for different times and for two values of the system-environment coupling parameter γ. Note that the scaling function $g(p/t)$ is directly given by the right down plot of figure 5.9 since the system is initially prepared with $m_0 = 1$.

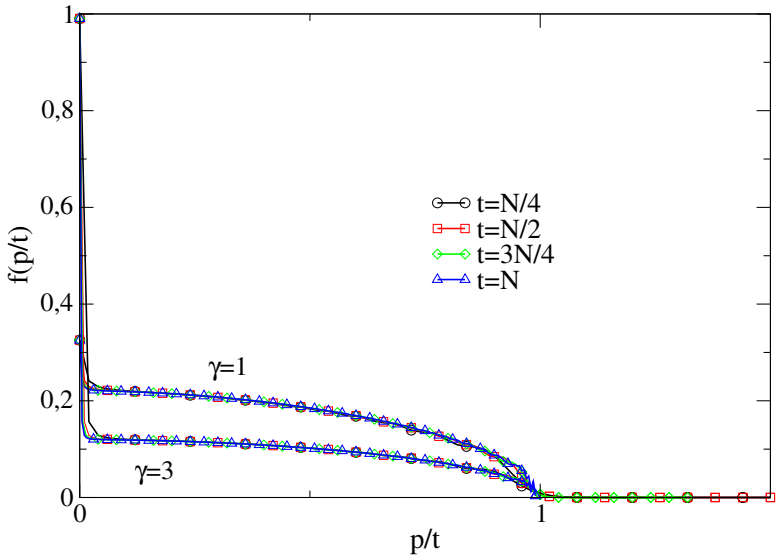

Figure 5.11 – *Scaling function $f(p/t)$ at different times for a system with $N = 300$ spins and two values of the system-environment coupling γ.*

The stationary current presents a non monotonic behavior with the coupling strength γ, as shown in figure 5.12. It appears that the good variable to use is the ratio between the intra chain coupling J (which is set to $1/2$ in our case) and the square of the coupling to the environment γ, which we will call $K = \gamma^2/2J$. The stationary current is weak in the limits $K \ll 1$ and $K \gg 1$, as already observed in [KP09].

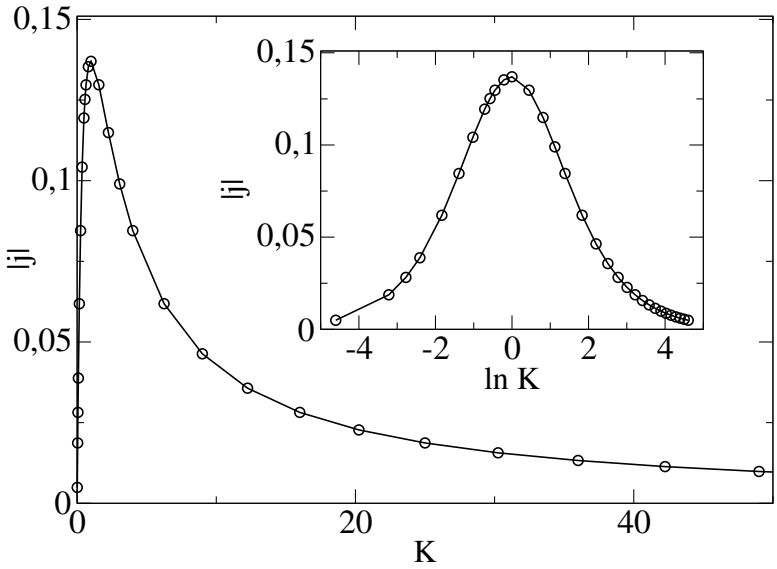

Figure 5.12 – *Stationary current evaluated at $t = N$ as a function of the parameter $K = \gamma^2/2J$ (main graph) and as a function of* $\ln(K)$ *(insert). The initial magnetization is* $m_0 = 1$.

Indeed, in the first limit, it is difficult to inject a particle, leading to a small value of the current. In the second limit, the contrary situation happens, it is easy to inject a particle at the interaction point, but it is difficult to propagate it along the chain, leading once again to a small value of the current. The maximum of the current is reached when the ratio is equal to unity, $K = 1$. We observe moreover that the current is invariant under the duality transformation

$$K \to \frac{1}{K}. \tag{5.147}$$

We check, in the insert of figure 5.12 where we plot $|j|$ as a function of $\ln(K)$ that the curve is well symmetric with respect to the point $\ln(K) = 0$, validating the duality (5.147).

The travel of the excitations injected at the interaction point has for consequence the correlation between the different sites of the system. The correlation between two sites belonging to the same chain (intra-chain correlators) is a direct consequence of the same quasiparticle flow, whereas the correlation between two sites belonging to different chains (inter-chain correlator) is the consequence of the passage of two quasiparticles initially entangled through the entanglement present into the two spins forming each pair of the bath. We show in figure 5.13 the real and imaginary parts of the correlators $\langle c_i^\dagger c_j \rangle$, with $i = 96$ (corresponding to $p = 4$) as a function of the position j taken at time $t = N$ for a system made of two chains of size $N = 100$, and for two different initial magnetizations $m_0 = 1$ and $m_0 = 0.5$.
Considering intra-chain correlators ($j < N$), the real part reaches its maximum value for $j = i$, corresponding to the local density, and decreases with the distance $d = |i - j|$, provided that $i + d \leq N$. Interestingly, the real part of the correlator vanishes for odd values of d. For even values of d, the correlations seem to decay algebraically

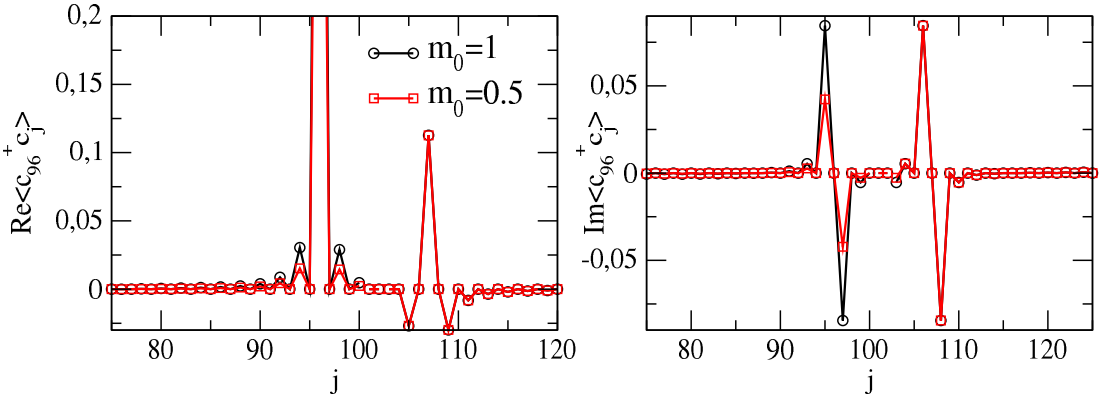

Figure 5.13 – *Real (left) and imaginary (right) part of the fermionic correlator* $\langle c_{96}^\dagger c_j \rangle$ *between site* 96 *the other sites taken at time* $t = N$ *for two initial magnetizations of* $m_0 = 1$ *and* $m_0 = 0.5$. *The other parameters are* $N = 100$ *and* $\gamma = 0.5$. *Here we show only the range* $j \in [75 : 125]$ *for clarity reason.*

with the distance following

$$\Re e\langle c_i^\dagger c_{i\pm d}\rangle \sim d^{-2}. \tag{5.148}$$

The imaginary part presents two packs corresponding, up to the sign, to the current of particles traveling along the chains. Of course, these two peaks are equal in absolute value but with different sign, the first one being proportional to the current of particles moving from the right to the left, and the second to the current of particles moving from the left to the right. As for the real part, some of the correlators have a vanishing imaginary part, namely those with an even value of d. For odd values of d, the decay of the peaks is, as for the real part, algebraic with the distance, but with a different exponent

$$|\Im m\langle c_i^\dagger c_{i\pm d}\rangle| \sim d^{-3}. \tag{5.149}$$

The real part of the inter-chain correlators presents a peak at position $j = 2N + 3 - i$, indicating that the site sharing the most correlation with one site i is the site facing it, the correlations decreasing with the distance to this particular site.
One can note that the intra-chain correlators are dependent on the initial magnetization m_0 of the system, whereas the inter-chain are not. This can be explained by looking at the evolution equation of the correlation matrix (5.141). The evolution equations of the matrices G_S^1 and G_S^2 containing the intra-chain correlators depend on the initial magnetization whereas the equation governing G_S^{12} only depends on the initial correlations between the two chains (set to zero in our case) and the coupling strength and then not on the value of m_0.

The correlations between the different sites are responsible for two kinds of entanglement, the longitudinal one between two neighboring sites p and $p + 1$, measured by the concurrence $\mathcal{C}_L^{(p)}$, and the cross one, measured by the cross concurrence $\mathcal{C}^{(p)}$, between two sites facing each others $N - p$ and $N + 3 + p$. We present in the left panel of figure 5.14 the longitudinal concurrence profile, extracted at time $t = N$, for different sizes of the chain. As for the magnetization and current, the entanglement between sites close to the boundary interacting with the environment has reached its steady state value. The longitudinal concurrence is equal to zero between the spins

composing the pair $(N, N-1)$, and starts to grow for the next pairs. Like for the magnetization, and the current, the longitudinal concurrence is scale invariant in the scaling region, as we can see on the right panel of figure 5.14 where we plot $\mathcal{C}_L^{(p/t)}$ as a function of p/t at different times, and where we can observe the perfect collapse of the curves.

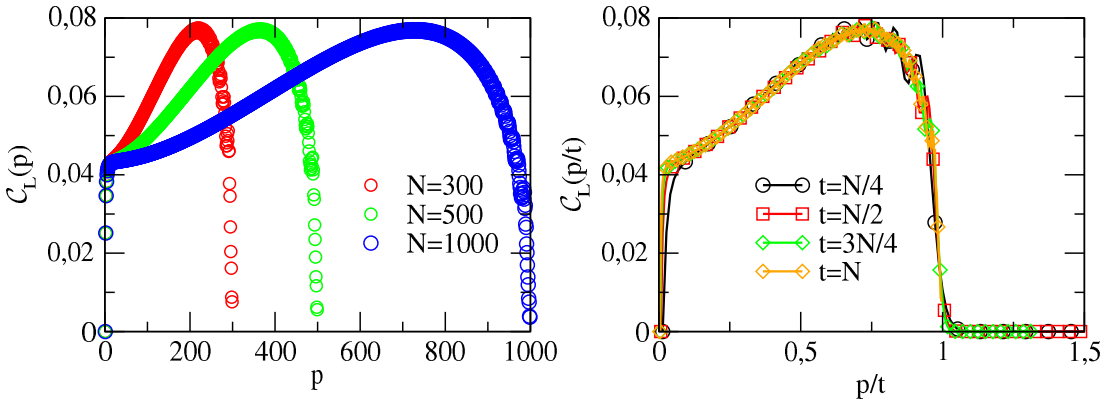

Figure 5.14 – *Longitudinal concurrence profile extracted a time $t = N$ for different sizes of the chains (left). Longitudinal concurrence profile as a function of the rescaled variable p/t at different times in the case of a chain of size $N = 300$ (right). For both plots, the initial magnetization is $m_0 = 1$, and $\gamma = 0.5$.*

Moreover, we define the total longitudinal concurrence by summing all the concurrences associated to first neighboring spins

$$\mathcal{C}_{tot}^{(p)} = \sum_{p=0}^{N-1} \mathcal{C}_L^{(p)}, \tag{5.150}$$

and we study its time evolution. This will gives us informations about how this entanglement is established and how it behaves after the breaking of the ness regime, i.e after time $t = N$. The results are shown on figure 5.15 for different sizes of the chain. One can observe that the total longitudinal entanglement grows linearly in time with a slope independent of the size. This linear regime is broken at the time $t = N$ when the first excitation emitted reaches the edge of the chain. After this time, the travel in opposite direction of the excitations creates destructive interferences, which have for consequence the decrease of the correlations, and the logarithmic decay of the total longitudinal concurrence. We can observe that the longitudinal concurrence is already killed after a time $t \approx 2N$, indicating that one return of the first excitation is enough to kill all the first neighbor entanglement.

We finish our study of the non-equilibrium-steady-state properties of the system by the cross entanglement, measured by the concurrence $\mathcal{C}^{(p)}$, between sites facing each other in the two chains. This entanglement is the consequence of the inter chain correlations created through the travel of entangled quasiparticles along the two chains. We plot in figure 5.16 the cross concurrence between the twenty first spin pairs (labeled, from top to bottom in the graphs by $p = 0$ to $p = 19$) of a system made of two chains of $N = 60$ spins for two values of the coupling parameter, $\gamma = 0.5$ (left)

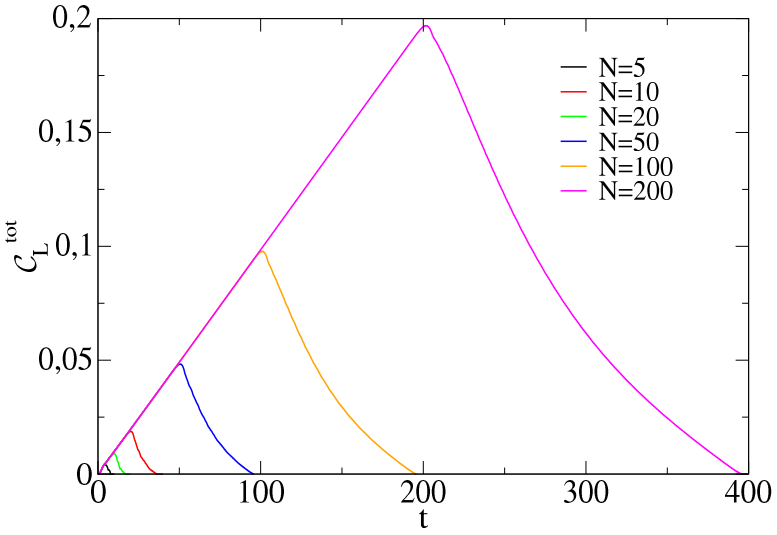

Figure 5.15 – *Time evolution of the total longitudinal concurrence for different sizes of the chain. The coupling parameter is set to* $\gamma = 0.5$.

and $\gamma = 0.1$ (right). These two coupling strengths correspond respectively to strong and weak current regime.

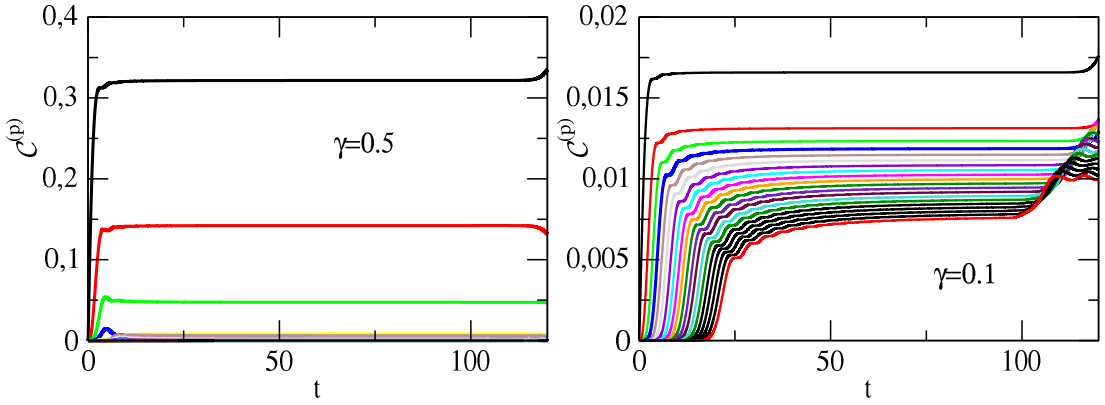

Figure 5.16 – *Cross concurrence* $\mathcal{C}^{(p)}$ *for, from top to bottom,* $p = 0$ *to* $p = 19$ *for a coupling strength* $\gamma = 0.5$ *(left) and* $\gamma = 0.1$ *(right). The size of the two chains is* $N = 60$*, and the initial magnetization is* $m_0 = 1$.

As for other observables like magnetization or current, the cross concurrence converges to a steady state value. This non-equilibrium-steady-state entanglement is maximum in the pair of spins $p = 0$ directly interacting with the environment, and decreases with the distance to the interaction point. One can here make two observations: the concurrence is about one order of magnitude bigger when the current is strong than when it is weak. Nevertheless, the decay of the cross concurrence with respect to the distance is faster in the strong current than in the weak current regime. Indeed, when the current is strong, it is easy for the entangled quasiparticles to distribute the entanglement along the spins, leading to a strong concurrence on the few first pairs, but also to a rapid decay of it. On the contrary, for weak current, it is

difficult to transfer the entanglement, leading to a small value of the concurrence, but this transfer can be done in a longer distance than in the strong current regime. Numerical results seem to indicate an exponential decay of the concurrence with the distance to the interaction point (see left panel of figure 5.17)

$$\mathcal{C}^{(p)} \sim \exp\left(-p/\xi_{ent}\right), \tag{5.151}$$

where ξ_{ent} is a typical entanglement length depending on the parameters of the system. Interestingly, in the small current regime, we find that the entanglement length is proportional to the inverse of the stationary current in the chain $\xi_{ent} \propto 1/|j|$, whereas deviations can be observed in the strong current regime, as shown in the right panel of figure 5.17.

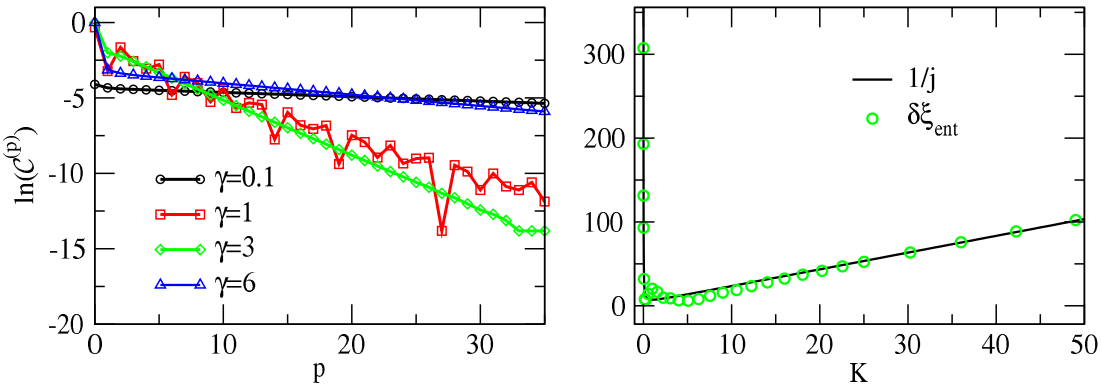

Figure 5.17 – *Left: logarithm of the cross concurrence measured at $t = N$ as a function of the pair p for three values of the coupling strength γ. Right: Inverse of the current and entanglement length ξ_{ent}. The proportionality coefficient is in this case $\delta \equiv 5.67$. The size of the chains is $N = 60$ and the initial magnetization is $m_0 = 1$.*

The impossibility to solve the evolution equation for $t < 2N$ and the non locality of the Jordan-Wigner transformation render the analytical determination of the non equilibrium steady state value of the cross concurrence difficult. Nevertheless, for the pair formed by the two spins in contact with the environment, i.e $p = 0$, we can determined the value of the concurrence as a function of the initial magnetization using some hypothesis. Indeed, because the sites close to the edge interacting with the environment are into a steady state, one can reasonably set the temporal derivative of these elements to zero. Solving the equation evolution

$$\partial_t G_S(t) = -i[T_S, G_S(t)] - \frac{1}{2}\left(\left\{G_S(t), \Theta^\dagger\Theta\right\} - 2\Theta^\dagger G_B \Theta\right) \tag{5.152}$$

for spins N and $N+3$, we find that their magnetization in the ness is directly proportional to the steady state current established in the chains for $t < N$

$$m_i = \frac{2J}{\gamma^2}|j| = \frac{1}{K}|j|, \quad i = N, N+3. \tag{5.153}$$

We can check this relation by plotting $m_N/|j|$ as a function of $1/K$ (see figure 5.18). We get, as expected, a linear relation with a slope equal to one, validating the relation (5.153).

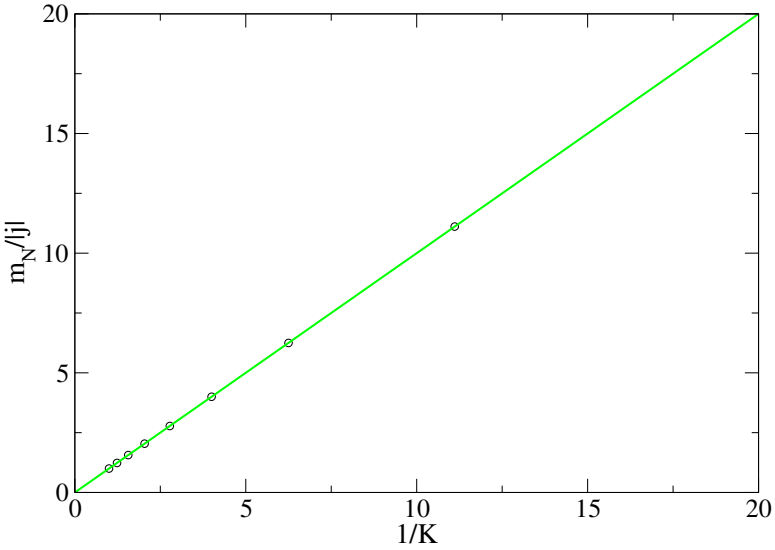

Figure 5.18 – *Steady state magnetization on the spin N divided by the stationary current as a function of $1/K$ (dots). The straight line is a linear function with slope* 1.

Following [Plao8], we can write the stationary current like

$$j \propto m_0 - m_B = m_0. \tag{5.154}$$

It appears then that the magnetization of spins N and $N+3$ is proportional to the initial magnetization of the chain, and we write

$$m_i = (1-\alpha)m_0, \quad i = N, N+3, \tag{5.155}$$

where the coefficient α depends only on the coupling constants. In the same way, we do the hypothesis that the fermionic correlator $\langle c_N^\dagger c_{N+3}\rangle$ is proportional to the initial fermionic correlator of the pair of spins forming one copy of the environment

$$\langle c_N^\dagger c_{N+3}\rangle = \alpha\langle c_{N+1}^\dagger c_{N+2}\rangle = \frac{\alpha}{2}, \tag{5.156}$$

with the same real coefficient α as previously. This coefficient is difficult to find analytically, and will be extracted numerically by looking the magnetization of spin N or $N+3$. We can now write down the spin-spin correlation functions between spins N and $N+3$

$$\begin{aligned}
\langle \sigma_N^x \sigma_{N+3}^x\rangle &= \langle \sigma_N^y \sigma_{N+3}^y\rangle = -\alpha,\\
\langle \sigma_N^x \sigma_{N+3}^y\rangle &= \langle \sigma_N^y \sigma_{N+3}^x\rangle = 0,\\
\langle \sigma_N^z \sigma_{N+3}^z\rangle &= (1-\alpha)^2 m_0^2 - \alpha^2,
\end{aligned} \tag{5.157}$$

where we have used the Wick theorem for the correlator in the z direction. This leads to the following reduced density matrix

$$\rho_{ij} = \begin{pmatrix} a & 0 & 0 & c \\ 0 & x & z & 0 \\ 0 & z^* & y & 0 \\ c^* & 0 & 0 & b \end{pmatrix}, \tag{5.158}$$

with the elements

$$\begin{aligned} a =& \frac{(1+(1-\alpha)m_0)^2}{4} - \frac{\alpha^2}{4}, \\ x =& y = \frac{(1+\alpha^2)\,(1-m_0^2)}{4} - \frac{\alpha m_0^2}{2}, \\ b =& \frac{(1-(1-\alpha)m_0)^2}{4} - \frac{\alpha^2}{4}, \\ c =& 0, \\ z =& -\alpha. \end{aligned} \tag{5.159}$$

Finally, with these matrix elements, we find a steady state concurrence in the pair $p = 0$ given by

$$\mathcal{C}^{(0)}(m_0, \alpha) = \max\left\{0, \alpha - \frac{1}{2}\sqrt{(1-\alpha)^2(1-m_0^2)^2\left(1+\alpha^2+2\alpha\left(\frac{1+m_0^2}{1-m_0^2}\right)\right)}\right\}. \tag{5.160}$$

One can remark that for $m_0 = 1$ (resp. $m_0 = -1$), $b = 0$ (resp. $a = 0$), leading to a maximum concurrence of $\mathcal{C}^{(0)} = \alpha$. The stationary entanglement in the first pair is then maximum for $|m_0| = 1$ and decreases with $|m_0|$. Depending on the value of the parameter α (and then on the value of the coupling γ), it may exist a threshold value $|m_{thre}|$, satisfying $\mathcal{C}^{(0)} = 0 \,\forall |m_0| < |m_{thre}|$, below which the entanglement between spins N and $N+3$ is lost in the ness. The value α^* above which the threshold value $|m_{thre}|$ does not exist is given by the solution of the equation $\mathcal{C}^{(0)}(m_0 = 0, \alpha^*) = 0$, leading to

$$\alpha^* = \sqrt{2} - 1. \tag{5.161}$$

We have checked numerically that the parameter α is a monotonically increasing function of the coupling γ. There is, as a consequence, only one value γ^* leading to α^*, and we find $\gamma^* = 0.5916$. For $\gamma < \gamma^*$, the threshold value $|m_{thre}|$ is found by solving the equation $\mathcal{C}^{(0)}(m_0, \alpha) = 0$, and we find

$$|m_{thre}| = \frac{\sqrt{\alpha^2 - 2\alpha\sqrt{2} + 1}}{1-\alpha}, \quad \gamma < \gamma^*. \tag{5.162}$$

We plot in figure 5.19 the concurrence for $p = 0, 1, 2$ computed numerically as a function of the initial magnetization for two different values of γ, together with equation (5.160).

First, we can see that the behavior of the pairs with $p = 1$ and $p = 2$ is similar to the behavior of the first pair, the concurrence being maximal for $|m_0| = 1$ and decreases with the initial magnetization. Secondly, the theoretical prediction (5.160) of the concurrence in the first pair as a function of the initial magnetization fits pretty well the numerical data, validating the hypothesis made above. In the case $\gamma = 2$, corresponding to the situation $\gamma > \gamma^*$, one can check that the threshold value $|m_{thre}|$ does not exist, and the first pair is entangled whatever the initial magnetization. In the case $\gamma = 0.5$, we extract numerically, by looking at the magnetization of the spin $i = N$, the value $\alpha = 0.324861586$, leading to a calculated value of the threshold magnetization $|m_{thre}| = 0.639978$. This value is in relatively good agreement with the value found numerically $m_{thre} = 0.643250$.

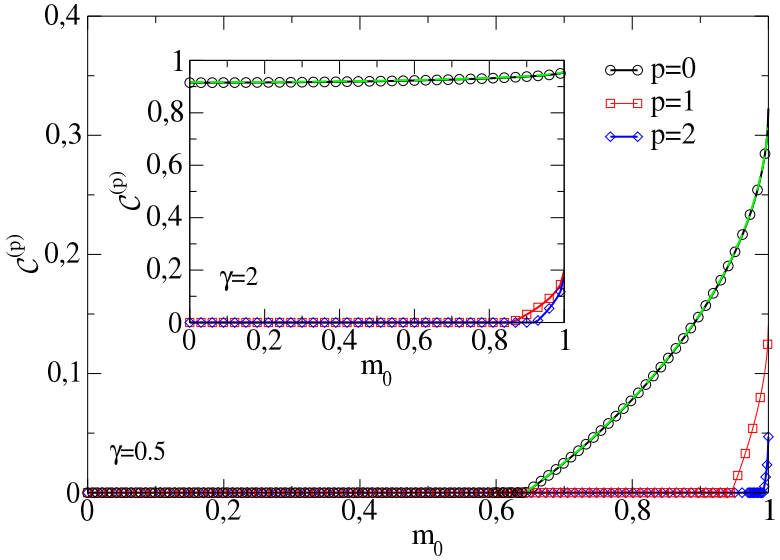

Figure 5.19 – *Cross concurrence for $p = 0, 1, 2$ as a function of the initial magnetization obtained numerically (dots), and equation (5.160) (dashed line). The coupling γ is set to $\gamma = 0.5$ in the main graph and to $\gamma = 2$ in the insert. In the case $\gamma = 0.5$, the extracted value of α is $\alpha = 0.324861586$.*

5.4.3 Steady state

We now consider the long times $t \gg N$, and we derive what is the steady state of the finite size system. For $t > 2N$, the excitations injected by the interaction are traveling forward and backward along the two chains. This will have for effect to destroy the correlation between spins belonging to the same chain, and increase entanglement between spins facing each others.
Let's introduce the matrices N_k and J_k $(k = N, B)$ such that the correlation matrices G_k becomes

$$G_k = N_k + iJ_k, \quad k = S, B, \tag{5.163}$$

with $N_k^T = N_k$ and $J_k^T = -J_k$. The local density of fermions is given by the diagonal of the N_S matrix, whereas the particles current is included in the J_S one. Plugging this decomposition into the evolution equation, one get two coupled equations governing the dynamics of the N_S and J_S matrices

$$\partial_t J_S + [A, N_S] + \frac{1}{2}\{\Theta\Theta^\dagger, J_S\} = \Theta J_B \Theta^\dagger = 0, \tag{5.164}$$

$$\partial_t N_S - [A, J_S] + \frac{1}{2}\{\Theta\Theta^\dagger, N_S\} = \Theta N_B \Theta^\dagger. \tag{5.165}$$

Since the system does not evolve any more in the steady state, we can set the time derivatives in the previous equations to zero. Moreover, in the steady state, the J_S matrix vanishes as well, since it represents current-like of the form $\langle ic_n^\dagger c_m - ic_m^\dagger c_n \rangle$. Plugging these assumptions into equations (5.164) and (5.165), one arrives to

$$[T_S, N_S^*] = 0, \tag{5.166}$$

$$\{\Theta^\dagger\Theta, N_S^*\} = 2\Theta N_B^* \Theta^\dagger, \tag{5.167}$$

where the star indicates steady state value.
For latter convenience, we reorganize the row vector $\mathbf{\Psi}^\dagger$ like

$$\mathbf{\Psi}^\dagger = (\tilde{\boldsymbol{c}}_S^\dagger, \boldsymbol{c}_B^\dagger) = (c_N^\dagger, c_{N+3}^\dagger, c_{N-1}^\dagger, c_{N+4}^\dagger, \ldots, c_1^\dagger, c_{2N+2}^\dagger, c_{N+1}^\dagger, c_{N+2}^\dagger) \tag{5.168}$$

such that the Θ matrix has now the structure $(\Theta)_{ij} = \gamma^2 \delta_{ij}(\delta_{i1} + \delta_{i2})$, and

$$\Theta N_B \Theta^\dagger = \gamma^2 \left(\begin{array}{c|c} N_B & 0 \\ \hline 0 & 0 \end{array}\right), \quad \Theta\Theta^\dagger = \gamma^2 \left(\begin{array}{c|c} \mathbb{1}_{2\times 2} & 0 \\ \hline 0 & 0 \end{array}\right). \tag{5.169}$$

Explicitly, the equation (5.167) is

$$\left(\begin{array}{cc|ccc} 2(N_S)_{11} & 2(N_S)_{12} & (N_S)_{13} & \ldots & (N_S)_{1,2N} \\ 2(N_S)_{12} & 2(N_S)_{12} & (N_S)_{23} & \ldots & (N_S)_{2,2N} \\ \hline (N_S)_{13} & (N_S)_{23} & & & \\ \vdots & \vdots & & 0 & \\ \vdots & \vdots & & & \\ (N_S)_{1,2N} & (N_S)_{2,2N} & & & \end{array}\right) = 2 \left(\begin{array}{c|c} N_B & 0 \\ \hline 0 & 0 \end{array}\right). \tag{5.170}$$

This last result is interesting, we find that the reduced fermionic correlation matrix associated to the two sites directly in contact with the environment is equal, in the steady state, to the fermionic correlation matrix N_B of each pair forming the bath. Moreover, these two sites are completely decorrelated from the rest of the system.

Now, let's have a look on equation (5.166). With the new ordering, the matrix T_S takes now the form

$$T_S = \begin{pmatrix} h & 0 & -J & & & & & \\ 0 & h & \ddots & \ddots & & & & \\ -J & \ddots & \ddots & \ddots & \ddots & & & \\ & \ddots & \ddots & \ddots & \ddots & \ddots & & \\ & & \ddots & \ddots & \ddots & \ddots & \ddots & \\ & & & \ddots & \ddots & \ddots & \ddots & -J \\ & & & & \ddots & \ddots & \ddots & 0 \\ & & & & & -J & 0 & h \end{pmatrix} = h\mathbb{1}_{2N\times 2N} - J\Delta, \tag{5.171}$$

where Δ is the matrix

$$\Delta = \begin{pmatrix} 0 & 0 & 1 & & & \\ 0 & 0 & \ddots & 1 & & \\ 1 & \ddots & \ddots & \ddots & \ddots & \\ & 1 & \ddots & \ddots & \ddots & \ddots \\ & & \ddots & \ddots & \ddots & \ddots & \ddots \end{pmatrix} = \begin{pmatrix} 0 & \mathbb{1}_{2\times 2} & & \\ \mathbb{1}_{2\times 2} & \ddots & \ddots & \\ & \ddots & \ddots & \ddots \end{pmatrix} \tag{5.172}$$
$$= \kappa \otimes \mathbb{1}_{2\times 2}$$

with $(\kappa)_{ij} = \delta_{j,i+1} + \delta_{j,i-1}$. This leads to

$$-J[\Delta, N_S^*] = -J[\kappa \otimes \mathbb{1}_{2\times 2}, N_S^*] = 0. \tag{5.173}$$

The previous result concerning the sites in contact with the bath, together with the toy model bring us to put the ansatz

$$N_S^* = \left(\begin{array}{c|c|c|c} N_B & & & \\ \hline & N_B & & \\ \hline & & \ddots & \\ \hline & & & N_B \end{array}\right) = \mathbb{1}_{N\times N} \otimes N_B. \tag{5.174}$$

Calculating the commutator of the Δ matrix with the previous ansatz, one finds

$$[\Delta, N_S^*] = -J[\kappa \otimes \mathbb{1}, \mathbb{1} \otimes N_B] = 0. \tag{5.175}$$

The ansatz satisfies the equation (5.167). The steady state of the system being unique [PPcv08, Proo8, KP09], this expression is then the correct solution. The fermionic representation of the steady state of the system is then characterized in the following way: the reduced fermionic correlation matrix associated to each pair of sites facing each other is equal to the fermionic correlation matrix of the copies of the environment. Moreover, all these pairs are completely decorrelated from each other.

The fermionic representation of the steady state is now known. But to know the state of each pair p, one need to determined what are the associated spin-spin correlation function. One can show that, in the steady state, one has

$$\langle \sigma^x_{N-p} \sigma^x_{N+3+p} \rangle^* = \langle \sigma^y_{N-p} \sigma^y_{N+3+p} \rangle^* = (-1)^{p+1}. \tag{5.176}$$

The demonstration of the last equality for $\langle \sigma^x_{N-p} \sigma^x_{N+3+p} \rangle^*$ is presented in appendix C. One can note that the value of these correlators depends of the considered pair of spins. In the same way, we have

$$\langle \sigma^x_{N-p} \sigma^y_{N+3+p} \rangle^* = \langle \sigma^y_{N-p} \sigma^x_{N+3+p} \rangle^* = 0, \quad \langle \sigma^z_{N-p} \sigma^z_{N+3+p} \rangle^* = -1 \tag{5.177}$$

whatever the pair into consideration. We plot on figure 5.20 the correlation functions $\langle \sigma^x_{N-p} \sigma^x_{N+3+p} \rangle^*$ (left) and $\langle \sigma^z_{N-p} \sigma^z_{N+3+p} \rangle^*$ (right) as a function of time for two chains of $N = 5$ spins obtained numerically.

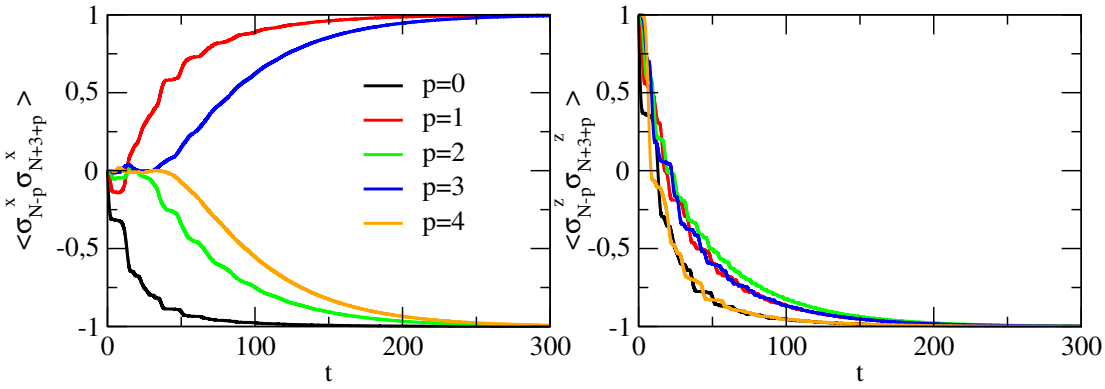

Figure 5.20 – *Time evolution of the $\langle \sigma^x_{N-p}\sigma^x_{N+3+p}\rangle$ (left) and $\langle \sigma^z_{N-p}\sigma^z_{N+3+p}\rangle$ (right) correlators for a system composed of two chains of $N = 5$ spins. The coupling parameters is fixed to $\gamma = 0.5$.*

One can check that the sign of the steady state value of the correlator in the x direction depends of the considered pairs, whereas, in the z direction, the correlator goes to the value -1 whatever the value of p.

We are now in position to write the steady state of the system, and in particular the reduced density matrix of one pair p. We obtain

$$\rho^*_p = \frac{1}{2}\begin{pmatrix} 0 & 0 & 0 & 0 \\ 0 & 1 & (-1)^{p+1} & 0 \\ 0 & (-1)^{p+1} & 1 & 0 \\ 0 & 0 & 0 & 0 \end{pmatrix}, \tag{5.178}$$

whereas the density matrix of one spin $i = N - p$ together with any spin $j \neq N+3+p$ is given by the (separable) thermal state

$$\rho^*_{ij} = \frac{1}{4}\begin{pmatrix} 1 & 0 & 0 & 0 \\ 0 & 1 & 0 & 0 \\ 0 & 0 & 1 & 0 \\ 0 & 0 & 0 & 1 \end{pmatrix}. \tag{5.179}$$

In the steady state, the system is then characterized by an alternation of pairs p of spins in the two states

$$\begin{aligned} |\psi^-\rangle &= \frac{1}{\sqrt{2}}(|\uparrow\downarrow\rangle - |\downarrow\uparrow\rangle) \quad \text{for } p \text{ even}, \\ |\psi^+\rangle &= \frac{1}{\sqrt{2}}(|\uparrow\downarrow\rangle + |\downarrow\uparrow\rangle) \quad \text{for } p \text{ odd}, \end{aligned}$$

these pairs being completely decorrelated from each others. Note that the state $|\psi^+\rangle$ is exactly the state of the copies of the environment. Nevertheless, these two states are two Bell states and are, as a consequence maximally entangled. The steady state value of the concurrence is equal to $\mathcal{C}^{(p)} = 1$ whatever the value of p. The full stationary state of the system can then be written like

$$\rho^*_S = (\rho^-)^{\otimes q} \otimes (\rho^+)^{\otimes N-q}, \tag{5.180}$$

where $\rho^{\pm} = |\psi^{\pm}\rangle\langle\psi^{\pm}|$ and $q = N/2$ if N is odd and $q = (N+1)/2$ if N is even. This steady state is independent of the system size, the initial magnetization of the two chains or the value of the different couplings, and is only driven by the state of the environment. Indeed, the entanglement present initially in the copies is replicated and transferred through the double array. A pictural representation of the steady state is presented on figure 5.21.

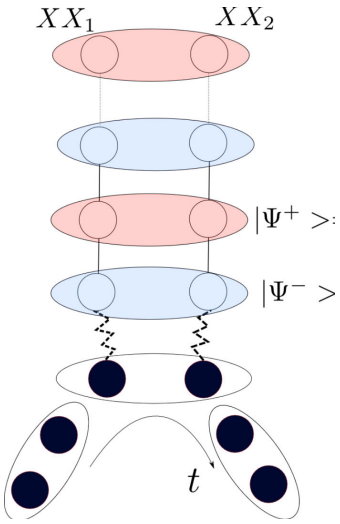

Figure 5.21 – *Pictural representation of the steady state of the system (here, N is chosen to be even). The red pairs are in the state $|\Psi^+\rangle$ whereas the blue ones are in the state $|\Psi^-\rangle$.*

We show on the left panel of figure 5.22 the evolution of the concurrence obtained numerically as a function of the time and the position for two chains with $N = 10$ spins. The right panels shows the time evolution of the concurrence for $p = 0$ to $p = 4$ for two chains with $N = 5$ spins.

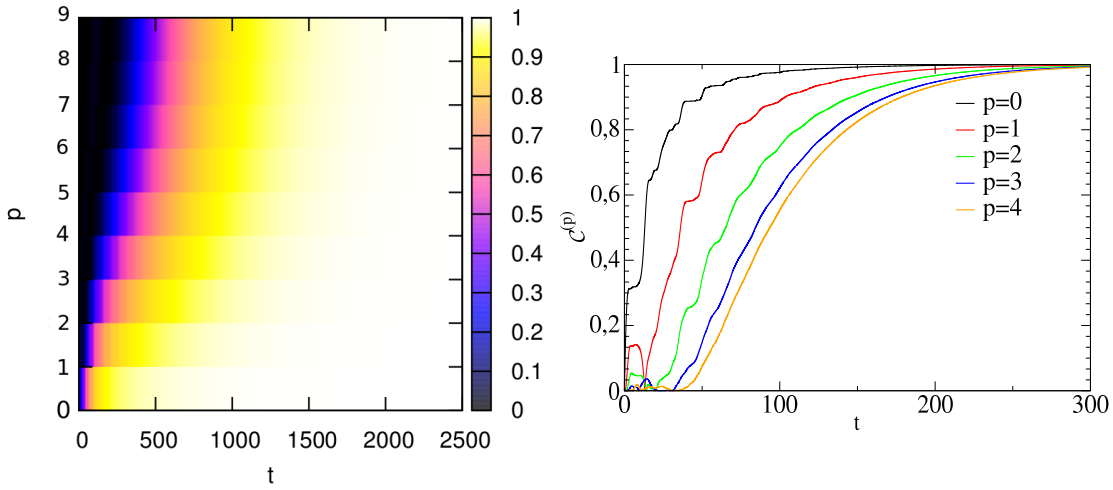

Figure 5.22 – *Left: Snapshot of the concurrence as a function of time and the pair considered for a system with $N = 10$. Right: Time evolution of the concurrence for $p = 0$ to $p = 4$ for a system with $N = 5$. In both plots, we set $m_0 = 1$ and $\gamma = 0.5$.*

In both plots, we can see that the concurrence corresponding to a pair p converges

asymptotically to the value $\mathcal{C}_p = 1$, indicating maximal entanglement between spins facing each others.

5.4.4 Convergence toward the steady state

Here we study the relaxation of the system toward the steady state. We start by focusing on the transverse magnetization m and pair concurrence $\mathcal{C}^{(p)}$. We plot on figure 5.23 the transverse magnetization on the first chain (left) and the pair concurrence (right) profiles, obtained numerically, for times $t > 2000$ for two chains of $N = 10$ spins and an initial magnetization of $m_0 = 1$.

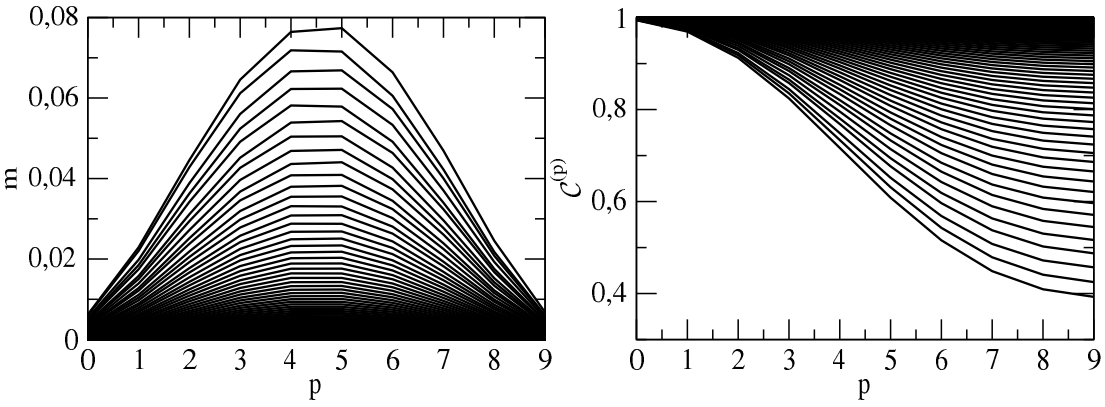

Figure 5.23 – *Transverse magnetization (left) and pair concurrence (right) profiles for times $t > 2000$ for $N = 10$ and an initial magnetization equal to $m_0 = 1$. The γ parameters is set to $\gamma = 0.5$. All the curves correspond to times $t_n = 2000 + 20n$.*

We can see that, as expected by the analysis of the previous section, the magnetization profile converges into a flat magnetization driven by the state of the bath $m(p) = m_B = 0$. Note that the value of the magnetization is smaller at the two edges of the chains than in the bulk. One can also check that the pair concurrence converges asymptotically to the value $\mathcal{C}^{(p)} = 1$. Contrary to the magnetization, the maximum value of the concurrence is found in the interaction point.

As we mentioned previously, the steady state is independent of the size or the initial state of the system. However, the relaxation toward the stationary state depends on these parameters. To study this dependance, we will use a global quantity which does not depend on the position in the chains. We define then the total cross concurrence by

$$\mathcal{C}^{tot}(t) = \sum_{p=0}^{N-1} \mathcal{C}^{(p)}(t), \tag{5.181}$$

and study its evolution toward the steady state. Initially, because all the pairs p are disentangled, the total concurrence must be equal to $\mathcal{C}^{tot} = 0$, whereas in the steady state, because all the pairs p are maximally entangled, the total concurrence is $\mathcal{C}^{tot} = N$. The two spins case treated in section 5.3 brings us to make the hypothesis that, for long times, the relaxation is exponential

$$\mathcal{C}^{tot}(t) = N\left(1 - \phi(m_0)e^{-t/T}\right), \tag{5.182}$$

where $\phi(m_0)$ is a function depending only on the initial magnetization, and T is a characteristic relaxation time depending on the coupling parameters. We plot on figure 5.24 $1 - \mathcal{C}^{(p)}/N$ extracted numerically as a function of time for different initial magnetizations. One can check that the relaxation is well exponential with a charac-

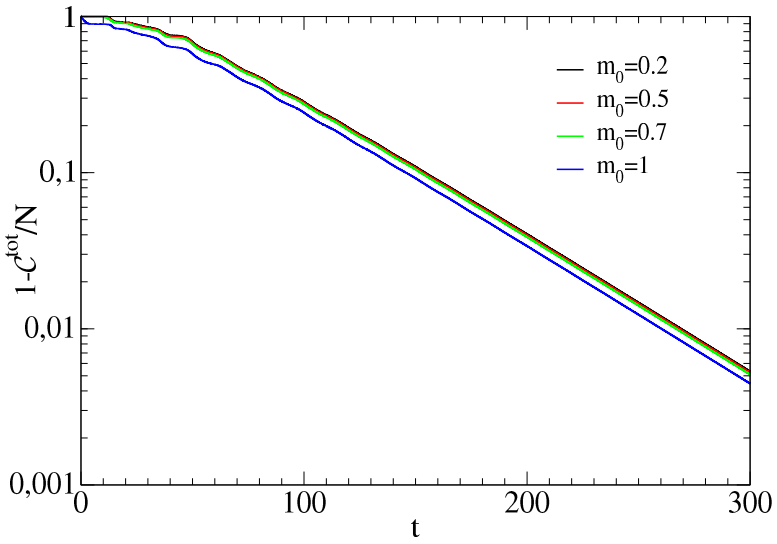

Figure 5.24 – *Relaxation of the total concurrence toward the maximal value as a function of time in semi logarithmic scale for different initial magnetization of the chains.*

teristic relaxation time independent on the initial magnetization. A numerical fit of the relaxation of the total concurrence allows us to have access to the function $\phi(m_0)$. The results are presented on figure 5.25

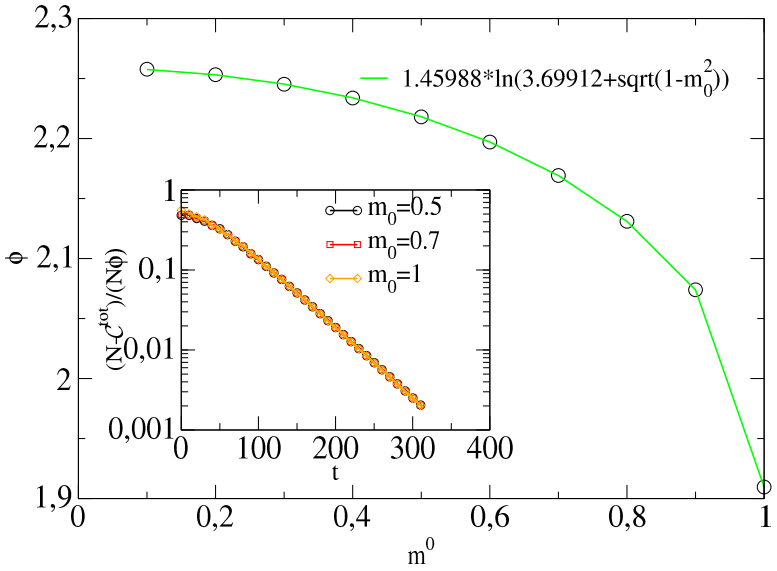

Figure 5.25 – *Function $\phi(m_0)$ characterizing the dependance of the relaxation on the initial magnetization. On the insert is shown $(N - \mathcal{C}^{tot})/(N\phi)$ as a function of time for different initial magnetizations.*

We find a magnetization dependance of the relaxation of the form

$$\phi(m_0) = 1.45988 \ln\left(3.69912 + \sqrt{1-(m_0)^2}\right). \tag{5.183}$$

We show on the insert of figure 5.25 $(N - \mathcal{C}^{tot})/(N\phi(m_0))$ as a function of time for different initial magnetizations. The curves perfectly collapse validating the form of the ϕ function.

5.5 Conclusion

In this chapter, we analyzed the entanglement dynamics of a open quantum system coupled to a bath by means of the repeated interactions process. We studied in a first time a simple system composed by two single spins, and we found that its fermionic correlators relaxed exponentially to steady state values fixed by the bath properties. The concurrence measured between the two system's spins reaches asymptotically its maximal value, reflecting the final Bell state and the entanglement transfer from the bath to the system.
After that, we moved to the general case where the system is now composed by two arrays of spins with XX interaction coupled at one edge to the bath. We identified two physical time regimes: the times of the order of the size of the chain $t \sim N$, and the times much larger than N. In the first regime, the state of the spins close to the interaction points is well described by a non-equilibrium-steady-state (ness) with stationary current traveling along the chains. We described numerically the scaling behavior of observables like local magnetization, current or longitudinal entanglement, and we found a decay of the cross concurrence with respect to the interaction point with a typical entanglement length. Finally, in the long times regime $t \gg N$, the current vanishes and the state of the system is a scale-free product of Bell states maximalising the cross entanglement.
If we have considered in this study two identical chains, an interesting continuation of this work could consist into the introduction of inhomogeneities in the system, like different intra-chain coupling, or different size of the two chains. This will lead to a dephasing in the quasi-particles movement, and to a modification of the observed behaviors.

Conclusion

In this thesis, we have investigated the behavior of one-dimensional quantum systems driven out-of-equilibrium, and more particularly, their entanglement dynamics. Indeed, understanding such a dynamics is of primary importance in quantum information processing or condensed matter theory. The dynamics of these systems, exhibiting very rich behaviors, has been assessed both analytically and numerically using exact diagonalization.

After having presented in the first chapter the theoretical and mathematical framework of this work, we moved, in the four next chapters, to our main results.
The first model we studied consisted in a bosonic cloud loaded in an one-dimensional optical lattice and described by the Bose-Hubbard Hamiltonian. This system is driven out-of-equilibrium by the sudden quench of its confining potential. In the infinite bosonic repulsion limit, we developed a hydrodynamical theory based on a local equilibrium hypothesis which perfectly reproduced the numerically observed dynamics.
We considered two different kinds of quench, namely the sudden release of the trap, and the sudden release of the trap and the loading of a linear potential. For this last protocol, we have identified different oscillations regimes of the trapped particle density, depending on the initial state and on the linear force F. Each of these regimes has been explained thanks to the aforementioned hydrodynamics theory. In addition, we have also studied the associated current dynamics, as well as the entanglement entropy between trapped and ejected particles.
The next three chapters are devoted to the dynamics of open quantum systems. In the first of these chapters, we analyzed the dynamics of two initially separable defect spins locally coupled to an environment modeled by a spin chain with Ising interaction. This environment has been mapped into an interacting harmonic bath thanks to the Holstein-Primakoff transformation. After the introduction of symmetric and antisymmetric variables for both the environment and defect spins descriptions, together with a degenerate spins approximation, we were able to write down the time evolution of the reduced density matrix, allowing us to have access to the concurrence. We considered the cases of vanishing and non-vanishing distance between the defect spins. We found in both cases that the entanglement performs oscillations with period and maxima highly dependent on the parameters of the system.
After that, we focused our attention to the decoherence and disentanglement dynamics of two spins, prepared in a Bell state, locally coupled to an Ising chain. In addition to this coupling, a sudden quench in the transverse field of the environment has been realized. We have shown that the concurrence can be related to the evolution of the Loschmidt echo, itself expressed in terms of the evolution of the fermionic correlation matrix, which has been computed numerically by exact diagonalization. After having identified two different coupling regimes, we have compared our results to

the equilibrium situation already treated in the literature [CPo8b]. We found that the quench situation is always unfavorable for the spins, in the sense that it increases and speeds-up the disentanglement dynamics. This dynamics has been studied in short times, and times of the order of the length of the chain. In the first limit, the echo is Gaussian and independent on the quench, whereas it exhibits revivals in the other limit. These revivals occur at times twice shorter than in the equilibrium case, reflecting the fact that all sites are excitations emitters when a global quench is performed. In all these studies, we also pointed out the role of an initial critical environment. In particular, we showed that the derivative of the echo with respect to the initial field at a given time exhibits a logarithmic divergence close to the critical point $h_i = 1$. Moreover, we found thanks to finite size scaling analysis, that the position of the peak behaves as a power law of the size of the chain, whereas its position behaves logarithmically with N.

Finally, we have analyzed in the last chapter the dynamics of an open quantum system coupled to an environment by means of the repeated interactions process. We first reminded in details the description of this kind of interactions [Plao8], where we showed in particular that, if the initial state is Gaussian and if the Hamiltonians are quadratics in terms of fermionic operators, the system can be described by the evolution of the fermionic correlation matrix.

We have in a first part considered a toy model where the system is only composed of two spins 1/2. Despite its apparent simplicity, this model is exactly solvable and the concurrence can be found analytically as a function of the parameters like initial magnetization and coupling constant. For asymptotic times, the system converges into a steady state with maximal entanglement. Afterward, we moved to a more general case where two arrays of spins are substituted to the two single spins. We analyzed the dynamics into two different time scales: the times shorter than the length of the arrays, and times much larger than N. This first time scale reproduces the behavior of a semi-infinite system on the sites close to the interaction point. In this limit, the state is well described by a non-equilibrium steady-state characterized by a stationary current traveling along the chains. We also evaluated numerically the relaxation of observables like magnetization, correlations, and two kinds of entanglement: the longitudinal and the cross ones. We pointed-out the scaling behavior of magnetization, current and longitudinal concurrence. Concerning the cross concurrence, we found an exponential decay with respect to the distance to the interaction point with a typical entanglement length. Finally, for long times, the system reaches a size-independent equilibrium steady state with a vanishing current. In this steady state, the concurrence between spins facing each other is maximal, indicating a perfect replication of bath entanglement.

Time evolution of the reduced density matrix

A

In this first appendix, we derive the formula of the time evolution of the reduced density matrix used in chapter 3 . We remind that the total Hamiltonian is $\widetilde{H} = \widetilde{H}^S + \widetilde{H}^A$ with

$$\widetilde{H}^S = \frac{1}{2}(\widetilde{\mathbf{p}}^S)^2 + \frac{1}{2}(\widetilde{\mathbf{x}}^S)^T D^S \widetilde{\mathbf{x}}^S - S_x^S (\widetilde{\gamma}^S)^T \widetilde{\mathbf{x}}^S, \tag{A.1}$$

$$\widetilde{H}^A = \frac{1}{2}(\widetilde{\mathbf{p}}^A)^2 + \frac{1}{2}(\widetilde{\mathbf{x}}^A)^T D^A \widetilde{\mathbf{x}}^A - S_x^A (\widetilde{\gamma}^A)^T \widetilde{\mathbf{x}}^A, \tag{A.2}$$

where the $S(A)$ subscript holds for the center-of-mass (relative) coordinates, and where we consider degenerate spins, such that the Zeeman term in the total Hamiltonian vanishes.

The first step for the derivation is to go into the interaction picture with respect to the bath degrees of freedom. Using the commutation relations

$$[\widetilde{H}_i^S, \widetilde{H}_b^A] = [\widetilde{H}_i^A, \widetilde{H}_b^S] = 0,$$

we can write

$$\begin{aligned} \widetilde{H}^{(I)} =& e^{i(\widetilde{H}_b^S + \widetilde{H}_b^A)t} (\widetilde{H}_i^S + H_i^A) e^{-i(\widetilde{H}_b^S + \widetilde{H}_b^A)t} \\ =& e^{i\widetilde{H}_b^S t} \widetilde{H}_i^S e^{-i\widetilde{H}_b^S t} + e^{i\widetilde{H}_b^A t} \widetilde{H}_i^A e^{-i\widetilde{H}_b^A t}. \end{aligned} \tag{A.3}$$

This expression can be evaluated using the formula [Wil67]

$$e^{\alpha \hat{X}} \hat{Y} e^{-\alpha \hat{X}} = \sum_{\nu=0}^{\infty} \frac{\alpha^\nu}{\nu!} \{\hat{X}^\nu, \hat{Y}\}, \tag{A.4}$$

where

$$\begin{aligned} \{\hat{X}^0, \hat{Y}\} =& \hat{Y}, \\ \{\hat{X}^1, \hat{Y}\} =& [\hat{X}, \hat{Y}], \\ \{\hat{X}^2, \hat{Y}\} =& [\hat{X}, [\hat{X}, \hat{Y}]], \end{aligned} \tag{A.5}$$

and so on. For the Hamiltonian (A.2), one gets for the four first terms

$$\begin{aligned}
&\nu = 0 : I_0 = \widetilde{H}_i = \sum_i \left(\widetilde{\gamma}_i^S S_x^S \widetilde{x}_i^S + \widetilde{\gamma}_i^A S_x^A \widetilde{x}_i^A \right), \\
&\nu = 1 : I_1 = [\widetilde{H}_b^S, \widetilde{H}_i^S] + [\widetilde{H}_b^A, \widetilde{H}_i^A] = -i \sum_i \left(\widetilde{\gamma}_i^S S_x^S \widetilde{p}_i^S + \widetilde{\gamma}_i^A S_x^A \widetilde{p}_i^A \right), \\
&\nu = 2 : I_2 = [\widetilde{H}_b^S, I_1] + [\widetilde{H}_b^A, I_1] = \sum_i \left(\widetilde{\gamma}_i^S (\widetilde{\omega}_i^S)^2 S_x^S \widetilde{x}_i^S + \widetilde{\gamma}_i^A (\widetilde{\omega}_i^A)^2 S_x^A \widetilde{x}_i^A \right), \\
&\nu = 3 : I_3 = [\widetilde{H}_b^S, I_2] + [\widetilde{H}_b^A, I_2] = -i \sum_i \left(\widetilde{\gamma}_i^S (\widetilde{\omega}_i^S)^2 S_x^S \widetilde{p}_i^S + \widetilde{\gamma}_i^A (\widetilde{\omega}_i^A)^2 S_x^A \widetilde{p}_i^A \right). \qquad \text{(A.6)}
\end{aligned}$$

We see a recursive expression that can be put in the form

$$\begin{aligned}
\widetilde{H}^{(I)} &= \sum_i \Bigg(\sum_{\nu=0}^{\infty} \left[\frac{(it)^\nu}{(2\nu)!} (\widetilde{\omega}_i^S)^{2\nu} \widetilde{\gamma}_i^S S_x^S \widetilde{x}_i^S + \frac{(it)^\nu}{(2\nu)!} (\widetilde{\omega}_i^A)^{2\nu} \widetilde{\gamma}_i^A S_x^A \widetilde{x}_i^A \right] \qquad \text{(A.7)} \\
&+ \left[\frac{(it)^{2\nu+1}}{(2\nu+1)!} (-i) \frac{(\widetilde{\omega}_i^S)^{2\nu+1}}{\widetilde{\omega}_i^S} \widetilde{\gamma}_i^S S_x^S \widetilde{x}_i^S + \frac{(it)^{2\nu+1}}{(2\nu+1)!} (-i) \frac{(\widetilde{\omega}_i^A)^{2\nu+1}}{\widetilde{\omega}_i^A} \widetilde{\gamma}_i^A S_x^A \widetilde{x}_i^A \right] \Bigg) \\
&= \sum_i \left(\widetilde{\gamma}_i^S \cos(\widetilde{\omega}_i^S t) S_x^S \widetilde{x}_i^S + \widetilde{\gamma}_i^A \cos(\widetilde{\omega}_i^A t) S_x^A \widetilde{x}_i^A + \frac{\widetilde{\gamma}_i^S}{\widetilde{\omega}_i^S} \sin(\widetilde{\omega}_i^S t) S_x^S \widetilde{p}_i^S + \frac{\widetilde{\gamma}_i^A}{\widetilde{\omega}_i^A} \sin(\widetilde{\omega}_i^A t) S_x^A \widetilde{p}_i^A \right).
\end{aligned}$$

Neglecting the free Hamiltonian $\widetilde{H}_d$ allows us to write the full time evolution operator as the product of evolution operators associated to the center-of-mass and relative coordinates, $\widetilde{U}(t) = \widetilde{U}^S(t)\widetilde{U}^A(t)$. These two operators $\widetilde{U}^{S(A)}(t)$ can be obtained with the ansatz

$$\widetilde{U}^{S(A)}(t) = \exp\left(i \sum_i \delta_i^{S(A)}(t) \right) \exp\left(i \sum_i (\phi_i^{S(A)}(t) \widetilde{p}_i^{S(A)} + \theta_i^{S(A)}(t) \widetilde{x}_i^{S(A)}) \right), \qquad \text{(A.8)}$$

where $\delta^{S(A)}(t), \phi^{S(A)}(t)$ and $\theta^{S(A)}(t)$ are functions to be specified. Let's now take the differentiate of $\widetilde{U}(t)$ with respect to time. We obtain

$$\begin{aligned}
\dot{\widetilde{U}} &= i \sum_i \left(\dot{\delta}_i^S + \dot{\phi}_i^S \widetilde{p}_i^S - \frac{1}{2} \frac{d}{dt} (\phi_i^S \theta_i^S) \right) \widetilde{U}^S \widetilde{U}^A + i \sum_i \left(\dot{\phi}_i^S \widetilde{x}_i^S + \dot{\theta}_i^S \phi_i^S \right) \widetilde{U}^S \widetilde{U}^A \\
&+ i \sum_i \left(\dot{\delta}_i^A + \dot{\phi}_i^A \widetilde{p}_i^A - \frac{1}{2} \frac{d}{dt} (\phi_i^A \theta_i^A) \right) \widetilde{U}^S \widetilde{U}^A + i \sum_i \left(\dot{\phi}_i^A \widetilde{x}_i^A + \dot{\theta}_i^A \phi_i^A \right) \widetilde{U}^S \widetilde{U}^A, \qquad \text{(A.9)}
\end{aligned}$$

where we have used

$$\exp\left(i \sum_i \phi_i \widetilde{p}_i^{S(A)} \right) \widetilde{x}_i^{S(A)} \exp\left(-i \sum_i \phi_i \widetilde{p}_i^{S(A)} \right) = \sum_i \left(x_i^{S(A)} + \phi_i^{S(A)} \right) \qquad \text{(A.10)}$$

and where we have dropped the explicit time dependence. The evolution operator $\widetilde{U}(t)$ fulfills the Shrödinger equation

$$\frac{d\widetilde{U}}{dt} = -i \widetilde{H}^{(I)}(t) \widetilde{U}(t), \qquad \text{(A.11)}$$

equation that will be used in order to find the functions $\delta^{S(A)}(t), \phi^{S(A)}(t)$ and $\theta^{S(A)}(t)$. By identification of eq.(A.9) with eq.(A.11), we obtain six differential equations

$$\begin{aligned}
\sum_i \dot{\theta}_i^{S(A)}(t) &= -\sum_i \widetilde{\gamma}_i^{S(A)} \cos(\widetilde{\omega}_i^{S(A)} t) S_x^{S(A)}, \\
\sum_i \dot{\phi}_i^{S(A)}(t) &= -\sum_i \frac{\widetilde{\gamma}_i^{S(A)}}{\widetilde{\omega}_i^{S(A)}} \sin(\widetilde{\omega}_i^{S(A)} t) S_x^{S(A)}, \\
\sum_i \dot{\delta}_i^{S(A)}(t) &= -\sum_i \dot{\theta}_i^{S(A)}(t) + \frac{1}{2}\sum_i \frac{d}{dt}\left(\dot{\phi}^{S(A)}(t)\phi_i^{S(A)}(t)\right),
\end{aligned} \tag{A.12}$$

which can be solved using the initial condition $\widetilde{U}(0) = \mathbb{1}$. We find

$$\begin{aligned}
\phi_i^{S(A)}(t) &= -\frac{\widetilde{\gamma}_i^{S(A)} S_x^{S(A)}}{\widetilde{\omega}_i^{S(A)}} \sin(\widetilde{\omega}_i^{S(A)} t) \\
\theta_i^{S(A)}(t) &= -\frac{\widetilde{\gamma}_i^{S(A)} S_x^{S(A)}}{(\widetilde{\omega}_i^{S(A)})^2} (\cos(\widetilde{\omega}_i^{S(A)} t) - 1) \\
\delta_i^{S(A)}(t) &= \frac{(\widetilde{\gamma}_i^{S(A)})^2 (S_x^{S(A)})^2}{(\widetilde{\omega}_i^{S(A)})^2} \left(t - \frac{\sin(\widetilde{\omega}_i^{S(A)} t)}{\widetilde{\omega}_i^{S(A)}} \right).
\end{aligned} \tag{A.13}$$

The final expression for the evolution operators $U^{S(A)}(t)$ is then

$$\begin{aligned}
\widetilde{U}^{S(A)}(t) = \exp\left(i \sum_i \delta_i^{S(A)}(t) \right) \exp\Bigg[i \sum_i \Bigg(\frac{\widetilde{\gamma}_i^{S(A)}}{\widetilde{\omega}_i^{S(A)}} \left(\frac{1}{\widetilde{\omega}_i^{S(A)}} (\cos(\widetilde{\omega}_i^{S(A)} t) - 1 \right) S_x^{S(A)} \widetilde{p}_i^{S(A)} \\
- \sin(\widetilde{\omega}_i^{S(A)} t) S_x^{S(A)} \widetilde{x}_i^{S(A)} \Bigg) \Bigg].
\end{aligned} \tag{A.14}$$

This full time evolution operator $\widetilde{U}(t)$ can be seen as a displacement operator, responsible of the displacement of a quantum state in the phase space

$$\widetilde{U}(t) = e^{i \sum_i \left(\delta_i^S(t) + \delta_i^A(t) \right)} e^{i(\mathbf{Q}^S(S_x^S)\widetilde{\mathbf{x}}^S - \mathbf{R}^S(S_x^S)\widetilde{\mathbf{p}}^S)} e^{i(\mathbf{Q}^A(S_x^A)\widetilde{\mathbf{x}}^A - \mathbf{R}^A(S_x^A)\widetilde{\mathbf{p}}^A)}, \tag{A.15}$$

with

$$\begin{aligned}
\mathbf{Q}^{S(A)}(S_x^{S(A)}) &= -\sum_i \frac{\widetilde{\gamma}_i^{S(A)}}{\widetilde{\omega}_i^{S(A)}} \sin(\widetilde{\omega}_i^{S(A)} t) S_x^{S(A)} \mathbf{e}_i^{S(A)}, \\
\mathbf{R}^{S(A)}(S_x^{S(A)}) &= -\sum_i \frac{\widetilde{\gamma}_i^{S(A)}}{(\widetilde{\omega}_i^{S(A)})^2} (\cos(\widetilde{\omega}_i^{S(A)} t) - 1) S_x^{S(A)} \mathbf{e}_i^{S(A)}
\end{aligned} \tag{A.16}$$

and the $\mathbf{e}_j$ are unit vectors on the j-th direction.
We now turn to the computation of the time evolution of the reduced density matrix. It is formally given by

$$\rho_d(t) = Tr_b\{\widetilde{U}(t)(\rho_d(0) \otimes \rho_b(0))\widetilde{U}^\dagger(t)\}, \tag{A.17}$$

where we have assumed that the two spins are uncorrelated to the bath at the initial time. For the time evolution, we use the 4-dimensional common eigenbase $\{|s_i\rangle\}$ of the operators $S_x^{S(A)}$ fulfilling $S_x^{S(A)}|s_i\rangle = s_i^{S(A)}|s_i\rangle$ with $s_i^{S(A)} = 0, \pm 1$. In this base, the matrix elements of ρ_d at a time t are

$$\begin{aligned}
\langle s_i|\rho_d(t)|s_j\rangle = \mathrm{Tr}_b\Big\{ &\langle s_i| \exp\left(i\sum_i \delta_i^S\right) \exp\left(i(\boldsymbol{Q}^S(S_x^S)\widetilde{\boldsymbol{x}}^S - \boldsymbol{R}^S(S_x^S)\widetilde{\boldsymbol{p}}^S)\right) \exp\left(i\sum_i \delta_i^A\right) \\
&\times \exp\left(i(\boldsymbol{Q}^A(S_x^A)\widetilde{\boldsymbol{x}}^A - \boldsymbol{R}^A(S_x^A)\widetilde{\boldsymbol{p}}^A)\right) (\rho_b(0)\otimes\rho_d(0)) \exp\left(-i\sum_i \delta_i^S\right) \\
&\times \exp\left(-i(\boldsymbol{Q}^S(S_x^S)\widetilde{\boldsymbol{x}}^S - \boldsymbol{R}^S(S_x^S)\widetilde{\boldsymbol{p}}^S)\right) \exp\left(-i\sum_i \delta_i^A\right) \exp\left(i(\boldsymbol{Q}^A(S_x^A)\widetilde{\boldsymbol{x}}^A - \boldsymbol{R}^A(S_x^A)\widetilde{\boldsymbol{p}}^A)\right) |s_j\rangle\Big\} \\
= \exp&\left(i\left(\varphi^S((s_i^S)^2 - (s_j^S)^2) + \varphi^A((s_i^A)^2 - (s_j^A)^2)\right)\right) \langle s_i|\rho_d(0)|s_j\rangle \\
&\times \mathrm{Tr}_b\Big\{ \exp\left(i(\mathbf{Q}^S(s_i^S)\widetilde{\mathbf{x}}^S - \mathbf{R}^S(s_i^S)\widetilde{\mathbf{p}}^S)\right) \exp\left(i(\mathbf{Q}^A(s_i^A)\widetilde{\mathbf{x}}^A - \mathbf{R}^A(s_i^A)\widetilde{\mathbf{p}}^A)\right) \rho_b(0) \\
&\times \exp\left(-i(\mathbf{Q}^S(s_j^S)\widetilde{\mathbf{x}}^S - \mathbf{R}^S(s_j^S)\widetilde{\mathbf{p}}^S)\right) \exp\left(-i(\mathbf{Q}^A(s_j^A)\widetilde{\mathbf{x}}^A - \mathbf{R}^A(s_j^A)\widetilde{\mathbf{p}}^A)\right) \Big\} \\
= C \times \mathrm{Tr}_b\Big\{ &\rho_b(0) \exp\left(-i(\mathbf{Q}^S(s_j^S)\widetilde{\mathbf{x}}^S - \mathbf{R}^S(s_j^S)\widetilde{\mathbf{p}}^S)\right) \exp\left(i(\mathbf{Q}^S(s_i^S)\widetilde{\mathbf{x}}^S - \mathbf{R}^S(s_i^S)\widetilde{\mathbf{p}}^S)\right) \\
&\times \exp\left(-i(\mathbf{Q}^A(s_j^A)\widetilde{\mathbf{x}}^A - \mathbf{R}^A(s^A)\widetilde{\mathbf{p}}^A)\right) \exp\left(i(\mathbf{Q}^A(s_i^A)\widetilde{\mathbf{x}}^A - \mathbf{R}^A(s_i^A)\widetilde{\mathbf{p}}^A)\right) \Big\}, \qquad \text{(A.18)}
\end{aligned}$$

where we have used the cyclic permutation of the trace, and the fact that $\exp\left(i(\mathbf{Q}^S(s_i^S)\mathbf{x}^S - \mathbf{R}^S(s_i^S)\mathbf{p}^S)\right)$ and $\exp\left(-i(\mathbf{Q}^A(s_j^A)\mathbf{x}^A - \mathbf{R}^A(s_j^A)\mathbf{p}^A)\right)$ commute. Note that now $\mathbf{Q}^{S(A)}(s_i^{S(A)})$ and $\mathbf{R}^{S(A)}(s_i^{S(A)})$ are function of the eigenvalues $s_i^{S(A)}$ of the operators $S_x^{S(A)}$. The C number appearing in equation (A.18) is given by

$$C = \exp\left(i\left(\varphi^S(t)((s_i^S)^2 - (s_j^S)^2) + \varphi^A(t)((s_i^A)^2 - (s_j^A)^2)\right)\right) \langle s_i|\rho_d(0)|s_j\rangle, \qquad \text{(A.19)}$$

with

$$\varphi^{S(A)}(t) = \sum_i \frac{\left(\widetilde{\gamma}_i^{S(A)}\right)^2}{2\left(\widetilde{\omega}_i^{S(A)}\right)^2}\left(t - \frac{\sin\left(\widetilde{\omega}_i^{S(A)}t\right)}{\widetilde{\omega}_i^{S(A)}}\right). \qquad \text{(A.20)}$$

Sicne the baths are initially not correlated $\rho_b(0) = \rho_{b^S}\otimes\rho_{b^A}$, (A.18) reduces to

$$\begin{aligned}
\langle s_i|\rho_d(t)|s_j\rangle = &C \times \mathrm{Tr}_{b^S}\left\{\rho_b^S \exp\left(i(\mathbf{Q}^S(s_i^S - s_j^S)\widetilde{\mathbf{x}}^S - \mathbf{R}^S(s_i^S - s_j^S)\widetilde{\mathbf{p}}^S)\right)\right\} \\
&\times \mathrm{Tr}_{b^A}\left\{\rho_b^A \exp\left(i(\mathbf{Q}^A(s_i^A - s_j^A)\widetilde{\mathbf{x}}^A - \mathbf{R}^A(s_i^A - s_j^A)\widetilde{\mathbf{p}}^A)\right)\right\}, \qquad \text{(A.21)}
\end{aligned}$$

with

$$\mathbf{R}^{S(A)}(s_i^{S(A)} - s_j^{S(A)}) = -\sum_k \frac{\widetilde{\gamma}_k^{S(A)}}{(\widetilde{\omega}_k^{S(A)})^2}(\cos(\widetilde{\omega}_k^{S(A)}t) - 1))(s_i^{S(A)} - s_j^{S(A)})\mathbf{e}_k^{S(A)},$$
$$\mathbf{Q}^{S(A)}(s_i^{S(A)} - s_j^{S(A)}) = \sum_k \frac{\widetilde{\gamma}_k^{S(A)}}{\widetilde{\omega}_k^{S(A)}} \sin(\widetilde{\omega}_i^{S(A)}t)(s_i^{S(A)} - s_j^{S(A)})\mathbf{e}_k^{S(A)}. \tag{A.22}$$

We are then left with two thermal averages of displacement operators $D^{S(A)}(\chi^{S(A)})$ with $(\chi^{S(A)})^T = (\mathbf{R}^{S(A)}(s_i^{S(A)} - s_j^{S(A)}), \mathbf{Q}^{S(A)}(s_i^{S(A)} - s_j^{S(A)}))$. These traces can be evaluated using to the formula

$$\mathrm{Tr}\{\rho D(\chi)\} = \exp\left(-\frac{1}{2}\chi^T J^T \Sigma J \chi\right), \tag{A.23}$$

where

$$J = \begin{pmatrix} 0 & \mathbb{1} \\ -\mathbb{1} & 0 \end{pmatrix}, \tag{A.24}$$

and Σ is the covariance matrix of the bath

$$\Sigma = \begin{pmatrix} \sigma_{xx} & \sigma_{xp} \\ \sigma_{px} & \sigma_{pp} \end{pmatrix}, \tag{A.25}$$

where the blocks are defined by

$$\begin{aligned}(\sigma_{xx})_{ij} &= \langle \widetilde{x}_i \widetilde{x}_j \rangle - \langle \widetilde{x}_i \rangle \langle \widetilde{x}_j \rangle, \\ (\sigma_{pp})_{ij} &= \langle \widetilde{p}_i \widetilde{p}_j \rangle - \langle \widetilde{p}_i \rangle \langle \widetilde{p}_j \rangle, \\ (\sigma_{xp})_{ij} &= \langle \widetilde{x}_i \widetilde{p}_j \rangle - \langle \widetilde{x}_i \rangle \langle \widetilde{p}_j \rangle. \end{aligned} \tag{A.26}$$

Using the expression of the covariance matrix of a thermal bosonic bath [FKM65, KWLM12], we finally arrive at the expression

$$\begin{aligned}\langle s_i|\rho_d(t)|s_j\rangle = \exp\Big\{&-\left[f^S(t)(s_i^S - s_j^S)^2 + f^A(t)(s_i^A - s_j^A)^2\right] \\ &+ i\left[\varphi^S(t)((s_i^S)^2 - (s_j^S)^2) + \varphi^A(t)(s_i^A)^2 - (s_j^A)^2)\right]\Big\} \langle s_i|\rho_d(0)|s_j\rangle,\end{aligned} \tag{A.27}$$

with the two functions

$$f^{S(A)}(t) = \sum_i \frac{\left(\widetilde{\gamma}_i^{S(A)}\right)^2 (2\widetilde{n}_i^{S(A)} + 1)}{2\left(\widetilde{\omega}_i^{S(A)}\right)^3} \left(1 - \cos\left(\widetilde{\omega}_i^{S(A)}t\right)\right), \tag{A.28}$$

$$\varphi^{S(A)}(t) = \sum_i \frac{\left(\widetilde{\gamma}_i^{S(A)}\right)^2}{2\left(\widetilde{\omega}_i^{S(A)}\right)^2} \left(t - \frac{\sin\left(\widetilde{\omega}_i^{S(A)}t\right)}{\widetilde{\omega}_i^{S(A)}}\right), \tag{A.29}$$

where $\widetilde{n}_i^{S(A)} = \left(\exp\left(\widetilde{\omega}_i^{S(A)}/T\right) - 1\right)^{-1}$ is the thermal occupation of the bosonic mode i of the symmetric (antisymmetric) bath.

Gaussian character of the Bell state

B

In this appendix, we show that the density matrix associated to the Bell state $|\psi_B\rangle = \frac{1}{\sqrt{2}}(|\uparrow\downarrow\rangle + |\downarrow\uparrow\rangle)$ can be written as the low temperature limit of a thermal density matrix ρ_{th}, and is as a consequence Gaussian.

Consider the operator $\widetilde{H} = \frac{1}{2}\mathbb{1} - \frac{1}{4}\left(\sigma_2^x\sigma_3^x + \sigma_2^y\sigma_3^y\right)$. Its matricial representation in the base of the bath Hilbert space spanned by the vectors $\{|\uparrow\uparrow\rangle, |\uparrow\downarrow\rangle, |\downarrow\uparrow\rangle, |\downarrow\downarrow\rangle\}$ is

$$\widetilde{H} = \frac{1}{2}\begin{pmatrix} 1 & 0 & 0 & 0 \\ 0 & 1 & -1 & 0 \\ 0 & -1 & 1 & 0 \\ 0 & 0 & 0 & 1 \end{pmatrix}, \tag{B.1}$$

with eigenvectors

$$v_1 = \begin{pmatrix} 1 \\ 0 \\ 0 \\ 0 \end{pmatrix}, \quad v_2 = \begin{pmatrix} 0 \\ 0 \\ 0 \\ 1 \end{pmatrix}, \quad v_3 = \frac{1}{\sqrt{2}}\begin{pmatrix} 0 \\ 1 \\ 1 \\ 0 \end{pmatrix}, \quad v_4 = \frac{1}{\sqrt{2}}\begin{pmatrix} 0 \\ 1 \\ -1 \\ 0 \end{pmatrix}. \tag{B.2}$$

The thermal density matrix at inverse temperature β

$$\rho_{th} = \frac{1}{Z}e^{-\beta\widetilde{H}} \tag{B.3}$$

becomes then

$$\rho_{th} = \frac{1}{2e^{-\beta/2} + e^{-\beta} + 1}\begin{pmatrix} e^{-\beta/2} & 0 & 0 & 0 \\ 0 & \frac{1}{2}e^{-\beta} + \frac{1}{2} & -\frac{1}{2}e^{-\beta} + \frac{1}{2} & 0 \\ 0 & -\frac{1}{2}e^{-\beta} + \frac{1}{2} & \frac{1}{2}e^{-\beta} + \frac{1}{2} & 0 \\ 0 & 0 & 0 & e^{-\beta/2} \end{pmatrix} \tag{B.4}$$

$$\overset{\beta\to\infty}{=} \frac{1}{2}\begin{pmatrix} 0 & 0 & 0 & 0 \\ 0 & 1 & 1 & 0 \\ 0 & 1 & 1 & 0 \\ 0 & 0 & 0 & 0 \end{pmatrix} = |\psi_B\rangle\langle\psi_B|. \tag{B.5}$$

The density matrix associated to the state of the bath can then be written like the low temperature limit of a thermal density matrix with a quadratic operator in term

of fermion, and is, as a consequence, Gaussian.

Note that we could choose any initial amount of entanglement between the spins of the bath by tuning properly the temperature. Indeed, equation (B.4) leads to a concurrence of

$$\mathcal{C}_B(\beta) = \max\left\{0, \frac{\sinh(\beta/2) - 1}{\cosh(\beta/2) + 1}\right\}. \tag{B.6}$$

Then we can always find a value of β such that $\mathcal{C}_B(\beta) = x,\ x \in [0:1]$, as shown in figure B.1, where we plot $\mathcal{C}_B(\beta)$.

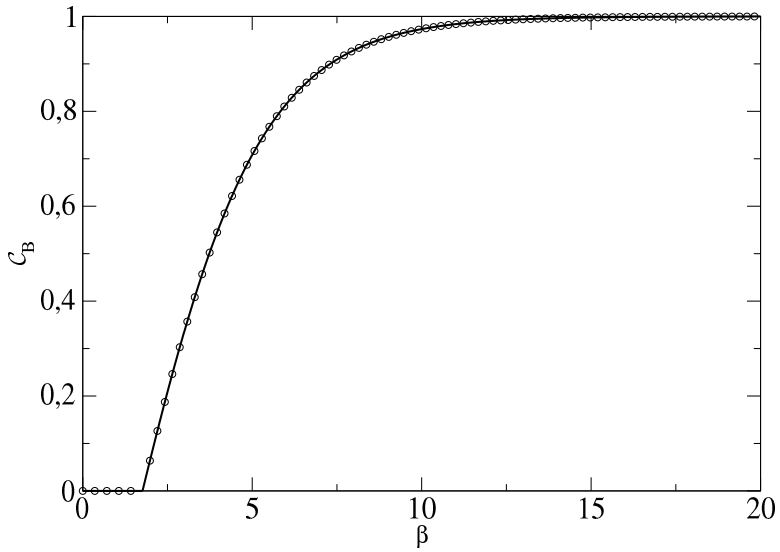

Figure B.1 – *Concurrence in the copies of the bath as a function of the inverse temperature β.*

Stationary spin-spin correlation functions

C

Finally, the last appendix is devoted to the steady state expression of the spin-spin correlation functions in the repeated interaction process.
Here, we show in details the case of $\langle \sigma^x_{N-p}\sigma^x_{N+3+p}\rangle$ but the other correlators are calculated exactelly in the same way. For writing reason, let's call $i = N-p$ and $i+R = N+3+p$. Due to the geometry of the system, R is always an odd number. We remind that in the steady state, the only non vanishing fermionic correlators are

$$\langle c_n^\dagger c_m\rangle = \frac{1}{2}\left(\delta_{nm} + \delta_{m,n+R}\right), \tag{C.1}$$

i.e the local correlators, corresponding to the local density, and the correlator between sites facing each others. Using Jordan-Wigner transformation, we have

$$\begin{aligned}\langle \sigma^x_i\sigma^x_{i+R}\rangle =& \Big\langle (c_i^\dagger - c_i)\prod_{k=i+1}^{i+R-1}(2c_k^\dagger c_k - 1)(c_{i+R}^\dagger + c_{i+R})\Big\rangle \\ =& \Big\langle c_i^\dagger \prod_{k=i+1}^{i+R-1}(2c_k^\dagger c_k - 1)c_{i+R}^\dagger\Big\rangle + \Big\langle c_i^\dagger \prod_{k=i+1}^{i+R-1}(2c_k^\dagger c_k - 1)c_{i+R}\Big\rangle \\ &-\Big\langle c_i \prod_{k=i+1}^{i+R-1}(2c_k^\dagger c_k - 1)c_{i+R}^\dagger\Big\rangle - \Big\langle c_i \prod_{k=i+1}^{i+R-1}(2c_k^\dagger c_k - 1)c_{i+R}\Big\rangle.\end{aligned} \tag{C.2}$$

Using the fact that $i < k < i+R$, equation (C.1) and the Wick theorem, the last expression can be written

$$\begin{aligned}\langle \sigma^x_i\sigma^x_{i+R}\rangle =& \big\langle c_i^\dagger c_{i+R}^\dagger\big\rangle\Big\langle \prod_{k=i+1}^{i+R-1}(2c_k^\dagger c_k - 1)\Big\rangle + \big\langle c_i^\dagger c_{i+R}\big\rangle\Big\langle \prod_{k=i+1}^{i+R-1}(2c_k^\dagger c_k - 1)\Big\rangle \\ &-\big\langle c_i c_{i+R}^\dagger\big\rangle\Big\langle \prod_{k=i+1}^{i+R-1}(2c_k^\dagger c_k - 1)\Big\rangle - \big\langle c_i c_{i+R}\big\rangle\Big\langle \prod_{k=i+1}^{i+R-1}(2c_k^\dagger c_k - 1)\Big\rangle \\ =& \Big(\big\langle c_i^\dagger c_{i+R}^\dagger\big\rangle + \big\langle c_i^\dagger c_{i+R}\big\rangle - \big\langle c_i c_{i+R}^\dagger\big\rangle - \big\langle c_i c_{i+R}\big\rangle\Big)\Big\langle \prod_{k=i+1}^{i+R-1}(2c_k^\dagger c_k - 1)\Big\rangle \\ =& 2\Re\mathrm{e}\big\langle c_i^\dagger c_{i+R}\big\rangle\Big\langle \prod_{k=i+1}^{i+R-1}(2c_k^\dagger c_k - 1)\Big\rangle \\ =& \Big\langle \prod_{k=i+1}^{i+R-1}(2c_k^\dagger c_k - 1)\Big\rangle,\end{aligned} \tag{C.3}$$

where we have used the fact that $\langle c_i c_{i+R}^\dagger \rangle = -\langle c_i^\dagger c_{i+R} \rangle^* = -1/2$ and $\langle c_i c_{i+R} \rangle = \langle c_i^\dagger c_{i+R}^\dagger \rangle = 0$. Developing the product, we get

$$\Big\langle \prod_{k=i+1}^{i+R-1} (2c_k^\dagger c_k - 1) \Big\rangle = \Bigg(1 - 2\Big\langle \sum_{k_1} c_{k_1}^\dagger c_{k_1} \Big\rangle + 2^2 \Big\langle \sum_{k_1<k_2} c_{k_1}^\dagger c_{k_1} c_{k_2}^\dagger c_{k_2} \Big\rangle$$
$$- \cdots + 2^{R-1} \Big\langle \sum_{k_1<k_2\cdots<k_{R-1}} c_{k_1}^\dagger c_{k_1} c_{k_2}^\dagger c_{k_2} \cdots c_{k_{R-1}}^\dagger c_{k_{R-1}} \Big\rangle \Bigg). \tag{C.4}$$

where the $k's$ indices take values between $i+1$ and $i+R-1$. Each sum with n ($n = 1, \cdots, R-1$) indices in the previous expression contains $\binom{R-1}{n}$ terms. To proceed further, we need to know the number of couples of indices corresponding to sites facing each others $\langle c_j^\dagger c_{j+R} \rangle$ present in one term of the development of each sum. In one term with n indices, we have the possibility to have $m = 0, 1, \cdots, n/2$ couples if $n \leq (R-1)/2$. If $n > (R-1)/2$, it is impossible to have 0 couple in the sum, at least one couple will appear in the sum. One can show that one term like

$$(-2)^n \Big\langle \sum_{k_1<k_2\cdots<k_n} c_{k_1}^\dagger c_{k_1} c_{k_2}^\dagger c_{k_2} \cdots c_{k_n}^\dagger c_{k_n} \Big\rangle \tag{C.5}$$

is equal to zero if the number of couples m present in the sum is different from zero. Indeed, using the Wick theorem, we find

$$(-2)^n \Big\langle \sum_{k_1<k_2\cdots<k_n} c_{k_1}^\dagger c_{k_1} c_{k_2}^\dagger c_{k_2} \cdots c_{k_n}^\dagger c_{k_n} \Big\rangle = \frac{(-2)^n}{2^n} \sum_{l=0}^{m} \binom{m}{l} (-1)^l = \frac{(-2)^n}{2^n} \delta_{m0}. \tag{C.6}$$

In consequence, we just need to consider the terms with 0 couple in equation (C.4). In each sum with $n > 1$ indices, there is

$$\frac{1}{n!} \prod_{j=0}^{n-1} ((R-1) - 2j) \tag{C.7}$$

terms with 0 couple with the same average of $\frac{(-2)^n}{2^n}$. Using

$$\frac{1}{n!} \prod_{j=0}^{n-1} ((R-1) - 2j) = \frac{(R-1)}{n} 2^{n-1} \binom{\frac{R-1}{2} - 1}{n-1}, \tag{C.8}$$

we obtain finally

$$\Big\langle \prod_{k=i+1}^{i+R-1} (2c_k^\dagger c_k - 1) \Big\rangle = 1 + \sum_{j=1}^{(R-1)/2} 2^{j-1} \frac{(-1)^j}{j} (R-1) \binom{\frac{R-1}{2} - 1}{j-1} = (-1)^{(R-1)/2}, \tag{C.9}$$

or, written in terms of the pair index p

$$\langle \sigma_{N-p}^x \sigma_{N+3+p}^x \rangle = (-1)^{p+1}. \tag{C.10}$$

Bibliography

[ABV01] M.C. Arnesen, S. Bose, and V. Vedral, *Natural thermal and magnetic entanglement in the 1D Heisenberg model*, Phys. Rev. Lett., **87** 017901 (2001).

[AD10] S. Attal and A. Dhahri, *Repeated quantum interactions and unitary random walks*, J. Theor. Prob., **23** 345 (2010).

[ADP14] S. Attal, J. Deschamps, and C. Pellegrini, *Entanglement of Bipartite Quantum Systems Driven by Repeated Interactions*, J. Stat. Phys., **154** 819 (2014).

[AFOV08] L. Amico, R. Fazio, A. Osterloh, and V. Vedral, *Entanglement in many-body systems*, Rev. Mod. Phys., **80** 517 (2008).

[AJ07] S. Attal and A. Joye, *The Langevin equation for a quantum heat bath*, J. Func. Analysis, **247** 253 (2007).

[AJP06a] S. Attal, A. Joye, and C-A. Pillet. *Open Quantum Systems I: The Hamiltonian Approach*, volume 1880. Springer (2006)a.

[AJP06b] S. Attal, A. Joye, and C-A. Pillet. *Open Quantum Systems II: The Markovian Approach*, volume 1880. Springer (2006)b.

[AOP+04] L. Amico, A. Osterloh, F. Plastina, R. Fazio, and G.M. Palma, *Dynamics of entanglement in one-dimensional spin systems*, Phys. Rev. A., **69** 022304 (2004).

[AP06] S. Attal and Y. Pautrat, *From repeated to continuous quantum interactions*, **7** 59 (2006).

[AP07] L. Amico and D. Patanè, *Entanglement crossover close to a quantum critical point*, Europhys. Lett., **77** 17001 (2007).

[BB84] C. H. Bennett and G. Brassard. *Quantum cryptography: Public key distribution and coin tossing*. In *Proceedings of IEEE International Conference on Computers, Systems and Signal Processing*, volume 175 (1984).

[BBC+93] C. H. Bennett, G. Brassard, C. Crépeau, R. Jozsa, A. Peres, and W. K. Wootters, *Teleporting an unknown quantum state via dual classical and Einstein-Podolsky-Rosen channels*, Phys. Rev. Lett., **70** 1895 (1993).

[BDZ08] I. Bloch, J. Dalibard, and W. Zwerger, *Many-body physics with ultracold gases*, Rev. Mod. Phys., **80** 885 (2008).

[BJM08] L. Bruneau, A. Joye, and M. Merkli, *Random repeated interaction quantum systems*, Comm. Math. Phys., **284** 553 (2008).

[BJM10] L. Bruneau, A. Joye, and M. Merkli. *Repeated and continuous interactions in open quantum systems*. In *Ann. Henri Poincaré*, volume 10, page 1251 (2010).

[BJM14] L. Bruneau, A. Joye, and M. Merkli, *Repeated interactions in open quantum systems*, J. Math. Phys., **55** 075204 (2014).

[Blo28] F. Bloch, *Über der Quantenmechanik der elektronen in Kristallgittern*, Z. Phys, **52** 555 (1928).

[Blo05] I. Bloch, *Ultracold quantum gases in optical lattices*, Nature Physics, **1** 23 (2005).

[BM71a] E. Barouch and B.M. McCoy, *Statistical mechanics of the XY model. II. Spin-correlation functions*, Phys. Rev. A, **3** 786 (1971)a.

[BM71b] E. Barouch and B.M. McCoy, *Statistical mechanics of the xy model. III*, Phys. Rev. A, **3** 2137 (1971)b.

[BMD70] E. Barouch, B.M. McCoy, and M. Dresden, *Statistical mechanics of the XY model. I*, Phys. Rev. A, **2** 1075 (1970).

[BP02] H.P. Breuer and F. Petruccione. *The theory of open quantum systems*. Oxford university press (2002).

[BPM+97] D. Bouwmeester, J-W Pan, K. Mattle, M. Eibl, H. Weinfurter, and A. Zeilinger, *Experimental quantum teleportation*, Nature, **390** 575 (1997).

[BR13] S. Boughn and M. Reginatto, *A pedestrian approach to the measurement problem in quantum mechanics*, Euro. Phys. J. H, **38** 443 (2013).

[Bra02] D. Braun, *Creation of Entanglement by Interaction with a Common Heat Bath*, Phys. Rev. Lett., **89** 277901 (2002).

[BRK11] J-S Bernier, G. Roux, and C. Kollath, *Slow Quench Dynamics of a One-Dimensional Bose Gas Confined to an Optical Lattice*, Phys. Rev. Lett., **106** 200601 (2011).

[CARK12] M. Collura, H. Aufderheide, G. Roux, and D. Karevski, *Entangling many-body bound states with propagative modes in Bose-Hubbard systems*, Phys. Rev. A, **86** 013615 (2012).

[CC05] P. Calabrese and J. Cardy, *Evolution of entanglement entropy in one-dimensional systems*, J. Stat. Mech.: Theor. Exp., **2005** P04010 (2005).

[CC09] P. Calabrese and J. Cardy, *Entanglement entropy and conformal field theory*, J. Phys. A: Math .and Theor., **42** 504005 (2009).

[CCW11] X. Cai, S. Chen, and Y. Wang, *Quantum dynamics of hard-core bosons in tilted bichromatic optical lattices*, Phys. Rev. A, **84** 033605 (2011).

[CEF12a] P. Calabrese, F.H.L Essler, and M. Fagotti, *Quantum quench in the transverse field Ising chain: I. Time evolution of order parameter correlators*, J. Stat. Mech.: Theor. Exper., **2012** P07016 (2012)a.

[CEF12b] P. Calabrese, F.H.L Essler, and M. Fagotti, *Quantum quenches in the transverse field Ising chain: II. Stationary state properties*, J. Stat. Mech.: Theor. Exper., **2012** P07022 (2012)b.

[CFVP07] F.M. Cucchietti, S. Fernandez-Vidal, and J.P. Paz, *Universal decoherence induced by an environmental quantum phase transition*, Phys. Rev. A, **75** 032337 (2007).

[CG07] P. Calabrese and A. Gambassi, *Slow dynamics in critical ferromagnetic vector models relaxing from a magnetized initial state*, J. Stat. Mech: Theor. Exp., **2007** P01001 (2007).

[Che07] H. Chen, *Two-point entanglement near a quantum phase transition*, J. Phys. A: Math. Theor, **40** 10215 (2007).

[CKW00] V. Coffman, J. Kundu, and W.K. Wootters, *Distributed entanglement*, Phys. Rev. A, **61** 052306 (2000).

[Col12] M. Collura. *Nonequilibrium aspects in strongly correlated one-dimensional quantum systems*. PhD thesis, Université de Lorraine (2012).

[Cor09] C. Cormick. *Decoherencia y simulaciones cuánticas: ambientes con dinámica propia*. PhD thesis, Universidad de Buenos Aires (2009).

[CP01] M-C Chung and I. Peschel, *Density-matrix spectra of solvable fermionic systems*, Phys. Rev. B, **64** 064412 (2001).

[CP08a] C. Cormick and J. P. Paz, *Decoherence induced by a dynamic spin environment: The universal regime*, Phys. Rev. A, **77** 022317 (2008)a.

[CP08b] C. Cormick and J. P. Paz, *Decoherence of Bell states by local interactions with a dynamic spin environment*, Phys. Rev. A, **78** 012357 (2008)b.

[CPZ05] F.M. Cucchietti, J.P. Paz, and W.H. Zurek, *Decoherence from spin environments*, Phys. Rev. A, **72** 052113 (2005).

[CVDEBR06] L. Campos Venuti, C. Degli Esposti Boschi, and M. Roncaglia, *Long-Distance Entanglement in Spin Systems*, Phys. Rev. Lett., **96** 247206 (2006).

[CVDEBR07] L. Campos Venuti, C. Degli Esposti Boschi, and M. Roncaglia, *Qubit Teleportation and Transfer across Antiferromagnetic Spin Chains*, Phys. Rev. Lett., **99** 060401 (2007).

[CVGIZ07] L. Campos Venuti, S.M. Giampaolo, F. Illuminati, and P. Zanardi, *Long-distance entanglement and quantum teleportation in XX spin chains*, Phys. Rev. A, **76** 052328 (2007).

[DCLLS12] G. De Chiara, L. Lepori, M. Lewenstein, and A. Sanpera, *Entanglement Spectrum, Critical Exponents, and Order Parameters in Quantum Spin Chains*, Phys. Rev. Lett., **109** 237208 (2012).

[Dha08] A. Dhahri, *A Lindblad model for a spin chain coupled to heat baths*, J. Phys. A: Math. and Theor., **41** 275305 (2008).

[DPR+96] M. B Dahan, E. Peik, Jakob Reichel, Y. Castin, and C. Salomon, *Bloch oscillations of atoms in an optical potential*, Phys. Rev Let., **76** 4508 (1996).

[DQZ11] B. Damski, H. T Quan, and W.H. Zurek, *Critical dynamics of decoherence*, Phys. Rev. A, **83** 062104 (2011).

[dSDS03] R. de Sousa and S. Das Sarma, *Electron spin coherence in semiconductors: Considerations for a spin-based solid-state quantum computer architecture*, Phys. Rev. B, **67** 033301 (2003).

[DV95] D. Di Vicenzo, *Quantum Computation*, Science, **270** 255 (1995).

[EK95] A. Ekert and P. L. Knight, *Entangled quantum systems and the Schmidt decomposition*, Amer. J. of Phys., **63** 415 (1995).

[EPR35] A. Einstein, B. Podolsky, and N. Rosen, *Can quantum-mechanical description of physical reality be considered complete ?*, Phys Rev, **47** 777 (1935).

[Eve57] H. Everett, *"Relative State" Formulation of Quantum Mechanics*, Rev. Mod. Phys., **29** 454 (1957).

[FK87] G.W. Ford and M. Kac, *On the quantum Langevin equation*, J. Stat. Phys., **46** 803 (1987).

[FKM65] G.W. Ford, M Kac, and P Mazur, *Statistical mechanics of assemblies of coupled oscillators*, J. Math Phys, **6** 504 (1965).

[FKT+13] T. Fogarty, E. Kajari, B. G. Taketani, A. Wolf, Th. Busch, and Giovanna Morigi, *Entangling two defects via a surrounding crystal*, Phys. Rev. A, **87** 050304 (2013).

[FS13] A. Faribault and D. Schuricht, *Spin decoherence due to a randomly fluctuating spin bath*, Phys. Rev. B, **88** 085323 (2013).

[FWGF89] M.P.A. Fisher, P.B. Weichman, G. Grinstein, and D.S. Fisher, *Boson localization and the superfluid-insulator transition*, Phys. Rev. B, **40** 546 (1989).

[GI10] S. M. Giampaolo and F. Illuminati, *Long-distance entanglement in many-body atomic and optical systems*, New. J. Phys., **12** 025019 (2010).

[GJPW12] A. Goussev, R.A. Jalabert, H.M. Pastawski, and D. Wisniacki, *Loschmidt Echo*, arXiv:1206.6348, (2012).

[GKVB01] D. Gunlycke, V.M. Kendon, V. Vedral, and S. Bose, *Thermal concurrence mixing in a one-dimensional Ising model*, Phys. Rev. A., **64** 042302 (2001).

[GLL03] S. Gu, H. Lin, and Y. Li, *Entanglement, quantum phase transition, and scaling in the XXZ chain*, Phys. Rev. A., **68** 042330 (2003).

[GRTZ02] N. Gisin, G.e Ribordy, W. Tittel, and H. Zbinden, *Quantum cryptography*, Rev. mod. phys., **74** 145 (2002).

[GT07] N. Gisin and R. Thew, *Quantum communication*, Nature Photonic, **1** 165 (2007).

[GTL06] S. Gu, G. Tian, and H. Lin, *Local entanglement and quantum phase transition in spin models*, New J. Phys., **8** 61 (2006).

[Hen99] M. Henkel. *Conformal invariance and critical phenomena*. Springer (1999).

[HHH96] M. Horodecki, P. Horodecki, and R. Horodecki, *Separability of mixed states: necessary and sufficient conditions*, Phys. Lett. A, **223** 1 (1996).

[HMMR+09] F. Heidrich-Meisner, S. R. Manmana, M. Rigol, A. Muramatsu, A. E. Feiguin, and E. Dagotto, *Quantum distillation: Dynamical generation of low-entropy states of strongly correlated fermions in an optical lattice*, Phys. Rev. A, **80** 041603 (2009).

[Hor01] M. Horodecki, *Entanglement measures*, Quant. Inf. Comp., **1** 3 (2001).

[HP40] T. Holstein and H. Primakoff, *Field Dependence of the Intrinsic Domain Magnetization of a Ferromagnet*, Phys. Rev., **58** 1098–1113 (1940).

[HRS04] V. Hunyadi, Z. Rácz, and L. Sasvári, *Dynamic scaling of fronts in the quantum XX chain*, Phys. Rev. E, **69** 066103 (2004).

[Hub63] J. Hubbard, *Electron correlations in narrow energy bands*, Proc. Roy. Soc. London, **276** 238 (1963).

[HW97] S. Hill and W.K. Wootters, *Entanglement of a Pair of Quantum Bits*, Phys. Rev. Lett., **78** 5022 (1997).

[JW28] P. Jordan and E. Wigner, *Über das Paulische Äquivalenzverbot*, Zeitschrift für Physik, **47** 631 (1928).

[Kar06] D. Karevski. *Ising quantum chains* (2006). arXiv:cond-mat/0611327.

[KK04] A.R. Kolovsky and H.J. Korsch, *Bloch oscillations of cold atoms in optical lattices*, Inter. Jour. Mod. Phys. B, **18** 1235 (2004).

[KP09] D. Karevski and T. Platini, *Quantum Nonequilibrium Steady States Induced by Repeated Interactions*, Phys. Rev. Lett., **102** 207207 (2009).

[KPS13] D. Karevski, V. Popkov, and G.M. Schütz, *Exact Matrix Product Solution for the Boundary-Driven Lindblad X X Z Chain*, Phys. Rev. Lett., **110** 047201 (2013).

[KS06] H.G. Krojanski and D. Suter, *Decoherence in large NMR quantum registers*, Phys. Rev. A, **74** 062319 (2006).

[KS10] M. Keyl and D.M. Schlingemann, *The algebra of Grassmann canonical anticommutation relations and its applications to fermionic systems*, J. Math. Phys., **51** 023522 (2010).

[KWLM12] E. Kajari, A. Wolf, E. Lutz, and G. Morigi, *Statistical mechanics of entanglement mediated by a thermal reservoir*, Phys. Rev. A, **85** 042318 (2012).

[LH08] H. Li and F.D.M. Haldane, *Entanglement Spectrum as a Generalization of Entanglement Entropy: Identification of Topological Order in Non-Abelian Fractional Quantum Hall Effect States*, Phys. Rev. Lett., **101** 010504 (2008).

[Lin76] G. Lindblad, *On the generators of quantum dynamical semigroups*, Commun. Math. Phys., **48** 119 (1976).

[LSM61] E. Lieb, T. Schultz, and D. Mattis, *Two soluble models of an antiferromagnetic chain*, Ann. Phys, **16** 407 (1961).

[LW03] D.A Lidar and K. B. Whaley. *Decoherence-free subspaces and subsystems*. In *Irreversible Quantum Dynamics*, page 83. Springer (2003).

[MBA71] B.M. McCoy, E. Barouch, and D. B. Abraham, *Statistical mechanics of the XY model. IV. Time-dependent spin-correlation functions*, Phys. Rev. A, **4** 2331 (1971).

[MDDS07] V. Mukherjee, U. Divakaran, A. Dutta, and D. Sen, *Quenching dynamics of a quantum XY spin-$\frac{1}{2}$ chain in a transverse field*, Phys. Rev. B, **76** 174303 (2007).

[MDRT+03] I. Marcikic, H. De Riedmatten, W. Tittel, H. Zbinden, and N. Gisin, *Long-distance teleportation of qubits at telecommunication wavelengths*, Nature, **421** 509 (2003).

[MG05] A. Minguzzi and D. M. Gangardt, *Exact Coherent States of a Harmonically Confined Tonks-Girardeau Gas*, Phys. Rev. Lett., **94** 240404 (2005).

[MHS+12] X-S Ma, T. Herbst, T. Scheidl, D. Wang, Se. Kropatschek, W. Naylor, B. Wittmann, A. Mech, J. Kofler, E. Anisimova, et al., *Quantum teleportation over 143 kilometres using active feed-forward*, Nature, **489** 269 (2012).

[MSD12] V. Mukherjee, S. Sharma, and A. Dutta, *Loschmidt echo with a nonequilibrium initial state: Early-time scaling and enhanced decoherence*, Phys. Rev. B, **86** 020301 (2012).

[NC00] Michael A. Nielsen and Isaac L. Chuang. *Quantum Computation and Quantum Information*. Cambridge University Press (2000).

[NDD12] T. Nag, U. Divakaran, and A. Dutta, *Scaling of the decoherence factor of a qubit coupled to a spin chain driven across quantum critical points*, Phys. Rev. B, **86** 020401 (2012).

[OAFF02] A. Osterloh, L. Amico, G. Falci, and R. Fazio, *Scaling of entanglement close to a quantum phase transition*, Nature, **416** 608 (2002).

[ON02] T.J Osborne and M.A. Nielsen, *Entanglement in a simple quantum phase transition*, Phys. Rev. A., **66** 032110 (2002).

[OW01] K.M. O'Connor and W.K. Wootters, *Entangled rings*, Phys. Rev. A, **63** 052302 (2001).

[Per84] A. Peres, *Stability of quantum motion in chaotic and regular systems*, Phys. Rev. A, **30** 1610 (1984).

[Per96] A. Peres, *Separability Criterion for Density Matrices*, Phys. Rev. Lett., **77** 1413 (1996).

[Pes03] I. Peschel, *Calculation of reduced density matrices from correlation functions*, J. Phys. A: Math. Gen, **36** L205 (2003).

[Pfe70] P. Pfeuty, *The one-dimensional Ising model with a transverse field*, Ann. Pys, **57** 79 (1970).

[PK05] T. Platini and D. Karevski, *Scaling and front dynamics in Ising quantum chains*, Eur. Phys. J. B., **48** 225 (2005).

[PKS13] V. Popkov, D. Karevski, and G. M. Schütz, *Driven isotropic Heisenberg spin chain with arbitrary boundary twisting angle: Exact results*, Phys. Rev. E, **88** 062118 (2013).

[Pla08] T. Platini. *Chaînes de spins quantiques hors de l'équilibre*. PhD thesis, Université Henri Poincaré (2008).

[PPcv08] T. Prosen and I. Pižorn, *Quantum Phase Transition in a Far-from-Equilibrium Steady State of an XY Spin Chain*, Phys. Rev. Lett., **101** 105701 (2008).

[PR08] J. P. Paz and A. J. Roncaglia, *Dynamics of the Entanglement between Two Oscillators in the Same Environment*, Phys. Rev. Lett., **100** 220401 (2008).

[PR09] J. P. Paz and A. J. Roncaglia, *Dynamical phases for the evolution of the entanglement between two oscillators coupled to the same environment*, Phys. Rev. A, **79** 032102 (2009).

[Pre00] J. Preskill, *Quantum information and physics: some future directions*, J. Mod. Opt., **47** 127 (2000).

[Pro08] T. Prosen, *Third quantization: a general method to solve master equations for quadratic open Fermi systems*, New J. Phys., **10** 043026 (2008).

[PS05] V. Popkov and M. Salerno, *Logarithmic divergence of the block entanglement entropy for the ferromagnetic Heisenberg model*, Phys. Rev. A, **71** 012301 (2005).

[PSSV11] A. Polkovnikov, K. Sengupta, A. Silva, and M. Vengalattore, *Colloquium: Nonequilibrium dynamics of closed interacting quantum systems*, Rev. Mod. Phys., **83** 863 (2011).

[PV07] M.B. Plenio and S. Virmani, *An Introduction to Entanglement Measures*, Quant. Info. Comput., **7** 1 (2007).

[PZ01] J.P. Paz and W.H. Zurek. *Environment-induced decoherence and the transition from quantum to classical*. In *Coherent atomic matter waves*, page 533. Springer (2001).

[QSL+06] H.T. Quan, Z. Song, X.F. Liu, P. Zanardi, and C.P. Sun, *Decay of Loschmidt echo enhanced by quantum criticality*, Phys. Rev. Lett., **96** 140604 (2006).

[RCG+07a] D. Rossini, T. Calarco, V. Giovannetti, S. Montangero, and R. Fazio, *Decoherence by engineered quantum baths*, J. Phys A: Math. and Theor., **40** 8033 (2007)a.

[RCG+07b] D. Rossini, T. Calarco, V. Giovannetti, S. Montangero, and R. Fazio, *Decoherence induced by interacting quantum spin baths*, Phys. Rev. A, **75** 032333 (2007)b.

[RFF+08] D. Rossini, P. Facchi, R. Fazio, G. Florio, D. A. Lidar, S. Pascazio, F. Plastina, and P. Zanardi, *Bang-bang control of a qubit coupled to a quantum critical spin bath*, Phys. Rev. A, **77** 052112 (2008).

[RM05] M. Rigol and A. Muramatsu, *Quantum criticality in ultracold atoms on optical lattices*, phys Stat. Sol. (b), **242** 1850 (2005).

[Rou09] G. Roux, *Quenches in quantum many-body systems: One-dimensional Bose-Hubbard model reexamined*, Phys. Rev. A, **79** 021608 (2009).

[RSMS09] D. Rossini, A. Silva, G. Mussardo, and G.E. Santoro, *Effective Thermal Dynamics Following a Quantum Quench in a Spin Chain*, Phys. Rev. Lett., **102** 127204 (2009).

[Sac00] S. Sachdev. *Quantum phase transitions*. Cambridge University Press (2000).

[Sch06] E. Schmidt, *Zur Theorie der linearen une nichtlinearen Integralgleichungen*, Math. Annalen, **63** 433 ((1906)).

[Sch05] M. A. Schlosshauer, *Decoherence, the measurement problem, and interpretations of quantum mechanics*, Rev. Mod. Phys., **76** 1267 (2005).

[Sch07] M. A. Schlosshauer. *Decoherence: and the quantum-to-classical transition*. Springer (2007).

[Sch13] N. Schuch. *Condensed Matter Applications of Entanglement Theory*. Lecture Notes of the 44th IFF Spring School "Quantum Information Processing" (2013). arXiv:1306.5551 [quant-ph].

[SG09] T. Stauber and F. Guinea, *Entanglement of spin chains with general boundaries and of dissipative systems*, Ann. Phys. (Berlin), **18** 561 (2009).

[SLRD13] J. Schachenmayer, B. P. Lanyon, C. F. Roos, and A. J. Daley, *Entanglement Growth in Quench Dynamics with Variable Range Interactions*, Phys. Rev. X, **3** 031015 (2013).

[SMD12] Shraddha Sharma, Victor Mukherjee, and Amit Dutta, *Study of Loschmidt Echo for a qubit coupled to an XY-spin chain environment*, Euro. Phys. J. B, **85** 1 (2012).

[SSG06] S. Su, J. Song, and S. Gu, *Local entanglement and quantum phase transition in a one-dimensional transverse field Ising model*, Phys. Rev. A, **74** 032308 (2006).

[TFK+14] B.G. Taketani, T. Fogarty, E. Kajari, Th. Busch, and G. Morigi, *Quantum reservoirs with ion chains*, Phys. Rev. A, **90** 012312 (2014).

[UJA+04] R. Ursin, T. Jennewein, M. Aspelmeyer, R. Kaltenbaek, M. Lindenthal, P. Walther, and A. Zeilinger, *Communications: Quantum teleportation across the Danube*, Nature, **430** 849 (2004).

[Ver04] V. Verdal, *High-temperature macroscopic entanglement*, New J. Phys., **6** 102 (2004).

[VL98] L. Viola and S. Lloyd, *Dynamical suppression of decoherence in two-state quantum systems*, Phys. Rev. A, **58** 2733 (1998).

[VLRK03] G. Vidal, J.I. Latorre, E. Rico, and A. Kitaev, *Entanglement in quantum critical phenomena*, Phys. Rev Lett., **90** 227902 (2003).

[VMD04] J. Vidal, R. Mosseri, and J. Dukelsky, *Entanglement in a first-order quantum phase transition*, Phys. Rev. A, **69** 054101 (2004).

[VPM04] J. Vidal, G. Palacios, and R. Mosseri, *Entanglement in a second-order quantum phase transition*, Phys. Rev. A, **69** 022107 (2004).

[Wan01] X. Wang, *Effects of anisotropy on thermal entanglement*, Phys. Lett. A, **281** 101 (2001).

[WDCK+11] A. Wolf, G. De Chiara, E. Kajari, E. Lutz, and G. Morigi, *Entangling two distant oscillators with a quantum reservoir*, Europhys. Lett., **95** 60008 (2011).

[Wei99] U. Weiss. *Quantum dissipative systems*. World Scientific (1999).

[Wer89] R.F. Werner, *Quantum states with Einstein-Podolsky-Rosen correlations admitting a hidden-variable model*, Phys. Rev. A, **40** 4277 (1989).

[Wil67] R.M Wilcox, *Exponential Operators and Parameter Differentiation in Quantum Physics*, J. Math. Phys, **8** 962 (1967).

[Woo98] W.K. Wootters, *Entanglement of Formation of an Arbitrary State of Two Qubits*, Phys. Rev. Lett., **80** 2245 (1998).

[Woo01] W.K. Wootters, *Entanglement of formation and concurrence.*, Quant. Inf. Comp., **1** 27 (2001).

[WSL04] L-A Wu, M.S Sarandy, and D.A Lidar, *Quantum phase transitions and bipartite entanglement*, Phys Rev Lett, **93** 250404 (2004).

[WZ82] W.K. Wootters and W.H. Zurek, *A single quantum cannot be cloned*, Nature, **299** 802 (1982).

[Yan05] M-F Yang, *Reexamination of entanglement and the quantum phase transition*, Phys. Rev. A, **71** 030302 (2005).

[YZL07] Z-G Yuan, P. Zhang, and S-S. Li, *Disentanglement of two qubits coupled to an X Y spin chain: Role of quantum phase transition*, Phys. Rev. A, **76** 042118 (2007).

[Zen34] C. Zener, *A theory of the electrical breakdown of solid dielectrics*, Proc. R. Soc. London. A, **145** 523 (1934).

[ZI14] S. Zippilli and F. Illuminati, *Non-Markovian dynamics and steady-state entanglement of cavity arrays in finite-bandwidth squeezed reservoirs*, Phys. Rev. A, **89** 033803 (2014).

[ZPAI13] S. Zippilli, M. Paternostro, G. Adesso, and F. Illuminati, *Entanglement Replication in Driven Dissipative Many-Body systems*, Phys. Rev. Lett., **110** 040503 (2013).

[Zur82] W.H. Zurek, *Environment-induced superselection rules*, Phys. Rev. D., **26** 1862 (1982).

[Zur02] W.H. Zurek, *Decoherence and the transition from quantum to classical-revisited*, Los Alamos Science, **27** 86 (2002).

[Zur03] W.H. Zurek, *Decoherence, einselection, and the quantum origins of the classical*, Rev. Mod. Phys., **75** 715 (2003).

[ZZL08] H-Q. Zhou, J-H. Zhao, and B. Li, *Fidelity approach to quantum phase transitions: finite-size scaling for the quantum Ising model in a transverse field*, J. Phys. A: Math. Theor., **41** 492002 (2008).

Intrication et dynamique de trempe dans les chaînes de spins quantiques

Résumé: L'étude menée dans cette thèse concerne la dynamique de systèmes quantiques hors de l'équilibre, et plus particulièrement leurs propriétés d'intrication. En effet, l'intrication est devenue un concept fondamental dans la physique moderne, grâce notamment au développement de l'information quantique. Nous avons dans un premier temps étudié la dynamique d'un modèle de bosons sur réseau après la trempe de leur potentiel de confinement. Dans la limite de cœur dur, nous avons développé une théorie hydrodynamique qui reproduit parfaitement les différents comportements observés. Nous nous sommes ensuite intéressés à la dynamique de deux spins défauts couplés à une chaîne d'Ising. Dans un premier temps, ces défauts ont été préparés dans un état séparable. Nous avons dans ce cas établi une formule donnant l'évolution temporelle de la matrice de densité réduite, qui nous a permis d'avoir accès à l'intrication créée par l'intermédiaire du couplage à la chaîne. Puis, nous avons considéré le cas de deux spins défauts initialement intriqués, et nous avons étudié l'influence d'un environnement hors de l'équilibre sur leurs propriétés de désintrication. Finalement, la dernière partie de cette thèse est consacrée à l'étude d'un système couplé à un environnement décrit par le processus d'interactions répétées. Nous avons étudié la relaxation du système dans deux régimes temporels différents. Pour des temps courts, l'état est bien décrit par un état stationnaire hors équilibre, dans lequel nous avons mis en évidence les propriétés d'échelle de certaines observables. Enfin, pour des temps longs, le système atteint un état stationnaire d'équilibre composé d'un produit d'états de Bell.

Mots-clés: Dynamique hors équilibre, systèmes quantiques ouverts, intrication quantique, concurrence, chaînes de spins, auto-piègeage bosonique

Entanglement and quench dynamics in quantum spin chains

Abstract: The study carried in this thesis concerns the dynamics of out-of-equilibrium quantum systems, and more particularly their entanglement properties. Indeed, entanglement became a fundamental concept in modern physics, especially with the development of quantum information. We have in a first part studied the dynamics of a model of bosons on a lattice after the quench of their trapping potential. In the hard-core limit, we developed an hydrodynamical theory which perfectly reproduced the observed behavior. Then, we have looked at the dynamics of two defect spins coupled to an Ising chain. When these defects have been prepared into a separable state, we have established a formula giving the evolution of the reduced density matrix, allowing us to have access to the entanglement create through the coupling to the chain. We considered then the case of two initially entangled defect spins, and we studied the influence of a non-equilibrium environment on the disentanglement properties. Finally, the last part of this thesis is devoted to the study of a system coupled to an environment by means of the repeated interactions process. We studied the relaxation of the system in two different time regimes. For short times, the state is well described by a non-equilibrium-steady-state, in which we highlighted the scaling properties of some observables. For long times, the system reaches an equilibrium steady state made of a product of Bell states.

Keywords: Out-of-equilibrium dynamics, open quantm systems, quantum entanglement, concurrence, spins chains, bosonic self-trapping